



**Universidade do Minho**  
Escola de Ciências da Saúde

Ana Sofia Teixeira Esteves

**Pre-clinical trials for Machado-Joseph Disease:  
Hypothesis-based and hypothesis-free  
therapeutic approaches**

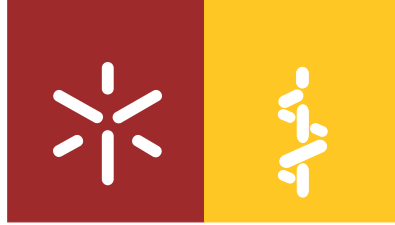
**Ensaio pré-clínico para a Doença de  
Machado-Joseph: Estratégias terapêuticas  
baseadas em hipótese e independentes de  
hipótese**

**Pre-clinical trials for Machado-Joseph Disease: Hypothesis-based and hypothesis-free therapeutic approaches**  
**Ensaio pré-clínico para a Doença de Machado-Joseph: Estratégias terapêuticas baseadas em hipótese e independentes de hipótese**

Ana Sofia Teixeira Esteves

UMinho | 2015

outubro de 2015



**Universidade do Minho**

Escola de Ciências da Saúde

Ana Sofia Teixeira Esteves

**Pre-clinical trials for Machado-Joseph Disease:  
Hypothesis-based and hypothesis-free  
therapeutic approaches**

**Ensaio pré-clínico para a Doença de  
Machado-Joseph: Estratégias terapêuticas  
baseadas em hipótese e independentes de  
hipótese**

Tese de Doutoramento em Ciências da Saúde

Trabalho efectuado sob a orientação da

**Professora Doutora Patrícia Espinheira de Sá Maciel**

## DECLARAÇÃO DE INTEGRIDADE

Declaro ter atuado com integridade na elaboração da presente tese. Confirmando que em todo o trabalho conducente à sua elaboração não recorri à prática de plágio ou a qualquer forma de falsificação de resultados.

Mais declaro que tomei conhecimento integral do Código de Conduta Ética da Universidade do Minho.

Universidade do Minho, 29 de Outubro de 2015

Nome completo: Ana Sofia Teixeira Esteves

Assinatura: \_\_\_\_\_ Sofia Esteves \_\_\_\_\_

This work was supported by Fundação para a Ciência e Tecnologia (FCT) and QREN – POPH through a *Bolsa de Doutoramento* (SFRH/BD/78554/2011) and ATAXIA UK Grant through the project: *Pharmacologic therapy for Machado-Joseph Disease: from a C.elegans drug screen to a mouse model validation*.



## **Agradecimentos**

---

Uma tese de Doutorado é uma longa viagem, com muitos altos e baixos, e foi sem dúvida, o desafio mais importante e marcante da minha vida académica. Embora uma tese seja um trabalho individual, há contributos de natureza diversa que não podem nem devem deixar de ser realçados. Por esta razão, desejo expressar os meus sinceros agradecimentos:

À Fundação para a Ciência e Tecnologia (FCT) por ter permitido a realização deste projeto através de uma bolsa de doutoramento (SFRH/BD/78554/2011) - financiada no âmbito do QREN – POPH.

À Escola de Ciências da Saúde da Universidade do Minho (ECS/UM), em nome da Professora Cecília Leão, por me ter aceitado como aluna de Doutorado desta Escola.

Ao Instituto de Ciências da Vida e da Saúde da Universidade do Minho (ICVS/3B's), em nome do Professor Jorge Pedrosa e ao Domínio das Neurociências (NeRD), em nome do Professor Nuno Sousa, pelo apoio a este projeto e pelas excelentes condições de acolhimento que me propiciou o desenvolvimento deste trabalho de Doutorado.

Aos funcionários da ECS que de uma forma ou de outra também contribuíram para o sucesso do meu trabalho. Um agradecimento especial à Goreti Pinto, Manuela Carneiro, Celina Barros e Maria José Tarroso.

Ao Programa Inter-universitário de Doutorado em Envelhecimento e Doenças Crónicas (PhDOC) ao qual tive o enorme privilégio de pertencer. É sem dúvida um excelente programa, que me permitiu abrir portas e partilhar novas experiências noutros laboratórios, com outros colegas e investigadores.

À Professora Patrícia Maciel por todo o apoio e confiança que depositou em mim nestes anos. Por me ter dado oportunidade de realizar um trabalho de Doutorado como eu realmente gostaria de o fazer. Pelo conhecimento profundo de todas as áreas que me transmitiu, pelas críticas construtivas que me ensinaram a tornar cada vez mais madura e profissional, pela disponibilidade, pela simpatia, por arranjar sempre forma de resolver os problemas. Obrigada!

Ao Professor Pedro, “o tempo, esse grande senhor das nossas vidas”, pela enorme paciência e carinho com que sempre me ajudou nas dificuldades em compreender estatística. Foi uma ajuda verdadeiramente preciosa pela qual estou imensamente grata. Pelos incansáveis exemplos de percentis de bebés, que sem eles tudo seria mais difícil de compreender.

À Sara Silva, pela qual sinto uma enorme gratidão. Por me teres ensinado a dar os primeiros passos no ICVS, pela tua disponibilidade e amizade constante. Por saber que sempre pude contar contigo. Por termos caminhado lado a lado nesta aventura, desde Coimbra, a Lisboa, a Braga e até Londres. Pelo teu “relaxa” que tanto me “stressa”, mas que no fim vale sempre a pena. Obrigada!

À Anabela, a fundadora das ratices. Por teres sido mais que uma colega, uma orientadora, uma amiga, sempre demasiado relaxada e desorganizada para o meu estilo, mas sempre com questões pertinentes, com aquele perfeccionismo característico mas imprescindível. Por teres criado um ratinho espetacular, mas que continua sempre a dar luta. Pelo teu sentido de humor, que não existe igual e por saber que te vais sempre lembrar de mim e eu de ti quando ouvir “*Thinking out loud*” and “*Wake me up*”. Obrigada!

À Andreia Castro pela criatividade, pelo exemplo de determinação, garra, luta, pelas críticas construtivas. Pelas imensas discussões produtivas, pelas questões pertinentes, por conseguires por à prova o meu espírito crítico e por me teres feito crescer enquanto cientista. Pelos desafios superados nesta longa caminhada chamada citalopram. Obrigada!

À Li. Porque tudo começou com “um dia vai ser o dia” e a partir daí nunca caminhei só. Por partilharmos o ginásio, o carro, o almoço, o lanche, a vida para além do trabalho, mas acima de tudo, as alegrias e tristezas, os sucessos e os fracassos. Se poderia ter feito esta caminhada sem ti? Poder podia, mas não seria a mesma coisa. Obrigada!

À Martinha Costa, pela “péssima” companhia calórica, porque só tu me fazes quebrar a dieta, mas que sabe tão bem. Por seres sempre tão natural e transparente, por seres boa amiga e teres um sentido de humor peculiar. Porque andas sempre a correr... a correr para chegar ao trabalho, a correr para fazer meio, a correr para extrair *pellets*, a correr para o *Real-Time*, a correr para sair, a correr de um lado para o outro, mas que torna o meu dia tão mais engraçado, mesmo quando tudo parece correr mal. Porque sei que foi apenas o início de uma grande amizade! Obrigada!

À Andreia Carvalho, pelos bons momentos de biotério e sacrifícios, pela ajuda preciosa nos últimos quilómetros do percurso, que embora pareça rápido, são os mais difíceis. Pelo exemplo dado em conseguir superar os limites e abraçar novos projetos, ideias e perspetivas. A vida não falha para quem tem coragem de arriscar. Obrigada!

À Ana Jalles, pelo teu sentido de humor, pelas piadas, pelos bons momentos. Por teres também caminhado lado a lado nesta longa aventura do citalopram, será sempre o nosso (da minhoca e do ratinho também) antidepressivo mais marcante! Obrigada!

À Dulce e Stephanie, boas meninas e colegas de trabalho, muita sorte para vocês! Não podia esquecer a Marina Amorim, pela qual tenho um carinho muito grande pela sua simplicidade e generosidade, pelas ajudas valiosas no biotério e por sempre me fazer rir. Obrigada!

Ao Carlos Bessa, por me ter salvado várias e várias vezes o computador, por saber que posso sempre estar descansada quando te coloco o computador nas mãos. Obrigada pela preciosa ajuda, pela disponibilidade, atenção e carinho!

A tantos outros colegas de trabalho, de *open space*, de lanches e almoços, de terraços, de NeRD meetings, de boas conversas, que pela sua individualidade marcaram também estes meus quatro anos, o meu muito obrigado! Joana Silva, Cristina Mota, Mónica Morais, Fábio Teixeira, Gonçalo Gonçalves, Bárbara Coimbra, Carina Cunha, Adriana Miranda, Dani Torres!

E porque a vida não é só Doutoramento, apesar de ter exigido uma enorme dedicação e ter sido um grande orgulho para mim, como teria tudo isto sido possível se não tivesse os amigos e a família?

Obrigada a todos os meus amigos, que sempre estiveram ao meu lado, me apoiaram, me deram valor e força, presenciaram as minhas vitórias, as minhas derrotas, mas que acima de tudo me ajudaram a levantar e fizeram sempre que o meu sorriso prevalecesse. Vocês sabem quem são e que estão aqui ♥ sempre!

À minha tia Guidinha, porque sei que estás sempre a pensar em mim e que celebras sempre as minhas vitórias. Obrigada titia!

Aos meus sogros, pela constante compreensão e extremo carinho, porque me sinto também uma filha e isso é um grande privilégio para mim. Obrigada!

Ao meu príncipe, meu Bruno, amor da minha vida, meu companheiro, minha família. O mais difícil de agradecer pois parece que as palavras nunca serão suficientes. Por me teres dado sempre uma enorme força, por teres acreditado tanto em mim e teres caminhado ao meu lado todos os dias, todos os segundos, por me teres compreendido e ouvido sempre que precisei, por teres uma enorme paciência quando tenho que ficar a estudar, por viveres as minhas vitórias como se fossem tuas, por seres também o meu melhor amigo e confidente. Por me fazeres sentir a mulher mais feliz do mundo, todos os dias das nossas vidas. Obrigada Bé ♥

Aos meus pais, amores eternos da minha vida, as pessoas mais importantes, esta tese é vossa, é a vós que devo tudo que hoje sou, vocês são os grandes impulsionadores do meu sucesso, das minhas vitórias, são o meu eterno porto de abrigo, são tudo para mim. Porque sempre acreditaram em mim, sempre me deram força e motivação para continuar e enfrentar os desafios, pela paciência, e compreensão... Não existem palavras suficientes para expressar o enorme amor e gratidão que tenho por vocês ♥ Esta tese é vossa!



## Abstract

---

### **“Pre-clinical trials for Machado-Joseph Disease: Hypothesis-based and hypothesis-free therapeutic approaches”**

Polyglutamine (PolyQ) diseases are a family of neurodegenerative disorders characterized by the expansion of a CAG trinucleotide repeat in specific genes. This leads to the production of pathogenic proteins containing critically expanded tracts of glutamines. Although polyQ diseases are rare disorders, this group includes nine progressive, severe and fatal disorders, which in general begin in adulthood and progress over 10 to 30 years, normally implicating the full time patient care by a member of the family. Thus, the economic and social impact of these neurodegenerative diseases is quite significant. This has led several researchers worldwide to investigate the pathogenesis mechanism and therapeutic strategies for polyQ diseases. In this study, hypothesis-based and hypothesis-free approaches were used in order to study candidate therapeutic compounds for Machado-Joseph Disease (MJD) using the CMVMJD135 mouse model.

Valproic acid (VPA) is an FDA-approved compound which showed therapeutic benefits in other neurodegenerative diseases, and also in *C.elegans* and *Drosophila* models of MJD, suggesting that it could be a promising compound for treatment of this disorder. Chronic pre-symptomatic VPA treatment (200mg/kg) led to mild improvements in balance and motor coordination in the CMVMJD135 mouse model, not changing the aggregation of mutant ataxin-3 (ATXN3) in affected brain regions. Although not a positive result, this pre-clinical trial still leaves an open window for other VPA dosages to be tested pre-clinically before exclusion of the compound's therapeutic potential.

In an unbiased screening of FDA/EMA-approved small molecules, citalopram was identified as a promising compound for suppression of neurological dysfunction and ATXN3 aggregation in *C.elegans*. Citalopram is an FDA-approved antidepressant, widely prescribed for clinical use, and therefore a good treatment opportunity. Chronic pre-symptomatic citalopram treatment at 8mg/kg led to significant balance and motor coordination improvement, rescued diminished body weight loss, suppressed ATXN3 nuclear inclusions in affected brain regions, reduced neuronal loss and astrogliosis in the CMVMJD135 mouse model. Chronic pre-symptomatic citalopram treatment with a higher dosage (13mg/kg) produced only mild effects at the behavior level and in ATXN3 aggregation phenotypes. This study also led to the characterization of new and relevant pathological features of the CMVMJD135 mouse model.

Chronic citalopram post-symptomatic treatment (at an 8mg/kg dosage) in a group of CMVMJD135 mice presenting higher severity of disease led to an improvement of some the motor symptoms, albeit much less marked than for pre-symptomatic treatment. The mechanisms of action of citalopram in MJD were explored by expression analysis of candidate pathways but they remain to be clarified.

In summary, this work suggests activation of serotonergic signaling as a relevant mechanism for protection against MJD pathogenesis, and suggests citalopram as a promising compound to be tested in human clinical trials in MJD.

## Resumo

---

### **“Ensaio pré-clínico para a Doença de Machado-Joseph: Estratégias terapêuticas baseadas em hipótese e independentes de hipótese”**

As doenças de poliglutaminas (poliQ) são uma família de doenças neurodegenerativas caracterizadas pela expansão de uma repetição do trinucleótido CAG em genes específicos. Esta expansão leva à produção de proteínas patogénicas contendo sequências altamente expandidas de glutaminas. Embora as doenças poliQ sejam doenças raras, este grupo inclui nove doenças progressivas, graves e fatais, que em geral começam na idade adulta e progridem ao longo de 10 a 30 anos, normalmente implicando a assistência ao paciente em tempo integral por um membro da família. Assim, o impacto económico e social destas doenças neurodegenerativas é bastante significativo. Isto tem levado diversos investigadores por todo o mundo a investigar o mecanismo de patogénese e estratégias terapêuticas para doenças poliQ. Neste estudo, foram utilizadas abordagens independentes de hipótese e baseadas em hipótese no estudo de compostos terapêuticos candidatos para a DMJ, utilizando o modelo de ratinho CMVMJD135.

O ácido valpróico (VPA) é um composto aprovado pela FDA, que mostrou benefícios terapêuticos noutras doenças neurodegenerativas, e também em modelos de *C.elegans* e *Drosophila melanogaster* da DMJ, sugerindo que pode ser um composto promissor para o tratamento desta doença. O tratamento crónico pré-sintomático com VPA (200mg/kg) levou a melhorias moderadas no equilíbrio e coordenação motora no modelo de ratinho CMVMJD135, não alterando a agregação da ataxina-3 (ATXN3) mutante em regiões afetadas do cérebro. Embora não seja um resultado muito positivo, este ensaio pré-clínico ainda deixa em aberto a possibilidade de outras dosagens de VPA serem testadas pré-clinicamente antes da exclusão do potencial terapêutico deste composto.

Num rastreio não dirigido de pequenas moléculas aprovadas pela FDA/EMA, o citalopram foi identificado como um composto promissor para a supressão da disfunção neurológica e da agregação de ATXN3 em *C. elegans*. O citalopram é um antidepressivo aprovado pela FDA, amplamente prescrito para uso clínico e, portanto, um bom candidato para tratamento. O tratamento crónico pré-sintomático com citalopram na dose de 8 mg/kg levou a uma melhoria bastante significativa da coordenação motora, resgatou a diminuição de peso corporal, suprimiu as inclusões nucleares de ATXN3 em regiões cerebrais afetadas, reduziu a perda neuronal e a astrogliose no ratinho CMVMJD135. O tratamento crónico pré-sintomático com citalopram numa dose mais elevada (13 mg/kg) produziu apenas efeitos moderados ao nível do fenótipo de comportamento e na agregação da ATXN3. Este

estudo também conduziu à caracterização de novas características patológicas relevantes do modelo de ratinho CMVMJD135.

O tratamento crónico pós-sintomático com citalopram na dose de 8mg/kg num grupo de ratinhos CMVMJD135 que apresentavam maior gravidade da doença levou à melhoria de alguns dos sintomas motores, embora muito menos marcada do que para o tratamento pré-sintomático. Os mecanismos de ação do citalopram na DMJ foram também explorados através da análise da expressão de genes de vias candidatas, precisando ainda de serem mais amplamente esclarecidos.

Em resumo, este trabalho sugere a activação da sinalização serotoninérgica como um mecanismo importante para a protecção contra a patogénese da DMJ, e sugere o citalopram como um composto promissor para ser testado em ensaios clínicos em humanos.

## Table of contents

Agradecimientos.....	v
Abstract.....	ix
Resumo .....	xi
Abbreviations .....	xv
CHAPTER 1.....	1
1. Neurodegenerative diseases .....	3
1.1 Polyglutamine diseases.....	4
1.1.1 The modulatory role of protein context of polyQ diseases .....	6
1.2 Pathogenic mechanisms of neurodegeneration in polyQ diseases.....	7
1.2.1 Misfolding and aggregation of mutant polyQ proteins - proteostasis disruption .....	9
1.2.2. Post-translational modifications of mutant polyQ proteins .....	10
1.2.3 Mitochondrial dysfunction and oxidative stress .....	11
1.2.4 Role of nuclear localization of mutant polyQ proteins .....	12
1.2.5 Transcriptional dysregulation in polyQ diseases .....	13
1.2.6 Defects in Axonal transport.....	15
1.2.7 Apoptosis in polyQ diseases.....	15
1.3 Therapeutic strategies for polyQ diseases.....	17
1.3.1 Hypothesis-based approaches.....	18
1.3.1.1 Gene silencing .....	18
1.3.1.2 Preventing/reducing aggregation.....	19
1.3.1.3 Inducing degradation: UPS and Autophagy .....	20
1.3.1.4 Proteolysis inhibition.....	22
1.3.1.5 Mitochondria stabilization and reduction of oxidative stress.....	23
1.3.1.6 Transcription modulation .....	24
1.3.1.7 Other treatment possibilities.....	26
1.3.2 Hypothesis-free approaches.....	27
1.3.2.1 Aggregation assays.....	31
1.3.2.2 Cell death assays .....	32
1.3.2.3 Clearance/Degradation assays.....	34
1.3.2.4 Transcription dysregulation and other targets.....	35
1.4 Clinical Trials in polyQ diseases .....	36
1.5 Machado-Joseph Disease (MJD) .....	39
1.2.3 Clinical and Neuropathology presentation .....	40

1.2.3	MJD Genetics.....	41
1.5.3	MJD protein: ATXN3 .....	42
1.5.4	Mouse models of MJD .....	43
1.6	Aims of the study .....	45
1.2.3	Thesis planning.....	45
1.7	References.....	47
CHAPTER 2.....		83
Limited effect of chronic valproic acid treatment in a mouse model of Machado-Joseph Disease .....		83
CHAPTER 3.....		109
Serotonergic signaling suppresses ataxin-3 aggregation, improves motor balance and coordination and exerts neuroprotection effects in a mouse model of Machado-Joseph disease .....		109
CHAPTER 4.....		137
Exploring the molecular mechanisms of chronic citalopram treatment in MJD mouse.....		137
Model.....		137
CHAPTER 5.....		151
Assesment of chronic citalopram post-symptomatic treatment in a MJD mouse model of increased severity .....		151
CHAPTER 6.....		171
General discussion and future perspectives .....		171
6.	Introduction.....	173
6.1	Pre-clinical trials design: Strengths and limitations .....	173
6.1.1	Validity of mouse models of disease .....	173
6.1.2	Sample size.....	174
6.1.3	Gender Balance, Randomization and Blindness .....	174
6.1.4	Drug treatment considerations .....	175
6.1.5	Statistical methods.....	177
6.1.6	Reproducibility .....	178
6.1.7	Reporting results.....	179
6.2	Hypothesis-based vs non-hypothesis based therapeutic approaches applied to polyQ diseases .....	179
6.3	Selective Serotonin Reuptake Inhibitors (SSRI's) for neurodegenerative disorders .....	181
6.3.1	Citalopram for MJD: future perspectives.....	181
Appendix I .....		191

## Abbreviations

---

<b>5-HT:</b> Serotonin	<b>CSF:</b> Cerebrospinal fluid
<b>7N:</b> Facial motor nucleus	<b>DAB:</b> 3, 3'-diaminobenzidine
<b>AD:</b> Alzheimer's disease	<b>DN:</b> Dentate nuclei
<b>ALS:</b> Amyotrophic Lateral Sclerosis	<b>DNA:</b> Deoxyribonucleic acid
<b>ANOVA:</b> Analysis of variance	<b>DRLPA:</b> Dentatorubral-pallidolusian atrophy
<b>AR:</b> Androgen receptor	<b>DTT:</b> Dithiothreitol
<b>ARE:</b> Antioxidant response element	<b>DUB:</b> Deubiquitylating enzyme
<b>ARRIVE:</b> Animal Research: Reporting of <i>In Vivo</i> Experiments	<b>EGFP:</b> Enhanced Green Fluorescent Protein
<b>ATXN1:</b> Ataxin-1 protein	<b>EGTA:</b> Ethylene glycol tetracetic acid
<b>ATXN2:</b> Ataxin-2 protein	<b>EMA:</b> European Medicines Agencies
<b>ATXN3:</b> Ataxin-3 protein	<b>ER:</b> Endoplasmic Reticulum
<b>ATXN7:</b> Ataxin-7 protein	<b>ERAD:</b> Endoplasmic reticulum-associated degradation
<b>B2m:</b> Beta-2-Microglobulin	<b>ES:</b> Embryonic stem
<b>BBB:</b> Blood brain barrier	<b>FDA:</b> Food and Drug Administration
<b>BDNF:</b> Brain-derived neurotrophic factor	<b>FELASA:</b> Federation for Laboratory Animal Science Associations
<b>BIM:</b> Bcl-2-like <i>protein</i> 11	<b>FRET:</b> Fluorescence resonance energy transfer
<b>BSA:</b> Bovine Serum Albumin	<b>GABA:</b> Gamma-Aminobutyric acid
<b><i>C. elegans:</i></b> <i>Caenorhabditis elegans</i>	<b>GADD45<math>\alpha</math>:</b> Growth arrest and DNA damage inducible, alpha
<b>CAG:</b> Cytosine-Adenine-Guanine	<b>GFAP:</b> Glial Fibrillary Acidic Protein
<b>CBP:</b> CREB-binding protein	<b>GRP78:</b> Endoplasmic reticulum luminal Ca <sup>(2+)</sup> -binding protein
<b>CBX:</b> Cerebellar cortex	<b>GSK3<math>\beta</math>:</b> Glycogen synthase kinase 3 $\beta$
<b>CGRP1:</b> Calcitonin gene-related peptide $\alpha$	<b>H3:</b> Histone 3
<b>ChAT:</b> Choline Acetyltransferase	<b>HAP1:</b> Huntingtin-associated protein
<b>Cit:</b> Citalopram	<b>HAT:</b> Histone acetyltransferase
<b>CMV:</b> Cytomegalovirus	<b>HD:</b> Huntington's disease
<b>CNS:</b> Central nervous system	<b>HDAC:</b> Histone deacetylase
<b>CoQ10:</b> Coenzyme Q10	
<b>CRE:</b> cyclicAMP responsive element	
<b>CREB:</b> cyclicAMP response element-binding protein	

**HDACi:** Histone Deacetylase inhibitor

*Hdh:* mouse huntingtin gene

**HED:** Human Equivalent Dose

**HO-1:** Heme oxygenase 1

**HPRT:** Hypoxanthine Phosphoribosyl Transferase

**HSF-1:** Heat-shock factor 1

**HSP:** Heat shock protein

**HSR:** Heat shock response

**HTS:** High Throughput Screening

**HTS:** Highthroughput screening

**Htt:** huntingtin

**iRNA:** Interference RNA

**JNK:** c-Jun N-terminal kinases

**KI:** Knock-in

**KO:** Knock-out

**LDH:** Lactate dehydrogenase

**LRT:** Lateral Reticular Nucleus

**LSC:** Lumbar spinal cord

**MJD:** Machado-Joseph disease

**MMP:** Matrix metalloproteinase

**mRNA:** messenger RNA

**mTOR:** Mammalian target of rapamycin

**NaCl:** Sodium chloride

**NIIs:** Neuronal intranuclear inclusions

**NLS:** Nuclear localization signal

**NMDA:** N-methyl D-aspartate

**NQO-1:** NAD(P)H dehydrogenase (quinone 1)

**Nrf2:** NF-E2-related factor-2

**PBS:** Phosphate-Buffered Saline

**PCR:** Polymerase chain reaction

**PD:** Parkinson's disease

**PFA:** Paraformaldehyde

**PMSF:** Phenylmethylsulfonyl fluoride

**PN:** Pontine nuclei

**poliQ:** Poliglutamines

**PolyQ:** Polyglutamine

**Prnp:** Prion protein

**RNA:** Ribonucleic acid

**ROCK:** Rho kinase

**ROS:** Reactive oxygen species

**RtTg:** Reticulotegmental nucleus of the pons

**SAHA:** Suberoylanilide hydroxamic acid

**SB:** sodium butyrate

**SBMA:** Spinal and bulbar muscular atrophy

**SC:** Spinal cord

**SCA:** Spinocerebellar Ataxia

**SD:** Standard Deviation

**SDS:** Sodium dodecyl sulfate

**SEM:** Standard Error Mean

**SERT:** Serotonin Transporter

**SHIRPA:** SmithKline Beecham, Harwell, Imperial College, Royal London Hospital, phenotype assessment

**shRNA:** Short-hairpin RNA

**siRNA:** Small interference RNA

**SMER:** Small-molecule enhancer

**SMIR:** Small-molecule inhibitor

**SN:** Substantia nigra

**SNc:** Substantia nigra pars compacta

**SP1:** Specificity Protein 1

**SPSS:** Statistical Package for the Social Science

**SSRI:** Selective Serotonin Re-uptake Inhibitor



**TBP:** TATA-Binding Protein

**TBS:** Tris-buffered saline

**TF:** Transcriptional factor

**TH:** Thyrosine Hydroxylase

**TSE:** Transmissible spongiform  
encephalopathy

**TUNEL:** Terminal deoxynucleotidyl transferase  
dUTP nick end labeling assay

**Ub:** Ubiquitin

**UIMs:** Ubiquitin-interacting motifs

**UPR:** Unfolded protein response

**UPS:** Ubiquitin-Proteasome system

**VPA:** Valproic acid

**WT:** wild-type

**YAC:** Yeast artificial chromosome



# CHAPTER 1

---

Introduction



## 1. Neurodegenerative diseases

Over the last several decades, life expectancy in industrialized countries has been rising causing a higher prevalence of neurodegenerative diseases. These diseases are hereditary or sporadic age-related disorders that are a growing health problem, exerting a huge emotional burden of both affected patients and society as a whole. They are often associated with atrophy of the affected central and peripheral structures of the nervous system responsible for affecting memory, cognition, abstract thinking, emotional feelings, skilled movements and other abilities<sup>1</sup>. There is no effective and lasting treatment for the majority of these disorders, therefore there is an urgent need for novel therapies to either halt and/or reverse their progression. This group of disorders includes Alzheimer's disease (AD), Parkinson's disease (PD), Huntington's disease (HD), and other polyglutamine-related disorders (PolyQ) including several forms of Spinocerebellar Ataxias (SCA's), Amyotrophic Lateral Sclerosis (ALS) and transmissible spongiform encephalopathies (TSE)<sup>2,3</sup>. This complex group of pathologies are defined by two major hallmarks: i) the presence of altered processing and accumulation of misfolded proteins in inclusions and/or plaques (either sporadic or due to mutations in their respective disease-causing genes) and ii) the presence of neuronal specificity and vulnerability which defines the characteristic clinical symptoms associated with each disease (Figure 1). Since the past years, emerging studies and efforts *in vitro* and *in vivo* have been focusing in understanding the pathogenic mechanisms that lead to neuronal degeneration; however, despite the current knowledge, these molecular pathways are still unclear. Meanwhile, several therapeutic strategies based on the putative mechanisms hypothesis-based and free of hypothesis are being studied, although with no effective treatment so far.

This dissertation will focus on the development of therapeutic strategies for Machado-Joseph disease (MJD) or Spinocerebellar ataxia type 3 (SCA3) using two different FDA-approved compounds and the study of their mechanism of action on the context of this disease.

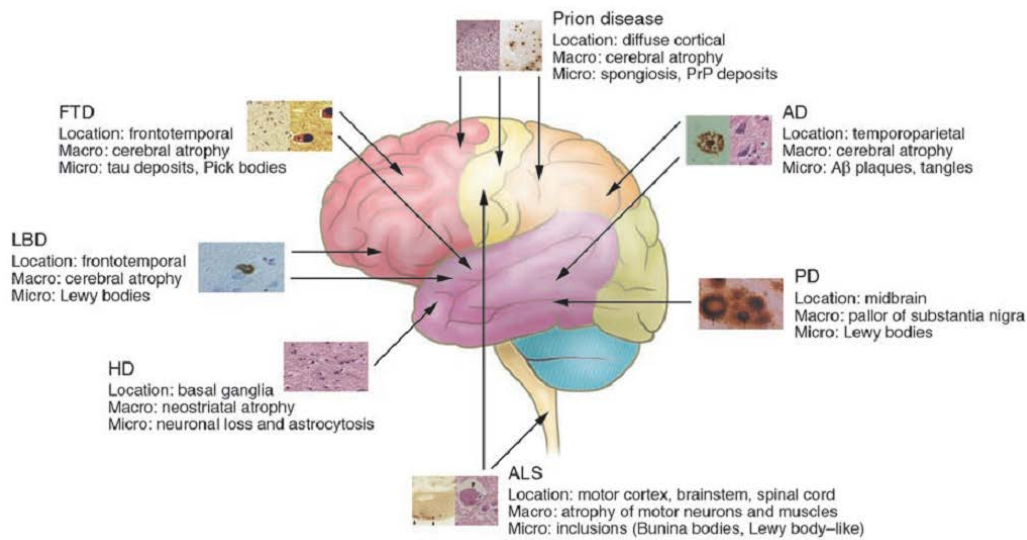


**Figure 1.** Overview of the anatomical location and characteristic macro and microscopic changes of the neurodegenerative diseases with evidence for histopathological aggregated proteins. Adapted from<sup>3</sup>.

### 1.1 Polyglutamine diseases

PolyQ diseases are a large group of inherited neurodegenerative disorders characterized by the pathological expansion of cytosine-adenine-guanine (CAG) repeats in the coding sequences of distinct genes. PolyQ diseases include Machado-Joseph disease (MJD/SCA3)<sup>4</sup>, Huntington's Disease (HD)<sup>5</sup>, spinal and bulbar muscular atrophy (SBMA)<sup>6</sup>, dentatorubral-pallidoluysian atrophy (DRPLA)<sup>7,8</sup>, and other spinocerebellar ataxias (SCA1, 2, 7, and 17)<sup>9-15</sup> (Table 1). The frequency of polyQ diseases averages 1–10 cases per 100,000 people<sup>16</sup>. Of these, HD and SCA3 have the highest prevalence worldwide<sup>17</sup>. All are progressive, ultimately fatal disorders which typically begin in mid-life and progress over 10 to 30 years. PolyQ diseases are dominantly inherited in an autosomal manner, with the exception of SBMA, which is X-linked, and they only manifest when the glutamine expansion exceeds a certain threshold<sup>18</sup>. Above the pathogenic threshold the CAG tracts are unstable across generations, and they can expand or contract, depending partially on the transmitter gender<sup>19</sup>. Frequently, but not always, maternal meioses tend to lead to contractions, while paternal transmissions tend to lead to expansions. This intergenerational instability causes earlier age-at-onset and increased severity of the symptoms in the successive generations, a phenomenon known as anticipation<sup>20-22</sup>. In addition to meiotic instability, tissue-specific mosaicism has been observed in some polyQ diseases resulting in cell populations, carrying different CAG repeat lengths, within or between tissues. CAG repeat instability is behind some features of polyQ disorders and may also contribute to their pathogenic mechanism.

At the molecular level, the disease-causing proteins are ubiquitously expressed in the Central Nervous System (CNS) and the peripheral tissues; however, each polyQ disease is characterized by the

loss of specific neuronal populations resulting in typical patterns of neurodegeneration and clinical symptoms<sup>23</sup>. A common feature of all polyQ disorders is the accumulation of the mutant protein in the cytoplasm and mostly in the nucleus of the neuronal cells, forming neuronal intranuclear inclusions (NIIs), which are found in patient brains and transgenic models of the disorders<sup>24</sup>. These inclusions are a common hallmark of all these diseases, however it is still controversial if they are pathogenic or not<sup>25-28</sup>. Several studies have explored which type of structure formed by the expanded polyQ is responsible for the disease. The theory that a toxic structure of the expanded polyQ causes the disease explains its length-dependence (specific for each polyQ disease) and implies a common pathogenic mechanism in these diseases. Nevertheless, it is not enough to clarify the selective toxicity pattern of these causative proteins, that leads to their different neuropathologic and clinical manifestations<sup>29</sup>.

**Table 1.** PolyQ diseases, causative genes, proteins, brain regions affected and main clinical features. Adapted from<sup>29-32</sup>.

PolyQ Disease	Locus	Protein	Protein localization	CAG repeat size		Brain regions	Clinical Features
				Normal	Pathological		
HD	4p16.3	Huntingtin	Cytoplasmic	6–35	36–12	Striatum and cerebral cortex	Chorea, dystonia, dementia
MJD/SCA3	14q24-q31	Ataxin-3	Nuclear and cytoplasmic	12–40	62–86	Cerebellum, brainstem and spinal cord	Ataxia, spasticity, polyneuropathy, diplopia, dystonia.
SBMA	Xq11-q12	Androgen receptor	Nuclear and cytoplasmic	6–36	38–62	Anterior horn of spinal cord, bulbar neurons and dorsal root ganglia	Weakness, bulbar symptom, fasciculations, tremors, gynecomastia
DRLPA	12p13	Atrophin-1	Cytoplasmic	3–38	49–88	Pallidum, subthalamic, dentate nuclei and red nucleus	Myoclonus epilepsy, ataxia, chorea, dementia.
SCA1	6p23	Ataxin-1	Nuclear	6–39	41–83	Cerebellum and brainstem	Ataxia, bulbar symptom, spasticity, polyneuropathy, cognitive impairment.
SCA2	12q24	Ataxin-2	Nuclear and cytoplasmic	14–32	34–77	Cerebellum, pons, medulla oblongata and spinal cord	Ataxia, slow saccades, ataxia, polyneuropathy, parkinsonism
SCA6	19p13	CACNA1A	Cytoplasmic	4–18	21–30	Cerebellum and brainstem	Ataxia, dysarthria, down-beating nystagmus.
SCA7	3p21-p12	Ataxin-7	Nuclear	7–18	38–200	Cerebellum and brainstem	Ataxia, retinal degeneration, ophthalmoplegia.
SCA17	6q27	TBP	Nuclear	25–43	45–63	Cerebrum, cerebellum and brainstem	Ataxia, dementia, psychosis, seizures, extrapyramidal signs

### 1.1.1 The modulatory role of protein context of polyQ diseases

Since the polyQ-associated proteins share no sequence homology, except the presence of an expanded polyQ tract, it is generally accepted that this is the trigger for the development of neurodegeneration. Several studies suggest that the polyQ tract confers a toxic gain of function to the proteins, associated with protein misfolding and aggregation; however, the identity of the toxic species (i.e., misfolded monomers, soluble oligomers, and/or insoluble fibrils) remains unclear<sup>18,23,33-35</sup>. Furthermore, the protein context also seems to influence the initiation and progression rate of the polyQ diseases. PolyQ-mediated neuropathology is markedly specific, at least at early stages of the diseases, affecting well-defined subsets of cells, despite the ubiquitous expression of the proteins. The context of the polyQ proteins and their modifying or interacting proteins, which may function or be expressed in a cell-specific manner, may determine the selective neuronal loss seen in distinct brain regions in the different polyQ diseases<sup>36</sup>.

The first example of the polyQ tract as a trigger of neurotoxicity *per se*, was the generation of a transgenic mouse expressing an expanded CAG tract into a different genetic context (*HPRT* locus) leading to several common features of the human polyQ diseases. This study proved that CAG polyQ repeats do not need to reside in one of the typical repeat disorder genes to have neurotoxic effects<sup>34</sup>. On the other hand, in the absence of any additional protein context, the simple expression of a polyQ tract is also toxic, as demonstrated in cell culture, *Mus musculus*, *Drosophila melanogaster* and *Caenorhabditis elegans* (*C.elegans*) studies<sup>37-40</sup>. Concerning protein context, one example was the insertion of a polyQ tract of the human HD gene into the mouse huntingtin gene (*Hdh*). Mice with an insertion of 90-111 repeats, which is pathologic in humans, in the *Hdh* gene, revealed no neurological symptoms, with only mild functional alterations reported for 72 and 80 polyQ repeats in other models. A more severe neurological phenotype was only observed in Hdh150Q mice, although its phenotype was not as severe as in humans, even with similar polyQ length and expression levels<sup>41-45</sup>. Therefore, it is notable that a pathological number of glutamines in the human protein is not so deleterious in the context of the mouse protein. Additionally, the same CAG repeat size in human patients causes different ages at onset for different polyQ diseases, showing that the protein context plays an important role in these diseases<sup>46</sup>. Another interesting example of toxicity modulation determined by protein context is in the SCA1 study, where Emamian and colleagues replaced one single amino acid (aa) in ataxin-1 (ATXN1) out of its polyQ tract and observed a considerable reduction of the ability of mutant ATXN1 to cause disease *in vivo*<sup>47</sup>.



It is unquestionable that protein context plays an important role in pathogenesis, and despite the existence of common mechanism among polyQ diseases, the striking differences in clinical and pathological features also suggest disease-specific effects.

## **1.2 Pathogenic mechanisms of neurodegeneration in polyQ diseases**

In the last years, a growing number of studies has emerged with possible pathogenic mechanisms of polyQ diseases, and although the exact mechanisms are still unclear, several hypothesis and relevant clues are contributing to new insights in these diseases. PolyQ diseases most likely share similar pathogenic mechanisms and main characteristics, making them variations of a common polyQ neurological disorder. First, the onset of symptoms occurs in adulthood and progresses for decades. This suggest that there is something changing with aging that allows the toxic gain of function that is associated with polyQ expansion polypeptides to reveal itself. The accumulation of mutant proteins inside neurons, causing their dysfunction and eventually death, is another unifying feature of these disorders. Figure 2 summarizes the pathogenic mechanisms that have been suggested for polyQ diseases and the possible therapeutic strategies directed at these mechanisms (discussed in the next section).

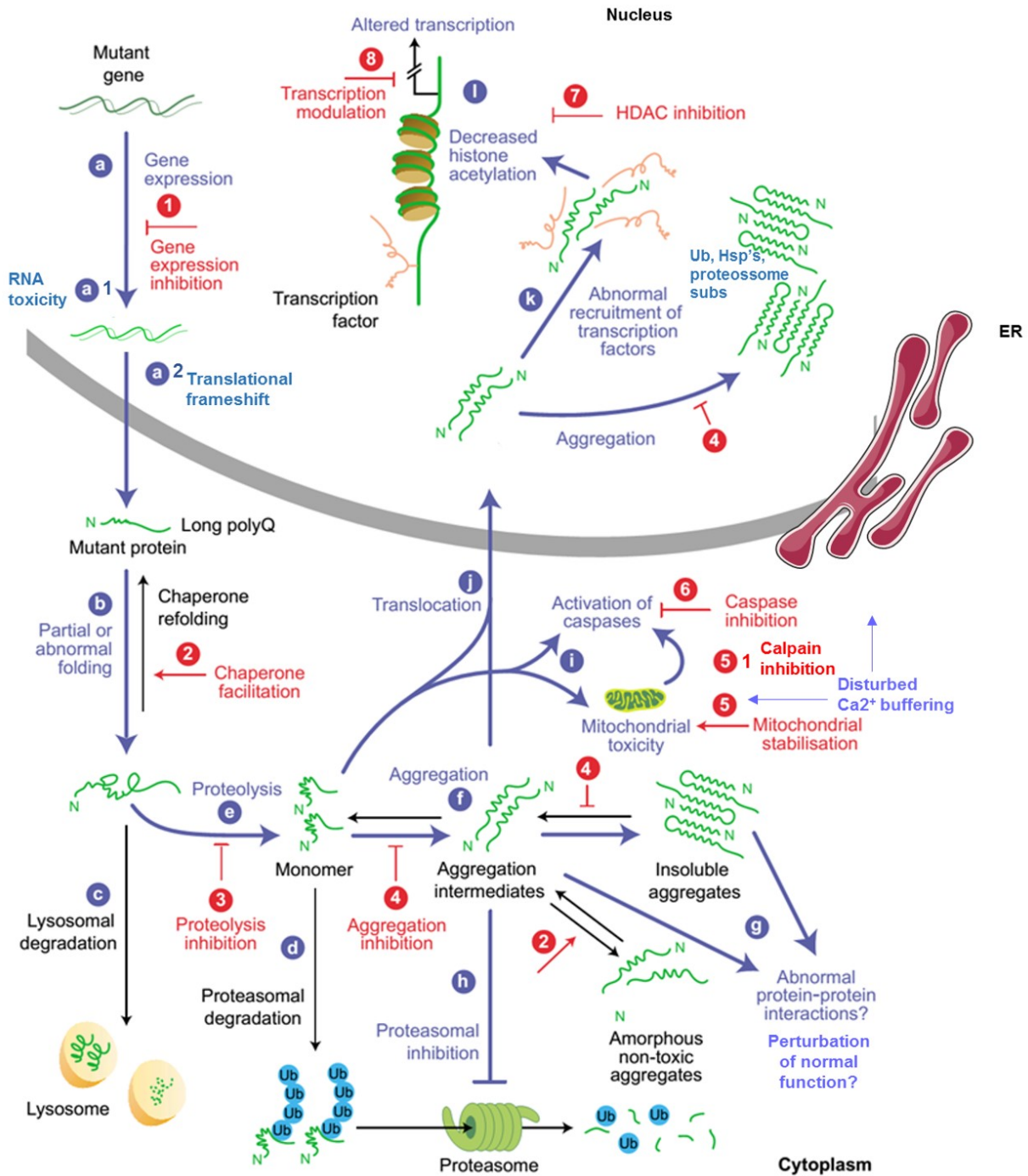


**Figure 2.** PolyQ pathogenesis and common possible therapeutic approaches. The disease proteins could be located in cytoplasm and/or in the nucleus, although, as a simplification, here they are shown originating in the cytoplasm. Pathogenic pathways (blue arrows); possible therapeutic approaches (red arrows). The pathogenic process generally starts with the synthesis of a protein with an expanded polyQ tract (a). This polyQ tract changes the native protein conformation dynamics, modulated by the presence of molecular chaperones (b). A fraction of abnormally folded proteins is addressed for lysosomal-dependent proteolysis (c) and the remaining fraction of the abnormal proteins is ubiquitinated (Ub) and subjected to proteasome degradation (d). Cleavage of the abnormal folded protein produces an N-terminal fragment that favors the aggregation process by a seeding effect (e). The mutant protein (whole or cleaved) could shift from a monomeric

**(Figure 2.) (cont.)** random coil or  $\beta$ -sheet into oligomeric  $\beta$ -sheets and ultimately into insoluble aggregates (amyloid fibrils) (f). These species could represent a protective mechanism to reduce the toxicity of the intermediate aggregates, or might contribute to pathology through abnormal interactions with cellular proteins (g). The intermediate aggregates inhibit proteasome processing (h). On the other hand, the monomers and oligomers directly activate caspases or disrupt mitochondrial and ER functions, leading to indirect activation of caspases (i). Proto-aggregates translocate into the nucleus (j) and recruit specific nuclear factors, co-activators and co-repressors (k) inhibiting their normal activities and resulting in transcriptional dysregulation (l). This pathogenic mechanisms suggests several potential therapeutic approaches, including: (1) inhibition of mutant protein expression at the level of transcription and translation; (2) improving the chaperone function; (3) proteolysis inhibition; (4) aggregation inhibition; (5) mitochondrial stabilization and protection; (6) caspase inhibition; (7) inhibition of histone deacetylation activity and (8) transcriptional modulation. Adapted from <sup>48</sup>.

### **1.2.1 Misfolding and aggregation of mutant polyQ proteins - proteostasis disruption**

It is hypothesized that polyQ diseases are the consequence of a toxic gain of function that occurs at the protein level. The role of aggregation in the pathogenesis of these diseases is still controversial. It is not entirely understood whether the toxicity of the expanded polyQ proteins results from the presence of visible aggregates or from smaller intermediary species during aggregation process and the question remains: are the inclusions toxic or protective to the cells?

NiIs were first described in an animal model of HD<sup>49</sup> and the major theory was that they are pathogenic as they may contain and/or sequester several proteins such as ubiquitin (Ub), chaperones, proteasome subunits as well as transcription activators and/or co-activators<sup>50-53</sup> interfering with their normal function<sup>54-56</sup> and representing the end products of the upstream toxic event. For example, in the case of SBMA, Apostolinas and colleagues described that neuronal death was associated with NiIs specifically restricted to the affected motor neurons of the spinal cord and brainstem<sup>57</sup>. Later, Poletti and colleagues described that in fact, motor neuronal cell death is not correlated with aggregate formation<sup>58</sup>. Additionally, several other studies have suggested that the NiIs could have a protective role showing the inconsistency between inclusion formation and cell death<sup>28,59</sup>. Indeed, in several polyQ diseases such as HD, SCA7 and SCA17, NiIs were detected in spared regions<sup>26,27,60,61</sup>, whereas in SCA1, SCA2, SCA3 and DRPLA, NiIs were absent in Purkinje cells, which are key targets of neurodegeneration in some of these polyQ diseases<sup>26,62</sup>. Even in cellular and animal model studies, it was demonstrated the presence of cell death when fewer or no NiIs was observed<sup>28,63-65</sup>. For instance, in rat primary striatal neurons, the NiIs were not a pre-requisite for cell death but mutant huntingtin (htt) had to be present in the nucleus to induce apoptosis<sup>64</sup>. In case of MJD, two transgenic mouse model were described showing a neurological phenotype with few and smaller NiIs which appeared later in

life<sup>66</sup> or even no inclusions<sup>67</sup>. On the contrary, a knock-in MJD mouse model was recently described with prominent aggregate pathology without evident neurological phenotype<sup>68</sup>.

Despite this scientific controversy in the field concerning NIs, it is undeniable that protein aggregates may be harmful for neurons by affecting their proteostasis. The cellular homeostasis disturbance hypothesis suggests that the sequestration of chaperones and proteasome subunits into polyQ aggregates could result in an increased protein misfolding and reduced clearance of other crucial cellular proteins, leading to a homeostatic imbalance<sup>69-71</sup>. This suggests the involvement of the ubiquitin-proteasome system (UPS) degradation pathway in these diseases, and also the activation of the heat shock response (HSR) machinery in order to either refold or degrade the mutant polyQ proteins. In fact, heat shock proteins (HSPs) play an important role in the cell stress response induced by the presence of polyQ expansion proteins. These proteins are able to move freely and only transiently associate with the aggregates<sup>72</sup>. Their overexpression in cellular and animal models of polyQ diseases has been demonstrated to modulate polyQ toxicity and/or disease manifestation<sup>73-75</sup>. Moreover, the proteasome appears to be permanently recruited into polyQ aggregates and it is functionally impaired by aggregated polyQ proteins, interfering with the degradation of other proteins<sup>76,77</sup>. Proteasome inhibition might also increase the intracellular load of misfolded, oxidized, or otherwise damaged proteins, leading to neuronal toxicity. Several reports have shown that reducing or inhibiting proteasomal activity is sufficient to induce neuronal death<sup>78-80</sup>.

A recent work also proposed that aggregate-associated chaperone competition leads to both gain- and loss-of-function phenotypes since chaperones become functionally depleted from multiple clients, leading to the decline of multiple cellular processes<sup>81</sup>. Altogether, these events may lead to a stressful cellular *milieu* that will finally culminate in neuronal dysfunction and eventually neuronal death.

### **1.2.2. Post-translational modifications of mutant polyQ proteins**

The pathogenic mechanism of several polyQ disorders including HD, SBMA and SCA3, appears linked to proteolytic cleavage resulting in production of toxic polyQ-containing fragments<sup>82-86</sup>, which may be required for the beginning of the aggregation process and for neuronal harmful effects. It is described that these fragments may also more easily translocate into the nucleus, where they can exert toxic effects<sup>87-89</sup>. Several studies have shown *in vitro* cleavage of several polyQ proteins, especially by caspases and calpains. Caspase-mediated cleavage sites were identified or predicted in htt, atrophin-1, ataxin-3 (ATXN3) and androgen receptor (AR)<sup>90-93</sup>. As a consequence, the resulting fragments could (i)

have an enhanced toxic effect<sup>37,85,94</sup>, (ii) more easily enter the nucleus<sup>95,96</sup> and/or (iii) more rapidly aggregate<sup>95,97</sup>. In fact, truncated proteins with polyQ expansions appear to be more prone than full-length proteins to form inclusions and/or cause cell death by apoptosis<sup>54,85,98,99</sup>. However, in a *C.elegans* model of MJD both full-length and truncated forms of ATXN3, with different Q-lengths, results in a consistent pattern of neuronal cell-type-specific aggregation, being the truncated protein more aggregation-prone<sup>100</sup>. Extensive research supports a model in which proteolysis of polyQ expanded proteins, formation of protein aggregates and subsequent sequestration of crucial cell proteins (including normal polyQ proteins) is required for disease onset. However, proteolytic cleavage may not be an essential step in the onset of pathogenesis of all polyQ diseases, rather in accelerating disease progression.

In addition to proteolytic cleavage, other post-translational modifications of mutant polyQ proteins, such as phosphorylation and sumoylation, have been shown to play a role in pathogenesis of polyQ diseases. In case of MJD, for instance, ATXN3 has been described to undergo phosphorylation at S256 by glycogen synthase kinase 3 $\beta$  (GSK3 $\beta$ ) causing a reduction in mutant ATXN3 aggregation *in vitro*<sup>101</sup>. CK2-dependent phosphorylation of ATXN3 at S236 and S340/S352 decreased the presence of NIs and controlled the nuclear translocation of ATXN3 providing a reasonable therapeutic strategy for MJD<sup>102</sup>. In contrast, phosphorylation of mutant ATXN1 at S776 is related with the increased formation of aggregates and neurodegeneration<sup>103</sup>. Collected, these observations suggest that post-translational modifications play an important role in the expression and/or progression of the disease, supporting the idea that the protein context in which the polyQ expansion is located influences the pathology of these diseases.

### 1.2.3 Mitochondrial dysfunction and oxidative stress

Neurons have very high energy demands and are very dependent on oxidative energy metabolism. This points to the impairment of mitochondrial function and impaired energy metabolism as key events of neurodegenerative diseases<sup>104,105</sup>, including polyQ diseases, leading to cell death. Most insights were gained in the field of HD<sup>106,107</sup> but several studies also highlight the role of mitochondria in the pathology of SCA's<sup>108-110</sup>. In polyQ diseases, the process of mitochondrial dysfunction is accompanied by impaired respiration, stress induced mitochondrial depolarization, increased reactive oxygen species (ROS) production leading to oxidative damage, and abnormal energy metabolism<sup>111,112</sup>. A mild or gradual energy disturbance may also lead to the release of pro-apoptotic factors, mainly cytochrome C from the mitochondria, and an apoptotic cascade being initiated. For instance, in SCA3 and SCA7 it was shown that the mRNA and protein levels of Bcl-xL were down-regulated in cerebellar

neurons when polyQ expanded ATXN3 and ataxin-7 (ATXN7), respectively, were overexpressed, causing activation of caspase-3 and caspase-9, two main caspases involved in mitochondrial induced apoptosis<sup>108,113</sup>. Then, a direct interaction was shown between ATXN3 and Bcl-xL suggesting that mutant ATXN3 promotes the interaction between Bcl-xL and Bax, activating the mitochondrial apoptotic pathway<sup>108</sup>.

Excessive Ca<sup>2+</sup> accumulation has also damaging effects, leading to the oxidative damage and activating an apoptotic cascade. In addition, but also important, non-excitabile cells, such as astrocytes and microglia, are likewise strongly dependent on the intracellular Ca<sup>2+</sup> concentration and signaling to maintain their normal function<sup>114</sup>.

Besides changes in mitochondrial bioenergetics and transcription of important proteins associated with mitochondrial function and cell death, modifications in mitochondria shape and motility have been observed in HD models<sup>115</sup>. Both retrograde and anterograde mitochondrial transport along axons were described to be impaired by mutant htt in cultured cortical neurons of mouse and rat models<sup>116,117</sup>. Therefore, a large body of evidence suggested that mitochondrial impairment, including fission/fusion dynamics, is also a common feature in the pathogenesis of polyQ diseases.

#### **1.2.4 Role of nuclear localization of mutant polyQ proteins**

The presence of polyQ proteins in the nucleus of cells has been shown to play an important role in the disease pathogenesis, disrupting nuclear organization and function<sup>118</sup> and/or affecting gene expression<sup>23,119,120</sup>. Yang and colleagues, demonstrated that in mammalian cells, polyQ aggregates were highly toxic when localized in the nucleus and less so in the cytoplasm<sup>121</sup>. Several studies showed that the nuclear accumulation of mutant proteins and inclusions is predominant in HD, SCA1, 3 and 7, DRPLA and SBMA patients<sup>22</sup>; however, inclusions in the cytoplasm, namely in axons, have also been found in affected brain regions of SCA2, SCA3 and HD patients<sup>122-125</sup>. In disease models, the presence of polyQ aggregates in the nucleus seems to be associated with more severe phenotypes. In the case of MJD, studies in mice showed that mutant ATXN3 nuclear localization is required for the disease manifestation, whereas the artificially induced export of ATXN3 out of the nucleus prevents the manifestation of the phenotype<sup>126</sup>.

### 1.2.5 Transcriptional dysregulation in polyQ diseases

Extensive evidence has reinforced the notion that major alterations in gene expression occur in polyQ diseases<sup>127</sup>. Interestingly, both htt, atrophin-1, ATXN1, ATXN3 and ATXN7 are capable of modulating transcription by related or unrelated mechanisms<sup>52,53,128-131</sup>. Three main mechanisms have been suggested to cause the polyQ-dependent transcription regulation/modulation: (i) the recruitment of transcription-related factors (TFs) in the NIIIs, (ii) the direct inhibition of acetyltransferase activity of transcription modulators and/or (iii) the direct repression of the transcriptional machinery.

The mutant polyQ proteins interact with several cellular proteins and may sequester them into cytoplasmic or nuclear aggregates contributing to cellular dysfunction<sup>74,132</sup>. In addition to proteasome subunits and molecular chaperones, poly-Q aggregates co-localize with crucial cellular components such as the TFs cyclic AMP response element-binding protein (CREB), CREB-binding Protein (CBP), TATA-Binding Protein (TBP), Specificity Protein 1 (SP1) and TAFII130 (which encodes a TBP-Associated Factor). The sequestration of TFs together with other relevant cellular components would be expected to promote profound effects on cellular homeostasis. Overexpression of some of these TFs was shown to overcome polyQ toxicity, both *in vitro* in cellular models of MJD, SBMA and HD<sup>53,133</sup>, as well as *in vivo* of a *Drosophila* polyQ model<sup>134</sup>. Additionally, the transcriptional activator CREB, along with its activator CBP, has been strongly associated in expanded polyQ-induced gene repression<sup>51</sup>. CBP is an essential mediator of survival signals in neurons. It has a histone acetyltransferase (HAT) activity, which is important for allowing TFs to access to DNA. In the presence of mutant htt or atrophin-1, CBP is sequestered into aggregates<sup>52</sup>. The recruitment of CBP into NIIIs or its interaction with mutant polyQ proteins are also described in SBMA, SCA3, and SCA7<sup>128,133,135</sup>. In SCA1, CBP is not irreversibly sequestered into NIIIs but it is quickly exchanged. Although CBP has a short residence time within the NIIIs, this may be enough to disrupt its normal function in sustaining cellular homeostasis<sup>136</sup>. It seems that the disruption of CREB/CBP-mediated gene expression may be a common mechanism of neurodegeneration in polyQ diseases. Contradicting this model, it was described that in the R6/2 HD mouse model, CREB-mediated transcription was increased<sup>137</sup> and CBP was not depleted in knock-in HD mouse brains<sup>138</sup>. TBP was also found to co-localize with htt, ataxin-2 (ATXN2), ATXN3, and atrophin-1 inclusions in human brains<sup>139-141</sup>, but like for CBP, the levels of TBP were not reduced in HD mouse model<sup>138</sup>.

SP1 contains a glutamine-rich activation domain, which is responsible for regulation of the transcriptional machinery of transcription factor II D (TFIID), a protein complex composed of TBP and multiple TBP-associated factors (TAFIIs), including TAFII130<sup>142</sup>. The role of SP1 in polyQ toxicity is not

completely clear. TAFII30 itself also interacts with mutant htt and it was shown to co-localize with atrophin-1 and ATXN3<sup>53,143</sup>. Another TAF, TAFII130, was described to be sequestered in ATXN7 NIIIs<sup>144</sup>. Alternatively, polyQ proteins might exert their toxic effect through direct inhibition of HATs or transcription modulators, causing a reduction in histone acetylation and consequently, gene transcription activation. Two TFs that regulate gene expression through their acetylase activity are CBP and PCAF<sup>145</sup>. A mutant truncated fragment of htt has been shown to inhibit transcription, through the repression of the HAT activity of CBP/p300/PCAF transcriptional co-activator<sup>146</sup>. Wild-type (WT) ATXN3 has been described to be a double co-repressor of transcription by the interaction with CBP, p300 and PCAF, inhibiting CREB-dependent gene transcription through its C-terminal and through its N-terminal interaction with histones<sup>128</sup>.

Relevant studies from Barco and colleagues concluded that the combination of histone acetylation and gene expression screenings demonstrates that histone deacetylation and transcriptional dysregulation are two early, largely independent, manifestations of polyQ diseases, and they propose that additional epigenetic marks or mechanisms are required to explain the full range of transcriptional alterations associated with these disorders<sup>147</sup>. On the other hand, microarray studies in polyQ diseases are crucial to understand the gene expression changes along the disease progression. For instance, in R6/2 HD mice a considerable number of genes have an altered pattern of expression but this pattern shows little sign of regional specificity<sup>148</sup>. Comparison of gene expression profiles of HD and SBMA mouse models revealed a considerable overlap in the genes showing altered gene expression. Such context-independent genes suggest the existence of pathways that are common among the different polyQ diseases<sup>149</sup>. Recently, several efforts are being performed in transcriptome profiling, providing valuable information regarding possible causes and consequences of the onset and progression of these diseases<sup>150-152</sup>.

Besides the analysis of the indirect consequences of the polyQ expression in cell or animal models, the connection of mutant polyQ proteins to the direct repression of the transcriptional machinery as cause of neurodegeneration remains to be fully understood. However, either by sequestration of TFs or by aberrant interactions with other transcription regulators, the transcriptional dysregulation seems to be a common hallmark of the polyQ diseases, which highlights the importance of studying this phenomenon as a potential therapeutic target.



### 1.2.6 Defects in Axonal transport

Mutant polyQ proteins can also affect cytoplasmic processes, such as axonal transport, which have a crucial role in building and maintaining the functional architecture of neurons. The precise mechanism is not completely clear but it has been suggested that some of the disease-causing proteins might have normal functions in the axonal transport system and cause axonal blockages when mutated, and/or that polyQ aggregates might physically block transport within the narrow axonal processes<sup>153-158</sup>.

It was described that htt is both anterogradely and retrogradely transported in rat sciatic nerve axons<sup>159</sup> and studies with *Drosophila* overexpressing mutant htt and ATXN3 constructs, showed an axonal accumulation of vesicles<sup>154,160</sup> that was comparable to that seen in axonal transport defects in kinesin- and dynein- mutants<sup>161</sup>. A few years ago, Li and colleagues suggested that htt interacted with motor proteins (namely a subunit of dynactin) via Huntingtin-associated protein 1 (HAP1)<sup>162</sup>. Studies in transgenic HD mouse models and human patient brains revealed evidence for axonal transport dysfunction in HD pathogenesis<sup>157,163-166</sup>. Additionally, a few studies described that HD dystrophic striatal and corticostriatal neurites exhibited characteristics of blocked axons, specifically, accumulation of vesicles and organelles in swollen axonal projections and termini associated with htt aggregates<sup>167,168</sup>. The presence of htt accumulations has also been demonstrated in axons of striatal projection neurons in R6/2 and knock-in mouse models of HD and in human patient brains<sup>165</sup>. ATXN3 was also shown to interact with dynein intermediate chain 2 (required for agosome formation and transport of misfolded proteins)<sup>169</sup> and to be a microtubule associated protein<sup>170</sup>, enhancing the idea that ATXN3 plays a critical role in the cytoskeleton; this was later proven to be true also in neurons<sup>171</sup>. However, evidence is still lacking for defects in axonal transport in MJD.

### 1.2.7 Apoptosis in polyQ diseases

The mechanism of cell death in polyQ diseases is likely very complex, and it seems to appear late in the polyQ disease process. Much of the attention in the cell death field has been focused in the major cell death pathway - apoptosis, which is often used as a synonym of programmed cell death. Additional programmed cell death pathways studies are gradually changing this notion. Activation of cell death pathways, even without resulting in cell death could be harmful to the neurons. The persistent activation of the cell death by the interaction of mutant polyQ proteins with their regulators or of stress responses, such as UPR and/or autophagy, together with the presence of mitochondrial abnormalities, transcriptional dysregulation, proteasome impairment and defects in axonal transport

may potentiate apoptosis phenomena in polyQ diseases. Several proteins usually involved in apoptosis are sequestered, redistributed or activated by expanded polyQ proteins. Activated caspases, which are a usual feature of apoptotic cell death<sup>108,172-175</sup>, can also be recruited in inclusions<sup>176</sup>. However, the morphological features of apoptosis do not always seem to accompany the neuronal cell death in polyQ disease models. Part of the struggle in resolving this issue lies in the fact that many model systems display polyQ toxicity on a time scale of days, whereas the human disease develops over decades.

In cellular models of polyQ toxicity, there is a divergent and contradictory amount of results concerning the relevance of apoptosis. This is given by the fact that several studies use different polyQ substrates to model toxicity in many types of cells<sup>64,94,99,176-182</sup>, and different cell types vary in the specific death modulators (e.g. Bcl-2 family members) and caspases (both initiators and effectors) that they express. Some researchers have described that polyQ toxicity is mediated, at least in part, by activated caspases<sup>64,181</sup>, whereas others have demonstrated that caspase inhibitors do not block death but only modify aggregate formation or the time course of death<sup>180,182</sup>. Some studies have shown morphologic features consistent with apoptosis<sup>37,64</sup>, whereas others shown cell death that contrasts with usual apoptosis<sup>178,182</sup>. Overall, these results seem to suggest that expanded polyQ proteins can cause neuronal cell death through a caspase-dependent mechanism that exhibits some features of apoptosis.

In animal models, the studies also show some divergence to answer these questions. In polyQ *Drosophila* models, the anti-apoptotic P35 gene has a slight or no ability to block degeneration<sup>183,184</sup>, showing that cell death mediated by expanded polyQ in flies is not only apoptotic. On the other hand, neuronal cell death in a *C. elegans* model of HD could comprise apoptotic pathways, since death required *Ced3* caspase activity<sup>185</sup>. Studies in mouse models also present some variability due to transgenic approach and/or transgene promoter used in each study. An HD mouse model expressing full length htt showed striatal degeneration along with positive TUNEL staining suggestive of apoptosis, however with no morphological changes typical of this type of cell death<sup>186</sup>. Another example is the YAC mouse model expressing full length htt which showed degenerative changes in the striatum consistent with apoptosis by electron microscopic approach<sup>187</sup>. However, the selective degeneration of striatal neurons was seen in transgenic mice expressing full length, but not in truncated htt. In case of MJD there is also some disagreement concerning the presence of cell death between different cells lines and models. Some studies proposed that the expanded ATXN3 induces apoptosis in cultured cells<sup>37</sup>, while *in vivo* some models presented apoptosis<sup>179</sup> and others did not<sup>67</sup>. Despite the controversy between different models in this field, it is undoubtedly important to study and identify which of the many molecules are implicated in apoptosis are contributing to neuronal dysfunction and cell death in polyQ

diseases. Furthermore, it is possible that other non-apoptotic cell death coexist with apoptosis in the brains of affected patients<sup>188-190</sup>.

### 1.3 Therapeutic strategies for polyQ diseases

Despite great progress in elucidating the pathomechanisms underlying polyQ diseases, an effective treatment is still lacking. The current strategies towards development of therapies for these diseases could be divided in hypothesis-based and hypothesis-free approaches. The most common are those based on hypothetic pathological mechanisms which can also be divided in two categories: i) those targeting the expression, processing or conformation of the polyQ protein and ii) those preventing the toxic effects of the polyQ protein, such as mitochondrial dysfunction and oxidative stress, transcriptional dysregulation, UPS impairment, excitotoxicity, or activation of apoptotic pathways<sup>191</sup>. On the other hand, hypothesis-free approaches are gaining relevance, mostly through the analysis of large libraries of compounds with high throughput methodologies. This approach often reveals interesting disease-modifying agents, contributing not only to provide new avenues for defining the pathomechanisms of the disease, but also for a direct pathway to therapy.

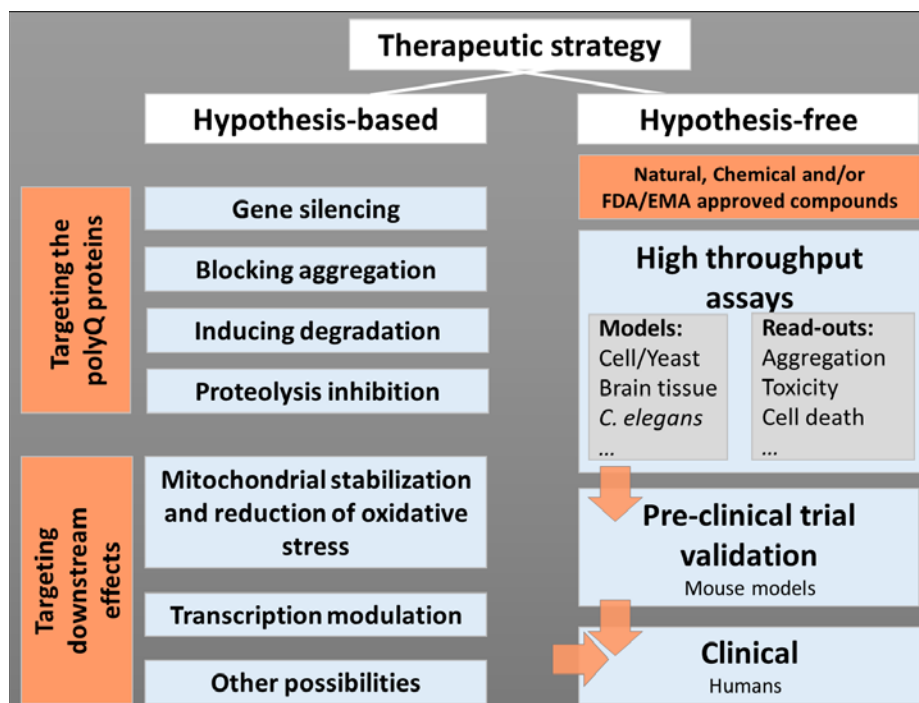


**Figure 3.** Therapeutic strategy workflow for polyQ diseases.

### 1.3.1 Hypothesis-based approaches

#### 1.3.1.1 Gene silencing

The most straightforward therapeutic approach for polyQ diseases may be decreasing the expression levels of the mutant protein and consequently prevent the downstream deleterious events. Down-regulation of the expression of the abnormal gene(s) was shown to be an effective strategy to halt disease progression in conditional tetracycline-regulated mouse and rat models of HD<sup>192,193</sup>, MJD<sup>194</sup> and in a doxycycline-regulated mouse model of SCA1<sup>195</sup>. Upon shutting down the mutant polyQ protein expression in these models, a reduction in the amount of NIIs as well as behavioral phenotype improvement was observed. Another example was shown in a pan-neuronal conditional *Drosophila* model of SCA7 in which the expression of truncated protein was interrupted leading to an increase in lifespan<sup>196</sup>. Once this proof-of-concept was obtained, several techniques targeting polyQ expression started being explored including small interference RNA (siRNA) and short-hairpin RNA (shRNA). The first description of interference RNA (iRNA) approaches for polyQ diseases, was made in an *in vitro* cell-based model, in which the inhibition of expression of a truncated version of the human AR through double-stranded RNA strikingly reduced polyQ-mediated cell death, caspase-3 activity and protein aggregation<sup>197</sup>. The applicability of iRNA *in vivo* was then validated in a SCA1 mouse model using shRNA for human ATXN1, which led to an improvement in motor coordination, reduction in NIIs and restored cerebellar morphology<sup>198</sup>. Later, microRNAs suppressing the expression of mRNA for ATXN1 and subsequently reducing the protein levels were shown to be effective in human cells<sup>199</sup>. Recently, the microRNA miR-25 was shown to reduce both WT and polyQ-expanded mutant ATXN3 protein levels, therefore increasing cell viability, decreasing early apoptosis, and down-regulating the accumulation of mutant ATXN3 protein aggregates in MJD model cells<sup>200</sup>. Extensive evidence for the efficacy of iRNA therapy was also presented in models of HD using different viral vector to deliver shRNA silencing the mutant htt. These treatments showed positive effects in behavior features, such as motor performance or clasping, and NIIs<sup>201–203</sup>. In case of MJD, several efforts were developed in the iRNA field by Pereira de Almeida and colleagues with successful results. Using lentiviral-mediated allele-specific silencing of the mutant ATXN3 the authors were able to prevent the development of the motor and neuropathological phenotype of rat and mouse models of MJD<sup>204,205</sup>. However, the model systems used did not closely mirror the human disease given the regionally limited expression of the transgenes and the treatment efficacy was only assessed in a short period. Another study with iRNA in MJD in a different model of the disease showed that despite efficacy, safety and lifelong suppression of ATXN3 expression in the deep

nuclei of the cerebellum, the motor impairment was not ameliorated in treated MJD mice during the pre-clinical trial and the lifespan was not prolonged<sup>206</sup>. This is likely due to the more widespread pathology presented by this model which expresses ATXN3 under its endogenous promoter and its native genomic context. However, there is still an open window to use other nucleotide-based gene silencing molecules more broadly to the brain and delivered at early stages of disease.

iRNA therapeutic application has progressed remarkably and reveals to be very promising due to efficient and specific gene silencing. However, in order to be delivered in the CNS, several challenges still need to be overcome to take full advantages of this potential technology.

### 1.3.1.2 Preventing/reducing aggregation

One major question still remains in polyQ diseases: are the inclusions as toxic as the monomeric species of the polyQ proteins? Although the question is continuously debated, it is more widely accepted that the polyQ proteins are toxic due to their acquired misfolded conformations when compared to their WT counterparts. In normal conditions, cells own an extremely well-organized protein quality control machinery to regulate proteostasis and to guarantee that misfolded proteins do not accumulate<sup>207,208</sup>. As a pathological hallmark of polyQ diseases, aggregation was one of the first therapeutic targets in the polyQ field.

Chaperones or HSPs are crucial proteins which maintain the normal folding and/or the assembly of other macromolecular structures and a defect in their normal function may *per se* have pathogenic implications<sup>209-211</sup>. A growing number of studies along the years reinforced that overexpression of molecular HSPs in cellular and animal models of polyQ diseases have a protective effect, decreasing polyQ aggregation and/or neurodegeneration. In 1999, Warrick and colleagues showed that overexpression of HSP70 was able to suppress polyQ toxicity even with no detectable effect on aggregation, in a *Drosophila* model<sup>212</sup>. In cell models of SBMA, the overexpression of HSP70 and HSP40 suppressed aggregate formation and apoptosis<sup>213</sup> and enhanced the degradation of expanded AR<sup>214</sup>. The protective role of HSP70 overexpression was also observed in SCA1 cell, fly and mouse models<sup>73,215</sup>. In the case of MJD, the overexpression of two HSP40s, DNAJ-1 and DNAJ-2, was able to suppress the aggregation of mutant ATXN3<sup>71</sup>. The HSR (including the HSP production) can also be induced through overexpression of heat shock transcription factors, which has also been described to reduce aggregation and cell death in polyQ disease cell models<sup>216-218</sup>.

Beyond transgenic overexpression of HSPs, the HSR and HSPs expression can also be induced by a number of promising small chemical compounds. Trehalose, a chemical chaperone, is able to

stabilize polyQ proteins in their native conformation and also activates autophagy. This compound was shown to be efficient in HD cellular and animal models<sup>219</sup> and recently in a SCA17 mouse model<sup>220</sup>. Geranylgeranylacetone, a molecule capable of enhancing the expression of HSP70, HSP90, and HSP105 through induction of heat-shock factor 1 (HSF-1) activity, proved to inhibit nuclear accumulation of mutant AR, ameliorate motor behavior and increase survival in a SBMA mouse model<sup>221</sup>. Another small molecule, with the ability to increase HSP70, YM-1, was recently described to increase degradation of mutant AR in cell culture and to rescue toxicity in a SBMA *Drosophila* model<sup>222</sup>. Extensive evidence supports the use of two analog compounds, 17-AAG and 17-DMAG, also capable of up-regulating HSP40, 70 and 90, dependently on HSF-1 induction. They have been described to have promising effects on aggregation load, toxicity and motor behavior in several cell, *Drosophila*, *C. elegans* and mouse models of polyQ diseases<sup>100,218,221,223–228</sup>. Recently, the compound arimoclolol, a coinducer of HSPs, has been shown to ameliorate the symptoms in SBMA and ALS mouse models<sup>229–231</sup>. Congo red, minocycline and chlorpromazine are valuable aggregation inhibitors *in vitro* and were tested in mouse models of HD, however, with mild or absent improvement in phenotype<sup>232–234</sup>. Cystamine may also reduce polyQ aggregation and survival by transglutaminase (TG) inhibition; TG is thought to crosslink expanded polyQ proteins and facilitate their aggregation. This compound improved survival in HD mice by decreasing htt aggregation<sup>235</sup>.

Another strategy in polyQ aggregation inhibition is centered on the use of small antibody fragments expressed intracellularly called intrabodies, which are a biotechnological tool to disturb, modulate or define the functions of a wide range of target antigens at the post-translational level<sup>236</sup>. In the case of htt, intrabodies were described to reduce neuropil aggregation and ameliorate neurological phenotypes in HD mouse models<sup>237,238</sup>. Results for ATXN3 have not been so promising, since only one aggregate-exacerbating intrabody against fibrillar polyQ proteins was tested, causing and increasing cytotoxicity and cell death when combined with ATXN3<sup>239</sup>.

### **1.3.1.3 Inducing degradation: UPS and Autophagy**

Increasing the clearance of the polyQ proteins to avoid their toxic downstream effects has been a focus of therapeutic strategies for several years. Cellular mechanisms for degrading unwanted proteins include the UPS and autophagy. In several cellular and animal models of polyQ diseases, as well as in the patients post-mortem brains, polyQ inclusions co-localize with Ub and proteasome subunits, raising the possibility of UPS involvement in these diseases<sup>167,215</sup>. Some studies show that stimulating ubiquitylation and degradation of polyQ proteins through the UPS can rescue pathology in cell and

animal models. By increasing UPS activity, the Y-27632 (rho-associated kinase inhibitor, already used in clinical trials as an anti-ischemic, anti-vasospastic and anti-hypertensive agent) decreased polyQ toxicity in a HD *Drosophila* model<sup>240</sup>, and reduced aggregation levels of mutant htt and ATXN3 cell models by its capability of modulating both UPS and autophagy<sup>241</sup>. Another compound shown to increase enzymatic activity of UPS is amilorid and its derivative, benzamil, also widely used in clinics; treatment with these compounds led to a reduction of mutant protein aggregation and toxicity in HD models<sup>242</sup>.

An additional strategy is the direct modulation of proteasome function. Ubiquitin-specific protease 14 (USP14) is a deubiquitylating enzyme (DUB) connected with the proteasome, which blocks the degradation of ubiquitylated substrates. IU1, a selective small molecule inhibitor of USP14, was described to accelerate proteasomal degradation of polyQ proteins, such as ATXN3, but also of other proteins associated with neurodegenerative diseases such as tau, TDP43 and oxidized proteins<sup>243</sup>. Interestingly, however, mutations in USP14 leads to an ataxic neurological phenotype in mice<sup>244</sup> which could be reverted upon USP14 neuronal specific-expression<sup>245</sup>. This urges caution in using inhibition of drug this target as therapy in SCA's.

Ub ligases are enzymes that determines the substrate UPS specificity. The overexpression of Ub ligase CHIP (C terminus of Hsc70 interacting protein) confers neuroprotection by enhancing ubiquitylation and consequent clearance of polyQ-expanded proteins, delaying the disease phenotype in SCA1 and SBMA animal models<sup>246,247</sup>. Parkin was also shown to ubiquitylate ATXN3 reducing polyQ toxicity in cells<sup>248,249</sup>. More recently, it was shown that the Nrf1 and Nrf2 transcription factors can regulate the UPS. Sulforaphane is a small molecule capable to induce Nrf2 activation, and therefore increase proteasome levels and activity<sup>250,251</sup> as well as enhance UPS function *in vivo*<sup>252</sup>. Through this action, this molecule was able to decrease the mutant htt and alleviate polyQ toxicity in neuronal cells<sup>252</sup>. These studies suggests that the UPS is a versatile system that can be targeted to increase the clearance of polyQ-expanded proteins.

Autophagy is another prominent therapeutic target for the degradation of aggregated proteins and is negatively regulated by the mammalian target of rapamycin (mTOR)<sup>253</sup>. Upregulation of autophagy by inhibiting mTOR with rapamycin in different animal models of neurodegenerative diseases showed beneficial effects by enhancing autophagy function<sup>254–258</sup>. For example, a rescue of polyQ toxicity in cell, fly and mouse models was observed upon rapamycin treatment, as well as an increase the clearance of both soluble and insoluble species of the polyQ-expanded proteins<sup>259,260</sup>. Autophagy can also be modulated independently of mTOR by the use of several compounds, such as

lithium chloride (LiCl), sodium valproate, carbamazepine, rilmenidine and compounds that inhibit inositol monophosphatase<sup>261,262</sup>. Since these compounds have been used for several years to treat human CNS and heart diseases, they may have also promising effects in polyQ diseases. LiCl treatment in an HD mouse model ameliorated motor performance and depression in post-symptomatic treatment, with no effect in survival<sup>263</sup>. In SCA1, treatment of the knock-in mouse model with LiCl also improved the neurological and pathological phenotypes<sup>264</sup>. In contrast, in the case of MJD, LiCl therapy led to no overall improvement in motor function<sup>265</sup>. Rilmenidine is a hypertensive agent that was also tested in an HD mouse model, leading to amelioration of the disease symptoms presented in these mice and also to a reduction in the mutant htt levels<sup>266</sup>. Other approaches may consist in modulating the expression of proteins or molecules to induce autophagic degradation<sup>267,268</sup>. For instance, upon *C. elegans bec-1*, *Ce-atg7* and *Ce-atg18* gene knockdown or knockout, the polyQ aggregate formation and polyQ-expanded protein toxicity increased<sup>269</sup>. Therefore, modulating these autophagic genes in the opposite direction could enhance the autophagic polyQ degradation. Overexpression of histone deacetylase 6 (HDAC6) leads to the autophagy process compensating for UPS impairment in a SBMA *Drosophila* model<sup>270</sup>. More recently, the lentiviral vector-mediated overexpression of beclin-1 was described to be protective in neuronal culture and in a lentivirus-based rat model of MJD<sup>271</sup>. Overall this strategy seems to be attractive, however, it is important to identify new safe autophagy modulators to be used in chronic treatment, and to validate them in clinical trials.

#### **1.3.1.4 Proteolysis inhibition**

Misfolded polyQ-expanded proteins may undergo proteolytic cleavage generating smaller fragments which could have an higher toxic effect<sup>179,272</sup> and/or more quickly aggregate<sup>95</sup>. The “toxic fragment hypothesis” suggests that proteolytic formation of polyQ fragments is a pre-requisite of polyQ disease manifestation. Therefore, modulation of the activity of cleavage proteases or decreasing the levels of toxic fragments seem to be reasonable therapeutic approaches for these diseases. There are several proteolytic enzymes associated with the cleavage of polyQ proteins. The first described were the caspases in HD<sup>90</sup>, followed by calpains (a class of calcium-dependent cysteine proteases); even if they contribute to the majority of cleavage effects, several other fragmentation events could not be explained by their proteolytic activity. A great number of studies in different cell and mouse models, demonstrated promising effects of caspase-1, -3 and -6 and calpain inhibition, as well as inhibition of matrix metalloproteinases (MMP's) activity in HD-associated toxicity<sup>175,180,273-276</sup>. Additionally, the cleavage of mutant htt by caspase-6 has been suggested to be required for the HD-related behavioral phenotype



and selective neuropathology in the YAC128 mouse model of HD. Furthermore, caspase-6 resistant mutant htt mice presented a delay in nuclear translocation of expanded htt<sup>277</sup>. More recently, a transgenic mouse expressing the N-terminal 586 aa of htt, a putative cleavage fragment mediated by caspase-6, showed behavioral deficits as well as nuclear accumulation of htt aggregates. Although their phenotype was less severe than that HD mouse models expressing shorter fragments, these studies suggest that the caspase-6 fragment is an intermediate of the cascade leading to disease progression<sup>278</sup>. Atrophin-1 is also cleaved by caspases at aspartate 109, and cleavage site mutations reduce nuclear localization, aggregate formation and cytotoxicity<sup>272</sup>. This was also shown in the context of MJD, in which general caspase inhibition in a *Drosophila* model delayed the neurodegeneration progression caused by the expanded ATXN3 expression<sup>279</sup>. Targeting the expression of endogenous inhibitors, such as calpastatin, was also proposed in MJD<sup>280-282</sup>, being this inhibition able to prevent the nuclear localization and aggregation of mutant ATXN3 and its toxicity. Recently, it was also described that calpain inhibition in a *Drosophila* model of HD mediates autophagy-dependent protection against polyQ toxicity<sup>283</sup>. Another strategy is to modulate alternative cleavage pathways. For example, the levels of caspase-1 and -3 were decreased by treating R6/2 mouse model of HD with a tetracycline derivative, retarding the disease progression and death<sup>284</sup>. Recently a genetic approach was also proposed using antisense oligonucleotide-mediated protein modification. Modulating cleavage by inducing the skipping of exon 12 in htt pre-mRNA inhibits the formation of an N-terminal fragment involved in HD toxicity<sup>285</sup>.

The generation and development of protease inhibitors to prevent the conversion of polyQ proteins into more toxic fragments seems to be a promising therapeutic strategy. However, it is important to be careful with the specificity of these inhibitors, since other several essential signaling pathways in which proteases are involved<sup>286,287</sup> could also be affected.

### **1.3.1.5 Mitochondria stabilization and reduction of oxidative stress**

Mitochondrial dysfunction and oxidative stress are thought to play an important role in polyQ pathogenesis<sup>288,289</sup>. Several compounds improving energy metabolism defects or reducing oxidative stress have been successfully tested in cellular and mouse models of polyQ diseases (described above). Although the degree of oxidative stress involvement is not completely known, antioxidant treatment may be able to exert some neuroprotective effects. Coenzyme Q10 (CoQ10) is a cofactor of the electron transport chain which supports mitochondrial energy function, preserves cell viability, acts as a potent antioxidant *in vivo* and induces increase of mitochondrial vitamin E concentrations<sup>290</sup>. Co-

treatment with CoQ10 and remacemide, an NMDA receptor antagonist, improved neurological symptoms and extended survival in different models of HD<sup>244</sup>. CoQ10 alone was also able to reduce weight loss and Nlls as well as greatly improve the motor performance in R6/2 mouse model of HD<sup>291,292</sup>. Supplementation of CoQ10 together with creatine, also exerted additive neuroprotective effects in HD models<sup>293</sup>. Creatine supplementation alone was also able to improve brain pathology, phenotype as well as increase survival in R6/2 mouse<sup>294</sup>. Also in the N171-82Q model of HD, survival was extended with creatine treatment<sup>295</sup>. Resveratrol, another natural phenol antioxidant, ameliorated the mutant polyQ toxicity in neuronal cells and *C. elegans* model of HD<sup>296</sup>. Tauroursodeoxycholic acid (TUDCA) is a hydrophilic endogeneous bile acid with multiple neuroprotective properties, including antioxidant and anti-apoptosis activities. This compound decreased the apoptosis of striatal neurons and improved motor and cognitive deficits in HD mouse models<sup>297</sup>. Several other antioxidants such as melatonin, selenium, quinolinic acid, idebenone, lycopene, lipoic acid, pyruvate or L-carnitine also proved to exert neuroprotective effects in HD models<sup>298</sup>.

Also related with this field is the Nrf2/antioxidant response element (ARE) signaling pathway, which is involved in antioxidant and anti-inflammatory responses<sup>299</sup>. For example, the triterpenoids CDDO-ethyl amide and CDDO-trifluoroethyl amide were described to up-regulate Nrf2/ARE genes, therefore reducing the oxidative stress and striatal atrophy, improving the motor deficits and increasing lifespan in the N171-82Q mouse model of HD<sup>300</sup>.

Together, these results indicate that a therapy based on antioxidants and other promising molecules capable of improving mitochondrial function and reducing oxidative stress could be effective for polyQ diseases. However, human clinical trials have not shown efficacy for CoQ or creatine in HD<sup>301,302</sup>. Several factors could underlie these failures, for example, the dosage used, the severity of the disease and the post-symptomatic treatment, among others.

### **1.3.1.6 Transcription modulation**

The current conceptual model is that mutant polyQ proteins frequently interact abnormally with HATs and/or histone deacetylases (HDACs), changing physiological histone modification patterns and thus altering gene expression<sup>303</sup>. The normalization of the dysregulated gene transcription, usually by targeting histone acetylation and methylation has been a growing field of research. The inhibition of HDAC activity, as a repressor of transcription, has been proposed as a transcription normalization method, and is the most widely tested in mouse models of polyQ diseases. Though HDAC inhibitor

(HDACi) molecules frequently lack specificity, and thus they may also perturb the expression of other unrelated genes, some of them exhibit promising therapeutic properties.

HDACi's such as sodium butyrate (SB), phenylbutyrate, suberoylanilide hydroxamic acid (SAHA or vorinostat) and valproic acid (VPA), which are proposed to increase gene expression, have shown efficacy in a variety of polyQ disease models. Pharmacological treatment of the R6/2 mouse model of HD with SB improved body weight loss and motor phenotype, significantly extended the lifespan by more than 20%, and delayed the neuropathological damage through the increase in acetylation of H3 and H4 and also of SP1<sup>304</sup>. An improvement in neurological phenotypes and increased survival, together with an increased acetylation of histones in neuronal tissues was also observed in a transgenic mouse model of SBMA treated with SB<sup>305</sup>. In a DRPLA transgenic mouse model presenting hypoacetylation of histone H3 in brain, SB treatment ameliorated the motor impairments and extended survival<sup>306</sup>. Chou and colleagues demonstrated that SB treatment in a transgenic mouse model of MJD reversed the histone hypoacetylation and the transcriptional down-regulation in the cerebellum, leading to an improvement in the ataxic symptoms and increased survival<sup>307</sup>. Also for SCA7, but in a conditional pan-neuronal *Drosophila* model with globally decreased histone acetylation, treatment with SB improved survival time of the neurons in primary neuronal cultures<sup>196</sup>. In spite of significant improvements in many neuropathological phenotypes, SB was not able to reduce the mutant polyQ protein aggregation in some cases<sup>304, 305</sup>.

Another HDACi, phenylbutyrate, reduced brain atrophy and ventricular enlargement, and improved lifespan in the N171-82Q model of HD<sup>96</sup>. SAHA has been tested in the R6/2 mouse model of HD showing beneficial effects in the motor phenotypes and neuronal atrophy, however with no improvement in body weight. Like SB, SAHA rescued the hypoacetylation of histones in these animals but with no effect on polyQ aggregates<sup>308</sup>. More recently, the same authors demonstrated that SAHA decreased HDAC2 and HDAC4 at the protein level in the cortex and brainstem, but not at the mRNA level<sup>309</sup>. VPA is a well-tolerated antiepileptic drug, also with HDACi properties. This compound has been proven to delay the disease onset, to reduce neurological deficits and/or to prolong survival in several models of neurodegenerative diseases, including HD, SBMA and ALS<sup>310-312</sup>. In MJD, VPA was reported to alleviate neurodegeneration in a *Drosophila* model of the disease<sup>313</sup> and to attenuate mutant ATXN3-induced cell toxicity in a human neuronal cell model<sup>314</sup>. Thomas and colleagues successfully treated R6/2 mouse model of HD with a benzamide-type HDACi, HDACi 4b. This compound showed a lower toxicity *in vitro* when compared with previously tested HDACi, together with prevention on motor deficits and neurodegenerative processes *in vitro* in a post symptomatic treatment approach<sup>315</sup>.

Other chromatin remodeling approaches, though not so well studied as the previous ones, comprise for instance the use of chromomycin and mithramycin antibiotics that were able to rescue the down-regulation of a subset of affected genes, improved motor and neuropathological phenotypes and increased the lifespan of transgenic mouse models of HD<sup>316,317</sup>. Another compound shown to alleviate the transcriptional dysfunction is the phosphodiesterase type IV inhibitor rolipram, which increases the phosphorylation and activity of CREB. Rolipram ameliorated neuropathology, slowed progression of neurological phenotype and extended lifespan in R6/2 mice. Additionally, BDNF levels, which are impaired in this HD mouse<sup>318,319</sup>, were induced in treated mice through restored function of CREB<sup>320</sup>. A subsequent study show that rolipram also prevented the sequestration of CBP into NIIs<sup>321</sup>. Dimethylcurcumin (ASC-J9), a drug that specifically disrupts the interaction of mutant AR with CBP, was shown to be symptomatically beneficial in an AR-97Q SBMA mouse model<sup>322</sup>.

In spite of the promising results obtained with HDCAi's in models of polyQ diseases, this strategy still lacks some specificity. In spite of their neuroprotective effects modulating the transcriptional defects, they could also increase the acetylation of other non-histone proteins, such as tubulin<sup>323</sup> and HSP90<sup>324</sup> and upregulate levels of HSPs<sup>325,326</sup> via transcription-independent mechanisms. These issues stickle the translation of some promising results to clinical application, together with some toxic effects associated with HDACi treatment. Further studies of their actual molecular mechanism, and development of more selective HDACi's with less toxicity, might offer better opportunities<sup>327</sup>. Lastly, and assuming the increased knowledge on HATs and their function in neuronal survival, the stimulation of HAT function appears to be a new therapeutic possibility in this field<sup>328</sup>.

### 1.3.1.7 Other treatment possibilities

The overactivation of NMDA glutamate receptors and consequent **excitotoxicity** leading to death has been supposed to have a role in pathogenesis of HD<sup>329</sup>. Supporting this concept, the use of compounds that block the excessive glutamate release, as riluzole, has been effective in HD mouse models concerning survival, motor performance and agregation<sup>330</sup>. Two compounds affecting the glutamate levels in the synaptic cleft, LY379268 and 2-methyl-6-(phenylethynyl)-pyridine, consistently with riluzole, significantly increased the lifespan of R6/2 mice<sup>331</sup>. Administration of remacemide (NMDA antagonist) and/or of CoQ10 also prolonged the lifespan rates of HD mice<sup>291</sup>. Another option is **apoptosis inhibition**; anti-apoptotic drugs, such as minocycline and caspase inhibitors have shown promise in polyQ animal models. Administration of minocycline in R6/2 mice extended the survival<sup>332</sup>, and when combined with CoQ10 further improved survival, neuropathology and motor phenotype when

compared with any of the treatments alone<sup>333</sup>. However, long-term studies will be required to find out possible side-effects associated with suppression of these key cellular pathways. Caspase inhibition could have other beneficial effects, through a decrease in generation of caspase-cleaved fragments of mutant proteins. In fact, a general caspase inhibitor, z-Val-Ala-Asp-fluoromethylketone, extended lifespan and ameliorated the rotarod performance in R6/2 mice<sup>276</sup>. The combined administration of caspase 1 and 3 inhibitors, Tyr-Val-Ala-Asp-chloromethylketone and Asp-Glu-Val-Asp-aldehyde-fluoromethylketone, respectively, also increased the lifespan in HD mice<sup>332</sup>. Other still emergent strategies for polyQ diseases may comprise **neural cell replacement therapy and neuroprotection strategies**. The replacement of dead and/or damaged neurons by new neural cells with the proper ability to integrate, function<sup>334</sup> and also contribute to neurogenesis and the production of trophic factors<sup>335,336</sup> may provide additional neuroprotection and promote the reestablishment of neuronal homeostasis. The attractiveness of these strategies lies partially in the fact that they might be effective even after disease manifestation.

### 1.3.2 Hypothesis-free approaches

Hypothesis-based drug design, although a theoretically rational approach, is only one strategy for drug discovery, and although this approach can offer promising results, it is limited to known targets and drugs, and it cannot unravel novel targets and disease pathways.

In the last years, hypothesis-free approaches for polyQ therapies are gaining relevance due to their numerous advantages and the novel technical possibilities for screening. High-throughput screening (HTS) allows the testing of the effects of thousands of compounds in one or more biological assays against a chosen set of defined targets. The small molecules used in HTS's are often readily commercially available and are generally classified into three groups: i) Food and Drug Administration (FDA)/European Medicines Agency (EMA) approved compounds, which comprise bioactive, natural products and synthetic small organic molecules; ii) novel synthetic compounds, comprising a vast collection of novel organic molecules and iii) natural products. The FDA/EMA approved compounds have the potential to rapidly translate into the clinic and of a faster interpretation of pathophysiological mechanism due to their often known targets and mechanisms of action. The synthetic compounds could comprise molecules for additional unexpected targets and can be easily improved and modified for increased potency or decreased side effects, for instance, together with their lower costs. The natural products could also contain novel structures and may be superior in terms of biological activities and chemical complexity but are usually associated with higher costs and limited availability.

Besides the compound library selection, the most critical step is the choice of the target which must faithfully reflect the disease process and be compatible with automation. In polyQ diseases, the drug discovery is hampered by to the lack of validated targets and the incomplete knowledge of the molecular pathways. Nevertheless, the strategy consists in screening against a specific disease hallmark in the available cellular or inferior animal models, since they can recapitulate at least some disease-associated phenotype. In these diseases the most common target is polyQ protein aggregation, which is an important aspect of cellular pathology, either as a primary event or as a robust indicator of abnormal protein conformation. Other described targets for polyQ HTS have been cell death, mutant protein clearance (degradation), transcriptional dysregulation and other events thought to contribute to toxicity. The HTS assays can be *in vitro*, cell-based or, less often, whole organism based. Any such model will have intrinsic advantages as well as limitations. A summary of the described polyQ HTS's is depicted in Table 2. Although the majority of the HTS's have been centered on HD, several concepts could be applied to the other polyQ diseases.

**Table 2.** Chemical HTS for polyQ diseases.

Target	PolyQ construct	Assay system/readout	Compounds tested	Hits	Secondary assays	Ref.
<b>Aggregation</b>	GST-HTT exon 1 Q51	<i>In vitro</i> screen by filter retardation assay	184,880 small molecules	Benzothiazoles	Immunoblotting, electron microscopy, mass spectrometry, 293 Tet-Off cells	337
	GST-HTT171 Q58	<i>In vitro</i> screen by filter retardation assay	1,040 FDA-approved drugs and bioactive compounds	Gossypol, gambogic acid, juglone, celastrol, sanguinarine and anthralin	Htt localization phenotype in Hdh <sup>Q111/Q111</sup> striatal cells	338
	GST Q62	<i>In vitro</i> screen	Phage display library	Six tryptophan-rich peptides (polyQ-binding peptide 1)	PolyQ turbidity, CFP/YFP FRET in HD COS-7 cell model, cell death and aggregation	339
	AR127 Q65	<i>In vitro</i> screen by CFP/YFP FRET assay	2,800 biologically active compounds	Y-27632 (Rho associated-kinase p160ROCK inhibitor)	Aggregation and neurodegeneration in HD <i>Drosophila</i> model	340
	GST-HTT exon 1 Q51	<i>In vitro</i> screen by filter retardation assay	11 small molecules	Congo red, thioflavine S, chrysamine G and direct fast yellow	Electron microscopy, SDS/PAGE, and MS and HD COS-7 cells	340
	HTT <sup>WT</sup> fragment	<i>In vitro</i> screen	15 peptides	HTT <sup>WT</sup> -related inhibitor peptides	Cell-penetrance and cytoplasmic localization in SH-SY5Y cells	341
	HTT Q72-Luciferase	HEK-293 cell-based screen by luciferase activity and FRET	2,687 small molecules	Leflunomide and teriflunomide	Size and number of aggregates upon treatment and cycloheximide (CHX)-chase experiments	342

Target	PolyQ construct	Assay system/readout	Compounds tested	Hits	Secondary assays	Ref.
<b>Aggregation and toxicity</b>	GST-HTT exon 1 Q51	<i>In vitro</i> screen by filter retardation assay	5,000 natural substances	EGCG and related polyphenols	Aggregation in HD Yeast model and photoreceptor degeneration and motor function in <i>Drosophila</i> model	343
	AR127 Q65	HEK-293 cell-based screen by CFP/YFP FRET	3 libraries (4,140 compounds)	EGFR inhibitor #3, EGFR inhibitor #4, gefitinib, nadolol, fosfosal, piceatannol, levonordefrin, todralazine, hydralazine, molsidomine, Ac-YVAD-cmk	Aggregation in PC12 cells, phenotype in Htt exon1 in <i>Drosophila</i>	344
	HTT Q103-EGFP	Yeast cell-based screen by growth and EGFP fluorescence	16,000 compound library	C2-8	Microscopy and PC12-Q103 cells, HD COS-7 cells, brain-slices and HD <i>Drosophila</i> and R6/2 models	345
	$\Delta$ ProQ103	Yeast-based assay by growth readout	11,000 natural extracts compounds	Actinomycin D	Chaperone levels and PC12 cell aggregation	346
<b>Cell death</b>	AR Q112	HEK-293 cell-based assay by caspase-3 activation and fluorescence	1,400 compounds	Nerifolin, Peruvoside, Digoxin, Suloctidil	Rescue of Q112-related cell death by FACS	347
	HTT exon 1 Q103-EGFP	PC12 cell-based by LDH release and absorption	1,040 compounds	12 compounds including cannabinoids and caspase inhibitors	NA	348
	HTT Q148	Inducible PC12 cell-based by LDH release and absorption	1,040 compounds	Nipecotic acid, Mycophenolic acid, acivicin, isoproterenol HCl and Propafenone	HTT aggregation by immunofluorescence cytochemistry	349
	HTT Q120	Temperature sensitive ST14A striatal cell-based assay by calcein AM cell viability and fluorescence	43,685 compounds	29 compounds (R1-R29)	Survival of Q103-related cell death in PC12, yeast, <i>C. elegans</i> and <i>Drosophila</i> and brain slices	350
<b>Cell death and toxicity</b>	HTT exon 1 Q25 and Q103-EGFP	PC12 cell-based screen by cycloaddition chemistry and in-gel fluorescence scanning	68,887 synthetic and natural compounds	16F16, thiomuscimol, cystamine	HD and AD cortico-striatal brain slice models	351
	HTT exon 1 Q150	<i>C. elegans</i> ASH neuron-based screen by GFP expression	9 compounds	LiCl, TSA, SAHA and mithramycin	NA	352
<b>Toxicity</b>	HTT480 Q68	Striatal neuronal primary culture-based screen	40,000 compounds	NA	NA	353

Target	PolyQ construct	Assay system/readout	Compounds tested	Hits	Secondary assays	Ref.
	HTTN90 Q8 and Q73	Cortical and Striatal neuronal primary culture-based screen by fluorescence scanning	400 small molecules	Inhibitors of Rho kinase, phosphodiesterase, adenosine 2A receptor and IKK $\beta$	NA	354
	HTTN90 Q73	Rat brain slice-based screen	74 drug-like compounds	Inhibitors of IKK complex, CXCR3 chemokine receptor, c-Jun N-terminal kinase and adenosine 2A receptor	NA	355
	HTT 588 C38 and Q15	<i>Drosophila</i> primary neuronal culture-based screen	2,600 small molecule	Camptothecin, OH-camptothecin, 18 $\beta$ -glycylrrhethinic acid and carbenoxolone	HD <i>Drosophila</i> larvae survival, pupal lethality and climbing behavior	356
<b>Clearance (Degradation)</b>	HTT573 Q72	HN10 neuronal cell-based screen by time-resolved FRET	10,000 natural compounds	TSA analogue, staurosporine, anisomycin, cycloheximide, borrelidin, BAY 61-3606	NA	357
	HTT573 Q25 and Q72	HN10 neuronal cell-based screen by time-resolved FRET	2x10 <sup>6</sup> compounds	Heat shock protein 90 inhibitors as NVP-AUY922	HdhQ150 embryonic stem cells and embryonic stem cell-derived neurons	358
	Q103-EGFP	Inducible PC12 cell-based by protein concentration with EGFP fluorescence	37,000 synthetic compounds	31 compounds	$\alpha$ -complementation, Q103-related cell death	359
	NA	Yeast-based assay by growth readout	50,729 compounds	21 SMIRs and 12 SMERs	PC12 (A53T $\alpha$ -synuclein) clearance, HD exon 1 (Q74)-EGFP, autophagy with embryonic fibroblasts, COS, HeLa cells and <i>Drosophila</i>	360
<b>HSF-1 activation</b>	NA	HeLa cell-based screen	1x10 <sup>6</sup> compounds	A1, A3, C1, D1, F1	HD mammalian cellular and <i>C. elegans</i> model	361
	NA	Yeast-based assay	10,000 compounds	HSF1A (TRiC/CCT complex)	HD mammalian cellular and <i>C. elegans</i> model	362
<b>Transcription dysregulation</b>	HTT Q138	Inducible HEK-293 cell-based assay by Luciferase reporter gene	24,000 compounds	47 compounds	Cell viability adenosine triphosphate assay in primary striatal neurons transfected with N171-Q82	363
<b>Fly motor impairment</b>	HTT Q128	<i>Drosophila</i> neuron-based screen	521 quinazoline-derived compounds	EVP4593	YAC128 medium spiny neurons	364

**Abbreviations:** GST = glutathione S-transferase; FDA = Food and drug administration; CFP/YFP = cyan fluorescent protein/yellow fluorescent protein; FRET = fluorescence resonance energy transfer; EGCG = Epigallocatechin gallate; EGFR = Epidermal growth factor receptor; EGFP = Enhanced Green Fluorescent Protein; FACS = Fluorescence-activated cell sorting; LDH = Lactate dehydrogenase; GFP = Green fluorescent protein; LiCl = Lithium chloride; TSA = Trichostatin A; SAHA = suberoyl anilide hydroxamic acid; NA = Not available; SMER = Small-molecule enhancer; SMIR = Small-molecule inhibitor.



### 1.3.2.1 Aggregation assays

The first HT screens were planned to identify compounds that would avoid the formation of and/or disrupt HD aggregates *in vitro*. Examples of these assays include aggregate quantification by filter retardation assay with fluorescent ELISA readouts<sup>337,338,340,343</sup>. Although optimization of this method required much more time than the current HTS's, Heiser and colleagues were able to screen 18,4880 small molecules and to identify 25 benzothiazoles able to inhibit aggregation of the HTTQ51 protein, some of them already described to be effective for ALS treatment<sup>365</sup>. As a second assay, these compounds were tested in HEK293 cell, expressing HTTQ51, the majority of them being toxic to cells and later to *in vivo* models. This HTS emphasized the importance of the risks of translation from *in vitro* to cell cultures. Another *in vitro* aggregation assay was performed by Wang and colleagues, with a longer htt fragment, identifying 19 compounds inhibiting aggregation by more than 50%<sup>338</sup>. Curiously, one of the hits was celastrol which is an anti-inflammatory and antioxidant compound that has been also proposed for AD therapeutics<sup>366</sup>. To incorporate cellular context, a pioneering screen to monitor polyQ aggregation in cells was developed using a fluorescence resonance energy transfer (FRET)-based assay which is based on the transfer of energy between two fluorophores that are in close spatial proximity. With this method, Pollit and colleagues screened a 2,800 compound library and identified the Rho kinase (ROCK) inhibitor Y-27632 of mutant AR aggregation as a hit compound<sup>240</sup> and consequent validate it in a HD *Drosophila* model. The discovery of the ROCK inhibitors in aggregation context allowed the characterization of the ROCK-profilin signaling pathway<sup>367,368</sup>. For instance, the FDA-approved ROCK inhibitor HA-1077 was able to rescue retinal degeneration in the R6/2 mouse model of HD, showing that ROCK inhibition is an HD-related mechanistic pathway<sup>369</sup>. With the same strategy, the group screened a set of biologically active compounds and found hits capable of inhibiting the aggregation of a pure polyQ stretch, suggesting that these compounds could be essential tools for understanding and counteracting the aggregation mechanisms in polyQ diseases. Some of the compounds were also able to alleviate the neurodegeneration in a HD *Drosophila* model<sup>344</sup>. Recently, in search of a more robust and quantitative method to assess protein aggregation dynamics, Fuentalba and colleagues developed a novel aggregation-sensitive luciferase-based reporter to quantify polyQ aggregation *in cellulo*, based on an expanded htt fragment<sup>342</sup>. With this method the authors identified leflunomide and its active metabolite teriflunomide, which prevent incorporation of expanded polyQ proteins into aggregates. This compound could hold promise for polyQ diseases, as it was already tested in multiple sclerosis patients, however its long-term safety profile remains unknown<sup>370</sup>. In addition to the use of mammalian cells in these assays, aggregation of htt has also been studied in simple yeast

systems. This biological system is less susceptible to polyQ-mediated toxicity, and easily subject to genetic analysis, allowing the study of other cellular factors in the aggregation process. In 2005, a primary aggregation screen was established with 16,000 compounds in a yeast strain, using a galactose-inducible htt construct with 103Q's tagged with EGFP<sup>346</sup>. Nine hits were identified and microscopically validated. Four compounds were found to inhibit the aggregation of this fusion protein also in PC12 cells. However, the compound activity was weak in a cell-filter retardation assay, demonstrating that the compound did not directly interfere with polyQ aggregation. A recent study also used a yeast model of polyQ proteotoxicity to screen a large amount of natural product extracts, identifying actinomycin D as a strong inhibitor of polyQ aggregation, an effect that was accompanied by its impact in increasing the levels of different HSPs<sup>346</sup>. This compound also suppressed aggregation in mammalian cells, suggestive of a conserved mechanism and therefore placing this as an interesting compound for polyQ diseases. Efforts were also made to establish brain slice assays that could closely mirror the aggregation events in mouse models for HD<sup>371-374</sup> and although the authors could confirm the anti-aggregation properties of Congo Red in this system, the predictive value of this assay for the compounds activity in animals and patients still needs to be validated.

Diverse *in vitro* and cell-based assays have allowed the identification of several small molecule inhibitors and some of them were also found to be active *in vivo* (for e.g. in the *Drosophila* model). However, some limitations are still present and platforms need to be optimized and to evolve in terms of comparing different toxicity patterns in different systems, or different genetic constructs that could led to different compound outcomes.

### **1.3.2.2 Cell death assays**

In addition to aggregation assays, more complex biological assays aiming at phenotypic endpoints associated with the disease process could be used. Though the exact role of cell death in polyQ pathogenesis is still discussed<sup>375,376</sup>, this downstream consequence of toxicity is being used as an assay readout for the identification of novel small molecules. Caspase-3 activation is a key event in the apoptotic cell death and its genetic or small molecule inhibition showed to be beneficial in cell cultures and mouse models of HD<sup>377,378</sup>. A cell-based assay was used to identify inhibitors of caspase activation in a model of SBMA, in which expression of mutant AR Q112 induces caspase-3 activation and cell death<sup>347</sup>. A 1,400 compound collection was screened and the researchers identified 15 compounds inhibiting caspase-3 activity by more than 70%, however only four cardiac glycosides were confirmed to enhance cell viability without causing cytotoxicity. Curiously, these compounds do not inhibit caspase-3

directly, suggesting that there are other targets upstream in the cascade of death pathway. Thus, the study of the mechanisms of action of these compounds could disclose new and unexpected biological targets in the HD context. Apart from this molecular endpoint, there are also HTS's based on the phenotypic endpoint, the cell death itself. Aiken and colleagues used an inducible PC12 cell model, with a construct containing 103Q's, previously described<sup>379</sup>, which underwent rapid cell death and quantified lactate dehydrogenase (LDH) or measured mitochondrial activity with an MTS assay. With this model, the group screened 1,040 compounds and identified 12 that completely rescued cell death. Among these compounds, cannabinoids were efficient for protection against cell death<sup>348</sup>, through a possible mechanism related with their described antioxidant effects<sup>380</sup>. Another screen with the same compounds, in an inducible PC12 cell model, but with a construct with 148Qs, identified 5 compounds preventing cell death, three of them (acivicin, nipecotic acid and mycophenolic acid) also decreasing aggregation<sup>349</sup>. It is important to note that, although performed with the same inducible model and the same compound library, these two HTS's do not present overlap in the hit compounds with the exception of caspase inhibitors, alerting for the importance of the cellular model and polyQ construct when designing the assay and for validation of findings in several models. Thus, it is valuable to perform HTS's in cell lines that mirror as much as possible the cell types known to be affected in the disease context. With that purpose, Varma and colleagues used a stable striatal neuronal cell line expressing N-terminal 548 aa fragment of htt with 120Qs, which undergoes cell death upon serum deprivation at 39°C<sup>350</sup>. In a collection of 43,685 compounds, they identified 29 hits rescuing cell death specifically in mutant but not in parental striatal cells suggesting that the targets of these compounds are specifically activated by mutant htt and consequently are possibly relevant therapeutic targets. As secondary assay, the authors tested these 29 compounds in three additional HD models – PC12 cells, yeast and *C.elegans* – four of them being active in these models, and two of them also active in a rat brain slice HD assay. Although their mechanism of action is still under study, these compounds seem to specifically target mutant htt toxicity across cell, tissue and organism-based HD models.

One of the major concerns of *in vitro* and cell-based assays is whether the hits will be also effective in a whole animal model of the disease. In this context, *C. elegans* is a powerful model for drug-testing in whole animal context, due to its short life cycle, small size and easiness of culturing in liquid medium. Moreover, several neurobiological and anti-parasitic drug studies in *C.elegans* provide a strong basis to use this organism in drug discovery identification<sup>381, 382</sup>. Voisine and colleagues used a *C.elegans* model of polyQ neurotoxicity expressing N-terminal 171 aa fragment of human htt with 151Qs in neurons, and mimicking the degeneration and cell death of the human disease (dependent

on both age and the length of the polyQ tract)<sup>185</sup>. The authors tested different candidate compounds previously identified in cell cultures and animal studies in the *C.elegans* model and found that two FDA approved compounds, LiCl and mithramycin, independently and in combination, alleviated HD neurotoxicity<sup>352</sup>. Due to its easiest genetic manipulation, *C.elegans* is also valuable to study the drugs' mechanisms of action by turning on/off possible targets, accelerating drug discovery field for polyQ diseases.

### 1.3.2.3 Clearance/Degradation assays

A different strategy than those referred above is to perform a HTS to tackle the cellular degradation of soluble or aggregated forms of mutant polyQ proteins. With the purpose of identifying compounds promoting clearance of the mutant polyQ protein in mammalian cells, Coufal and colleagues used the htt gene encoding a protein with 103Qs in fusion with EGFP, placed under control of an inducible ecdysone control element in PC12 cells<sup>379</sup>. These authors screened a library of 37,000 compounds, basing their screen on fast degradation of the Q130-EGFP fusion proteins 24 hours succeeding of the inducer removal. After toxicity studies, they identified 31 compounds that accelerated degradation, of which two structurally similar compounds, A28 and A31. For this last one, a second assay aiming to study these compounds in terms of their specificity for a mutant (Q79) or a WT (Q23) htt protein in PC12 cells, showed that A31 increased clearance and cell viability for the mutant htt but not for the WT protein<sup>359</sup>. Another HTS screening to search for modulators of autophagy was performed in a *Saccharomyces cerevisiae* model by Sarkar and colleagues<sup>360</sup>. The mTOR kinase is a major negative regulator of autophagy<sup>383</sup>, and thus an interesting drug target in protein aggregation-related diseases, although the utility/safety of its chronic inhibition is under debate. In this HTS, 15,000 compounds were screened and the authors identified 12 novel small-molecule enhancers (SMERs) of autophagy, modulating the levels of htt and A35T  $\alpha$ -synuclein, and 21 inhibitors (SMIRs) of the cytostatic effects of rapamycin in yeast. The SMERs were shown to be independent or functioning downstream of mTOR, and proved to attenuate mutant htt toxicity in HD cell and *Drosophila* models.

Another cell-based assay through a time-resolved FRET analysis was performed by Paganetti and colleagues, the main advantage of which was the possibility to adapt the design for protein visualization in intracellular imaging assays, with fixed and permeabilized cells<sup>357</sup>. To validate the system, the authors tested 10,000 compounds for their ability to modulate intracellular htt levels with a parallel cytotoxicity readout. Then, by screening a natural product library, the authors identified six molecules that efficiently reduced or increased the mutant htt present in the neuronal HN10 cells.

Recently, a HTS using a hippocampal HN10 cell line expressing mutant htt through a time-resolved FRET assay, identified several hits, including heat shock protein 90 (HSP90) inhibitors<sup>358</sup>. These compounds strikingly decreased mutant htt levels without major toxic effects. The hit NVP-AUY922 was picked to deepen the degradation mechanism in HdhQ150 embryonic stem (ES) cells and ES cell-derived neurons. This compound significantly decreased the soluble full-length mutant htt levels and enhanced mutant htt proteasomal degradation without induction of HSP70, suggesting it as a promising therapeutic molecule.

#### **1.3.2.4 Transcription dysregulation and other targets**

As the knowledge of the pathogenic mechanisms of polyQ diseases evolves, more relevant quantifiable readouts could be used for HTS's. Although the most of the pieces of the puzzle of transcription dysregulation of polyQ diseases are still not well understood, the fact is that this mechanism seems to play an important role in their pathogenesis. In this line, it is known that mutant htt is able to sequester the CREB co-activator CBP through direct polyQ interactions leading to reduced CREB-mediated transcription<sup>52</sup>. Taking this into consideration a recently study from Lazzeroni and colleagues described a novel phenotypic screening assay to identify modulators of htt-induced transcriptional dysregulation<sup>363</sup>. The authors used a stable cell line expressing a full-length mutant htt gene (138Q), together with a reporter gene under the control of the CRE. The full-length protein used here enabled a more disease-relevant cellular phenotype than that measured for models expressing exon-1 or other htt fragments previously described. As a proof-of-concept, upon treatment with Rho kinase inhibitor Y27632, one clone showed reversible inhibition of the reporter activity and was then used for a HTS of 24,000 compounds. 64 compounds were identified with different specificity levels for CRE-mediated transcriptional regulation and secondary assays needs to be performed to tackle their mechanisms of action and their effects on mutant htt aggregation.

Recent studies have also been focusing on other parameters of polyQ pathogenesis. One is the activation of the heat shock transcription-factor 1 (HSF-1) which has been shown to restore proteostasis in a wide range of neurodegenerative diseases<sup>218,223,226,362</sup>. A few small molecules were already identified as regulators of protein conformation through the activation of HSF-1 in cell<sup>361</sup> and yeast-based assays<sup>362</sup>.

Although the majority of the HTS's are performed in a simple cell-based assays and the *in vivo* rodent models are only used as a last part of the screening before testing the compounds in clinical trials, other non-rodent *in vivo* models can actually be used for primary library screenings. Despite their

higher cost and throughput limitations, *Drosophila* and *C.elegans* are two models that can be used with the higher advantage of being multicellular organisms displaying polyQ disease-related quantifiable phenotypes for HTS. PolyQ-associated phenotypes, as motor impairment, for instance, could be used as first line readouts in *Drosophila*<sup>64</sup> and *C.elegans* models in the future of polyQ HTS's.

In summary, in the last decade, a significant number of HTS assays have been established which lead to the identification of multiple of polyQ disease-modifying compounds, comprising both FDA/EMA approved drugs and novel chemical molecules. The next challenge is to test these molecules in clinical trials and use them as tools to enhance the understanding of the polyQ disease mechanisms, therefore unravelling novel therapeutics targets. So far, the best candidates will be the FDA/EMA approved compounds which cross the blood brain barrier (BBB) which, once they prove to be effective in animal models, they fast translate to clinical trials. The hurdles for the novel molecules are more complex, as they need to pass several filters including their analysis in different secondary assays in terms of their toxicity, potency, metabolic stability, adequate pharmacokinetic profile and their capability to cross the BBB. At this moment, a unifying handicap in polyQ disease therapeutics is that mutant polyQ expression is associated with the disturbance of several cellular mechanisms. These multi-affected mechanisms make the process of drug discovery difficult since it turns out to be difficult to know exactly which might be the most important aspect of disease mechanism to target. However, the hard but also productive pathway that we have travelled so far in this field, together with the improvement in biotechnology, means that we will have the best tools to tackle the emerging and old questions towards better therapeutic approaches for these devastating diseases.

#### **1.4 Clinical Trials in polyQ diseases**

Despite the enormous efforts in the past decades, there is no effective treatment for polyQ diseases. However, several clinical trials were performed and numerous are ongoing in which, despite no clear overall improvement, some specific symptoms of the disease could be attenuated. Table 3 summarizes the completed double-blinded, phase 2 and/or phases 3 randomized controlled clinical trials (RCTs), for polyQ diseases with 20 or more patients, available at [clinicaltrials.gov](http://clinicaltrials.gov) and/or Pubmed, excluding open-label and retrospective trials. The main objective of this categorization was to cover the high quality evidence RCTs.

**Table 3.** Completed RCTs for polyQ diseases with available results at [clinicaltrials.gov](http://clinicaltrials.gov) and/or Pubmed.

PolyQ disease	Therapeutic molecule	Mechanism of action	Treatment duration	N	Overall efficacy	Ref.
HD	Latrepidine	Antihistamine, mitochondrial membrane stabilizer	90 days	91	Improvement in the MMSE score mean	384
			26 weeks	403	No significant effect in cognition or global function	385
	Creatine	Energy metabolism regulator	1 year	41	No significant effect in functional, neuromuscular, and cognitive status	301
	Pridopidine	Dopaminergic stabilizer	4 weeks	58	Trend towards improvement in affective symptoms. No significant effect in voluntary motor symptoms	386
	Nabilone	Cannabinoid CB1 and CB2 agonist	15 weeks	44	Significant effect for total motor score, chorea, UHDRS cognition, UHDRS behavior and for NPI.	387
	Ethyl-EPA	Multiple Targets mitochondrial function	6 months	316	No significant effect	388
			1 year	135	No significant effect	389
	Atomoxetine	NARI	10 weeks	20	No significant effect	390
	Fluoxetine	SSRI	4 months	30	No significant effect	391
	Citalopram	SSRI	20 weeks	33	No significant effect in executive functions	392
	Lamotrigine	Glutamate release inhibitor	30 weeks	64	No significant effect in delayed disease progression. Symptomatic improvement in some patients and a trend towards chorea decrease.	393
	Riluzole	Glutamate release inhibitor	3 years	537	No neuroprotective or beneficial symptomatic effects	394
			8 weeks	63	Improvement in chorea intensity. No improvement in functional capacity or other clinical features	395
	Tetrabenazine	Catecholamine-depleting agent	12 weeks	84	Improvement in chorea symptoms	396
			5 days	30		397
	Clozapine	D2 receptor antagonist	31 days	33	Little beneficial effects.	398
	Tiapride	D2 receptor antagonist	4 weeks	22	No significant effect in involuntary movements	399
			9 weeks	29	Significant improvement in chorea and motor symptoms	400
	Amantadine	NMDA-receptor antagonist	4 weeks	24	Only palliative benefit	401
			2 weeks	24	No significant effect in chorea symptoms	402
Remacemide hydrochloride	NMDA receptor antagonist	5 weeks	31	No significant effect	403	
Remacemide hydrochloride and Coenzyme Q10	NMDA receptor antagonist and antioxidant	30 months	347	No significant effect	302	
Donepezil	Acetylcholinesterase inhibitor	12 weeks	30	No significant effect	404	
Baclofen	GABA agonist	42 months	60	No significant effect	405	
Modafinil	Analeptic	3 weeks	20	Improvement in alertness but not in cognition or mood	406	
Mavoglurant	Selective metabotropic	32 days	42	No significant effect in chorea symptoms	407	

PolyQ disease	Therapeutic molecule	Mechanism of action	Treatment duration	N	Overall efficacy	Ref.
	(AFQ056)	glutamate receptor 5 antagonist				
	PBT2	metal protein-attenuating compound	26 weeks	109	No significant effect in cognition	408
<b>SBMA</b>	Leuprorelin	gonadotrophin-releasing hormone (GnRH) analogue	48 weeks	199	No significant effects on swallowing function	409
	Dutasteride	Dual 5- $\alpha$ reductase inhibitor	2 years	50	No significant effect on the progression of muscle weakness	410
<b>SCA1,2,6</b>	Dalfampridine	Potassium channel blocker	10 weeks	20	Unreliable or uninterpretable data	NPP
	Dalfampridine	Potassium channel blocker	10 weeks	20	Unreliable or uninterpretable data	NPP
	Varenicline (Chantix)	$\alpha$ 4 $\beta$ 2 neuronal nicotinic acetylcholine receptor agonist	8 weeks	20	Improvement of axial symptoms and rapid alternating movements. Nausea as a side effect. Large percentage of dropouts.	411
<b>SCA3/MJD</b>	Lithium carbonate	Anti-maniac	24 weeks	62	No significant effect in NESSCA scores; minor progression on the PATA speech-rate, nondominant Click test, Spinocerebellar Ataxia Functional Index and in the Composite Cerebellar Functional Score	412
	Trimethoprim and sulfamethoxazole (Bactrim)	Antibiotic	24 weeks	22	No significant effect	413

**Abbreviations:** N = number of patients (treatment and placebo); MMSE = Mini-Mental State Examination; UHDRS = Unified Huntington's Disease Rating Scale; NPI = neuropsychiatric inventory; NARI = Noradrenaline reuptake inhibitor; SSRI = Selective serotonin reuptake inhibitor; Ethyl-EPA = Ethyl-eicosapentaenoic acid; NPP = No publication provided; NESSCA = Neurological Examination Score for the Assessment of Spinocerebellar Ataxia.

The vast majority of the clinical trials in polyQ diseases have been performed for HD, which is the most common of these disorders; however, in the case of remarkable outcomes, they may function as a good hypothesis to test in other polyQ diseases which frequently share some symptoms. Nevertheless, the design and success of polyQ clinical trials constitutes a challenging issue due to the particularities of these diseases, namely: i) highly variable clinical presentation and slow progression of symptoms; ii) lack of reliable and specific targetable biomarkers; iii) small number of patients and iv) high costs of clinical trials for rare diseases. In fact, the majority of clinical trials performed up to now have failed or produced slight success. Therefore, it is crucial to critically analyze the results obtained so far, to be able to design novel trials with novel suggestions for the future success of polyQ clinical trials. Some issues regarding patient risks and side effects, study duration, sample size, trial rationale and pre-clinical study results,



pharmacological and methodology questions and clinical trial design could underlie the current results. On the other hand, despite the considerable improvement of the knowledge on the genetics and pathophysiology of the polyQ diseases in the past decade, the field is still lacking relevant biomarkers of the disease manifestation. Improving the reliability and validity of performance measures of the composite rating scales and neuroimaging studies are also major investments that should be kept in the field and, finally, a more effective approach to early phase clinical trials is required to speed up the identification of suitable drugs for these diseases.

While no overall effective treatment is available, physical and/or palliative therapies to maintain the individual's independence in all environmental contexts should be implemented for as long as possible. The working goal of this kind of therapy is to establish strategies to optimize sensorial information, to improve cognition through different activities, to enhance communication, to increase the quality and control of movement in different body postures, to improve approaches for an independent gait, to exercise against resistance, to improve hypotonia and motor control and speech therapy<sup>414-417</sup>. These small steps could may represent a great help and motivation leading to an improvement and sustainable life quality of patients and their families.

### **1.5 Machado-Joseph Disease (MJD)**

MJD, also known as SCA3, is the most common autosomal dominant ataxia worldwide<sup>22,418,419</sup>. The disease was first described in 1972 in a patient with Portuguese/Azorean ancestors, William Machado, by Nakano and colleagues, as an “autosomal dominant ataxia” and named as “Machado Disease”<sup>420</sup>. The Thomas family, also of Azorean ancestry, was reported in 1972 by Woods and colleagues with a disease characterized by some similar symptoms that was defined as “Nigro-spino-dentatal degeneration with nuclear ophthalmoplegia”<sup>421</sup>. A few years later, Rosenberg and colleagues described a “particular type of autosomal dominant hereditary ataxia” in the family of Antone Joseph, which was designated as Joseph disease<sup>422</sup>. In 1978, Coutinho and Andrade carry out several studies in a large number of Azorean families and presented an “autosomal dominant system degeneration in Portuguese families of the Azores Islands”<sup>423</sup>. In the 80's, Lima and Coutinho proposed for the first time the name MJD, and described this as a single disorder characterized by a high clinical variability, proposing the clinical classification of patients into three types that clustered all this variability<sup>424</sup>. MJD is considered rare, (global prevalence of 1:100000<sup>22,425</sup>) with its prevalence varying according to the population studied; however, in the Azorean island of Flores its prevalence is reported to be 1:140.

Initially, MJD was considered a “Portuguese disease”, but nowadays numerous families have been all diagnosed around the world<sup>426,427</sup>.

### 1.2.3 Clinical and Neuropathology presentation

The central clinical feature in MJD is a slowly progressive ataxia, being the average age at onset 37 years and the mean survival time of 21 years<sup>424</sup>, during which the intellect is preserved<sup>423</sup>. The maintenance of the cognitive function is a key feature of MJD in its differential diagnosis among the vast group of SCAs. The severity of the disease is associated to the age of onset, an earlier onset being related with a more severe and rapidly progressive form of the disease. MJD patients usually present ataxia, pyramidal and extrapyramidal signs, progressive external ophthalmoplegia, peripheral amyotrophies, with weakness in the arms and legs, intention fasciculation-like movements of facial and lingual muscles, rigidity, and bulging eyes<sup>422,423,428</sup>. The clinical spectrum of MJD is highly pleomorphic and led to the definition of four clinical sub-types, according to the age of clinical onset and major symptoms of the disorder. **MJD type I** includes the MJD forms with early age at onset (10-30 years of age), faster progression and more intense pyramidal and extra-pyramidal signs such as dystonia, tremors and parkinsonism. **MJD type II** is the most frequent, and is characterized by intermediate age-at-onset (20-50 years of age) and progression, with patients presenting ataxia and ophthalmoplegia. MJD patients with **MJD type III** exhibit the latest age at onset (40-70 years of age), slow disease progression and more peripheral signs (peripheral neuropathy and amyotrophy). In 1983, Roger Rosenberg further added a **fourth type**, which is the rarest and includes MJD patients exhibiting Parkinsonic symptoms associated with the most typical symptoms of MJD<sup>418,429</sup>.

At neuropathological level, MJD is characterized by neuronal loss in the deep cerebellar nuclei, substantia nigra, thalamus, striatum, pontine nuclei, spinal cord and cranial nerves, pre-cerebellar brainstem, cholinergic and dopaminergic midbrain, as well as visual, auditory, vestibular, somatosensory, and ingestion and urination-related systems (Figure 4). Preserved integrity of the cortical and subcortical regions of the limbic system and mild degeneration of cerebral and cerebellar cortices, white matter of cerebellum, inferior olive and Purkinje cells, are also characteristic of MJD<sup>423,430-435</sup>. The majority of the MJD patients' brains with disease duration of more than 15 years showed reduced brain weight when compared with individuals without medical histories of neurological or psychiatric diseases<sup>436</sup>. An enlargement of the fourth ventricle, atrophy of the pons, cerebellar vermis and hemispheres, basal ganglia, midbrain, medulla oblongata and spinal cord was revealed through magnetic resonance imaging (MRI) and neuroimaging studies<sup>437-440</sup>. Concerning brain functionality, a

decreased metabolism in the cerebellum, brainstem, cerebral cortex, thalamus and putamen was observed through magnetic spectroscopy analysis, suggestive of axonal dysfunction, at symptomatic ages<sup>441-445</sup>.

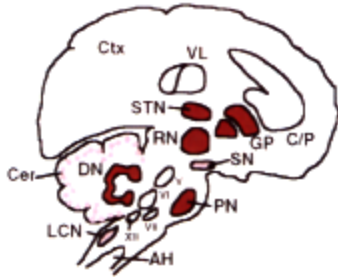


**Figure 4.** Main MJD affected brain regions are depicted in red. Adapted from<sup>31</sup>. STN: subthalamic nucleus, GP: globus pallidus, RN: red nucleus, SN: substantia nigra, PN: pontine nucleus, DN: dentate nucleus, LCN: lateral cuneate nucleus, Cer: cerebellum.

Another neuropathological feature of MJD, as of other polyQ diseases, is the presence of neuronal ubiquitinated inclusions; in which several other proteins are found, such as molecular chaperones, proteasomal components, TFs and both normal and pathogenic ATXN3<sup>139,177,446</sup>.

### 1.2.3 MJD Genetics

MJD is transmitted in an autosomal dominant manner and, as other polyQ diseases, shows intergenerational instability of the expanded CAG repeat. Frequently in polyQ diseases, longer CAG tracts are associated with earlier onset and more severe symptoms<sup>20</sup>, a phenomenon called “anticipation”<sup>20,447</sup>. However, some factors other than the increase of the number of CAG repeat units, may play also a role in genetic anticipation of MJD<sup>448</sup>.

MJD is caused by a mutation in the *ATXN3* gene mapped to the long arm of chromosome 14 (14q32.1)<sup>4</sup>. The gene has around 48 kb and contains 13 exons (two of them recently described), with the (CAG)<sub>n</sub> tract located at exon 10<sup>449,450</sup>. The number of CAG repeats ranges from 12 to 44 CAG’s in the healthy population, whereas expanded alleles typically contain from 52 to 87 repeat units<sup>451,452</sup>. Individuals carrying intermediate CAG repeat units (45-51) may or may not manifest the disease<sup>451,453,454</sup>. It encodes at least, four different transcripts of approximately 1.4, 1.8, 4.5 and 7.5 kb ubiquitously expressed in neuronal and non-neuronal human tissues, reported by Northern-blot<sup>450,455</sup>. These different mRNA types are probably a result from differential splicing of exons 2, 10 and 11 of *ATXN3* gene, and alternative polyadenylation of exon 10<sup>4,450,456</sup>. From sequence analysis of cDNA clones, Ichikawa and colleagues described five cDNA variants: MJD1a, MJD1-1, MJD5-1, MJD2-1 and H2<sup>4,450,456</sup>. The MJD1a was the first variant described and uses exon 10 to provide the 3’-terminal sequence. The MJD1-1 and MJD5-1 variants simply contrast in the size of their 3’ UTR, and have exon 11 as 3’-terminal sequence.

The MJD2-1 is similar to MJD1a except for the single nucleotide substitution in the exon 10 stop codon<sup>456</sup> and in the H2, exon 2 is absent<sup>450</sup>.

A more recent study suggested the existence of 50 additional alternative splicing variants of ATXN3 gene, generated by different types of splicing events<sup>449</sup> proposing that alternative splicing might be an important mechanism regulating ATXN3 expression.

### 1.5.3 MJD protein: ATXN3

The *ATXN3* gene encodes for a 42 KDa protein, ATXN3, which is ubiquitously expressed and contains a conserved N-terminal Josephin domain (1-198 aa), containing the putative catalytic triad aminoacids cysteine (C14), histidine (H119) and asparagine (N134). This domain is followed by two or three ubiquitin-interacting motifs (UIMs), depending on the protein isoform, and the polyQ region of variable length, whose expansion beyond a certain threshold is associated with MJD<sup>457,458</sup>. The UIMs can act either to bind ubiquitin or ubiquitylated proteins, or to promote ubiquitylation (mono-, oligo- and polyubiquitylation)<sup>459</sup>. In the case of ATXN3 they are thought to bind poly ubiquitylated chains. ATXN3 also contains a conserved nuclear-localization signal (NLS)<sup>460</sup>. Similarly, 6 putative nuclear export signal (NES) sequences were found within the ataxin-3 primary structure<sup>449</sup>.

The *ATXN3* gene is present in different organisms, including plants, nematodes and human. Sequence analysis shown that there is a high degree of conservation, at the DNA level, between human *ATXN3* and the corresponding orthologues in rat<sup>461</sup>, mouse<sup>462</sup>, chicken<sup>463</sup>, and *C. elegans*<sup>464</sup>, suggesting evolutionary conserved functions and properties<sup>465</sup>. However, the long polyQ tract seems to be human-specific because it is absent in other species such as mouse and worms that have only six and one glutamines in the ATXN3 homologue, respectively.

A crucial finding in the understanding of ATXN3 function was the discovery of its deubiquitylating (DUB) activity *in vitro*<sup>458,466,467</sup>. Although DUBs are frequently promiscuous, specific substrates have been suggested for ATXN3, namely proteins involved in endoplasmic reticulum-associated degradation (ERAD)<sup>468</sup>. Lately, alpha5 integrin subunit<sup>469</sup> and parkin<sup>470,471</sup> were also found to be specific substrates of ATXN3. Several studies also described the involvement of ATXN3 in transcription regulation<sup>128,464,472</sup>, cytoskeletal organization<sup>170,171,469</sup> and stress responses<sup>473-475</sup>.

#### 1.5.4 Mouse models of MJD

Since the description of the disease-causing gene in MJD, several *in vitro* and *in vivo* models were generated in order to gain insight into the pathogenic mechanism(s) and to develop potential therapies. Although more difficult to generate and less genetically manipulable than cell and invertebrate models, rodent models share important molecular, anatomical and physiological similarities with humans and are relevant for pre-clinical studies aiming at drug discovery and development.

Several mouse (and rat) models have been described for MJD comprising 9 transgenic mouse models<sup>37,66,67,85,126,194,228,476,477</sup>, 1 lentiviral rat model<sup>478</sup>, 2 knock-out (KO) mouse models<sup>461,479</sup> and 2 knock-in (KI) mouse models<sup>68,480</sup>. Transgenic models are the more appropriate not only to study several biological and mechanism feature of the disease, but also for pathology and behavioral phenotype and therefore for pre-clinical trials.

The first transgenic mouse model of MJD was generated in 1996 by Ikeda and colleagues using the truncated and full length cDNA of the *ATXN3* gene, under the control of the L7 promoter which drives expression specifically to the Purkinje cells, which are only mildly affected in MJD<sup>37</sup>. No pathological changes were observed when full-length ataxin3 cDNA was expressed in the cells, while expression of the truncated cDNA led to an early and severe phenotype, together with an extensive degeneration of the cerebellar cortex, which does not reproduce the typical pathology in MJD patients.

Later, another mouse model was generated in an attempt to better replicate the temporal and spatial expression of the human disease gene, using yeast artificial chromosome (YAC) constructs carrying the full-length *ATXN3* gene (plus two additional genes flanking it) with expanded polyQ and its regulatory elements<sup>476</sup>. This was the first heterozygous model expressing the entire human *ATXN3* gene and it developed very mild and slowly progressive cerebellar deficits. With the disease progression, pelvic elevation became significantly flattened, accompanied by hypotonia, motor and sensory loss, tremors and reduced weight gain. This model also displayed cytoplasmic and nuclear ATXN3 aggregates, and neurodegeneration in later stages<sup>476,481,482</sup>. The homozygous version of this model showed more pronounced effects, as characterized later<sup>206</sup>.

Three additional mouse models were generated by Goti, Bichelmeier, Chou and respective colleagues, expressing a pathogenic *ATXN3* isoform (mjd1a or c) under the control of prion protein (Prnp) promoter<sup>85,126,477</sup>. These models display similar phenotypes with early onset motor dysfunction and intranuclear inclusions replicating the MJD symptoms, however, the neurodegeneration profile was not very noteworthy in any of these models. The referred mouse models reproduce many MJD features

such as ataxic symptoms, behavioral deficits, tremors and neuronal dysfunction, however, contrary to what occurs in human patients the neurological symptoms arise very early and the disease progression is very fast. Therefore, Boy and colleagues used the rat *htt* promoter to directly express the mutant ATXN3 in brain which led to weaker expression of the ATXN3 protein but in a ubiquitous manner and a brain distribution consistent with that seen in human patients<sup>66</sup>. This model presents late onset decline of motor coordination with slow progression, Nlls, significant neurodegeneration, however with hyperactivity during the first months. The same authors developed a conditional mouse model with the full-length human *ATXN3* cDNA using a Tet-Off system, in order to analyze whether symptoms caused by ATXN3 with an expanded repeat were reversible *in vivo*<sup>94</sup>. These mice showed motor symptoms and reduced body weight gain but when the expanded ataxin-3 expression was turned off in early symptomatic stages, the phenotype was reversed. However, in this model the expression of the mutant protein in the cerebellum was limited to the glial cells, the involvement of which in MJD has not been described. Also, neurodegeneration was mostly present in Purkinje cells, typically not affected in MJD.

Another rodent model was obtained in 2008 by Alves and colleagues who injected lentivirus expressing human ATXN3 in the striatum of the rat reproducing several cellular aspects of MJD neuropathology such as formation of ubiquitinated Nlls and neuronal demise<sup>478, 483, 484</sup>.

One more model able to recapitulate many features of human disease was described in 2010 by Silva-Fernandes and colleagues, directing the expression of mutant *ATXN3* under the control of cytomegalovirus (CMV) promoter<sup>67</sup>. The mutant protein was ubiquitously distributed throughout the body but only the cerebellum, pontine nuclei, substantia nigra and thalamus were shown to degenerate as the disease progresses. No Nll's were observed in any age of the transgenic mice even with the early symptoms of motor uncoordination. More recently, the same authors described an identical model but with a higher number of repeats which closely recapitulates the human disease in terms of motor symptoms, neuropathology, with severe and progressive phenotype<sup>228</sup>. Recently, two knock-in MJD models have also been described, displaying prominent aggregate pathology but with only one of them displaying a very mild and late onset of motor symptoms<sup>68, 480</sup>.

The importance of having many different animal models of MJD is unquestionable since together they provide the improvement in the clarification of several MJD features and pathogenesis. Despite the pros and cons of each model, some are valuable to understand the different mechanisms of disease progression and others for the development of therapeutic strategies, as they exhibit several MJD-like symptoms.

## 1.6 Aims of the study

Since there is no effective treatment so far for Machado-Joseph disease, the overall objective of this thesis was to develop potential therapeutic strategies for this disorder (hypothesis-based and -free) using the CMVMJD135 mouse model, with phenotypic and neuropathologic features of MJD. With this purpose we aimed to:

1. Study the therapeutic efficacy of chronic treatment with valproic acid in the CMVMJD135 mouse model;
2. Study the therapeutic efficacy of citalopram in the CMVMJD135 mouse model;
3. Unravel the molecular effects of citalopram in the CMVMJD135 mouse model;
4. Study the therapeutic efficacy of citalopram in the CMVMJD135 mouse model using a post-symptomatic treatment and a more severe disease state.

### 1.2.3 Thesis planning

The current thesis is divided into 6 chapters. The Chapter 1 consists of a general introduction; Chapter 2 to 5 comprises the hypothesis-based and hypothesis-free therapeutic approaches in the CMVMJD135 mouse model (in research articles form, published and in preparation); and, in Chapter 6 is provided a general discussion of the thesis.

In **Chapter 1** a general introduction to the thesis is provided. A brief overview on polyglutamine diseases and the major potential pathomechanisms underlying these diseases is presented. A more extensive part of the introduction centers on a general state of the art of the existent therapeutic strategies as well as the complete clinical trials in humans patients for polyQ diseases. In addition, a summary of Machado-Joseph disease and its available mouse models is presented.

In **Chapter 2** the work “Limited effect of chronic valproic acid treatment in a mouse model of Machado-Joseph Disease”, describes a hypothesis-based therapeutic approach with valproic acid. We show that chronic VPA treatment in the CMVMJD135 mouse model had limited effects in the motor deficits of these mice seen, mostly at late stages, without changing the ATXN3 inclusion load in affected brain regions.

In **Chapter 3** the work entitled “Serotonergic signaling suppresses ataxin-3 aggregation, improves motor balance and coordination and exerts neuroprotection effects in a mouse model of Machado-Joseph disease” is provided. In this work, we tested the therapeutic efficacy of chronic pre-symptomatic citalopram treatment in CMVMJD135 with two different dosages. This compound reduced ataxin-3 neuronal inclusions, mitigated neuronal loss and astrogliosis, strikingly ameliorated motor symptoms and exert molecular neuroprotective effects. These results suggest that modulation of serotonergic signaling could be a promising therapeutic strategy for MJD.

**Chapter 4**, “Dissecting the molecular effects of chronic citalopram treatment in an MJD mouse model” focuses on unraveling the molecular changes in the brain responsible for the phenotype amelioration upon citalopram treatment. Some interesting trends was observed towards an increase in neuroprotective molecules, however; without statistical differences. The continuous efforts in understanding, at pathological and molecular levels, the citalopram mode of action in MJD may shed light into the underlying pathogenesis of this disease and into the identification of novel therapeutic targets.

In **Chapter 5**, “Assesment of chronic citalopram post-symptomatic treatment in a MJD mouse model with increased severity“ is presented. In an attempt to better mirror the patients treatment, we performed a post-symptomatic citalopram treatment in a high severity disease condition of the CMVMJD135 mouse model. Citalopram post-symptomatic treatment led to mild improvement in balance and motor coordination in this group of animals with no impact on ATXN3 aggregation and astrogliosis. Efficacy post-symptomatic treatment of citalopram may not be able to improve the symptoms when the disease condition is too severe and fully established, validating this approach but also suggesting that early onset of treatment may be more effective in human patients.

A general discussion of this thesis work and future perspectives are presented in **Chapter 6**.



## 1.7 References

1. Martin, J. B. Molecular basis of the neurodegenerative disorders. *N. Engl. J. Med.* **340**, 1970–1980 (1999).
2. Soto, C. Unfolding the role of protein misfolding in neurodegenerative diseases. *Nat. Rev. Neurosci.* **4**, 49–60 (2003).
3. Bertram, L. & Tanzi, R. E. The genetic epidemiology of neurodegenerative disease. *J. Clin. Invest.* **115**, 1449–1457 (2005).
4. Kawaguchi, Y. *et al.* CAG expansions in a novel gene for Machado-Joseph disease at chromosome 14q32.1. *Nat. Genet.* **8**, 221–228 (1994).
5. A novel gene containing a trinucleotide repeat that is expanded and unstable on Huntington's disease chromosomes. The Huntington's Disease Collaborative Research Group. *Cell* **72**, 971–983 (1993).
6. La Spada, A. R., Wilson, E. M., Lubahn, D. B., Harding, A. E. & Fischbeck, K. H. Androgen receptor gene mutations in X-linked spinal and bulbar muscular atrophy. *Nature* **352**, 77–79 (1991).
7. Nagafuchi, S. *et al.* Dentatorubral and pallidolusian atrophy expansion of an unstable CAG trinucleotide on chromosome 12p. *Nat. Genet.* **6**, 14–18 (1994).
8. Koide, R. *et al.* Unstable expansion of CAG repeat in hereditary dentatorubral-pallidolusian atrophy (DRPLA). *Nat. Genet.* **6**, 9–13 (1994).
9. Orr, H. T. *et al.* Expansion of an unstable trinucleotide CAG repeat in spinocerebellar ataxia type 1. *Nat. Genet.* **4**, 221–226 (1993).
10. Nechiporuk, A. *et al.* Genetic mapping of the spinocerebellar ataxia type 2 gene on human chromosome 12. *Neurology* **46**, 1731–1735 (1996).
11. Imbert, G. *et al.* Cloning of the gene for spinocerebellar ataxia 2 reveals a locus with high sensitivity to expanded CAG/glutamine repeats. *Nat. Genet.* **14**, 285–291 (1996).
12. Sanpei, K. *et al.* Identification of the spinocerebellar ataxia type 2 gene using a direct identification of repeat expansion and cloning technique, DIRECT. *Nat. Genet.* **14**, 277–284 (1996).
13. Zhuchenko, O. *et al.* Autosomal dominant cerebellar ataxia (SCA6) associated with small polyglutamine expansions in the alpha 1A-voltage-dependent calcium channel. *Nat. Genet.* **15**, 62–69 (1997).
14. David, G. *et al.* Molecular and clinical correlations in autosomal dominant cerebellar ataxia with progressive macular dystrophy (SCA7). *Hum. Mol. Genet.* **7**, 165–170 (1998).

15. Holmes, S. E. *et al.* Expansion of a novel CAG trinucleotide repeat in the 5' region of PPP2R2B is associated with SCA12. *Nat. Genet.* **23**, 391–392 (1999).
16. Margulis, B. A., Vigont, V., Lazarev, V. F., Kaznacheyeva, E. V. & Guzhova, I. V. Pharmacological protein targets in polyglutamine diseases: mutant polypeptides and their interactors. *FEBS Lett.* **587**, 1997–2007 (2013).
17. Bauer, P. O. & Nukina, N. The pathogenic mechanisms of polyglutamine diseases and current therapeutic strategies. *J. Neurochem.* **110**, 1737–1765 (2009).
18. Ross, C. A. Intranuclear neuronal inclusions: a common pathogenic mechanism for glutamine-repeat neurodegenerative diseases? *Neuron* **19**, 1147–1150 (1997).
19. Duyao, M. *et al.* Trinucleotide repeat length instability and age of onset in Huntington's disease. *Nat. Genet.* **4**, 387–392 (1993).
20. Maciel, P. *et al.* Correlation between CAG repeat length and clinical features in Machado-Joseph disease. *Am. J. Hum. Genet.* **57**, 54–61 (1995).
21. Rubinsztein, D. C. *et al.* Phenotypic characterization of individuals with 30-40 CAG repeats in the Huntington disease (HD) gene reveals HD cases with 36 repeats and apparently normal elderly individuals with 36-39 repeats. *Am. J. Hum. Genet.* **59**, 16–22 (1996).
22. Schöls, L., Bauer, P., Schmidt, T., Schulte, T. & Riess, O. Autosomal dominant cerebellar ataxias: clinical features, genetics, and pathogenesis. *Lancet Neurol.* **3**, 291–304 (2004).
23. Zoghbi, H. Y. & Orr, H. T. Glutamine repeats and neurodegeneration. *Annu. Rev. Neurosci.* **23**, 217–247 (2000).
24. Davies, S. W. *et al.* Are neuronal intranuclear inclusions the common neuropathology of triplet-repeat disorders with polyglutamine-repeat expansions? *Lancet* **351**, 131–133 (1998).
25. Becher, M. W. & Ross, C. A. Intranuclear neuronal inclusions in DRPLA. *Mov. Disord. Off. J. Mov. Disord. Soc.* **13**, 852–853 (1998).
26. Rolfs, A. *et al.* Clinical features and neuropathology of autosomal dominant spinocerebellar ataxia (SCA17). *Ann. Neurol.* **54**, 367–375 (2003).
27. Holmberg, M. *et al.* Spinocerebellar ataxia type 7 (SCA7): a neurodegenerative disorder with neuronal intranuclear inclusions. *Hum. Mol. Genet.* **7**, 913–918 (1998).
28. Arrasate, M., Mitra, S., Schweitzer, E. S., Segal, M. R. & Finkbeiner, S. Inclusion body formation reduces levels of mutant huntingtin and the risk of neuronal death. *Nature* **431**, 805–810 (2004).
29. Takahashi, T., Katada, S. & Onodera, O. Polyglutamine diseases: where does toxicity come from? what is toxicity? where are we going? *J. Mol. Cell Biol.* **2**, 180–191 (2010).

30. Fan, H.-C. *et al.* Polyglutamine (PolyQ) diseases: genetics to treatments. *Cell Transplant.* **23**, 441–458 (2014).
31. Ross, C. A. When more is less: pathogenesis of glutamine repeat neurodegenerative diseases. *Neuron* **15**, 493–496 (1995).
32. Seidel, K. *et al.* Brain pathology of spinocerebellar ataxias. *Acta Neuropathol. (Berl.)* **124**, 1–21 (2012).
33. Hands, S. L. & Wyttenbach, A. Neurotoxic protein oligomerisation associated with polyglutamine diseases. *Acta Neuropathol. (Berl.)* **120**, 419–437 (2010).
34. Ordway, J. M. *et al.* Ectopically expressed CAG repeats cause intranuclear inclusions and a progressive late onset neurological phenotype in the mouse. *Cell* **91**, 753–763 (1997).
35. Davies, S. W. *et al.* Formation of neuronal intranuclear inclusions underlies the neurological dysfunction in mice transgenic for the HD mutation. *Cell* **90**, 537–548 (1997).
36. Havel, L. S., Li, S. & Li, X.-J. Nuclear accumulation of polyglutamine disease proteins and neuropathology. *Mol. Brain* **2**, 21 (2009).
37. Ikeda, H. *et al.* Expanded polyglutamine in the Machado-Joseph disease protein induces cell death in vitro and in vivo. *Nat. Genet.* **13**, 196–202 (1996).
38. Marsh, J. L. *et al.* Expanded polyglutamine peptides alone are intrinsically cytotoxic and cause neurodegeneration in *Drosophila*. *Hum. Mol. Genet.* **9**, 13–25 (2000).
39. Morley, J. F., Brignull, H. R., Weyers, J. J. & Morimoto, R. I. The threshold for polyglutamine-expansion protein aggregation and cellular toxicity is dynamic and influenced by aging in *Caenorhabditis elegans*. *Proc. Natl. Acad. Sci. U. S. A.* **99**, 10417–10422 (2002).
40. Brignull, H. R., Moore, F. E., Tang, S. J. & Morimoto, R. I. Polyglutamine proteins at the pathogenic threshold display neuron-specific aggregation in a pan-neuronal *Caenorhabditis elegans* model. *J. Neurosci. Off. J. Soc. Neurosci.* **26**, 7597–7606 (2006).
41. Shelbourne, P. F. *et al.* A Huntington's disease CAG expansion at the murine *Hdh* locus is unstable and associated with behavioural abnormalities in mice. *Hum. Mol. Genet.* **8**, 763–774 (1999).
42. Wheeler, V. C. *et al.* Long glutamine tracts cause nuclear localization of a novel form of huntingtin in medium spiny striatal neurons in *HdhQ92* and *HdhQ111* knock-in mice. *Hum. Mol. Genet.* **9**, 503–513 (2000).
43. Lin, C. H. *et al.* Neurological abnormalities in a knock-in mouse model of Huntington's disease. *Hum. Mol. Genet.* **10**, 137–144 (2001).

44. Levine, M. S. *et al.* Enhanced sensitivity to N-methyl-D-aspartate receptor activation in transgenic and knockin mouse models of Huntington's disease. *J. Neurosci. Res.* **58**, 515–532 (1999).
45. Usdin, M. T., Shelbourne, P. F., Myers, R. M. & Madison, D. V. Impaired synaptic plasticity in mice carrying the Huntington's disease mutation. *Hum. Mol. Genet.* **8**, 839–846 (1999).
46. Gusella, J. F. & MacDonald, M. E. Molecular genetics: unmasking polyglutamine triggers in neurodegenerative disease. *Nat. Rev. Neurosci.* **1**, 109–115 (2000).
47. Emamian, E. S. *et al.* Serine 776 of ataxin-1 is critical for polyglutamine-induced disease in SCA1 transgenic mice. *Neuron* **38**, 375–387 (2003).
48. Rudnicki, D. D. & Margolis, R. L. Repeat expansion and autosomal dominant neurodegenerative disorders: consensus and controversy. *Expert Rev. Mol. Med.* **5**, (2003).
49. Mangiarini, L. *et al.* Exon 1 of the HD gene with an expanded CAG repeat is sufficient to cause a progressive neurological phenotype in transgenic mice. *Cell* **87**, 493–506 (1996).
50. Zoghbi, H. Y. & Botas, J. Mouse and fly models of neurodegeneration. *Trends Genet. TIG* **18**, 463–471 (2002).
51. Steffan, J. S. *et al.* The Huntington's disease protein interacts with p53 and CREB-binding protein and represses transcription. *Proc. Natl. Acad. Sci. U. S. A.* **97**, 6763–6768 (2000).
52. Nucifora, F. C. *et al.* Interference by huntingtin and atrophin-1 with cbp-mediated transcription leading to cellular toxicity. *Science* **291**, 2423–2428 (2001).
53. Dunah, A. W. *et al.* Sp1 and TAFII130 transcriptional activity disrupted in early Huntington's disease. *Science* **296**, 2238–2243 (2002).
54. Paulson, H. L. *et al.* Intracellular inclusions of expanded polyglutamine protein in spinocerebellar ataxia type 3. *Neuron* **19**, 333–344 (1997).
55. Stenoien, D. L. *et al.* Polyglutamine-expanded androgen receptors form aggregates that sequester heat shock proteins, proteasome components and SRC-1, and are suppressed by the HDJ-2 chaperone. *Hum. Mol. Genet.* **8**, 731–741 (1999).
56. Chai, Y., Wu, L., Griffin, J. D. & Paulson, H. L. The role of protein composition in specifying nuclear inclusion formation in polyglutamine disease. *J. Biol. Chem.* **276**, 44889–44897 (2001).
57. Apostolinas, S., Rajendren, G., Dobrjansky, A. & Gibson, M. J. Androgen receptor immunoreactivity in specific neural regions in normal and hypogonadal male mice: effect of androgens. *Brain Res.* **817**, 19–24 (1999).
58. Simeoni, S. *et al.* Motoneuronal cell death is not correlated with aggregate formation of androgen receptors containing an elongated polyglutamine tract. *Hum. Mol. Genet.* **9**, 133–144 (2000).

59. Caron, N. S., Hung, C. L., Atwal, R. S. & Truant, R. Live cell imaging and biophotonic methods reveal two types of mutant huntingtin inclusions. *Hum. Mol. Genet.* **23**, 2324–2338 (2014).
60. Becher, M. W. *et al.* Intranuclear neuronal inclusions in Huntington's disease and dentatorubral and pallidoluysian atrophy: correlation between the density of inclusions and IT15 CAG triplet repeat length. *Neurobiol. Dis.* **4**, 387–397 (1998).
61. Reina, C. P., Zhong, X. & Pittman, R. N. Proteotoxic stress increases nuclear localization of ataxin-3. *Hum. Mol. Genet.* **19**, 235–249 (2010).
62. Koyano, S., Iwabuchi, K., Yagishita, S., Kuroiwa, Y. & Uchihara, T. Paradoxical absence of nuclear inclusion in cerebellar Purkinje cells of hereditary ataxias linked to CAG expansion. *J. Neurol. Neurosurg. Psychiatry* **73**, 450–452 (2002).
63. Lunkes, A. & Mandel, J. L. A cellular model that recapitulates major pathogenic steps of Huntington's disease. *Hum. Mol. Genet.* **7**, 1355–1361 (1998).
64. Saudou, F., Finkbeiner, S., Devys, D. & Greenberg, M. E. Huntingtin acts in the nucleus to induce apoptosis but death does not correlate with the formation of intranuclear inclusions. *Cell* **95**, 55–66 (1998).
65. Lunkes, A. *et al.* Properties of polyglutamine expansion in vitro and in a cellular model for Huntington's disease. *Philos. Trans. R. Soc. Lond. B. Biol. Sci.* **354**, 1013–1019 (1999).
66. Boy, J. *et al.* A transgenic mouse model of spinocerebellar ataxia type 3 resembling late disease onset and gender-specific instability of CAG repeats. *Neurobiol. Dis.* **37**, 284–293 (2010).
67. Silva-Fernandes, A. *et al.* Motor uncoordination and neuropathology in a transgenic mouse model of Machado-Joseph disease lacking intranuclear inclusions and ataxin-3 cleavage products. *Neurobiol. Dis.* **40**, 163–176 (2010).
68. Ramani, B. *et al.* A knockin mouse model of spinocerebellar ataxia type 3 exhibits prominent aggregate pathology and aberrant splicing of the disease gene transcript. *Hum. Mol. Genet.* **24**, 1211–1224 (2015).
69. Chai, Y., Koppenhafer, S. L., Shoemith, S. J., Perez, M. K. & Paulson, H. L. Evidence for proteasome involvement in polyglutamine disease: localization to nuclear inclusions in SCA3/MJD and suppression of polyglutamine aggregation in vitro. *Hum. Mol. Genet.* **8**, 673–682 (1999).
70. Schmidt, T. *et al.* Protein surveillance machinery in brains with spinocerebellar ataxia type 3: redistribution and differential recruitment of 26S proteasome subunits and chaperones to neuronal intranuclear inclusions. *Ann. Neurol.* **51**, 302–310 (2002).

71. Chai, Y., Koppenhafer, S. L., Bonini, N. M. & Paulson, H. L. Analysis of the role of heat shock protein (Hsp) molecular chaperones in polyglutamine disease. *J. Neurosci. Off. J. Soc. Neurosci.* **19**, 10338–10347 (1999).
72. Kim, S., Nollen, E. A. A., Kitagawa, K., Bindokas, V. P. & Morimoto, R. I. Polyglutamine protein aggregates are dynamic. *Nat. Cell Biol.* **4**, 826–831 (2002).
73. Cummings, C. J. *et al.* Over-expression of inducible HSP70 chaperone suppresses neuropathology and improves motor function in SCA1 mice. *Hum. Mol. Genet.* **10**, 1511–1518 (2001).
74. Mitsui, K. *et al.* Purification of polyglutamine aggregates and identification of elongation factor-1alpha and heat shock protein 84 as aggregate-interacting proteins. *J. Neurosci. Off. J. Soc. Neurosci.* **22**, 9267–9277 (2002).
75. Ishihara, K. *et al.* Hsp105alpha suppresses the aggregation of truncated androgen receptor with expanded CAG repeats and cell toxicity. *J. Biol. Chem.* **278**, 25143–25150 (2003).
76. Holmberg, C. I., Staniszewski, K. E., Mensah, K. N., Matouschek, A. & Morimoto, R. I. Inefficient degradation of truncated polyglutamine proteins by the proteasome. *EMBO J.* **23**, 4307–4318 (2004).
77. Bence, N. F., Sampat, R. M. & Kopito, R. R. Impairment of the ubiquitin-proteasome system by protein aggregation. *Science* **292**, 1552–1555 (2001).
78. Keller, J. N. & Markesbery, W. R. Proteasome inhibition results in increased poly-ADP-ribosylation: implications for neuron death. *J. Neurosci. Res.* **61**, 436–442 (2000).
79. Ding, Q., Dimayuga, E., Markesbery, W. R. & Keller, J. N. Proteasome inhibition increases DNA and RNA oxidation in astrocyte and neuron cultures. *J. Neurochem.* **91**, 1211–1218 (2004).
80. Qiu, J. H. *et al.* Proteasome inhibitors induce cytochrome c-caspase-3-like protease-mediated apoptosis in cultured cortical neurons. *J. Neurosci. Off. J. Soc. Neurosci.* **20**, 259–265 (2000).
81. Yu, A. *et al.* Protein aggregation can inhibit clathrin-mediated endocytosis by chaperone competition. *Proc. Natl. Acad. Sci. U. S. A.* **111**, E1481–1490 (2014).
82. Paulson, H. L. Protein fate in neurodegenerative proteinopathies: polyglutamine diseases join the (mis)fold. *Am. J. Hum. Genet.* **64**, 339–345 (1999).
83. Paulson, H. L., Bonini, N. M. & Roth, K. A. Polyglutamine disease and neuronal cell death. *Proc. Natl. Acad. Sci. U. S. A.* **97**, 12957–12958 (2000).
84. Lunke, A. *et al.* Proteases acting on mutant huntingtin generate cleaved products that differentially build up cytoplasmic and nuclear inclusions. *Mol. Cell* **10**, 259–269 (2002).

85. Goti, D. *et al.* A mutant ataxin-3 putative-cleavage fragment in brains of Machado-Joseph disease patients and transgenic mice is cytotoxic above a critical concentration. *J. Neurosci. Off. J. Soc. Neurosci.* **24**, 10266–10279 (2004).
86. Gardian, G. *et al.* Neuroprotective effects of phenylbutyrate in the N171-82Q transgenic mouse model of Huntington's disease. *J. Biol. Chem.* **280**, 556–563 (2005).
87. Peters, M. F. *et al.* Nuclear targeting of mutant Huntingtin increases toxicity. *Mol. Cell. Neurosci.* **14**, 121–128 (1999).
88. Martín-Aparicio, E., Avila, J. & Lucas, J. J. Nuclear localization of N-terminal mutant huntingtin is cell cycle dependent. *Eur. J. Neurosci.* **16**, 355–359 (2002).
89. Yang, W., Dunlap, J. R., Andrews, R. B. & Wetzel, R. Aggregated polyglutamine peptides delivered to nuclei are toxic to mammalian cells. *Hum. Mol. Genet.* **11**, 2905–2917 (2002).
90. Goldberg, Y. P. *et al.* Cleavage of huntingtin by apopain, a proapoptotic cysteine protease, is modulated by the polyglutamine tract. *Nat. Genet.* **13**, 442–449 (1996).
91. Kobayashi, Y. *et al.* Caspase-3 cleaves the expanded androgen receptor protein of spinal and bulbar muscular atrophy in a polyglutamine repeat length-dependent manner. *Biochem. Biophys. Res. Commun.* **252**, 145–150 (1998).
92. Wellington, C. L. *et al.* Caspase cleavage of gene products associated with triplet expansion disorders generates truncated fragments containing the polyglutamine tract. *J. Biol. Chem.* **273**, 9158–9167 (1998).
93. Berke, S. J. S., Schmied, F. A. F., Brunt, E. R., Ellerby, L. M. & Paulson, H. L. Caspase-mediated proteolysis of the polyglutamine disease protein ataxin-3. *J. Neurochem.* **89**, 908–918 (2004).
94. Ellerby, L. M. *et al.* Kennedy's disease: caspase cleavage of the androgen receptor is a crucial event in cytotoxicity. *J. Neurochem.* **72**, 185–195 (1999).
95. Igarashi, S. *et al.* Suppression of aggregate formation and apoptosis by transglutaminase inhibitors in cells expressing truncated DRPLA protein with an expanded polyglutamine stretch. *Nat. Genet.* **18**, 111–117 (1998).
96. Hackam, A. S. *et al.* Evidence for both the nucleus and cytoplasm as subcellular sites of pathogenesis in Huntington's disease in cell culture and in transgenic mice expressing mutant huntingtin. *Philos. Trans. R. Soc. Lond. B. Biol. Sci.* **354**, 1047–1055 (1999).
97. Cooper, J. K. *et al.* Truncated N-terminal fragments of huntingtin with expanded glutamine repeats form nuclear and cytoplasmic aggregates in cell culture. *Hum. Mol. Genet.* **7**, 783–790 (1998).

98. Martindale, D. *et al.* Length of huntingtin and its polyglutamine tract influences localization and frequency of intracellular aggregates. *Nat. Genet.* **18**, 150–154 (1998).
99. Merry, D. E., Kobayashi, Y., Bailey, C. K., Taye, A. A. & Fischbeck, K. H. Cleavage, aggregation and toxicity of the expanded androgen receptor in spinal and bulbar muscular atrophy. *Hum. Mol. Genet.* **7**, 693–701 (1998).
100. Teixeira-Castro, A. *et al.* Neuron-specific proteotoxicity of mutant ataxin-3 in *C. elegans*: rescue by the DAF-16 and HSF-1 pathways. *Hum. Mol. Genet.* **20**, 2996–3009 (2011).
101. Fei, E. *et al.* Phosphorylation of ataxin-3 by glycogen synthase kinase 3 $\beta$  at serine 256 regulates the aggregation of ataxin-3. *Biochem. Biophys. Res. Commun.* **357**, 487–492 (2007).
102. Mueller, T. *et al.* CK2-dependent phosphorylation determines cellular localization and stability of ataxin-3. *Hum. Mol. Genet.* **18**, 3334–3343 (2009).
103. Chen, H.-K. *et al.* Interaction of Akt-phosphorylated ataxin-1 with 14-3-3 mediates neurodegeneration in spinocerebellar ataxia type 1. *Cell* **113**, 457–468 (2003).
104. Beal, M. F. Mitochondria, free radicals, and neurodegeneration. *Curr. Opin. Neurobiol.* **6**, 661–666 (1996).
105. Lenaz, G. *et al.* Mitochondrial bioenergetics in aging. *Biochim. Biophys. Acta* **1459**, 397–404 (2000).
106. Costa, V. & Scorrano, L. Shaping the role of mitochondria in the pathogenesis of Huntington's disease. *EMBO J.* **31**, 1853–1864 (2012).
107. Chakraborty, J., Rajamma, U. & Mohanakumar, K. P. A mitochondrial basis for Huntington's disease: therapeutic prospects. *Mol. Cell. Biochem.* **389**, 277–291 (2014).
108. Chou, A.-H. *et al.* Polyglutamine-expanded ataxin-3 activates mitochondrial apoptotic pathway by upregulating Bax and downregulating Bcl-xL. *Neurobiol. Dis.* **21**, 333–345 (2006).
109. Yu, Y.-C., Kuo, C.-L., Cheng, W.-L., Liu, C.-S. & Hsieh, M. Decreased antioxidant enzyme activity and increased mitochondrial DNA damage in cellular models of Machado-Joseph disease. *J. Neurosci. Res.* **87**, 1884–1891 (2009).
110. Kaplan, J. Spinocerebellar ataxias due to mitochondrial defects. *Neurochem. Int.* **40**, 553–557 (2002).
111. Grünewald, T. & Beal, M. F. Bioenergetics in Huntington's disease. *Ann. N. Y. Acad. Sci.* **893**, 203–213 (1999).
112. Panov, A. V. *et al.* Early mitochondrial calcium defects in Huntington's disease are a direct effect of polyglutamines. *Nat. Neurosci.* **5**, 731–736 (2002).



113. Wang, Q., Li, L. & Ye, Y. Regulation of retrotranslocation by p97-associated deubiquitinating enzyme ataxin-3. *J. Cell Biol.* **174**, 963–971 (2006).
114. Verkhratsky, A., Orkand, R. K. & Kettenmann, H. Glial calcium: homeostasis and signaling function. *Physiol. Rev.* **78**, 99–141 (1998).
115. Pandey, M., Mohanakumar, K. P. & Usha, R. Mitochondrial functional alterations in relation to pathophysiology of Huntington's disease. *J. Bioenerg. Biomembr.* **42**, 217–226 (2010).
116. Chang, D. T. W., Rintoul, G. L., Pandipati, S. & Reynolds, I. J. Mutant huntingtin aggregates impair mitochondrial movement and trafficking in cortical neurons. *Neurobiol. Dis.* **22**, 388–400 (2006).
117. Orr, A. L. *et al.* N-terminal mutant huntingtin associates with mitochondria and impairs mitochondrial trafficking. *J. Neurosci. Off. J. Soc. Neurosci.* **28**, 2783–2792 (2008).
118. Sun, J., Xu, H., Negi, S., Subramony, S. H. & Hebert, M. D. Differential effects of polyglutamine proteins on nuclear organization and artificial reporter splicing. *J. Neurosci. Res.* **85**, 2306–2317 (2007).
119. Mohan, R. D., Abmayr, S. M. & Workman, J. L. The expanding role for chromatin and transcription in polyglutamine disease. *Curr. Opin. Genet. Dev.* **26**, 96–104 (2014).
120. Kumar, A., Vaish, M. & Ratan, R. R. Transcriptional dysregulation in Huntington's disease: a failure of adaptive transcriptional homeostasis. *Drug Discov. Today* **19**, 956–962 (2014).
121. Yang, W., Dunlap, J. R., Andrews, R. B. & Wetzel, R. Aggregated polyglutamine peptides delivered to nuclei are toxic to mammalian cells. *Hum. Mol. Genet.* **11**, 2905–2917 (2002).
122. Huynh, D. P., Figueroa, K., Hoang, N. & Pulst, S. M. Nuclear localization or inclusion body formation of ataxin-2 are not necessary for SCA2 pathogenesis in mouse or human. *Nat. Genet.* **26**, 44–50 (2000).
123. DiFiglia, M. Huntingtin fragments that aggregate go their separate ways. *Mol. Cell* **10**, 224–225 (2002).
124. Hayashi, M., Kobayashi, K. & Furuta, H. Immunohistochemical study of neuronal intranuclear and cytoplasmic inclusions in Machado-Joseph disease. *Psychiatry Clin. Neurosci.* **57**, 205–213 (2003).
125. Hübener, J. *et al.* N-terminal ataxin-3 causes neurological symptoms with inclusions, endoplasmic reticulum stress and ribosomal dislocation. *Brain J. Neurol.* **134**, 1925–1942 (2011).
126. Bichelmeier, U. *et al.* Nuclear localization of ataxin-3 is required for the manifestation of symptoms in SCA3: in vivo evidence. *J. Neurosci. Off. J. Soc. Neurosci.* **27**, 7418–7428 (2007).

127. Okazawa, H. Polyglutamine diseases: a transcription disorder? *Cell. Mol. Life Sci. CMLS* **60**, 1427–1439 (2003).
128. Li, F., Macfarlan, T., Pittman, R. N. & Chakravarti, D. Ataxin-3 is a histone-binding protein with two independent transcriptional corepressor activities. *J. Biol. Chem.* **277**, 45004–45012 (2002).
129. Okazawa, H. *et al.* Interaction between mutant ataxin-1 and PQBP-1 affects transcription and cell death. *Neuron* **34**, 701–713 (2002).
130. Wood, J. D. *et al.* Atrophin-1, the dentato-rubral and pallido-luysian atrophy gene product, interacts with ETO/MTG8 in the nuclear matrix and represses transcription. *J. Cell Biol.* **150**, 939–948 (2000).
131. Helmlinger, D. *et al.* Ataxin-7 is a subunit of GCN5 histone acetyltransferase-containing complexes. *Hum. Mol. Genet.* **13**, 1257–1265 (2004).
132. Doi, H. *et al.* RNA-binding protein TLS is a major nuclear aggregate-interacting protein in huntingtin exon 1 with expanded polyglutamine-expressing cells. *J. Biol. Chem.* **283**, 6489–6500 (2008).
133. McCampbell, A. *et al.* CREB-binding protein sequestration by expanded polyglutamine. *Hum. Mol. Genet.* **9**, 2197–2202 (2000).
134. Taylor, J. P. *et al.* Aberrant histone acetylation, altered transcription, and retinal degeneration in a *Drosophila* model of polyglutamine disease are rescued by CREB-binding protein. *Genes Dev.* **17**, 1463–1468 (2003).
135. Ström, A.-L., Forsgren, L. & Holmberg, M. A role for both wild-type and expanded ataxin-7 in transcriptional regulation. *Neurobiol. Dis.* **20**, 646–655 (2005).
136. Stenoien, D. L., Mielke, M. & Mancini, M. A. Intranuclear ataxin1 inclusions contain both fast- and slow-exchanging components. *Nat. Cell Biol.* **4**, 806–810 (2002).
137. Obrietan, K. & Hoyt, K. R. CRE-mediated transcription is increased in Huntington's disease transgenic mice. *J. Neurosci. Off. J. Soc. Neurosci.* **24**, 791–796 (2004).
138. Yu, Z.-X., Li, S.-H., Nguyen, H.-P. & Li, X.-J. Huntingtin inclusions do not deplete polyglutamine-containing transcription factors in HD mice. *Hum. Mol. Genet.* **11**, 905–914 (2002).
139. Perez, M. K. *et al.* Recruitment and the role of nuclear localization in polyglutamine-mediated aggregation. *J. Cell Biol.* **143**, 1457–1470 (1998).
140. Uchihara, T. *et al.* Non-expanded polyglutamine proteins in intranuclear inclusions of hereditary ataxias—triple-labeling immunofluorescence study. *Acta Neuropathol. (Berl.)* **102**, 149–152 (2001).

141. van Roon-Mom, W. M. C. *et al.* Insoluble TATA-binding protein accumulation in Huntington's disease cortex. *Brain Res. Mol. Brain Res.* **109**, 1–10 (2002).
142. Tanese, N. & Tjian, R. Coactivators and TAFs: a new class of eukaryotic transcription factors that connect activators to the basal machinery. *Cold Spring Harb. Symp. Quant. Biol.* **58**, 179–185 (1993).
143. Shimohata, T. *et al.* Expanded polyglutamine stretches interact with TAFII130, interfering with CREB-dependent transcription. *Nat. Genet.* **26**, 29–36 (2000).
144. Yvert, G. *et al.* SCA7 mouse models show selective stabilization of mutant ataxin-7 and similar cellular responses in different neuronal cell types. *Hum. Mol. Genet.* **10**, 1679–1692 (2001).
145. Ogryzko, V. V., Schiltz, R. L., Russanova, V., Howard, B. H. & Nakatani, Y. The transcriptional coactivators p300 and CBP are histone acetyltransferases. *Cell* **87**, 953–959 (1996).
146. Steffan, J. S. *et al.* Histone deacetylase inhibitors arrest polyglutamine-dependent neurodegeneration in *Drosophila*. *Nature* **413**, 739–743 (2001).
147. Valor, L. M., Guiretti, D., Lopez-Atalaya, J. P. & Barco, A. Genomic landscape of transcriptional and epigenetic dysregulation in early onset polyglutamine disease. *J. Neurosci. Off. J. Soc. Neurosci.* **33**, 10471–10482 (2013).
148. Luthi-Carter, R. *et al.* Dysregulation of gene expression in the R6/2 model of polyglutamine disease: parallel changes in muscle and brain. *Hum. Mol. Genet.* **11**, 1911–1926 (2002).
149. Luthi-Carter, R. *et al.* Polyglutamine and transcription: gene expression changes shared by DRPLA and Huntington's disease mouse models reveal context-independent effects. *Hum. Mol. Genet.* **11**, 1927–1937 (2002).
150. Serra, H. G. *et al.* Gene profiling links SCA1 pathophysiology to glutamate signaling in Purkinje cells of transgenic mice. *Hum. Mol. Genet.* **13**, 2535–2543 (2004).
151. Friedrich, B. *et al.* Comparative analyses of Purkinje cell gene expression profiles reveal shared molecular abnormalities in models of different polyglutamine diseases. *Brain Res.* **1481**, 37–48 (2012).
152. Halievski, K., Mo, K., Westwood, J. T. & Monks, D. A. Transcriptional profile of muscle following acute induction of symptoms in a mouse model of Kennedy's disease/spinobulbar muscular atrophy. *PLoS One* **10**, e0118120 (2015).
153. Seidel, K. *et al.* Axonal inclusions in spinocerebellar ataxia type 3. *Acta Neuropathol. (Berl.)* **120**, 449–460 (2010).

154. Lee, W.-C. M., Yoshihara, M. & Littleton, J. T. Cytoplasmic aggregates trap polyglutamine-containing proteins and block axonal transport in a *Drosophila* model of Huntington's disease. *Proc. Natl. Acad. Sci. U. S. A.* **101**, 3224–3229 (2004).
155. Piccioni, F. *et al.* Androgen receptor with elongated polyglutamine tract forms aggregates that alter axonal trafficking and mitochondrial distribution in motor neuronal processes. *FASEB J. Off. Publ. Fed. Am. Soc. Exp. Biol.* **16**, 1418–1420 (2002).
156. Krench, M. & Littleton, J. T. Modeling Huntington disease in *Drosophila*: Insights into axonal transport defects and modifiers of toxicity. *Fly (Austin)* **7**, 229–236 (2013).
157. Charrin, B. C., Saudou, F. & Humbert, S. Axonal transport failure in neurodegenerative disorders: the case of Huntington's disease. *Pathol. Biol. (Paris)* **53**, 189–192 (2005).
158. Feany, M. B. & La Spada, A. R. Polyglutamines stop traffic: axonal transport as a common target in neurodegenerative diseases. *Neuron* **40**, 1–2 (2003).
159. Block-Galarza, J. *et al.* Fast transport and retrograde movement of huntingtin and HAP 1 in axons. *Neuroreport* **8**, 2247–2251 (1997).
160. Gunawardena, S. *et al.* Disruption of axonal transport by loss of huntingtin or expression of pathogenic polyQ proteins in *Drosophila*. *Neuron* **40**, 25–40 (2003).
161. Martin, M. *et al.* Cytoplasmic dynein, the dynactin complex, and kinesin are interdependent and essential for fast axonal transport. *Mol. Biol. Cell* **10**, 3717–3728 (1999).
162. Li, S. H., Gutekunst, C. A., Hersch, S. M. & Li, X. J. Interaction of huntingtin-associated protein with dynactin P150Glued. *J. Neurosci. Off. J. Soc. Neurosci.* **18**, 1261–1269 (1998).
163. Reddy, P. H. & Shirendeb, U. P. Mutant huntingtin, abnormal mitochondrial dynamics, defective axonal transport of mitochondria, and selective synaptic degeneration in Huntington's disease. *Biochim. Biophys. Acta* **1822**, 101–110 (2012).
164. Her, L.-S. & Goldstein, L. S. B. Enhanced sensitivity of striatal neurons to axonal transport defects induced by mutant huntingtin. *J. Neurosci. Off. J. Soc. Neurosci.* **28**, 13662–13672 (2008).
165. Li, H., Li, S. H., Yu, Z. X., Shelbourne, P. & Li, X. J. Huntingtin aggregate-associated axonal degeneration is an early pathological event in Huntington's disease mice. *J. Neurosci. Off. J. Soc. Neurosci.* **21**, 8473–8481 (2001).
166. Smith, G. A. *et al.* Progressive axonal transport and synaptic protein changes correlate with behavioral and neuropathological abnormalities in the heterozygous Q175 KI mouse model of Huntington's disease. *Hum. Mol. Genet.* **23**, 4510–4527 (2014).

167. DiFiglia, M. *et al.* Aggregation of huntingtin in neuronal intranuclear inclusions and dystrophic neurites in brain. *Science* **277**, 1990–1993 (1997).
168. Sapp, E. *et al.* Axonal transport of N-terminal huntingtin suggests early pathology of corticostriatal projections in Huntington disease. *J. Neuropathol. Exp. Neurol.* **58**, 165–173 (1999).
169. Burnett, B. G. & Pittman, R. N. The polyglutamine neurodegenerative protein ataxin 3 regulates aggresome formation. *Proc. Natl. Acad. Sci. U. S. A.* **102**, 4330–4335 (2005).
170. Rodrigues, A.-J. *et al.* Absence of ataxin-3 leads to cytoskeletal disorganization and increased cell death. *Biochim. Biophys. Acta* **1803**, 1154–1163 (2010).
171. Neves-Carvalho, A. *et al.* Dominant negative effect of polyglutamine expansion perturbs normal function of ataxin-3 in neuronal cells. *Hum. Mol. Genet.* **24**, 100–117 (2015).
172. Wellington, C. L. & Hayden, M. R. Caspases and neurodegeneration: on the cutting edge of new therapeutic approaches. *Clin. Genet.* **57**, 1–10 (2000).
173. Gervais, F. G. *et al.* Recruitment and activation of caspase-8 by the Huntingtin-interacting protein Hip-1 and a novel partner Hipp1. *Nat. Cell Biol.* **4**, 95–105 (2002).
174. Kouroku, Y. *et al.* Polyglutamine aggregates stimulate ER stress signals and caspase-12 activation. *Hum. Mol. Genet.* **11**, 1505–1515 (2002).
175. Gafni, J. *et al.* Inhibition of calpain cleavage of huntingtin reduces toxicity: accumulation of calpain/caspase fragments in the nucleus. *J. Biol. Chem.* **279**, 20211–20220 (2004).
176. Sánchez, I. *et al.* Caspase-8 is required for cell death induced by expanded polyglutamine repeats. *Neuron* **22**, 623–633 (1999).
177. Chai, Y., Koppenhafer, S. L., Bonini, N. M. & Paulson, H. L. Analysis of the role of heat shock protein (Hsp) molecular chaperones in polyglutamine disease. *J. Neurosci. Off. J. Soc. Neurosci.* **19**, 10338–10347 (1999).
178. Evert, B. O. *et al.* High level expression of expanded full-length ataxin-3 in vitro causes cell death and formation of intranuclear inclusions in neuronal cells. *Hum. Mol. Genet.* **8**, 1169–1176 (1999).
179. Ikeda, H. *et al.* Expanded polyglutamine in the Machado-Joseph disease protein induces cell death in vitro and in vivo. *Nat. Genet.* **13**, 196–202 (1996).
180. Kim, M. *et al.* Mutant huntingtin expression in clonal striatal cells: dissociation of inclusion formation and neuronal survival by caspase inhibition. *J. Neurosci. Off. J. Soc. Neurosci.* **19**, 964–973 (1999).
181. Miyashita, T. *et al.* Expression of extended polyglutamine sequentially activates initiator and effector caspases. *Biochem. Biophys. Res. Commun.* **257**, 724–730 (1999).

182. Moulder, K. L., Onodera, O., Burke, J. R., Strittmatter, W. J. & Johnson, E. M. Generation of neuronal intranuclear inclusions by polyglutamine-GFP: analysis of inclusion clearance and toxicity as a function of polyglutamine length. *J. Neurosci. Off. J. Soc. Neurosci.* **19**, 705–715 (1999).
183. Jackson, G. R. *et al.* Polyglutamine-expanded human huntingtin transgenes induce degeneration of *Drosophila* photoreceptor neurons. *Neuron* **21**, 633–642 (1998).
184. Warrick, J. M. *et al.* Expanded polyglutamine protein forms nuclear inclusions and causes neural degeneration in *Drosophila*. *Cell* **93**, 939–949 (1998).
185. Faber, P. W., Alter, J. R., MacDonald, M. E. & Hart, A. C. Polyglutamine-mediated dysfunction and apoptotic death of a *Caenorhabditis elegans* sensory neuron. *Proc. Natl. Acad. Sci. U. S. A.* **96**, 179–184 (1999).
186. Reddy, P. H. *et al.* Transgenic mice expressing mutated full-length HD cDNA: a paradigm for locomotor changes and selective neuronal loss in Huntington's disease. *Philos. Trans. R. Soc. Lond. B. Biol. Sci.* **354**, 1035–1045 (1999).
187. Hodgson, J. G. *et al.* A YAC mouse model for Huntington's disease with full-length mutant huntingtin, cytoplasmic toxicity, and selective striatal neurodegeneration. *Neuron* **23**, 181–192 (1999).
188. Rami, A. Review: autophagy in neurodegeneration: firefighter and/or incendiary? *Neuropathol. Appl. Neurobiol.* **35**, 449–461 (2009).
189. Offen, D., Elkon, H. & Melamed, E. Apoptosis as a general cell death pathway in neurodegenerative diseases. *J. Neural Transm. Suppl.* 153–166 (2000).
190. Tait, S. W. G., Ichim, G. & Green, D. R. Die another way—non-apoptotic mechanisms of cell death. *J. Cell Sci.* **127**, 2135–2144 (2014).
191. Bauer, P. O. & Nukina, N. The pathogenic mechanisms of polyglutamine diseases and current therapeutic strategies. *J. Neurochem.* **110**, 1737–1765 (2009).
192. Yamamoto, A., Lucas, J. J. & Hen, R. Reversal of neuropathology and motor dysfunction in a conditional model of Huntington's disease. *Cell* **101**, 57–66 (2000).
193. Régulier, E., Trottier, Y., Perrin, V., Aebischer, P. & Déglon, N. Early and reversible neuropathology induced by tetracycline-regulated lentiviral overexpression of mutant huntingtin in rat striatum. *Hum. Mol. Genet.* **12**, 2827–2836 (2003).
194. Boy, J. *et al.* Reversibility of symptoms in a conditional mouse model of spinocerebellar ataxia type 3. *Hum. Mol. Genet.* **18**, 4282–4295 (2009).

195. Zu, T. *et al.* Recovery from polyglutamine-induced neurodegeneration in conditional SCA1 transgenic mice. *J. Neurosci. Off. J. Soc. Neurosci.* **24**, 8853–8861 (2004).
196. Latouche, M. *et al.* A conditional pan-neuronal Drosophila model of spinocerebellar ataxia 7 with a reversible adult phenotype suitable for identifying modifier genes. *J. Neurosci. Off. J. Soc. Neurosci.* **27**, 2483–2492 (2007).
197. Caplen, N. J. *et al.* Rescue of polyglutamine-mediated cytotoxicity by double-stranded RNA-mediated RNA interference. *Hum. Mol. Genet.* **11**, 175–184 (2002).
198. Xia, H. *et al.* RNAi suppresses polyglutamine-induced neurodegeneration in a model of spinocerebellar ataxia. *Nat. Med.* **10**, 816–820 (2004).
199. Lee, Y. *et al.* miR-19, miR-101 and miR-130 co-regulate ATXN1 levels to potentially modulate SCA1 pathogenesis. *Nat. Neurosci.* **11**, 1137–1139 (2008).
200. Huang, F. *et al.* miR-25 alleviates polyQ-mediated cytotoxicity by silencing ATXN3. *FEBS Lett.* **588**, 4791–4798 (2014).
201. Harper, S. Q. *et al.* RNA interference improves motor and neuropathological abnormalities in a Huntington's disease mouse model. *Proc. Natl. Acad. Sci. U. S. A.* **102**, 5820–5825 (2005).
202. Rodriguez-Lebron, E., Denovan-Wright, E. M., Nash, K., Lewin, A. S. & Mandel, R. J. Intrastriatal rAAV-mediated delivery of anti-huntingtin shRNAs induces partial reversal of disease progression in R6/1 Huntington's disease transgenic mice. *Mol. Ther. J. Am. Soc. Gene Ther.* **12**, 618–633 (2005).
203. Machida, Y. *et al.* rAAV-mediated shRNA ameliorated neuropathology in Huntington disease model mouse. *Biochem. Biophys. Res. Commun.* **343**, 190–197 (2006).
204. Nóbrega, C. *et al.* Silencing mutant ataxin-3 rescues motor deficits and neuropathology in Machado-Joseph disease transgenic mice. *PLoS One* **8**, e52396 (2013).
205. Nóbrega, C. *et al.* RNA interference mitigates motor and neuropathological deficits in a cerebellar mouse model of Machado-Joseph disease. *PLoS One* **9**, e100086 (2014).
206. Costa, M. do C. *et al.* Toward RNAi therapy for the polyglutamine disease Machado-Joseph disease. *Mol. Ther. J. Am. Soc. Gene Ther.* **21**, 1898–1908 (2013).
207. Morimoto, R. I. Dynamic remodeling of transcription complexes by molecular chaperones. *Cell* **110**, 281–284 (2002).
208. Nollen, E. A. A. & Morimoto, R. I. Chaperoning signaling pathways: molecular chaperones as stress-sensing 'heat shock' proteins. *J. Cell Sci.* **115**, 2809–2816 (2002).

209. Li, L., Saegusa, H. & Tanabe, T. Deficit of heat shock transcription factor 1-heat shock 70 kDa protein 1A axis determines the cell death vulnerability in a model of spinocerebellar ataxia type 6. *Genes Cells Devoted Mol. Cell. Mech.* **14**, 1253–1269 (2009).
210. Zijlstra, M. P. *et al.* Levels of DNAJB family members (HSP40) correlate with disease onset in patients with spinocerebellar ataxia type 3. *Eur. J. Neurosci.* **32**, 760–770 (2010).
211. Huang, S., Ling, J. J., Yang, S., Li, X.-J. & Li, S. Neuronal expression of TATA box-binding protein containing expanded polyglutamine in knock-in mice reduces chaperone protein response by impairing the function of nuclear factor- $\kappa$ B transcription factor. *Brain J. Neurol.* **134**, 1943–1958 (2011).
212. Warrick, J. M. *et al.* Suppression of polyglutamine-mediated neurodegeneration in *Drosophila* by the molecular chaperone HSP70. *Nat. Genet.* **23**, 425–428 (1999).
213. Kobayashi, Y. *et al.* Chaperones Hsp70 and Hsp40 suppress aggregate formation and apoptosis in cultured neuronal cells expressing truncated androgen receptor protein with expanded polyglutamine tract. *J. Biol. Chem.* **275**, 8772–8778 (2000).
214. Bailey, C. K., Andriola, I. F. M., Kampinga, H. H. & Merry, D. E. Molecular chaperones enhance the degradation of expanded polyglutamine repeat androgen receptor in a cellular model of spinal and bulbar muscular atrophy. *Hum. Mol. Genet.* **11**, 515–523 (2002).
215. Cummings, C. J. *et al.* Chaperone suppression of aggregation and altered subcellular proteasome localization imply protein misfolding in SCA1. *Nat. Genet.* **19**, 148–154 (1998).
216. Rimoldi, M., Servadio, A. & Zimarino, V. Analysis of heat shock transcription factor for suppression of polyglutamine toxicity. *Brain Res. Bull.* **56**, 353–362 (2001).
217. Fujimoto, M. *et al.* Active HSF1 significantly suppresses polyglutamine aggregate formation in cellular and mouse models. *J. Biol. Chem.* **280**, 34908–34916 (2005).
218. Fujikake, N. *et al.* Heat shock transcription factor 1-activating compounds suppress polyglutamine-induced neurodegeneration through induction of multiple molecular chaperones. *J. Biol. Chem.* **283**, 26188–26197 (2008).
219. Tanaka, M. *et al.* Trehalose alleviates polyglutamine-mediated pathology in a mouse model of Huntington disease. *Nat. Med.* **10**, 148–154 (2004).
220. Chen, Z.-Z. *et al.* Trehalose attenuates the gait ataxia and gliosis of spinocerebellar ataxia type 17 mice. *Neurochem. Res.* **40**, 800–810 (2015).
221. Katsuno, M. *et al.* Pharmacological induction of heat-shock proteins alleviates polyglutamine-mediated motor neuron disease. *Proc. Natl. Acad. Sci. U. S. A.* **102**, 16801–16806 (2005).



222. Wang, A. M. *et al.* Activation of Hsp70 reduces neurotoxicity by promoting polyglutamine protein degradation. *Nat. Chem. Biol.* **9**, 112–118 (2013).
223. Sittler, A. *et al.* Geldanamycin activates a heat shock response and inhibits huntingtin aggregation in a cell culture model of Huntington's disease. *Hum. Mol. Genet.* **10**, 1307–1315 (2001).
224. Hay, D. G. *et al.* Progressive decrease in chaperone protein levels in a mouse model of Huntington's disease and induction of stress proteins as a therapeutic approach. *Hum. Mol. Genet.* **13**, 1389–1405 (2004).
225. Auluck, P. K., Meulener, M. C. & Bonini, N. M. Mechanisms of Suppression of {alpha}-Synuclein Neurotoxicity by Geldanamycin in *Drosophila*. *J. Biol. Chem.* **280**, 2873–2878 (2005).
226. Waza, M. *et al.* 17-AAG, an Hsp90 inhibitor, ameliorates polyglutamine-mediated motor neuron degeneration. *Nat. Med.* **11**, 1088–1095 (2005).
227. Tokui, K. *et al.* 17-DMAG ameliorates polyglutamine-mediated motor neuron degeneration through well-preserved proteasome function in an SBMA model mouse. *Hum. Mol. Genet.* **18**, 898–910 (2009).
228. Silva-Fernandes, A. *et al.* Chronic treatment with 17-DMAG improves balance and coordination in a new mouse model of Machado-Joseph disease. *Neurother. J. Am. Soc. Exp. Neurother.* **11**, 433–449 (2014).
229. Malik, B. *et al.* Co-induction of the heat shock response ameliorates disease progression in a mouse model of human spinal and bulbar muscular atrophy: implications for therapy. *Brain J. Neurol.* **136**, 926–943 (2013).
230. Kalmar, B., Edet-Amana, E. & Greensmith, L. Treatment with a coinducer of the heat shock response delays muscle denervation in the SOD1-G93A mouse model of amyotrophic lateral sclerosis. *Amyotroph. Lateral Scler. Off. Publ. World Fed. Neurol. Res. Group Mot. Neuron Dis.* **13**, 378–392 (2012).
231. Phukan, J. Arimoclomol, a coinducer of heat shock proteins for the potential treatment of amyotrophic lateral sclerosis. *IDrugs Investig. Drugs J.* **13**, 482–496 (2010).
232. Wood, N. I., Pallier, P. N., Wanderer, J. & Morton, A. J. Systemic administration of Congo red does not improve motor or cognitive function in R6/2 mice. *Neurobiol. Dis.* **25**, 342–353 (2007).
233. Smith, D. L. *et al.* Minocycline and doxycycline are not beneficial in a model of Huntington's disease. *Ann. Neurol.* **54**, 186–196 (2003).
234. Schilling, G. *et al.* Environmental, pharmacological, and genetic modulation of the HD phenotype in transgenic mice. *Exp. Neurol.* **187**, 137–149 (2004).

235. Dedeoglu, A. *et al.* Therapeutic effects of cystamine in a murine model of Huntington's disease. *J. Neurosci. Off. J. Soc. Neurosci.* **22**, 8942–8950 (2002).
236. Lo, A. S.-Y., Zhu, Q. & Marasco, W. A. Intracellular antibodies (intrabodies) and their therapeutic potential. *Handb. Exp. Pharmacol.* 343–373 (2008). doi:10.1007/978-3-540-73259-4\_15
237. Wang, C.-E. *et al.* Suppression of neuropil aggregates and neurological symptoms by an intracellular antibody implicates the cytoplasmic toxicity of mutant huntingtin. *J. Cell Biol.* **181**, 803–816 (2008).
238. Snyder-Keller, A., McLearn, J. A., Hathorn, T. & Messer, A. Early or late-stage anti-N-terminal Huntingtin intrabody gene therapy reduces pathological features in B6.HDR6/1 mice. *J. Neuropathol. Exp. Neurol.* **69**, 1078–1085 (2010).
239. Kvam, E. *et al.* Conformational targeting of fibrillar polyglutamine proteins in live cells escalates aggregation and cytotoxicity. *PLoS One* **4**, e5727 (2009).
240. Pollitt, S. K. *et al.* A rapid cellular FRET assay of polyglutamine aggregation identifies a novel inhibitor. *Neuron* **40**, 685–694 (2003).
241. Bauer, P. O. *et al.* Inhibition of Rho kinases enhances the degradation of mutant huntingtin. *J. Biol. Chem.* **284**, 13153–13164 (2009).
242. Wong, H. K. *et al.* Blocking acid-sensing ion channel 1 alleviates Huntington's disease pathology via an ubiquitin-proteasome system-dependent mechanism. *Hum. Mol. Genet.* **17**, 3223–3235 (2008).
243. Lee, B.-H. *et al.* Enhancement of proteasome activity by a small-molecule inhibitor of USP14. *Nature* **467**, 179–184 (2010).
244. Anderson, C. *et al.* Loss of Usp14 results in reduced levels of ubiquitin in ataxia mice. *J. Neurochem.* **95**, 724–731 (2005).
245. Crimmins, S. *et al.* Transgenic rescue of ataxia mice with neuronal-specific expression of ubiquitin-specific protease 14. *J. Neurosci. Off. J. Soc. Neurosci.* **26**, 11423–11431 (2006).
246. Al-Ramahi, I. *et al.* CHIP protects from the neurotoxicity of expanded and wild-type ataxin-1 and promotes their ubiquitination and degradation. *J. Biol. Chem.* **281**, 26714–26724 (2006).
247. Adachi, H. *et al.* CHIP overexpression reduces mutant androgen receptor protein and ameliorates phenotypes of the spinal and bulbar muscular atrophy transgenic mouse model. *J. Neurosci. Off. J. Soc. Neurosci.* **27**, 5115–5126 (2007).

248. Tsai, Y. C., Fishman, P. S., Thakor, N. V. & Oyler, G. A. Parkin facilitates the elimination of expanded polyglutamine proteins and leads to preservation of proteasome function. *J. Biol. Chem.* **278**, 22044–22055 (2003).
249. Morishima, Y. *et al.* CHIP deletion reveals functional redundancy of E3 ligases in promoting degradation of both signaling proteins and expanded glutamine proteins. *Hum. Mol. Genet.* **17**, 3942–3952 (2008).
250. Kwak, M.-K., Wakabayashi, N., Greenlaw, J. L., Yamamoto, M. & Kensler, T. W. Antioxidants enhance mammalian proteasome expression through the Keap1-Nrf2 signaling pathway. *Mol. Cell. Biol.* **23**, 8786–8794 (2003).
251. Kwak, M.-K., Cho, J.-M., Huang, B., Shin, S. & Kensler, T. W. Role of increased expression of the proteasome in the protective effects of sulforaphane against hydrogen peroxide-mediated cytotoxicity in murine neuroblastoma cells. *Free Radic. Biol. Med.* **43**, 809–817 (2007).
252. Liu, Y. *et al.* Sulforaphane enhances proteasomal and autophagic activities in mice and is a potential therapeutic reagent for Huntington's disease. *J. Neurochem.* **129**, 539–547 (2014).
253. Meijer, A. J. & Codogno, P. Regulation and role of autophagy in mammalian cells. *Int. J. Biochem. Cell Biol.* **36**, 2445–2462 (2004).
254. Rubinsztein, D. C. Autophagy induction rescues toxicity mediated by proteasome inhibition. *Neuron* **54**, 854–856 (2007).
255. Cuervo, A. M. Autophagy: in sickness and in health. *Trends Cell Biol.* **14**, 70–77 (2004).
256. Menzies, F. M. *et al.* Autophagy induction reduces mutant ataxin-3 levels and toxicity in a mouse model of spinocerebellar ataxia type 3. *Brain J. Neurol.* **133**, 93–104 (2010).
257. Yu, W. H. *et al.* Macroautophagy—a novel Beta-amyloid peptide-generating pathway activated in Alzheimer's disease. *J. Cell Biol.* **171**, 87–98 (2005).
258. Menzies, F. M., Ravikumar, B. & Rubinsztein, D. C. Protective roles for induction of autophagy in multiple proteinopathies. *Autophagy* **2**, 224–225 (2006).
259. Berger, Z. *et al.* Rapamycin alleviates toxicity of different aggregate-prone proteins. *Hum. Mol. Genet.* **15**, 433–442 (2006).
260. Ravikumar, B. *et al.* Inhibition of mTOR induces autophagy and reduces toxicity of polyglutamine expansions in fly and mouse models of Huntington disease. *Nat. Genet.* **36**, 585–595 (2004).
261. Sarkar, S. *et al.* Lithium induces autophagy by inhibiting inositol monophosphatase. *J. Cell Biol.* **170**, 1101–1111 (2005).

262. Xiong, N. *et al.* Potential autophagy enhancers attenuate rotenone-induced toxicity in SH-SY5Y. *Neuroscience* **199**, 292–302 (2011).
263. Wood, N. I. & Morton, A. J. Chronic lithium chloride treatment has variable effects on motor behaviour and survival of mice transgenic for the Huntington's disease mutation. *Brain Res. Bull.* **61**, 375–383 (2003).
264. Watase, K. *et al.* Lithium therapy improves neurological function and hippocampal dendritic arborization in a spinocerebellar ataxia type 1 mouse model. *PLoS Med.* **4**, e182 (2007).
265. Duarte-Silva, S. *et al.* Lithium chloride therapy fails to improve motor function in a transgenic mouse model of Machado-Joseph disease. *Cerebellum Lond. Engl.* **13**, 713–727 (2014).
266. Rose, C. *et al.* Rilmenidine attenuates toxicity of polyglutamine expansions in a mouse model of Huntington's disease. *Hum. Mol. Genet.* **19**, 2144–2153 (2010).
267. Shibata, M. *et al.* Regulation of intracellular accumulation of mutant Huntingtin by Beclin 1. *J. Biol. Chem.* **281**, 14474–14485 (2006).
268. Zhang, L. *et al.* Small molecule regulators of autophagy identified by an image-based high-throughput screen. *Proc. Natl. Acad. Sci. U. S. A.* **104**, 19023–19028 (2007).
269. Jia, K., Hart, A. C. & Levine, B. Autophagy genes protect against disease caused by polyglutamine expansion proteins in *Caenorhabditis elegans*. *Autophagy* **3**, 21–25 (2007).
270. Pandey, U. B., Batlevi, Y., Baehrecke, E. H. & Taylor, J. P. HDAC6 at the intersection of autophagy, the ubiquitin-proteasome system and neurodegeneration. *Autophagy* **3**, 643–645 (2007).
271. Nascimento-Ferreira, I. *et al.* Overexpression of the autophagic beclin-1 protein clears mutant ataxin-3 and alleviates Machado-Joseph disease. *Brain J. Neurol.* **134**, 1400–1415 (2011).
272. Ellerby, L. M. *et al.* Cleavage of atrophin-1 at caspase site aspartic acid 109 modulates cytotoxicity. *J. Biol. Chem.* **274**, 8730–8736 (1999).
273. Wellington, C. L. *et al.* Inhibiting caspase cleavage of huntingtin reduces toxicity and aggregate formation in neuronal and nonneuronal cells. *J. Biol. Chem.* **275**, 19831–19838 (2000).
274. Ratovitski, T. *et al.* N-terminal proteolysis of full-length mutant huntingtin in an inducible PC12 cell model of Huntington's disease. *Cell Cycle Georget. Tex* **6**, 2970–2981 (2007).
275. Miller, J. P. *et al.* Matrix metalloproteinases are modifiers of huntingtin proteolysis and toxicity in Huntington's disease. *Neuron* **67**, 199–212 (2010).
276. Ona, V. O. *et al.* Inhibition of caspase-1 slows disease progression in a mouse model of Huntington's disease. *Nature* **399**, 263–267 (1999).

277. Graham, R. K. *et al.* Levels of mutant huntingtin influence the phenotypic severity of Huntington disease in YAC128 mouse models. *Neurobiol. Dis.* **21**, 444–455 (2006).
278. Waldron-Roby, E. *et al.* Transgenic mouse model expressing the caspase 6 fragment of mutant huntingtin. *J. Neurosci. Off. J. Soc. Neurosci.* **32**, 183–193 (2012).
279. Jung, J., Xu, K., Lessing, D. & Bonini, N. M. Preventing Ataxin-3 protein cleavage mitigates degeneration in a Drosophila model of SCA3. *Hum. Mol. Genet.* **18**, 4843–4852 (2009).
280. Hübener, J. *et al.* Calpain-mediated ataxin-3 cleavage in the molecular pathogenesis of spinocerebellar ataxia type 3 (SCA3). *Hum. Mol. Genet.* **22**, 508–518 (2013).
281. Simões, A. T. *et al.* Calpastatin-mediated inhibition of calpains in the mouse brain prevents mutant ataxin 3 proteolysis, nuclear localization and aggregation, relieving Machado-Joseph disease. *Brain J. Neurol.* **135**, 2428–2439 (2012).
282. Haacke, A., Hartl, F. U. & Breuer, P. Calpain inhibition is sufficient to suppress aggregation of polyglutamine-expanded ataxin-3. *J. Biol. Chem.* **282**, 18851–18856 (2007).
283. Menzies, F. M. *et al.* Calpain inhibition mediates autophagy-dependent protection against polyglutamine toxicity. *Cell Death Differ.* **22**, 433–444 (2015).
284. Sancho, M. *et al.* Minocycline inhibits cell death and decreases mutant Huntingtin aggregation by targeting Apaf-1. *Hum. Mol. Genet.* **20**, 3545–3553 (2011).
285. Evers, M. M. *et al.* Preventing formation of toxic N-terminal huntingtin fragments through antisense oligonucleotide-mediated protein modification. *Nucleic Acid Ther.* **24**, 4–12 (2014).
286. Ono, Y. & Sorimachi, H. Calpains: an elaborate proteolytic system. *Biochim. Biophys. Acta* **1824**, 224–236 (2012).
287. Hyman, B. T. & Yuan, J. Apoptotic and non-apoptotic roles of caspases in neuronal physiology and pathophysiology. *Nat. Rev. Neurosci.* **13**, 395–406 (2012).
288. Weber, J. J., Sowa, A. S., Binder, T. & Hübener, J. From Pathways to Targets: Understanding the Mechanisms behind Polyglutamine Disease. *BioMed Res. Int.* **2014**, 1–22 (2014).
289. Chen, C.-M. Mitochondrial dysfunction, metabolic deficits, and increased oxidative stress in Huntington's disease. *Chang Gung Med. J.* **34**, 135–152 (2011).
290. Ibrahim, W. H., Bhagavan, H. N., Chopra, R. K. & Chow, C. K. Dietary coenzyme Q10 and vitamin E alter the status of these compounds in rat tissues and mitochondria. *J. Nutr.* **130**, 2343–2348 (2000).
291. Ferrante, R. J. *et al.* Therapeutic effects of coenzyme Q10 and remacemide in transgenic mouse models of Huntington's disease. *J. Neurosci. Off. J. Soc. Neurosci.* **22**, 1592–1599 (2002).

292. Smith, K. M. *et al.* Dose ranging and efficacy study of high-dose coenzyme Q10 formulations in Huntington's disease mice. *Biochim. Biophys. Acta* **1762**, 616–626 (2006).
293. Yang, L. *et al.* Combination therapy with coenzyme Q10 and creatine produces additive neuroprotective effects in models of Parkinson's and Huntington's diseases. *J. Neurochem.* **109**, 1427–1439 (2009).
294. Ferrante, R. J. *et al.* Neuroprotective effects of creatine in a transgenic mouse model of Huntington's disease. *J. Neurosci. Off. J. Soc. Neurosci.* **20**, 4389–4397 (2000).
295. Andreassen, O. A. *et al.* Creatine increase survival and delays motor symptoms in a transgenic animal model of Huntington's disease. *Neurobiol. Dis.* **8**, 479–491 (2001).
296. Parker, A. J. *et al.* [Resveratrol rescues mutant polyglutamine cytotoxicity in nematode and mammalian neurons]. *Médecine Sci. MS* **21**, 556–557 (2005).
297. Keene, C. D. *et al.* Tauroursodeoxycholic acid, a bile acid, is neuroprotective in a transgenic animal model of Huntington's disease. *Proc. Natl. Acad. Sci. U. S. A.* **99**, 10671–10676 (2002).
298. Johri, A. & Beal, M. F. Antioxidants in Huntington's disease. *Biochim. Biophys. Acta BBA - Mol. Basis Dis.* **1822**, 664–674 (2012).
299. Johnson, J. A. *et al.* The Nrf2-ARE pathway: an indicator and modulator of oxidative stress in neurodegeneration. *Ann. N. Y. Acad. Sci.* **1147**, 61–69 (2008).
300. Stack, C. *et al.* Triterpenoids CDDO-ethyl amide and CDDO-trifluoroethyl amide improve the behavioral phenotype and brain pathology in a transgenic mouse model of Huntington's disease. *Free Radic. Biol. Med.* **49**, 147–158 (2010).
301. Verbessem, P. *et al.* Creatine supplementation in Huntington's disease: a placebo-controlled pilot trial. *Neurology* **61**, 925–930 (2003).
302. Huntington Study Group. A randomized, placebo-controlled trial of coenzyme Q10 and remacemide in Huntington's disease. *Neurology* **57**, 397–404 (2001).
303. Butler, R. & Bates, G. P. Histone deacetylase inhibitors as therapeutics for polyglutamine disorders. *Nat. Rev. Neurosci.* **7**, 784–796 (2006).
304. Ferrante, R. J. *et al.* Histone deacetylase inhibition by sodium butyrate chemotherapy ameliorates the neurodegenerative phenotype in Huntington's disease mice. *J. Neurosci. Off. J. Soc. Neurosci.* **23**, 9418–9427 (2003).
305. Minamiyama, M. *et al.* Sodium butyrate ameliorates phenotypic expression in a transgenic mouse model of spinal and bulbar muscular atrophy. *Hum. Mol. Genet.* **13**, 1183–1192 (2004).

306. Ying, M. *et al.* Sodium butyrate ameliorates histone hypoacetylation and neurodegenerative phenotypes in a mouse model for DRPLA. *J. Biol. Chem.* **281**, 12580–12586 (2006).
307. Chou, A.-H., Chen, S.-Y., Yeh, T.-H., Weng, Y.-H. & Wang, H.-L. HDAC inhibitor sodium butyrate reverses transcriptional downregulation and ameliorates ataxic symptoms in a transgenic mouse model of SCA3. *Neurobiol. Dis.* **41**, 481–488 (2011).
308. Hockly, E. *et al.* Suberoylanilide hydroxamic acid, a histone deacetylase inhibitor, ameliorates motor deficits in a mouse model of Huntington's disease. *Proc. Natl. Acad. Sci. U. S. A.* **100**, 2041–2046 (2003).
309. Mielcarek, M. *et al.* SAHA decreases HDAC 2 and 4 levels in vivo and improves molecular phenotypes in the R6/2 mouse model of Huntington's disease. *PLoS One* **6**, e27746 (2011).
310. Feng, H.-L. *et al.* Combined lithium and valproate treatment delays disease onset, reduces neurological deficits and prolongs survival in an amyotrophic lateral sclerosis mouse model. *Neuroscience* **155**, 567–572 (2008).
311. Tsai, L.-K., Tsai, M.-S., Ting, C.-H. & Li, H. Multiple therapeutic effects of valproic acid in spinal muscular atrophy model mice. *J. Mol. Med. Berl. Ger.* **86**, 1243–1254 (2008).
312. Zádori, D., Geisz, A., Vámos, E., Vécsei, L. & Klivényi, P. Valproate ameliorates the survival and the motor performance in a transgenic mouse model of Huntington's disease. *Pharmacol. Biochem. Behav.* **94**, 148–153 (2009).
313. Yi, J. *et al.* Sodium valproate alleviates neurodegeneration in SCA3/MJD via suppressing apoptosis and rescuing the hypoacetylation levels of histone H3 and H4. *PLoS One* **8**, e54792 (2013).
314. Lin, X. P. *et al.* Valproic acid attenuates the suppression of acetyl histone H3 and CREB activity in an inducible cell model of Machado-Joseph disease. *Int. J. Dev. Neurosci. Off. J. Int. Soc. Dev. Neurosci.* **38**, 17–22 (2014).
315. Thomas, E. A. *et al.* The HDAC inhibitor 4b ameliorates the disease phenotype and transcriptional abnormalities in Huntington's disease transgenic mice. *Proc. Natl. Acad. Sci. U. S. A.* **105**, 15564–15569 (2008).
316. Ferrante, R. J. *et al.* Chemotherapy for the brain: the antitumor antibiotic mithramycin prolongs survival in a mouse model of Huntington's disease. *J. Neurosci. Off. J. Soc. Neurosci.* **24**, 10335–10342 (2004).
317. Stack, E. C. *et al.* Modulation of nucleosome dynamics in Huntington's disease. *Hum. Mol. Genet.* **16**, 1164–1175 (2007).

318. Zuccato, C. *et al.* Loss of huntingtin-mediated BDNF gene transcription in Huntington's disease. *Science* **293**, 493–498 (2001).
319. Zuccato, C. *et al.* Huntingtin interacts with REST/NRSF to modulate the transcription of NRSE-controlled neuronal genes. *Nat. Genet.* **35**, 76–83 (2003).
320. DeMarch, Z., Giampà, C., Patassini, S., Bernardi, G. & Fusco, F. R. Beneficial effects of rolipram in the R6/2 mouse model of Huntington's disease. *Neurobiol. Dis.* **30**, 375–387 (2008).
321. Giampà, C. *et al.* Phosphodiesterase type IV inhibition prevents sequestration of CREB binding protein, protects striatal parvalbumin interneurons and rescues motor deficits in the R6/2 mouse model of Huntington's disease. *Eur. J. Neurosci.* **29**, 902–910 (2009).
322. Yang, Z. *et al.* ASC-J9 ameliorates spinal and bulbar muscular atrophy phenotype via degradation of androgen receptor. *Nat. Med.* **13**, 348–353 (2007).
323. Hubbert, C. *et al.* HDAC6 is a microtubule-associated deacetylase. *Nature* **417**, 455–458 (2002).
324. Kovacs, J. J. *et al.* HDAC6 regulates Hsp90 acetylation and chaperone-dependent activation of glucocorticoid receptor. *Mol. Cell* **18**, 601–607 (2005).
325. Ren, M., Leng, Y., Jeong, M., Leeds, P. R. & Chuang, D.-M. Valproic acid reduces brain damage induced by transient focal cerebral ischemia in rats: potential roles of histone deacetylase inhibition and heat shock protein induction. *J. Neurochem.* **89**, 1358–1367 (2004).
326. Zhao, Y. *et al.* Lifespan extension and elevated hsp gene expression in *Drosophila* caused by histone deacetylase inhibitors. *J. Exp. Biol.* **208**, 697–705 (2005).
327. Fraczek, J., Vanhaecke, T. & Rogiers, V. Toxicological and metabolic considerations for histone deacetylase inhibitors. *Expert Opin. Drug Metab. Toxicol.* **9**, 441–457 (2013).
328. Selvi, B. R., Cassel, J.-C., Kundu, T. K. & Boutillier, A.-L. Tuning acetylation levels with HAT activators: therapeutic strategy in neurodegenerative diseases. *Biochim. Biophys. Acta* **1799**, 840–853 (2010).
329. Cepeda, C. *et al.* Transient and progressive electrophysiological alterations in the corticostriatal pathway in a mouse model of Huntington's disease. *J. Neurosci. Off. J. Soc. Neurosci.* **23**, 961–969 (2003).
330. Schiefer, J. *et al.* Riluzole prolongs survival time and alters nuclear inclusion formation in a transgenic mouse model of Huntington's disease. *Mov. Disord. Off. J. Mov. Disord. Soc.* **17**, 748–757 (2002).



331. Schiefer, J. *et al.* The metabotropic glutamate receptor 5 antagonist MPEP and the mGluR2 agonist LY379268 modify disease progression in a transgenic mouse model of Huntington's disease. *Brain Res.* **1019**, 246–254 (2004).
332. Chen, M. *et al.* Minocycline inhibits caspase-1 and caspase-3 expression and delays mortality in a transgenic mouse model of Huntington disease. *Nat. Med.* **6**, 797–801 (2000).
333. Stack, E. C. *et al.* Combination therapy using minocycline and coenzyme Q10 in R6/2 transgenic Huntington's disease mice. *Biochim. Biophys. Acta* **1762**, 373–380 (2006).
334. Chintawar, S. *et al.* Grafting neural precursor cells promotes functional recovery in an SCA1 mouse model. *J. Neurosci. Off. J. Soc. Neurosci.* **29**, 13126–13135 (2009).
335. Jin, K. *et al.* FGF-2 promotes neurogenesis and neuroprotection and prolongs survival in a transgenic mouse model of Huntington's disease. *Proc. Natl. Acad. Sci. U. S. A.* **102**, 18189–18194 (2005).
336. Ebert, A. D., Barber, A. E., Heins, B. M. & Svendsen, C. N. Ex vivo delivery of GDNF maintains motor function and prevents neuronal loss in a transgenic mouse model of Huntington's disease. *Exp. Neurol.* **224**, 155–162 (2010).
337. Heiser, V. *et al.* Identification of benzothiazoles as potential polyglutamine aggregation inhibitors of Huntington's disease by using an automated filter retardation assay. *Proc. Natl. Acad. Sci. U. S. A.* **99 Suppl 4**, 16400–16406 (2002).
338. Wang, J., Gines, S., MacDonald, M. E. & Gusella, J. F. Reversal of a full-length mutant huntingtin neuronal cell phenotype by chemical inhibitors of polyglutamine-mediated aggregation. *BMC Neurosci.* **6**, 1 (2005).
339. Nagai, Y. *et al.* Inhibition of polyglutamine protein aggregation and cell death by novel peptides identified by phage display screening. *J. Biol. Chem.* **275**, 10437–10442 (2000).
340. Heiser, V. *et al.* Inhibition of huntingtin fibrillogenesis by specific antibodies and small molecules: implications for Huntington's disease therapy. *Proc. Natl. Acad. Sci. U. S. A.* **97**, 6739–6744 (2000).
341. Mishra, R. *et al.* Inhibiting the nucleation of amyloid structure in a huntingtin fragment by targeting  $\alpha$ -helix-rich oligomeric intermediates. *J. Mol. Biol.* **415**, 900–917 (2012).
342. Fuentealba, R. A., Marasa, J., Diamond, M. I., Piwnicka-Worms, D. & Weihl, C. C. An aggregation sensing reporter identifies leflunomide and teriflunomide as polyglutamine aggregate inhibitors. *Hum. Mol. Genet.* **21**, 664–680 (2012).

343. Ehrnhoefer, D. E. *et al.* Green tea (-)-epigallocatechin-gallate modulates early events in huntingtin misfolding and reduces toxicity in Huntington's disease models. *Hum. Mol. Genet.* **15**, 2743–2751 (2006).
344. Desai, U. A. *et al.* Biologically active molecules that reduce polyglutamine aggregation and toxicity. *Hum. Mol. Genet.* **15**, 2114–2124 (2006).
345. Zhang, X. *et al.* A potent small molecule inhibits polyglutamine aggregation in Huntington's disease neurons and suppresses neurodegeneration in vivo. *Proc. Natl. Acad. Sci. U. S. A.* **102**, 892–897 (2005).
346. Walter, G. M. *et al.* High-throughput screen of natural product extracts in a yeast model of polyglutamine proteotoxicity. *Chem. Biol. Drug Des.* **83**, 440–449 (2014).
347. Piccioni, F., Roman, B. R., Fischbeck, K. H. & Taylor, J. P. A screen for drugs that protect against the cytotoxicity of polyglutamine-expanded androgen receptor. *Hum. Mol. Genet.* **13**, 437–446 (2004).
348. Aiken, C. T., Tobin, A. J. & Schweitzer, E. S. A cell-based screen for drugs to treat Huntington's disease. *Neurobiol. Dis.* **16**, 546–555 (2004).
349. Wang, W. *et al.* Compounds blocking mutant huntingtin toxicity identified using a Huntington's disease neuronal cell model. *Neurobiol. Dis.* **20**, 500–508 (2005).
350. Varma, H. *et al.* Selective inhibitors of death in mutant huntingtin cells. *Nat. Chem. Biol.* **3**, 99–100 (2007).
351. Hoffstrom, B. G. *et al.* Inhibitors of protein disulfide isomerase suppress apoptosis induced by misfolded proteins. *Nat. Chem. Biol.* **6**, 900–906 (2010).
352. Voisine, C. *et al.* Identification of Potential Therapeutic Drugs for Huntington's Disease using *Caenorhabditis elegans*. *PLoS ONE* **2**, e504 (2007).
353. Pruss, R. M. Phenotypic screening strategies for neurodegenerative diseases: a pathway to discover novel drug candidates and potential disease targets or mechanisms. *CNS Neurol. Disord. Drug Targets* **9**, 693–700 (2010).
354. Kaltenbach, L. S. *et al.* Composite primary neuronal high-content screening assay for Huntington's disease incorporating non-cell-autonomous interactions. *J. Biomol. Screen.* **15**, 806–819 (2010).
355. Reinhart, P. H. *et al.* Identification of anti-inflammatory targets for Huntington's disease using a brain slice-based screening assay. *Neurobiol. Dis.* **43**, 248–256 (2011).

356. Schulte, J., Sepp, K. J., Wu, C., Hong, P. & Littleton, J. T. High-content chemical and RNAi screens for suppressors of neurotoxicity in a Huntington's disease model. *PLoS One* **6**, e23841 (2011).
357. Paganetti, P. *et al.* Development of a method for the high-throughput quantification of cellular proteins. *Chembiochem Eur. J. Chem. Biol.* **10**, 1678–1688 (2009).
358. Baldo, B. *et al.* A screen for enhancers of clearance identifies huntingtin as a heat shock protein 90 (Hsp90) client protein. *J. Biol. Chem.* **287**, 1406–1414 (2012).
359. Coufal, M. *et al.* Discovery of a novel small-molecule targeting selective clearance of mutant huntingtin fragments. *J. Biomol. Screen.* **12**, 351–360 (2007).
360. Sarkar, S. *et al.* Small molecules enhance autophagy and reduce toxicity in Huntington's disease models. *Nat. Chem. Biol.* **3**, 331–338 (2007).
361. Calamini, B. *et al.* Small-molecule proteostasis regulators for protein conformational diseases. *Nat. Chem. Biol.* **8**, 185–196 (2012).
362. Neef, D. W., Turski, M. L. & Thiele, D. J. Modulation of heat shock transcription factor 1 as a therapeutic target for small molecule intervention in neurodegenerative disease. *PLoS Biol.* **8**, e1000291 (2010).
363. Lazzeroni, G. *et al.* A phenotypic screening assay for modulators of huntingtin-induced transcriptional dysregulation. *J. Biomol. Screen.* **18**, 984–996 (2013).
364. Wu, J. *et al.* Neuronal store-operated calcium entry pathway as a novel therapeutic target for Huntington's disease treatment. *Chem. Biol.* **18**, 777–793 (2011).
365. Jimonet, P. *et al.* Riluzole series. Synthesis and in vivo 'antiglutamate' activity of 6-substituted-2-benzothiazolamines and 3-substituted-2-imino-benzothiazolines. *J. Med. Chem.* **42**, 2828–2843 (1999).
366. Allison, A. C., Cacabelos, R., Lombardi, V. R., Alvarez, X. A. & Vigo, C. Celastrol, a potent antioxidant and anti-inflammatory drug, as a possible treatment for Alzheimer's disease. *Prog. Neuropsychopharmacol. Biol. Psychiatry* **25**, 1341–1357 (2001).
367. Shao, J., Welch, W. J. & Diamond, M. I. ROCK and PRK-2 mediate the inhibitory effect of Y-27632 on polyglutamine aggregation. *FEBS Lett.* **582**, 1637–1642 (2008).
368. Shao, J., Welch, W. J., Diprospero, N. A. & Diamond, M. I. Phosphorylation of profilin by ROCK1 regulates polyglutamine aggregation. *Mol. Cell. Biol.* **28**, 5196–5208 (2008).
369. Li, M. *et al.* Intravitreal administration of HA-1077, a ROCK inhibitor, improves retinal function in a mouse model of huntington disease. *PLoS One* **8**, e56026 (2013).

370. Pawate, S. & Bagnato, F. Newer agents in the treatment of multiple sclerosis. *The Neurologist* **19**, 104–117 (2015).
371. Murphy, R. C. & Messer, A. Gene transfer methods for CNS organotypic cultures: a comparison of three nonviral methods. *Mol. Ther. J. Am. Soc. Gene Ther.* **3**, 113–121 (2001).
372. Murphy, R. C. & Messer, A. A single-chain Fv intrabody provides functional protection against the effects of mutant protein in an organotypic slice culture model of Huntington's disease. *Brain Res. Mol. Brain Res.* **121**, 141–145 (2004).
373. Varma, H., Lo, D. C. & Stockwell, B. R. High throughput screening for neurodegeneration and complex disease phenotypes. *Comb. Chem. High Throughput Screen.* **11**, 238–248 (2008).
374. Smith, D. L. *et al.* Inhibition of polyglutamine aggregation in R6/2 HD brain slices-complex dose-response profiles. *Neurobiol. Dis.* **8**, 1017–1026 (2001).
375. Paulson, H. L. Toward an understanding of polyglutamine neurodegeneration. *Brain Pathol. Zurich Switz.* **10**, 293–299 (2000).
376. Blum, E. S., Schwendeman, A. R. & Shaham, S. PolyQ disease: misfiring of a developmental cell death program? *Trends Cell Biol.* **23**, 168–174 (2013).
377. Thornberry, N. A. & Lazebnik, Y. Caspases: enemies within. *Science* **281**, 1312–1316 (1998).
378. Sanchez Mejia, R. O. & Friedlander, R. M. Caspases in Huntington's disease. *Neurosci. Rev. J. Bringing Neurobiol. Neurol. Psychiatry* **7**, 480–489 (2001).
379. Apostol, B. L. *et al.* A cell-based assay for aggregation inhibitors as therapeutics of polyglutamine-repeat disease and validation in *Drosophila*. *Proc. Natl. Acad. Sci. U. S. A.* **100**, 5950–5955 (2003).
380. Marsicano, G., Moosmann, B., Hermann, H., Lutz, B. & Behl, C. Neuroprotective properties of cannabinoids against oxidative stress: role of the cannabinoid receptor CB1. *J. Neurochem.* **80**, 448–456 (2002).
381. Geary, T. G. & Thompson, D. P. *Caenorhabditis elegans*: how good a model for veterinary parasites? *Vet. Parasitol.* **101**, 371–386 (2001).
382. Rand, J. B. & Johnson, C. D. Genetic pharmacology: interactions between drugs and gene products in *Caenorhabditis elegans*. *Methods Cell Biol.* **48**, 187–204 (1995).
383. Levine, B. & Klionsky, D. J. Development by self-digestion: molecular mechanisms and biological functions of autophagy. *Dev. Cell* **6**, 463–477 (2004).
384. Kiebertz, K. *et al.* A randomized, placebo-controlled trial of latrepirdine in Huntington disease. *Arch. Neurol.* **67**, 154–160 (2010).

385. HORIZON Investigators of the Huntington Study Group and European Huntington's Disease Network. A randomized, double-blind, placebo-controlled study of latrepirdine in patients with mild to moderate Huntington disease. *JAMA Neurol.* **70**, 25–33 (2013).
386. Lundin, A. *et al.* Efficacy and safety of the dopaminergic stabilizer Pridopidine (ACR16) in patients with Huntington's disease. *Clin. Neuropharmacol.* **33**, 260–264 (2010).
387. Curtis, A., Mitchell, I., Patel, S., Ives, N. & Rickards, H. A pilot study using nabilone for symptomatic treatment in Huntington's disease. *Mov. Disord. Off. J. Mov. Disord. Soc.* **24**, 2254–2259 (2009).
388. Huntington Study Group TREND-HD Investigators. Randomized controlled trial of ethyl-eicosapentaenoic acid in Huntington disease: the TREND-HD study. *Arch. Neurol.* **65**, 1582–1589 (2008).
389. Puri, B. K. *et al.* Ethyl-EPA in Huntington disease: a double-blind, randomized, placebo-controlled trial. *Neurology* **65**, 286–292 (2005).
390. Beglinger, L. J. *et al.* Randomized controlled trial of atomoxetine for cognitive dysfunction in early Huntington disease. *J. Clin. Psychopharmacol.* **29**, 484–487 (2009).
391. Como, P. G. *et al.* A controlled trial of fluoxetine in nondepressed patients with Huntington's disease. *Mov. Disord. Off. J. Mov. Disord. Soc.* **12**, 397–401 (1997).
392. Beglinger, L. J. *et al.* Results of the citalopram to enhance cognition in Huntington disease trial. *Mov. Disord. Off. J. Mov. Disord. Soc.* **29**, 401–405 (2014).
393. Kremer, B. *et al.* Influence of lamotrigine on progression of early Huntington disease: a randomized clinical trial. *Neurology* **53**, 1000–1011 (1999).
394. Landwehrmeyer, G. B. *et al.* Riluzole in Huntington's disease: a 3-year, randomized controlled study. *Ann. Neurol.* **62**, 262–272 (2007).
395. Huntington Study Group. Dosage effects of riluzole in Huntington's disease: a multicenter placebo-controlled study. *Neurology* **61**, 1551–1556 (2003).
396. Huntington Study Group. Tetrabenazine as antichorea therapy in Huntington disease: a randomized controlled trial. *Neurology* **66**, 366–372 (2006).
397. Frank, S. *et al.* A study of chorea after tetrabenazine withdrawal in patients with Huntington disease. *Clin. Neuropharmacol.* **31**, 127–133 (2008).
398. van Vugt, J. P., Siesling, S., Vergeer, M., van der Velde, E. A. & Roos, R. A. Clozapine versus placebo in Huntington's disease: a double blind randomised comparative study. *J. Neurol. Neurosurg. Psychiatry* **63**, 35–39 (1997).

399. Roos, R. A., Buruma, O. J., Bruyn, G. W., Kemp, B. & van der Velde, E. A. Tiapride in the treatment of Huntington's chorea. *Acta Neurol. Scand.* **65**, 45–50 (1982).
400. Deroover, J., Baro, F., Bourguignon, R. P. & Smets, P. Tiapride versus placebo: a double-blind comparative study in the management of Huntington's chorea. *Curr. Med. Res. Opin.* **9**, 329–338 (1984).
401. Verhagen Metman, L. *et al.* Huntington's disease: a randomized, controlled trial using the NMDA-antagonist amantadine. *Neurology* **59**, 694–699 (2002).
402. O'Suilleabhain, P. & Dewey, R. B. A randomized trial of amantadine in Huntington disease. *Arch. Neurol.* **60**, 996–998 (2003).
403. Kiebertz, K. *et al.* A controlled trial of remacemide hydrochloride in Huntington's disease. *Mov. Disord. Off. J. Mov. Disord. Soc.* **11**, 273–277 (1996).
404. Cubo, E. *et al.* Effect of donepezil on motor and cognitive function in Huntington disease. *Neurology* **67**, 1268–1271 (2006).
405. Shoulson, I. *et al.* A controlled clinical trial of baclofen as protective therapy in early Huntington's disease. *Ann. Neurol.* **25**, 252–259 (1989).
406. Blackwell, A. D., Paterson, N. S., Barker, R. A., Robbins, T. W. & Sahakian, B. J. The effects of modafinil on mood and cognition in Huntington's disease. *Psychopharmacology (Berl.)* **199**, 29–36 (2008).
407. Reilmann, R. *et al.* A randomized, placebo-controlled trial of AFQ056 for the treatment of chorea in Huntington's disease. *Mov. Disord. Off. J. Mov. Disord. Soc.* **30**, 427–431 (2015).
408. Huntington Study Group Reach2HD Investigators. Safety, tolerability, and efficacy of PBT2 in Huntington's disease: a phase 2, randomised, double-blind, placebo-controlled trial. *Lancet Neurol.* **14**, 39–47 (2015).
409. Katsuno, M. *et al.* Efficacy and safety of leuprorelin in patients with spinal and bulbar muscular atrophy (JASMITT study): a multicentre, randomised, double-blind, placebo-controlled trial. *Lancet Neurol.* **9**, 875–884 (2010).
410. Fernández-Rhodes, L. E. *et al.* Efficacy and safety of dutasteride in patients with spinal and bulbar muscular atrophy: a randomised placebo-controlled trial. *Lancet Neurol.* **10**, 140–147 (2011).
411. Zesiewicz, T. A. *et al.* A randomized trial of varenicline (Chantix) for the treatment of spinocerebellar ataxia type 3. *Neurology* **78**, 545–550 (2012).
412. Saute, J. A. M. *et al.* A randomized, phase 2 clinical trial of lithium carbonate in Machado-Joseph disease. *Mov. Disord. Off. J. Mov. Disord. Soc.* **29**, 568–573 (2014).

413. Schulte, T. *et al.* Double-blind crossover trial of trimethoprim-sulfamethoxazole in spinocerebellar ataxia type 3/Machado-Joseph disease. *Arch. Neurol.* **58**, 1451–1457 (2001).
414. Matilla-Dueñas, A. *et al.* in *Handbook of the Cerebellum and Cerebellar Disorders* (eds. Manto, M., Schmahmann, J. D., Rossi, F., Gruol, D. L. & Koibuchi, N.) 2370–2394 (Springer Netherlands, 2013). at <[http://www.springerlink.com/index/10.1007/978-94-007-1333-8\\_106](http://www.springerlink.com/index/10.1007/978-94-007-1333-8_106)>
415. Phillips, W., Shannon, K. M. & Barker, R. A. The current clinical management of Huntington's disease. *Mov. Disord. Off. J. Mov. Disord. Soc.* **23**, 1491–1504 (2008).
416. Travers, E., Jones, K. & Nichol, J. Palliative care provision in Huntington's disease. *Int. J. Palliat. Nurs.* **13**, 125–130 (2007).
417. Moskowitz, C. B. & Marder, K. Palliative care for people with late-stage Huntington's disease. *Neurol. Clin.* **19**, 849–865 (2001).
418. Margolis, R. L. The spinocerebellar ataxias: order emerges from chaos. *Curr. Neurol. Neurosci. Rep.* **2**, 447–456 (2002).
419. Paulson, H. L. Dominantly inherited ataxias: lessons learned from Machado-Joseph disease/spinocerebellar ataxia type 3. *Semin. Neurol.* **27**, 133–142 (2007).
420. Nakano, K. K., Dawson, D. M. & Spence, A. Machado disease. A hereditary ataxia in Portuguese emigrants to Massachusetts. *Neurology* **22**, 49–55 (1972).
421. Woods, B. T. & Schaumburg, H. H. Nigro-spino-dentatal degeneration with nuclear ophthalmoplegia. A unique and partially treatable clinico-pathological entity. *J. Neurol. Sci.* **17**, 149–166 (1972).
422. Barbeau, A. *et al.* The natural history of Machado-Joseph disease. An analysis of 138 personally examined cases. *Can. J. Neurol. Sci. J. Can. Sci. Neurol.* **11**, 510–525 (1984).
423. Coutinho, P. & Andrade, C. Autosomal dominant system degeneration in Portuguese families of the Azores Islands. A new genetic disorder involving cerebellar, pyramidal, extrapyramidal and spinal cord motor functions. *Neurology* **28**, 703–709 (1978).
424. Coutinho, P. & Sequeiros, J. [Clinical, genetic and pathological aspects of Machado-Joseph disease]. *J. Génétique Hum.* **29**, 203–209 (1981).
425. van de Warrenburg, B. P. C. *et al.* Spinocerebellar ataxias in the Netherlands: prevalence and age at onset variance analysis. *Neurology* **58**, 702–708 (2002).
426. Sequeiros, J. & Coutinho, P. Epidemiology and clinical aspects of Machado-Joseph disease. *Adv. Neurol.* **61**, 139–153 (1993).

427. Gaspar, C. *et al.* Ancestral origins of the Machado-Joseph disease mutation: a worldwide haplotype study. *Am. J. Hum. Genet.* **68**, 523–528 (2001).
428. Lima, L. & Coutinho, P. Clinical criteria for diagnosis of Machado-Joseph disease: report of a non-Azorena Portuguese family. *Neurology* **30**, 319–322 (1980).
429. Rosenberg, R. N. Dominant ataxias. *Res. Publ. - Assoc. Res. Nerv. Ment. Dis.* **60**, 195–213 (1983).
430. Dürr, A. *et al.* Spinocerebellar ataxia 3 and Machado-Joseph disease: clinical, molecular, and neuropathological features. *Ann. Neurol.* **39**, 490–499 (1996).
431. Rosenberg, R. N. Machado-Joseph disease: an autosomal dominant motor system degeneration. *Mov. Disord. Off. J. Mov. Disord. Soc.* **7**, 193–203 (1992).
432. Sudarsky, L. & Coutinho, P. Machado-Joseph disease. *Clin. Neurosci. N. Y.* **N3**, 17–22 (1995).
433. Kanda, T., Isozaki, E., Kato, S., Tanabe, H. & Oda, M. Type III Machado-Joseph disease in a Japanese family: a clinicopathological study with special reference to the peripheral nervous system. *Clin. Neuropathol.* **8**, 134–141 (1989).
434. Rüb, U., Brunt, E. R. & Deller, T. New insights into the pathoanatomy of spinocerebellar ataxia type 3 (Machado-Joseph disease). *Curr. Opin. Neurol.* **21**, 111–116 (2008).
435. Shimizu, H. *et al.* Involvement of Onuf's nucleus in Machado-Joseph disease: a morphometric and immunohistochemical study. *Acta Neuropathol. (Berl.)* **120**, 439–448 (2010).
436. Iwabuchi, K., Tsuchiya, K., Uchihara, T. & Yagishita, S. Autosomal dominant spinocerebellar degenerations. Clinical, pathological, and genetic correlations. *Rev. Neurol. (Paris)* **155**, 255–270 (1999).
437. Etchebehere, E. C. *et al.* Brain single-photon emission computed tomography and magnetic resonance imaging in Machado-Joseph disease. *Arch. Neurol.* **58**, 1257–1263 (2001).
438. Klockgether, T. *et al.* Autosomal dominant cerebellar ataxia type I. MRI-based volumetry of posterior fossa structures and basal ganglia in spinocerebellar ataxia types 1, 2 and 3. *Brain J. Neurol.* **121 ( Pt 9)**, 1687–1693 (1998).
439. Taniwaki, T. *et al.* Positron emission tomography (PET) in Machado-Joseph disease. *J. Neurol. Sci.* **145**, 63–67 (1997).
440. Fahl, C. N. *et al.* Spinal cord damage in Machado-Joseph disease. *Cerebellum Lond. Engl.* **14**, 128–132 (2015).
441. Riess, O., Rüb, U., Pastore, A., Bauer, P. & Schöls, L. SCA3: neurological features, pathogenesis and animal models. *Cerebellum Lond. Engl.* **7**, 125–137 (2008).



442. Soong, B., Cheng, C., Liu, R. & Shan, D. Machado-Joseph disease: clinical, molecular, and metabolic characterization in Chinese kindreds. *Ann. Neurol.* **41**, 446–452 (1997).
443. Wüllner, U. *et al.* Dopamine transporter positron emission tomography in spinocerebellar ataxias type 1, 2, 3, and 6. *Arch. Neurol.* **62**, 1280–1285 (2005).
444. D'Abreu, A., França, M., Appenzeller, S., Lopes-Cendes, I. & Cendes, F. Axonal dysfunction in the deep white matter in Machado-Joseph disease. *J. Neuroimaging Off. J. Am. Soc. Neuroimaging* **19**, 9–12 (2009).
445. Soong, B. W. & Liu, R. S. Positron emission tomography in asymptomatic gene carriers of Machado-Joseph disease. *J. Neurol. Neurosurg. Psychiatry* **64**, 499–504 (1998).
446. Paulson, H. L. *et al.* Machado-Joseph disease gene product is a cytoplasmic protein widely expressed in brain. *Ann. Neurol.* **41**, 453–462 (1997).
447. Rubinsztein, D. C. *et al.* Sequence variation and size ranges of CAG repeats in the Machado-Joseph disease, spinocerebellar ataxia type 1 and androgen receptor genes. *Hum. Mol. Genet.* **4**, 1585–1590 (1995).
448. Takiyama, Y. *et al.* Maternal anticipation in Machado-Joseph disease (MJD): some maternal factors independent of the number of CAG repeat units may play a role in genetic anticipation in a Japanese MJD family. *J. Neurol. Sci.* **155**, 141–145 (1998).
449. Bettencourt, C. *et al.* Increased transcript diversity: novel splicing variants of Machado-Joseph disease gene (ATXN3). *Neurogenetics* **11**, 193–202 (2010).
450. Ichikawa, Y. *et al.* The genomic structure and expression of MJD, the Machado-Joseph disease gene. *J. Hum. Genet.* **46**, 413–422 (2001).
451. Maciel, P. *et al.* Improvement in the molecular diagnosis of Machado-Joseph disease. *Arch. Neurol.* **58**, 1821–1827 (2001).
452. Cummings, C. J. & Zoghbi, H. Y. Fourteen and counting: unraveling trinucleotide repeat diseases. *Hum. Mol. Genet.* **9**, 909–916 (2000).
453. Padiath, Q. S., Srivastava, A. K., Roy, S., Jain, S. & Brahmachari, S. K. Identification of a novel 45 repeat unstable allele associated with a disease phenotype at the MJD1/SCA3 locus. *Am. J. Med. Genet. Part B Neuropsychiatr. Genet. Off. Publ. Int. Soc. Psychiatr. Genet.* **133B**, 124–126 (2005).
454. Gu, W. *et al.* The shortest expanded allele of the MJD1 gene in a Chinese MJD kindred with autonomic dysfunction. *Eur. Neurol.* **52**, 107–111 (2004).
455. Schmitt, I., Brattig, T., Gossen, M. & Riess, O. Characterization of the rat spinocerebellar ataxia type 3 gene. *Neurogenetics* **1**, 103–112 (1997).

456. Goto, J. *et al.* Machado-Joseph disease gene products carrying different carboxyl termini. *Neurosci. Res.* **28**, 373–377 (1997).
457. Albrecht, M., Golatta, M., Wüllner, U. & Lengauer, T. Structural and functional analysis of ataxin-2 and ataxin-3. *Eur. J. Biochem. FEBS* **271**, 3155–3170 (2004).
458. Burnett, B., Li, F. & Pittman, R. N. The polyglutamine neurodegenerative protein ataxin-3 binds polyubiquitylated proteins and has ubiquitin protease activity. *Hum. Mol. Genet.* **12**, 3195–3205 (2003).
459. Miller, S. L. H., Malotky, E. & O'Bryan, J. P. Analysis of the role of ubiquitin-interacting motifs in ubiquitin binding and ubiquitylation. *J. Biol. Chem.* **279**, 33528–33537 (2004).
460. Tait, D. *et al.* Ataxin-3 is transported into the nucleus and associates with the nuclear matrix. *Hum. Mol. Genet.* **7**, 991–997 (1998).
461. Schmitt, I. *et al.* Inactivation of the mouse *Atxn3* (ataxin-3) gene increases protein ubiquitination. *Biochem. Biophys. Res. Commun.* **362**, 734–739 (2007).
462. Costa, M. do C. *et al.* Genomic structure, promoter activity, and developmental expression of the mouse homologue of the Machado-Joseph disease (MJD) gene. *Genomics* **84**, 361–373 (2004).
463. Linhartová, I. *et al.* Conserved domains and lack of evidence for polyglutamine length polymorphism in the chicken homolog of the Machado-Joseph disease gene product ataxin-3. *Biochim. Biophys. Acta* **1444**, 299–305 (1999).
464. Rodrigues, A.-J. *et al.* Functional genomics and biochemical characterization of the *C. elegans* orthologue of the Machado-Joseph disease protein ataxin-3. *FASEB J. Off. Publ. Fed. Am. Soc. Exp. Biol.* **21**, 1126–1136 (2007).
465. Albrecht, M. *et al.* Structural modeling of ataxin-3 reveals distant homology to adaptins. *Proteins* **50**, 355–370 (2003).
466. Doss-Pepe, E. W., Stenroos, E. S., Johnson, W. G. & Madura, K. Ataxin-3 interactions with rad23 and valosin-containing protein and its associations with ubiquitin chains and the proteasome are consistent with a role in ubiquitin-mediated proteolysis. *Mol. Cell. Biol.* **23**, 6469–6483 (2003).
467. Mao, Y. *et al.* Deubiquitinating function of ataxin-3: insights from the solution structure of the Josephin domain. *Proc. Natl. Acad. Sci. U. S. A.* **102**, 12700–12705 (2005).
468. Zhong, X. & Pittman, R. N. Ataxin-3 binds VCP/p97 and regulates retrotranslocation of ERAD substrates. *Hum. Mol. Genet.* **15**, 2409–2420 (2006).
469. do Carmo Costa, M. *et al.* Ataxin-3 plays a role in mouse myogenic differentiation through regulation of integrin subunit levels. *PLoS One* **5**, e11728 (2010).

470. Durcan, T. M., Kontogianna, M., Bedard, N., Wing, S. S. & Fon, E. A. Ataxin-3 deubiquitination is coupled to Parkin ubiquitination via E2 ubiquitin-conjugating enzyme. *J. Biol. Chem.* **287**, 531–541 (2012).
471. Durcan, T. M. & Fon, E. A. Mutant ataxin-3 promotes the autophagic degradation of parkin. *Autophagy* **7**, 233–234 (2011).
472. Evert, B. O. *et al.* Ataxin-3 represses transcription via chromatin binding, interaction with histone deacetylase 3, and histone deacetylation. *J. Neurosci. Off. J. Soc. Neurosci.* **26**, 11474–11486 (2006).
473. Rodrigues, A. J. *et al.* Absence of ataxin-3 leads to enhanced stress response in *C. elegans*. *PLoS One* **6**, e18512 (2011).
474. Reina, C. P., Nabet, B. Y., Young, P. D. & Pittman, R. N. Basal and stress-induced Hsp70 are modulated by ataxin-3. *Cell Stress Chaperones* **17**, 729–742 (2012).
475. Zhou, L. *et al.* Ataxin-3 protects cells against H<sub>2</sub>O<sub>2</sub>-induced oxidative stress by enhancing the interaction between Bcl-X(L) and Bax. *Neuroscience* **243**, 14–21 (2013).
476. Cemal, C. K. *et al.* YAC transgenic mice carrying pathological alleles of the MJD1 locus exhibit a mild and slowly progressive cerebellar deficit. *Hum. Mol. Genet.* **11**, 1075–1094 (2002).
477. Chou, A.-H. *et al.* Polyglutamine-expanded ataxin-3 causes cerebellar dysfunction of SCA3 transgenic mice by inducing transcriptional dysregulation. *Neurobiol. Dis.* **31**, 89–101 (2008).
478. Alves, S. *et al.* Striatal and nigral pathology in a lentiviral rat model of Machado-Joseph disease. *Hum. Mol. Genet.* **17**, 2071–2083 (2008).
479. Switonski, P. M. *et al.* Mouse ataxin-3 functional knock-out model. *Neuromolecular Med.* **13**, 54–65 (2011).
480. Switonski, P. M., Szlachcic, W. J., Krzyzosiak, W. J. & Figiel, M. A new humanized ataxin-3 knock-in mouse model combines the genetic features, pathogenesis of neurons and glia and late disease onset of SCA3/MJD. *Neurobiol. Dis.* **73**, 174–188 (2015).
481. Chen, X. *et al.* Deranged calcium signaling and neurodegeneration in spinocerebellar ataxia type 3. *J. Neurosci. Off. J. Soc. Neurosci.* **28**, 12713–12724 (2008).
482. Shakkottai, V. G. *et al.* Early changes in cerebellar physiology accompany motor dysfunction in the polyglutamine disease spinocerebellar ataxia type 3. *J. Neurosci. Off. J. Soc. Neurosci.* **31**, 13002–13014 (2011).
483. Alves, S. *et al.* Allele-specific RNA silencing of mutant ataxin-3 mediates neuroprotection in a rat model of Machado-Joseph disease. *PLoS One* **3**, e3341 (2008).

484. Alves, S. *et al.* Silencing ataxin-3 mitigates degeneration in a rat model of Machado-Joseph disease: no role for wild-type ataxin-3? *Hum. Mol. Genet.* **19**, 2380–2394 (2010).

## CHAPTER 2

---

Limited effect of chronic valproic acid treatment in a mouse model of Machado-Joseph

Disease

*(in press in PLoS One, doi: 10.1371/journal.pone.0141610)*

## **Limited effect of chronic valproic acid treatment in a mouse model of Machado-Joseph disease**

Sofia Esteves<sup>1,2</sup>, Sara Duarte-Silva<sup>1,2</sup>, Luana Naia<sup>3,4</sup>, Andreia Neves-Carvalho<sup>1,2</sup>, Andreia Teixeira-Castro<sup>1,2</sup>,  
A. Cristina Rego<sup>3,4</sup>, Anabela Silva-Fernandes<sup>1,2</sup> and Patricia Maciel<sup>1,2</sup>

- 1) Life and Health Sciences Research Institute (ICVS), School of Health Sciences, University of Minho, 4710-057 Braga, Portugal.
- 2) ICVS/3Bs - PT Government Associate Laboratory, Braga/Guimarães, Portugal.
- 3) CNC-Center for Neuroscience and Cell Biology, University of Coimbra, Coimbra, Portugal
- 4) Faculty of Medicine, University of Coimbra, Coimbra, Portugal.

## Abstract

Machado-Joseph disease (MJD) is an inherited neurodegenerative disease, caused by a CAG repeat expansion within the coding region of *ATXN3* gene, and which currently lacks effective treatment. In this work we tested the therapeutic efficacy of chronic treatment with valproic acid (VPA) (200mg/kg), a compound with known neuroprotection activity, and previously shown to be effective in cell, fly and nematode models of MJD. We show that chronic VPA treatment in the CMVMJD135 mouse model had limited effects in the motor deficits of these mice, seen mostly at late stages in the motor swimming, beam walk, rotarod and spontaneous locomotor activity tests, and did not modify the *ATXN3* inclusion load and astrogliosis in affected brain regions. However, VPA chronic treatment was able to increase GRP78 protein levels at 30 weeks of age, one of its known neuroprotective effects, confirming target engagement. In spite of limited results, the use of another dosage of VPA or of VPA in a combined therapy with molecules targeting other pathways, cannot be excluded as potential strategies for MJD therapeutics.

## Introduction

Polyglutamine (PolyQ) diseases are neurodegenerative disorders caused by an expansion of trinucleotide CAG repeats within the coding region of specific genes<sup>1</sup>. This group of disorders includes spinal bulbar muscular atrophy (SBMA), Huntington's disease (HD), Dentatorubral-Pallidoluysian atrophy (DRPLA), and six types of spinocerebellar ataxias (SCA's)<sup>2</sup>. Machado-Joseph disease (MJD) or Spinocerebellar Ataxia type 3 (SCA3) is the most common dominantly inherited SCA worldwide and is caused by the expansion of a polyQ tract in the C-terminus of the *ATXN3* gene product<sup>3</sup>. Both the normal and expanded ataxin-3 (*ATXN3*) proteins are expressed ubiquitously, although the neurodegeneration in MJD is limited to some brain regions, mainly in cerebellum, brainstem and spinal cord<sup>4</sup>. The symptoms include ataxia, progressive external ophthalmoplegia, pyramidal and extrapyramidal signs, peripheral amyotrophies, intention fasciculation-like movements of facial and lingual muscles, rigidity, and bulging eyes<sup>5-7</sup>. The pathological hallmark of the disease is the presence of neuronal intranuclear inclusions (NIIs) of aggregation-prone expanded *ATXN3* in the patients' brain, being the pathogenic relevance of these aggregates still unclear<sup>8-11</sup>.

Despite the recent efforts towards the understanding of the pathogenesis of this disorder, the molecular pathways that ultimately lead to neuronal demise remain mostly unknown and no effective treatments are yet available for MJD, as for other polyQ diseases. Nevertheless, there seem to be common pathways between all polyQ diseases that were shown to be altered, which could be explored

in the development of therapeutics, related to transcriptional dysregulation, mitochondrial dysfunction, oxidative stress, Ubiquitin Proteasome System (UPS) impairment, excitotoxicity, DNA damage and activation of apoptotic pathways<sup>12</sup>.

Nevertheless, the translation of candidate therapies to clinical trials is a very long process due to uncertainty for human safety and has not improved significantly in the last years. In this context, drug re-purposing strategies, which relies on finding new uses for existing FDA-approved compounds, has been gaining attractiveness due to the faster translation to the clinic, with predictably less safety issues.

VPA is an FDA-approved compound that has been used over the years as an anticonvulsant and mood-stabilizing drug in the treatment of epilepsy, bipolar disorder and migraine<sup>13</sup>, with a relatively safe profile in clinical use. In the last years, a growing body of evidence indicates that VPA holds promise in treating other neurodegenerative diseases due to its diverse mechanisms of action. Its pharmacological effects comprise a range of mechanisms, including inhibition of histone deacetylases, increased gamma-aminobutyric acid (GABA)-ergic transmission, reduced release and/or effects of excitatory amino acids, blockade of voltage-gated sodium channels and modulation of dopaminergic and serotonergic transmission<sup>14</sup>. VPA treatment is also known to produce changes in the expression of multiple genes, involved in transcription regulation, cell survival, ion homeostasis, cytoskeletal modifications, signal transduction, endoplasmic reticulum stress and longevity<sup>13,15</sup>. This drug has been shown to delay the disease onset, to reduce neurological deficits and/or to prolong survival in several models of neurodegenerative diseases, including HD, SBMA and Amyotrophic Lateral Sclerosis (ALS)<sup>16-18</sup>. In MJD, VPA was reported to alleviate neurodegeneration in a *Drosophila* model of the disease<sup>19</sup> and to attenuate mutant ATXN3-induced cell toxicity in a human neuronal cell model<sup>20</sup>. Moreover, we have previously shown a significant reduction of mutant ATXN3 aggregation and neurological dysfunction in a *C. elegans* model of MJD upon VPA treatment through the protective role of the transcription factor DAF-16, supporting a role in protection against proteotoxicity related to aging and cell survival<sup>21</sup>. However, its therapeutic efficacy is still not demonstrated in a mammalian model of MJD. The goal of this work was to test the therapeutic efficacy of chronic VPA treatment in a mouse model of MJD, CMVMJD135<sup>22</sup>. Our results show that chronic VPA treatment at the dosage used in this pre-clinical trial, lead to very limited and transient phenotypic effects in the CMVMJD135 mouse model, and did not change the ATXN3 inclusion load neither astrogliosis in affected brain regions.



## Material and Methods

**Ethics statement.** All animal procedures were conducted in accordance with European regulations (European Union Directive 2010/63/EU). Animal facilities and the people directly involved in animal experiments (SE, SDS, ANC and ASF) were certified by the Portuguese regulatory entity – Direcção Geral de Alimentação e Veterinária. All of the protocols performed were approved by the Ethics Subcommittee for Life and Health Sciences of the Life and Health Sciences Research Institute, University of Minho. All experiments were designed with commitment to the principles of refinement, reduction, and replacement and performed according to the FELASA guidelines to minimize discomfort, stress, and pain to the animals, with defined humane endpoints<sup>23</sup>. Humane endpoints for the pre-clinical trial were defined as 20% reduction of the body weight, inability to reach food and water, presence of wounds in the body and dehydration), however they were not needed as the study period was conceived to include ages at which animals do not reach these endpoints.

**Transgenic mice model and drug administration.** We used the CMVMJD135 (background C57BL/6) mouse model, expressing an expanded version of the human MJD1-1 cDNA (the 3 UIMs-containing variant of ATXN3) under the regulation of the CMV promoter, ubiquitously and at near-endogenous levels<sup>22</sup>. These animals show a slowly progressive motor phenotype and CNS pathology consistent with that of MJD patients<sup>22</sup>. Male transgenic and non-transgenic drug- and placebo- treated animals were sequentially assigned and housed at weaning in groups of 5 animals in filter-topped polysulfone cages 267 × 207 × 140 mm (370 cm<sup>2</sup> floor area) (Tecniplast, Buguggiate, Italy), with corncob bedding (Scobis Due, Mucedola SRL, Settimo Milanese, Italy) in a conventional animal facility. DNA extraction, animal genotyping and CAG repeat size analyses were performed as previously described<sup>24</sup>, with the mean repeat size (±SD) for all mice of (133±1). Male littermates wild-type (WT) animals were used as controls. All animals were maintained under standard laboratory conditions: an artificial 12 h light/dark cycle (lights on from 8:00 to 20:00 h), with an ambient temperature of 21±1 °C and a relative humidity of 50–60%; the mice were given a standard diet (4RF25 during the gestation and postnatal periods, and 4RF21 after weaning, Mucedola SRL, Settimo Milanese, Italy) and water *ad libitum*. We administered Valproic acid sodium salt (PG-4543, Sigma) during five consecutive days per week through intraperitoneal injection (i.p), in a dosage of 200mg/kg dissolved in 0,9% saline. Control animals were given a placebo of injection buffer (0.9% NaCl) with the same frequency. Treatment was initiated at five weeks of age, i.e. one week before the onset of the first neurological symptoms, until 30

weeks of age. for pre-clinical trial. For a pilot study, WT animals were treated for 5 consecutive days with i.p. injections of VPA at 200mg/k or saline.

**Western-blot.** Cerebellum tissues were thawed and homogenized with a Potter-Elvehjem 377 homogenizer with a Teflon pestle, at 300 rpm, in lysis buffer (150 mM NaCl, 50 mM Tris, 5 mM EGTA, 1% Triton X-100, 0.5% sodium deoxycholate, 0.1% SDS, pH 7.5) supplemented with 100 nM okadaic acid, 25 mM NaF, 1 mM Na<sub>3</sub>VO<sub>4</sub>, 1 mM DTT, 1 mM PMSF, 1 µg/mL of protease inhibitor cocktail (chymostatin, pepstatin A, leupeptin and antipain), 1 µM trichostatin A (HDACs inhibitor) and 10 mM nicotinamide (sirtuins inhibitor). The homogenates were then sonicated for 15 s and centrifuged at 20,800 g for 10 min to remove cell debris. The pellet was discarded, the supernatant (total extract) was collected and protein content quantified by Bio-Rad protein assay (Bio-Rad). Total extracts were denatured with denaturing buffer (50 mM Tris-HCl pH 6.8, 2% SDS, 5% glycerol, 600 mM DTT, 0.01% bromophenol blue) at 95 °C, for 5 min. Equivalent amounts of protein (30µg) were separated on a 15% SDS-PAGE gel electrophoresis and electroblotted onto polyvinylidene difluoride (PVDF) membranes. The membranes were blocked for 1 h in Tris-buffered saline (TBS) solution containing 0.1% Tween (TBS-Tween) and 5% BSA, followed by an overnight incubation with primary antibodies (rabbit anti-acH3 (1:1,000, Milipore), rabbit anti-Lamin B1 (1:1000, Abcam) rabbit anti-GRP78 (1:1000, Abcam) and mouse anti-actin (1:5000, Ambion), at 4°C, with gentle agitation. Membranes were then washed 3 times, for 10 min, with TBS-Tween, and incubated with secondary antibodies conjugated with alkaline phosphatase (1:10,000), for 1 h, at room temperature, with gentle agitation. Immunoreactive bands were visualized by alkaline phosphatase activity after incubation with ECL substrate, in a ChemiDoc Imaging System (Bio-Rad). Bands were quantified using the Image Lab software (Bio-Rad).

**Gene expression quantification (qRT-PCR).** Cerebellum total RNA was isolated from 18 week-old CMVMJD135 littermate mice, vehicle- and VPA-treated (n=4 for each group) using TRIZOL (15596-026, Invitrogen, Calrsbad, USA) according to the manufacturer's protocol. RNA samples were treated with DNase I (EN0525, Thermo Scientific®, USA) according to the manufacturer's protocol. First-strand cDNA, synthesized with iScript cDNA Synthesis kit (#170-8891, Bio-Rad, USA) was amplified by quantitative reverse-transcriptase PCR (qRT-PCR) as previously described<sup>24</sup>. The following primers were used for expression quantification: GADD45α (F 5'-AGACCGAAAGGATGGACACG-3'); GADD45α (R 5'-TGACTCCGAGCCTTGCTGA-3'); BIM (F 5'-CGGATCGGAGACGAGTTCA-3'); BIM (R 5'-TTCAGCCTCGCGTAATCA-3'); B2m (F 5'-CCTTCAGCAAGGACTGGTCT-3' and B2m (R 5'-

TCTCGATCCCAGTAGACGGT-3'). Primers were designed using PRIMER-BLAST (<http://www.ncbi.nlm.nih.gov/tools/primer-blast/>).

### **Behavioral analysis**

Behavioral analysis was performed during the diurnal period in groups of 5 male animals per cage including CMVMJD135 hemizygous transgenic mice and WT littermates (n=10-15 per genotype) treated and non-treated with VPA. All behavioral tests started in a pre-symptomatic stage of the disease (4 weeks of age) and were conducted until an age at which the phenotype is fully established (30 weeks)<sup>22</sup>. The animals were weighed one week before the start of drug treatment (4 weeks) and then every two weeks until 30 weeks of age (Fig. 2).

**Neurological examination (based on SHIRPA protocol).** Based on the SHIRPA protocol we established an adapted protocol for phenotypic assessment applied since 4 weeks until 24 weeks of age, in which we used the tests for which, based on our previous experience, CMVMJD135 mice usually present significant phenotypic alterations<sup>22</sup>. We assessed motor function through the spontaneous activity test, by counting wall-leanings during five minutes, and locomotor activity in which we counted the number of squares travelled over 30 secs, in an arena (55×33×18 cm) with 15 labeled squares. Other observational measurements included tremors and limb claspings, in which we suspended the animal by the tail and classified the extensor reflexes. In this protocol we also included the hanging wire test, as a measure of muscle strength and fine motor coordination of the paws. This protocol was adjusted in order to minimize animal handling and to generate uniformity in waiting times between the tests<sup>25</sup>.

**Footprint analysis.** To evaluate the dragging of the paws, the footprint test was used since 10 weeks of age. To obtain footprints, the hind- and forepaws of the mice were coated with black and red non-toxic paints, respectively. We used a clean rectangular paper sheet placed on the floor of the runway for each run. The animals were allowed to walk along a 100-cm-long × 4.2 cm width × 10 cm height corridor in the direction of an enclosed black box. Each animal was allowed to achieve one valid trial per age. To evaluate the severity of foot-dragging through age the footprinting pattern was classified at each time point considering six consecutive steps (0=absent dragging, up to three steps; 1=moderate dragging, less than three steps out of six; 2=severe dragging, all steps out of six show dragging). The

stride length was also measured through the footprinting pattern by measuring the length between three consecutive steps.

**Motor swimming test.** To assess swimming movement coordination, the time that animals take to reach a safe platform at the end of a container (60 cm distance) with 15 cm depth of water at 24-26°C was recorded bi-weekly since 22 weeks of age. The protocol consisted of 2 days of training with three trial followed by three days of test with two trials as previously described<sup>22,26</sup>.

**Beam walk test.** Balance and fine motor coordination of mice were assessed by measuring the ability of the mice to traverse, without falling, a graded series of narrow beams to reach an enclosed safety platform as previously described<sup>22,26</sup>. During training, mice were placed at the start of the 12 mm square beam and trained over 3 days (3 trials per day) to traverse the beam to the safe platform. On the fourth day, they were tested in the training beam (12 mm square) and 11mm round beam (2 trials per beam).

**Rotarod test.** To evaluate motor skill learning and coordination with another paradigm, mice were tested in a rotarod apparatus (TSE systems, Bad Homburg, Germany). The protocol is comprised of 3 training days at a constant speed (15 rpm) for a maximum of 60 s in four trials, with a 10 min interval between each trial. On the fourth day, animals were tested for each of 6 different speeds (5 rpm, 8 rpm, 15 rpm, 20 rpm, 24 rpm and 31 rpm) for a maximum of 60s in two trials, with a 10-min-long interval between each trial, as previously described<sup>24</sup>.

**Immunohistochemistry and quantification of ataxin-3 neuronal inclusions and astrogliosis.** Thirty week-old WT and CMVMJD135 littermate mice, VPA-treated and non-treated (n=4 for each group) were deeply anesthetized with a mixture of ketamine hydrochloride (150 mg/kg) plus medetomidine (0.3 mg/kg) and transcardially perfused with phosphate-buffered saline (PBS) followed by 4% paraformaldehyde (PFA) (Panreac, USA). Brains were removed and post fixed overnight in PFA 4% and embedded in paraffin. Slides with 4-µm-thick paraffin sections were subjected to antigen retrieval (Buffer Citrate, 1M) and then incubated with mouse anti-ATXN3 (1H9) (1:1000, MAB5360, Milipore) and GFAP (1:500, Z0334, Dako corporation) which were detected by incubation with a biotinylated anti-polyvalent antibody, followed by detection through biotin-streptavidin coupled to horseradish peroxidase and reaction with the DAB (3, 3'-diaminobenzidine) substrate (Lab Vision™

Ultra-Vision™ Detection kit, Thermo Scientific). The slides were counterstained with 25% hematoxylin according to standard procedures. ATXN3 positive inclusions in the facial motor nucleus (7N) and lateral reticular nucleus (LRt), and GFAP positive cells in substantia nigra (SN) of vehicle or VPA-treated animals (n=4 for each conditions, 4 slides per animal) were quantified and normalized for total area using the Olympus BX51 stereological microscope (Olympus, Japan) and the Visiopharma integrator system software (Visiopharm, Denmark) as previously described<sup>22</sup>. The total area of 7N,LRt and SN were chosen based on the mouse brain atlas<sup>27</sup>.

**Determination of Valproic acid Plasma Levels.** The plasma valproic acid levels were measured applying the VALP assay using the Dimension Vista® System (VALP Flex® reagent cartridge) – SIEMENS.

**Statistical analysis.** The experimental unit used in this study was a single animal. Experimental design was based on power analyses for optimization of sample size<sup>28</sup>. Mouse sample size calculations were performed for each behavioral test and pathological analyses assuming a power of 0.8 and a significance level of  $p < 0.05$ . The effect size was calculated aiming at detecting 50% improvement. We used  $n = 10$  to 15 per genotype/treatment for behavioral tests, and a group size of four animals per group for quantification of ATXN3 Nlls analysis. Data was analyzed through the non-parametric Mann-Whitney U-test when variables were non-continuous or when a continuous variable did not present a normal distribution (Kolmogorov-Smirnov test,  $p < 0.05$ ) (Rotarod). Continuous variables with normal distributions and with homogeneity of variance (Levene's test) were analyzed with Repeated-Measures ANOVA for longitudinal multiple comparisons, using Tukey test for post-hoc comparisons and One-way ANOVA for paired comparisons. Non-continuous categorical variables were analyzed through Chi-Square Fisher exact test. All statistical analyses were performed using SPSS 22.0 (SPSS Inc., Chicago, IL) and G-Power 3.1.9.2 (University Kiel, Germany). A critical value for significance of  $P < 0.05$  was used throughout the study. Values were expressed as mean  $\pm$  SEM for continuous variables and as percentages for non-continuous variables.

## Results

### Effect of VPA acute treatment in histone acetylation and neuroprotective molecules in the cerebellum

Although CMVMJD135 mouse model do not present a general hypoacetylation of histones in specific brain regions, we measured the H3 acetylation and we observed a trend towards an increase in H3 acetylation levels upon 5 days of VPA acute treatment (Fig. 1A).

This result did not present statistical difference due to high variability between samples, however, a trend was observed to an hyperacetylation of histone H3 in the cerebellum upon VPA treatment, when normalized to the nuclear protein Lamin B1. Furthermore, and considering our previous results in *C.elegans* model of MJD upon VPA treatment, we also assessed the mRNA levels of GADD45 $\alpha$  and BIM, two genes related to stress resistance and apoptosis regulation, respectively<sup>29-32</sup>, in the cerebellum of CMVMJD135 mice, where a trend towards an increase upon VPA acute treatment was also observed (Fig. 1B).

Plasma VPA concentration was also assessed after 30 and 120 minutes post-injection. An average of  $252 \pm 15.8$   $\mu\text{mol/L}$  after 30 minutes was observed in VPA-treated animals while a  $25.7 \pm 8.7$   $\mu\text{mol/L}$  concentration was detected after 120 minutes post-injection (Fig. 1C).

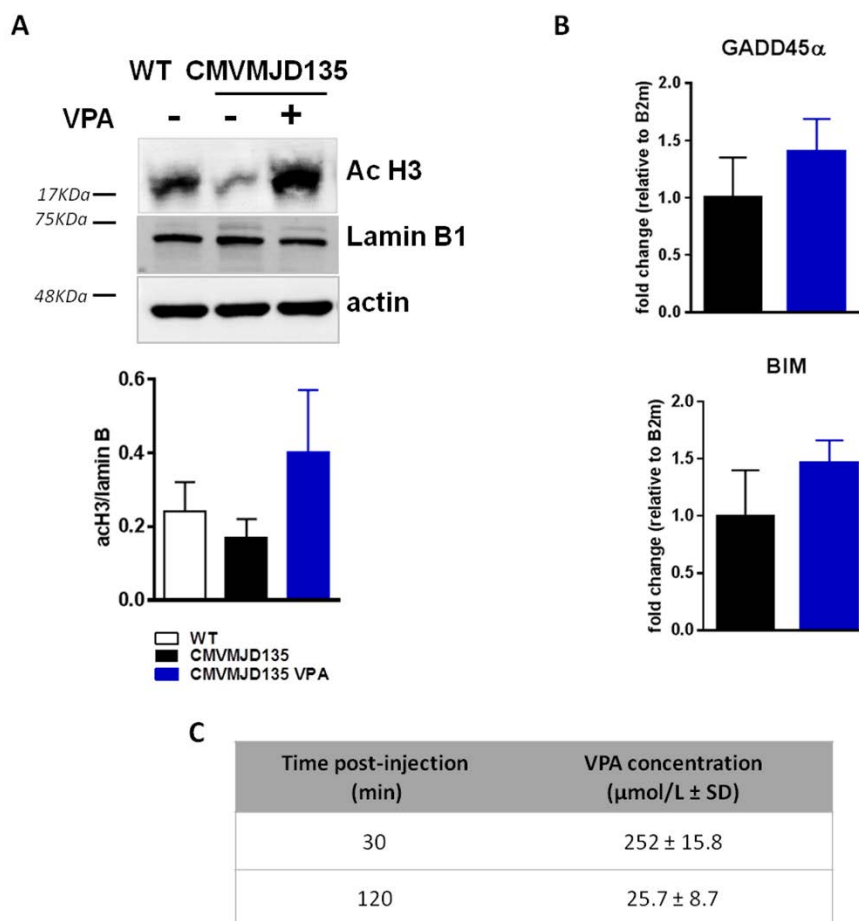


**Figure 1.** VPA acute treatment effects in cerebellum of CMVMJD135 mouse model. (A) A trend towards an increase in the H3 histone acetylation upon VPA acute treatment; (B) a trend towards an increase in GADD45 $\alpha$  and BIM mRNA levels upon VPA acute treatment and (C) VPA concentration in the plasma after 30 and 120 minutes post-injection. Bars represent the mean  $\pm$  SEM (n=4 males for each group), One-Way ANOVA.

### VPA treatment had limited effects in neurological deficits and decreased the body weight gain in CMVMJD135 mice

Chronic VPA treatment was initiated at 5 weeks of age, with a dosage of 200mg/kg, for 5 consecutive days each week, until 30 weeks of age. A battery of neurological and motor coordination tests was performed since 4 weeks of age until 30 weeks of age (Fig. 2).

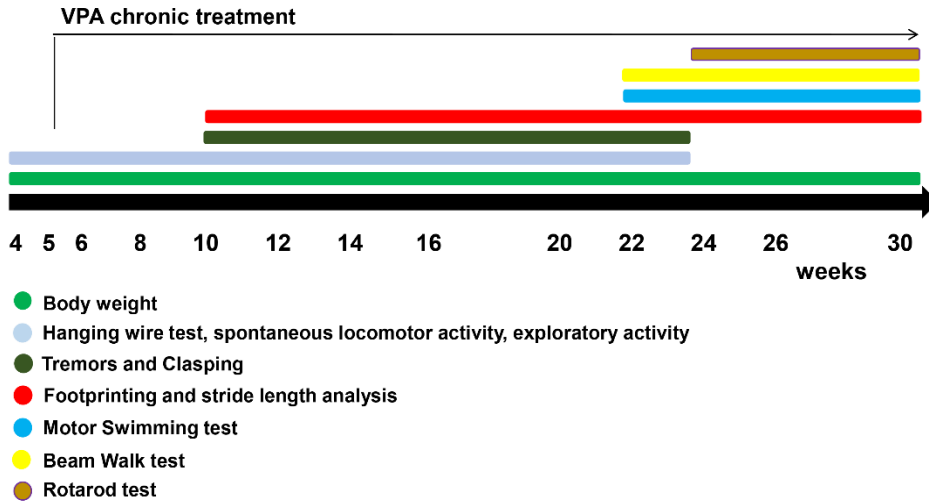


**Figure. 2.** Schematic representation of the VPA pre-clinical therapeutic trial.

No differences were found between WT and CMVMJD135 mice at 4 weeks of age before the beginning of the injections. CMVMJD135 mice start showing less body weight gain at 16 weeks of age, being statistically different from age-matched WT littermates at 24 weeks of age (Fig. 3A). VPA treatment significantly reduced the already diminished body weight gain of the transgenic animals since very early in this trial (Fig. 3A) suggesting some toxicity to these animals.



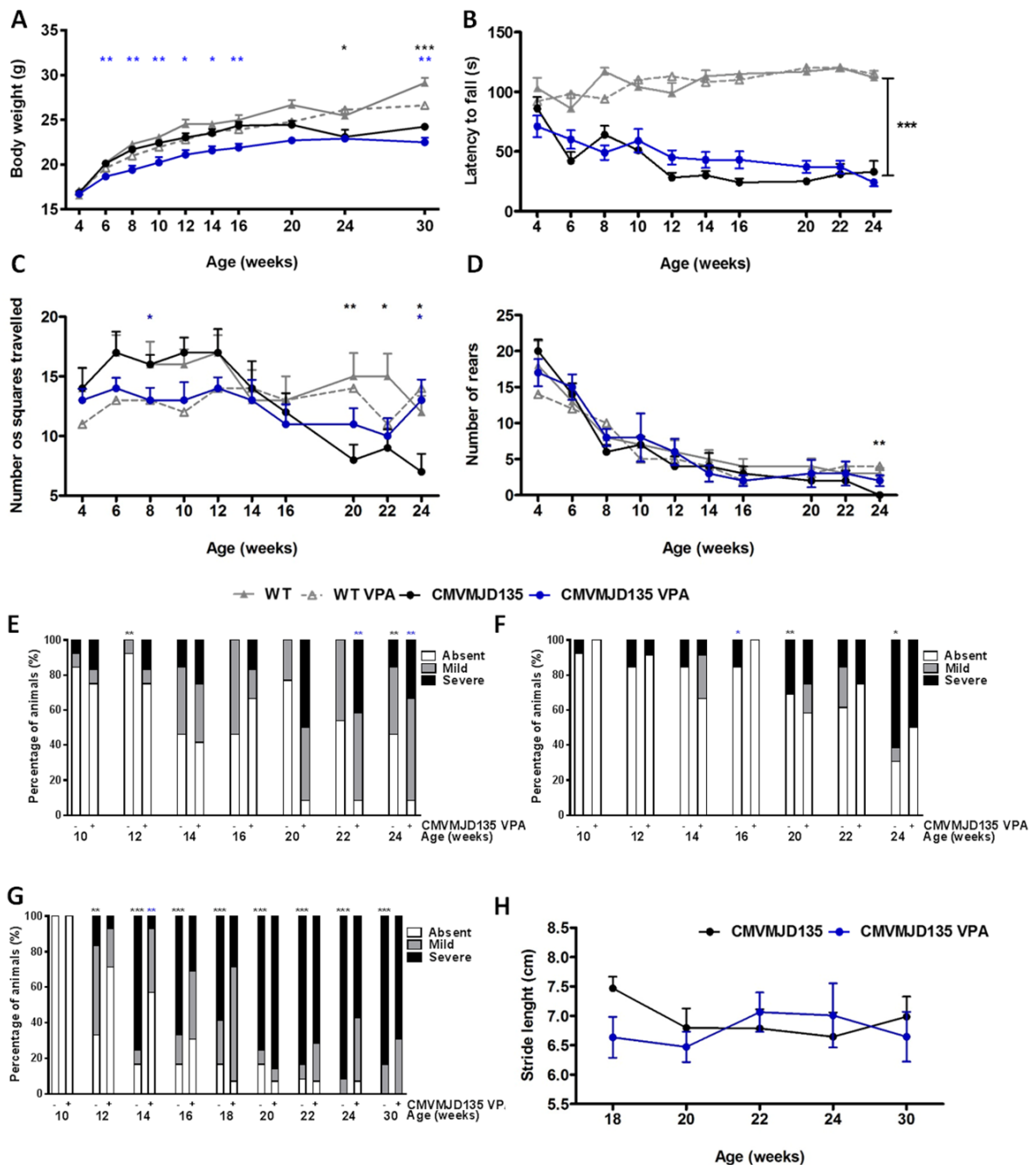


**Figure 3. Minor effects in neurological deficits and body weight gain presented by CMVMJD135 mice upon VPA treatment.** (A) Decreased body weight gain in CMVMJD135 VPA-treated animals compared to CMVMJD135 vehicle-treated animals; (B) no improvement of VPA-treated animals in grip strength as assessed through the hanging wire test; (C) Improvement in spontaneous locomotor activity at 24 weeks of age; (D,E,F) No improvement in spontaneous activity (vertical movement), in tremors and limb claspings, respectively, (G) transient improvement in footdragging severity at 14 weeks, and (H) tendency toward an improvement in stride length at 22 and 24 weeks of age. Bars represent the mean  $\pm$  SEM (WT veh, n=10; WT VPA, n=15; CMVMJD135 vehicle, n=10; CMVMJD135 VPA, n=13), \* represent  $p < 0.05$ , \*\* represent  $p < 0.01$  and \*\*\* represent  $p < 0.001$ , black asterisks represents the difference between WT and CMVMJD135, blue asterisks represents the difference between non-treated and VPA-treated CMVMJD135 (Repeated-measures ANOVA, Tukey correction for continuous variables, One-Way ANOVA for differences between groups in specific ages of the continuous variables and Chi-square Fisher's exact test for categorical non-continuous variables).

Other than reduced weight gain, no apparent clinical symptoms indicative of significant health impact were observed during long-term VPA treatment of WT and transgenic animals, and no more than 20% of their total body weight was lost at any instance. The first sign of neurological disease in the CMVMJD135 mouse model is the presence of muscular grip strength abnormalities at 6 weeks of age, given by the significant decrease in the latency to fall off in the hanging wire test <sup>22</sup>. VPA treatment did not alter the progression of the CMVMJD135 animals in the hanging wire, demonstrating an absence of effect in muscle strength and/or fine motor coordination of the paws (Fig. 3B). Spontaneous locomotor activity of transgenic animals, given by the number of squares travelled in the arena, was markedly increased upon VPA treatment at 24 weeks of age (Fig. 3C). However, spontaneous vertical exploratory activity, tremors and clasping were not improved by VPA treatment (Fig. 3D,E,F).

Gait abnormalities were assessed qualitatively by the analysis of the footprint pattern. CMVMJD135 mice model presented foot dragging already at 12 weeks progressing through age. VPA was able to decrease the severity of this phenotype only at 14 weeks (Fig. 3G), while no effect was observed at more advanced stages of the trial. In addition, stride length was also measured and although not significant, a trend towards and improvement in transgenic animals upon VPA treatment was observed at 22 and 24 weeks of age (Fig. 3H).

### **Long-term VPA treatment led to limited improvement in balance and motor coordination at later disease stages**

Since chronic VPA treatment induced a decrease in body weight of transgenic animals, behavior performance in the motor and balance coordination tests was normalized to body weight. Results of behavioral tests without normalization to body weight are included in supplementary data (Fig. S1).

VPA treatment ameliorated balance and motor coordination of CMVMJD135 mice at 24 weeks of age, after 20 weeks of daily treatment, as assessed by the time taken to cross the 11 mm circle and 12 mm beams in the balance beam walk test. However, this improvement was not maintained at 30 weeks of age (Fig. 4A,B).

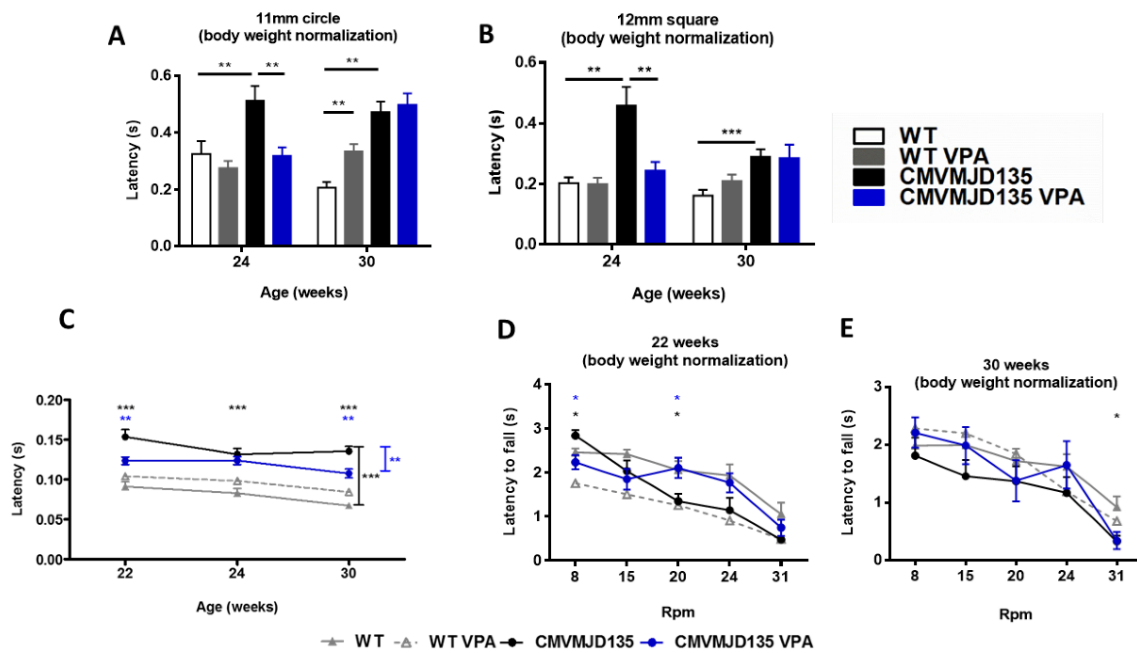


**Figure 4. Balance and motor coordination performance normalized for animal body weight.** (A,B) No differences were observed between non-normalized and normalized performance for body weight in balance beam walk test; (C) improvement motor swimming test at 22 and 30 weeks of age and (D) improvement at 22 weeks of in 8 and 20 rpm of Rotarod test. Bars represent the mean  $\pm$  SEM (WT veh, n=10; WT VPA, n=15; CMVMJD135 vehicle, n=10; CMVMJD135 VPA, n=13), \* represent  $p < 0.05$ , \*\* represent  $p < 0.01$  and \*\*\* represent  $p < 0.001$ , black asterisks represents the difference between WT and CMVMJD135, blue asterisks represents the difference between non-treated and VPA-treated CMVMJD135, (Repeated-measures ANOVA, Tukey correction for continuous variables, One-Way ANOVA for differences between groups in specific ages of the continuous variables and Mann-Whitney U test for continuous variables without normal distribution (Rotarod)).

In the motor swimming test, VPA-treated CMVMJD135 mice also had a better performance later in life (22 and 30 weeks of age) when compared to vehicle-treated mice (Fig. 4C). Other motor deficits observed in CMVMJD135 mice, namely the loss of motor coordination observed in the Rotarod test, were alleviated by VPA treatment at 22 weeks of age for 8 and 20 rpm, but not maintained at 30 weeks of age (Fig. 4D,E).

### VPA treatment did not change the ataxin-3 inclusion load and astrogliosis in specific brain regions of CMVMJD135 mice

At the pathological level, CMVMJD135 mice show presence of ATXN3 NIIs in the nucleus of cells in different regions of the CNS including the pontine nuclei, reticulotegmental nucleus of the pons, spinal cord neurons, facial motor nuclei, anterior olfactory nuclei, ventral tenia tecta, inferior olive, dentate nuclei, locus coeruleus, cuneate nuclei and lateral reticular nuclei<sup>22</sup>. The analysis of brain tissue of VPA-treated and non-treated CMVMJD135 by immunohistochemistry of ATXN3 in facial motor nuclei (7N) and lateral reticular nuclei (LRt), did not reveal significant differences between groups (Fig. 6A-D). Astrogliosis observed in substantia nigra of the CMVMJD135 mouse model, was also not mitigated upon VPA treatment (Fig. 6E,F).

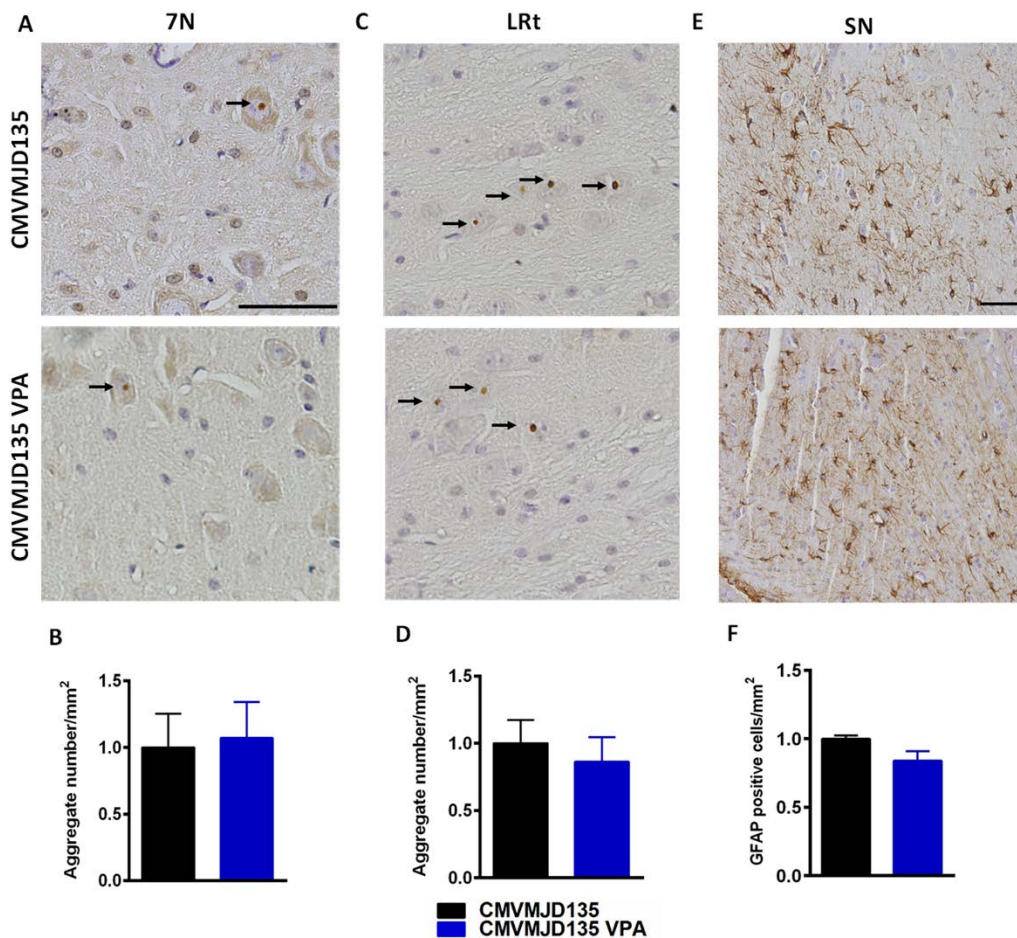


**Figure 5. Immunohistochemistry and quantification of ATXN3 neuronal inclusions and astrogliosis of VPA-treated and non-treated CMVMJD135.** No differences in nuclear ATXN3 inclusion load were observed between groups in (A,B) 7N and (C,D) LRt brain regions. No differences in astrogliosis in substantia nigra (SN) between VPA-treated and non-treated transgenic animals (E,F). Scale bar of ATXN3 figures, 20  $\mu$ m; Scale bar of GFAP figure, 200  $\mu$ m. Bars represent the mean  $\pm$  SEM (n=4 for each group), One-Way ANOVA.

## Chronic VPA treatment increases GRP78 protein levels in cerebellum of CMVMJD135 mice

One of the neuroprotective actions described for VPA is its ability to increase GRP78 protein levels, through HDAC inhibition<sup>15</sup>. GRP78, also known as binding immunoglobulin protein (BiP), is a stress chaperone protein found in the lumen of the endoplasmic reticulum (ER) which binds newly synthesized proteins as they are translocated into the ER, and keeps them in a competent state for subsequent folding and oligomerization<sup>33</sup>. We specifically investigated the potential role of HDAC inhibition by monitoring the GRP78 protein levels induction upon VPA treatment. We observe a striking increase in GRP78 protein levels in CMVMJD135-treated animals when compared to non-treated animals, in the cerebellum at 30 weeks of age (Fig. 6).

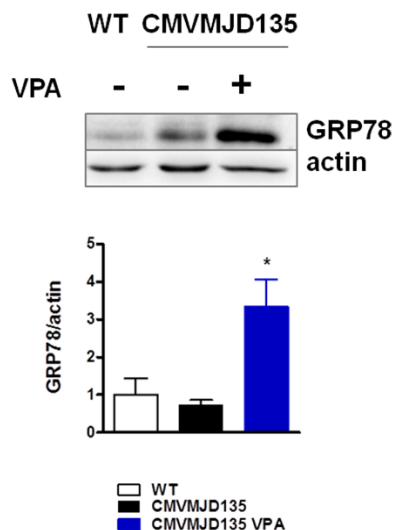


**Figure 6.** Cerebellum western-blot and quantification of GRP78 protein levels in 30 week-old WT, VPA-treated and non-treated CMVMJD135 mice. GRP78 protein induction in CMVMJD135 animals upon VPA treatment. Bars represent the mean  $\pm$  SEM (n=4 for each group), \* represent  $p < 0.05$ , One-way ANOVA.

## Discussion

In the past years, the use of VPA as a treatment for neurodegenerative disease models has been shown to improve neurological phenotypes, decrease cell degeneration and toxicity, together with the increase of histone acetylation and subsequent gene transcription activation<sup>34-39</sup>. The dosage of VPA of 200mg/kg used in this pre-clinical trial was previously described in a pre-clinical trial ALS, in which neuroprotective and histone acetylation effects were shown<sup>40,41</sup>. Here, we also show that five days treatment with 200mg/kg of VPA was able to exert a trend towards an increase in histone acetylation in cerebellum and a tendency to increase GADD45 $\alpha$  and BIM mRNA levels, which may be used as VPA target engagement<sup>42-44</sup>. The acute treatment and/or high variability between animals may account for the lack of statistical differences between groups. Acute VPA treated animals presented therapeutic

levels of  $252 \pm 15.8 \mu\text{mol/L}$  and  $25.7 \pm 8.7 \mu\text{mol/L}$  in plasma, after 30 and 120 minutes post-injection, respectively, which was within the usually accepted therapeutic range of VPA. Therefore, we performed a pre-clinical trial with five consecutive day treatment starting at 5 and ending at 30 weeks of age in CMVMJD135 mouse model. Animals in the pre-clinical trial were always maintained in an appropriate and healthy environment avoiding the development of any stressful condition that may interfere with their motor performance. Although previous findings by several groups suggested a therapeutic effect for VPA in cellular and invertebrate animal models of SCA3, in the present study, chronic VPA treatment of CMVMJD135 mice lead to a late and limited improvement in the motor performance, given by the beam balance, motor swimming, rotarod and spontaneous locomotor activity tests. For other general health and neuromuscular function, VPA-treatment had only marginal or even no effects comparing to vehicle-treated transgenic animals. In addition, the dosage used in this study is not considered toxic for mice and is already described as safe in the literature<sup>18,40,41,45</sup>. Nevertheless, chronic VPA treatment at similar dosage was already described to reduce the body mass gain in WT animals<sup>40</sup>, even though chronically treated human patients are known to increase their body weight upon VPA treatment<sup>46-48</sup>. Metabolic differences and biological system diversity could be the reason for these contradictory observations.

At the pathological level, we examined the presence of ATXN3 neuronal nuclear inclusions in facial nuclei (7N) and lateral reticular nuclei (LRt), two regions described to be affected in MJD human patients<sup>49,50</sup>, as well as in CMVMJD135 mouse model<sup>22</sup>. No differences were observed in the amount of nuclear neuronal inclusions of ATXN3 in both VPA-treated and non-treated CMVMJD135 mice. Additionally, astrogliosis is a consistent pathological phenotype of CMVMJD135 mouse model and human patients, which was also not mitigated by VPA chronic treatment.

The overexpression of specific chaperones has been shown to allow protection against cellular damage and/or death caused from an extensive group of agents and conditions including cytotoxic chemicals<sup>51</sup>, oxidative stress<sup>52</sup> and ER stress<sup>33</sup>. Here we show that the induction of GRP78 protein levels upon VPA chronic treatment, whose overexpression may be neuroprotective in proteinopathies, including MJD<sup>53,54</sup>, could be one of its cytoprotective actions in the MJD context, enhancing the folding capacity of the ER. The induction of GRP78 also indicates VPA target engagement during the chronic treatment in the pre-clinical trial, as this protein is known to be induced by VPA<sup>15</sup>. Although we did not observe a statistical difference in the CMVMJD135 animals when comparing to WT, enhancing the expression of this molecular chaperone in the cerebellum of these mice could be one of the

neuroprotective mechanisms responsible for the late and mild improvement of the CMVMJD135 animal motor performance.

The observed beneficial effects of VPA were transient, occurred mostly later in life and thus at an advanced stage of disease (between 22 and 30 weeks of age), mainly in behavioral tests more related with motor coordination. These results are comparable to some extent with previous findings, in which we have shown a significant reduction in neurological dysfunction in a *C. elegans* model of MJD after VPA treatment that was more relevant later in the worm's life (day10) in spite of early treatment<sup>21</sup>. Previous evidence also suggested a protective role for VPA in the context of MJD, both in cell and *Drosophila* models, by attenuating mutant ATXN3 induced cell toxicity and alleviating polyQ-induced phenotypic abnormalities, without major impact on ATXN3 inclusion<sup>19,20</sup>; in *C. elegans*, there was some improvement of aggregation, but less prominent than that observed for other compounds, for instance Hsp90 inhibitors<sup>21</sup>.

Although the effects observed in our mouse model were not striking, only one dosage of VPA was tested; thus, the possibility of testing other dosages, far from toxic and lethal ones<sup>55,56</sup>, should be considered, as they could exert more pronounced effects. Moreover, the complex activity and a broad range of VPA effects also create the need for further clarification of the effects of this drug not only at the symptom level, but also molecular and pathological levels in the CMVMJD135 mouse model. In fact, and although the use of HDACi's in the context of polyQ diseases has showed promising results, the evidence for a globally decreased histone acetylation is not fully consistent<sup>57</sup>, and this strategy still lacks some target specificity/selectivity<sup>58</sup> and requires a more in depth study of the mechanisms of action of these compounds in the central nervous system. Furthermore, chronic VPA treatment in human patients can produce some side effects, such as weight gain<sup>59,60</sup>, decreased reproductive potential<sup>61,62</sup> and increased susceptibility to birth defects<sup>63-65</sup>. Nevertheless, the strategy of re-purposing FDA/EMA-approved molecules, as VPA, could be of benefit for MJD and other rare diseases lacking effective therapies. Additionally, there is still an open window for different VPA dosages to be tested and since in the past years, a growing number of efforts are being developed for the formulation of a new generation of more selective and specific compounds this could be useful for the treatment not only of MJD, but also of other polyglutamine diseases.

## References

1. Bauer, P. O. & Nukina, N. The pathogenic mechanisms of polyglutamine diseases and current therapeutic strategies. *J. Neurochem.* **110**, 1737–1765 (2009).
2. Ross, C. A. *et al.* Pathogenesis of neurodegenerative diseases associated with expanded glutamine repeats: new answers, new questions. *Prog. Brain Res.* **117**, 397–419 (1998).
3. Kawaguchi, Y. *et al.* CAG expansions in a novel gene for Machado-Joseph disease at chromosome 14q32.1. *Nat. Genet.* **8**, 221–228 (1994).
4. Rüb, U., Brunt, E. R. & Deller, T. New insights into the pathoanatomy of spinocerebellar ataxia type 3 (Machado-Joseph disease). *Curr. Opin. Neurol.* **21**, 111–116 (2008).
5. Barbeau, A. *et al.* The natural history of Machado-Joseph disease. An analysis of 138 personally examined cases. *Can. J. Neurol. Sci. J. Can. Sci. Neurol.* **11**, 510–525 (1984).
6. Coutinho, P. & Andrade, C. Autosomal dominant system degeneration in Portuguese families of the Azores Islands. A new genetic disorder involving cerebellar, pyramidal, extrapyramidal and spinal cord motor functions. *Neurology* **28**, 703–709 (1978).
7. Lima, L. & Coutinho, P. Clinical criteria for diagnosis of Machado-Joseph disease: report of a non-Azorena Portuguese family. *Neurology* **30**, 319–322 (1980).
8. Hoffner, G. & Djian, P. Polyglutamine Aggregation in Huntington Disease: Does Structure Determine Toxicity? *Mol. Neurobiol.* (2014). doi:10.1007/s12035-014-8932-1
9. Seidel, K. *et al.* Axonal inclusions in spinocerebellar ataxia type 3. *Acta Neuropathol. (Berl.)* **120**, 449–460 (2010).
10. Evert, B. O. *et al.* Neuronal intranuclear inclusions, dysregulation of cytokine expression and cell death in spinocerebellar ataxia type 3. *Clin. Neuropathol.* **25**, 272–281 (2006).
11. Rüb, U. *et al.* Spinocerebellar ataxia type 3 (SCA3): thalamic neurodegeneration occurs independently from thalamic ataxin-3 immunopositive neuronal intranuclear inclusions. *Brain Pathol. Zurich Switz.* **16**, 218–227 (2006).
12. Weber, J. J., Sowa, A. S., Binder, T. & Hübener, J. From Pathways to Targets: Understanding the Mechanisms behind Polyglutamine Disease. *BioMed Res. Int.* **2014**, 1–22 (2014).
13. Rosenberg, G. The mechanisms of action of valproate in neuropsychiatric disorders: can we see the forest for the trees? *Cell. Mol. Life Sci. CMLS* **64**, 2090–2103 (2007).
14. Perucca, E. Pharmacological and therapeutic properties of valproate: a summary after 35 years of clinical experience. *CNS Drugs* **16**, 695–714 (2002).



15. Shi, Y., Gerritsma, D., Bowes, A. J., Capretta, A. & Werstuck, G. H. Induction of GRP78 by valproic acid is dependent upon histone deacetylase inhibition. *Bioorg. Med. Chem. Lett.* **17**, 4491–4494 (2007).
16. Zádori, D., Geisz, A., Vámos, E., Vécsei, L. & Klivényi, P. Valproate ameliorates the survival and the motor performance in a transgenic mouse model of Huntington's disease. *Pharmacol. Biochem. Behav.* **94**, 148–153 (2009).
17. Tsai, L.-K., Tsai, M.-S., Ting, C.-H. & Li, H. Multiple therapeutic effects of valproic acid in spinal muscular atrophy model mice. *J. Mol. Med. Berl. Ger.* **86**, 1243–1254 (2008).
18. Feng, H.-L. *et al.* Combined lithium and valproate treatment delays disease onset, reduces neurological deficits and prolongs survival in an amyotrophic lateral sclerosis mouse model. *Neuroscience* **155**, 567–572 (2008).
19. Yi, J. *et al.* Sodium valproate alleviates neurodegeneration in SCA3/MJD via suppressing apoptosis and rescuing the hypoacetylation levels of histone H3 and H4. *PLoS One* **8**, e54792 (2013).
20. Lin, X. P. *et al.* Valproic acid attenuates the suppression of acetyl histone H3 and CREB activity in an inducible cell model of Machado-Joseph disease. *Int. J. Dev. Neurosci. Off. J. Int. Soc. Dev. Neurosci.* **38**, 17–22 (2014).
21. Teixeira-Castro, A. *et al.* Neuron-specific proteotoxicity of mutant ataxin-3 in *C. elegans*: rescue by the DAF-16 and HSF-1 pathways. *Hum. Mol. Genet.* **20**, 2996–3009 (2011).
22. Silva-Fernandes, A. *et al.* Chronic treatment with 17-DMAG improves balance and coordination in a new mouse model of Machado-Joseph disease. *Neurother. J. Am. Soc. Exp. Neurother.* **11**, 433–449 (2014).
23. FELASA working group on revision of guidelines for health monitoring of rodents and rabbits *et al.* FELASA recommendations for the health monitoring of mouse, rat, hamster, guinea pig and rabbit colonies in breeding and experimental units. *Lab. Anim.* **48**, 178–192 (2014).
24. Silva-Fernandes, A. *et al.* Motor uncoordination and neuropathology in a transgenic mouse model of Machado-Joseph disease lacking intranuclear inclusions and ataxin-3 cleavage products. *Neurobiol. Dis.* **40**, 163–176 (2010).
25. Rafael, J. A., Nitta, Y., Peters, J. & Davies, K. E. Testing of SHIRPA, a mouse phenotypic assessment protocol, on Dmd(mdx) and Dmd(mdx3cv) dystrophin-deficient mice. *Mamm. Genome Off. J. Int. Mamm. Genome Soc.* **11**, 725–728 (2000).
26. Carter, R. J. *et al.* Characterization of progressive motor deficits in mice transgenic for the human Huntington's disease mutation. *J. Neurosci. Off. J. Soc. Neurosci.* **19**, 3248–3257 (1999).

27. Franklin, K. B. J. *Paxinos and Franklin's The mouse brain in stereotaxic coordinates*. (Academic Press, an imprint of Elsevier, 2013).
28. Zar, J. H. *Biostatistical analysis*. (Prentice Hall, 1999).
29. Sultan, F. A. & Sweatt, J. D. The role of the Gadd45 family in the nervous system: a focus on neurodevelopment, neuronal injury, and cognitive neuroepigenetics. *Adv. Exp. Med. Biol.* **793**, 81–119 (2013).
30. Akhtar, R. S., Ness, J. M. & Roth, K. A. Bcl-2 family regulation of neuronal development and neurodegeneration. *Biochim. Biophys. Acta BBA - Mol. Cell Res.* **1644**, 189–203 (2004).
31. Yamauchi, J. *et al.* Gadd45a, the gene induced by the mood stabilizer valproic acid, regulates neurite outgrowth through JNK and the substrate paxillin in N1E-115 neuroblastoma cells. *Exp. Cell Res.* **313**, 1886–1896 (2007).
32. Xie, C. *et al.* Mechanisms of synergistic antileukemic interactions between valproic acid and cytarabine in pediatric acute myeloid leukemia. *Clin. Cancer Res. Off. J. Am. Assoc. Cancer Res.* **16**, 5499–5510 (2010).
33. Morris, J. A., Dorner, A. J., Edwards, C. A., Hendershot, L. M. & Kaufman, R. J. Immunoglobulin binding protein (BiP) function is required to protect cells from endoplasmic reticulum stress but is not required for the secretion of selective proteins. *J. Biol. Chem.* **272**, 4327–4334 (1997).
34. Steffan, J. S. *et al.* Histone deacetylase inhibitors arrest polyglutamine-dependent neurodegeneration in *Drosophila*. *Nature* **413**, 739–743 (2001).
35. Ferrante, R. J. *et al.* Histone deacetylase inhibition by sodium butyrate chemotherapy ameliorates the neurodegenerative phenotype in Huntington's disease mice. *J. Neurosci. Off. J. Soc. Neurosci.* **23**, 9418–9427 (2003).
36. Hockly, E. *et al.* Suberoylanilide hydroxamic acid, a histone deacetylase inhibitor, ameliorates motor deficits in a mouse model of Huntington's disease. *Proc. Natl. Acad. Sci. U. S. A.* **100**, 2041–2046 (2003).
37. Chou, A.-H., Chen, S.-Y., Yeh, T.-H., Weng, Y.-H. & Wang, H.-L. HDAC inhibitor sodium butyrate reverses transcriptional downregulation and ameliorates ataxic symptoms in a transgenic mouse model of SCA3. *Neurobiol. Dis.* **41**, 481–488 (2011).
38. Hahnen, E. *et al.* Histone deacetylase inhibitors: possible implications for neurodegenerative disorders. *Expert Opin. Investig. Drugs* **17**, 169–184 (2008).
39. Minamiyama, M. *et al.* Sodium butyrate ameliorates phenotypic expression in a transgenic mouse model of spinal and bulbar muscular atrophy. *Hum. Mol. Genet.* **13**, 1183–1192 (2004).

40. Rouaux, C. *et al.* Sodium valproate exerts neuroprotective effects in vivo through CREB-binding protein-dependent mechanisms but does not improve survival in an amyotrophic lateral sclerosis mouse model. *J. Neurosci. Off. J. Soc. Neurosci.* **27**, 5535–5545 (2007).
41. Hoffmann, K., Czapp, M. & Löscher, W. Increase in antiepileptic efficacy during prolonged treatment with valproic acid: role of inhibition of histone deacetylases? *Epilepsy Res.* **81**, 107–113 (2008).
42. Yamauchi, J. *et al.* Gadd45a, the gene induced by the mood stabilizer valproic acid, regulates neurite outgrowth through JNK and the substrate paxillin in N1E-115 neuroblastoma cells. *Exp. Cell Res.* **313**, 1886–1896 (2007).
43. Stauber, R. H. *et al.* A combination of a ribonucleotide reductase inhibitor and histone deacetylase inhibitors downregulates EGFR and triggers BIM-dependent apoptosis in head and neck cancer. *Oncotarget* **3**, 31–43 (2012).
44. Mologni, L. *et al.* Valproic acid enhances bosutinib cytotoxicity in colon cancer cells. *Int. J. Cancer J. Int. Cancer* **124**, 1990–1996 (2009).
45. Tremolizzo, L. *et al.* An epigenetic mouse model for molecular and behavioral neuropathologies related to schizophrenia vulnerability. *Proc. Natl. Acad. Sci. U. S. A.* **99**, 17095–17100 (2002).
46. Corman, C. L., Leung, N. M. & Guberman, A. H. Weight gain in epileptic patients during treatment with valproic acid: a retrospective study. *Can. J. Neurol. Sci. J. Can. Sci. Neurol.* **24**, 240–244 (1997).
47. Martin, C. K., Han, H., Anton, S. D., Greenway, F. L. & Smith, S. R. Effect of valproic acid on body weight, food intake, physical activity and hormones: results of a randomized controlled trial. *J. Psychopharmacol. Oxf. Engl.* **23**, 814–825 (2009).
48. Verrotti, A., D'Egidio, C., Mohn, A., Coppola, G. & Chiarelli, F. Weight gain following treatment with valproic acid: pathogenetic mechanisms and clinical implications. *Obes. Rev. Off. J. Int. Assoc. Study Obes.* **12**, e32–43 (2011).
49. Rüb, U. *et al.* Degeneration of ingestion-related brainstem nuclei in spinocerebellar ataxia type 2, 3, 6 and 7. *Neuropathol. Appl. Neurobiol.* **32**, 635–649 (2006).
50. Rüb, U. *et al.* Spinocerebellar ataxia type 3 (Machado-Joseph disease): severe destruction of the lateral reticular nucleus. *Brain J. Neurol.* **125**, 2115–2124 (2002).
51. Reddy, R. K. *et al.* Endoplasmic reticulum chaperone protein GRP78 protects cells from apoptosis induced by topoisomerase inhibitors: role of ATP binding site in suppression of caspase-7 activation. *J. Biol. Chem.* **278**, 20915–20924 (2003).

52. Liu, H. *et al.* Endoplasmic reticulum chaperones GRP78 and calreticulin prevent oxidative stress, Ca<sup>2+</sup> disturbances, and cell death in renal epithelial cells. *J. Biol. Chem.* **272**, 21751–21759 (1997).
53. Gorbatyuk, M. S. & Gorbatyuk, O. S. The Molecular Chaperone GRP78/BiP as a Therapeutic Target for Neurodegenerative Disorders: A Mini Review. *J. Genet. Syndr. Gene Ther.* **4**, (2013).
54. Pereira, C. M. F. Crosstalk between Endoplasmic Reticulum Stress and Protein Misfolding in Neurodegenerative Diseases. *ISRN Cell Biol.* **2013**, 1–22 (2013).
55. Goodwin, D. G., Strobl, J., Mitchell, S. M., Zajac, A. M. & Lindsay, D. S. Evaluation of the mood-stabilizing agent valproic acid as a preventative for toxoplasmosis in mice and activity against tissue cysts in mice. *J. Parasitol.* **94**, 555–557 (2008).
56. Löscher, W. Pharmacological, toxicological and neurochemical effects of delta 2(E)-valproate in animals. *Pharm. Weekbl. Sci.* **14**, 139–143 (1992).
57. Valor, L. M., Guiretti, D., Lopez-Atalaya, J. P. & Barco, A. Genomic landscape of transcriptional and epigenetic dysregulation in early onset polyglutamine disease. *J. Neurosci. Off. J. Soc. Neurosci.* **33**, 10471–10482 (2013).
58. Kazantsev, A. G. & Thompson, L. M. Therapeutic application of histone deacetylase inhibitors for central nervous system disorders. *Nat. Rev. Drug Discov.* **7**, 854–868 (2008).
59. Wirrell, E. C. Valproic acid-associated weight gain in older children and teens with epilepsy. *Pediatr. Neurol.* **28**, 126–129 (2003).
60. Grosso, S., Mostardini, R., Piccini, B. & Balestri, P. Body mass index and serum lipid changes during treatment with valproic acid in children with epilepsy. *Ann. Pharmacother.* **43**, 45–50 (2009).
61. Isojärvi, J. Disorders of reproduction in patients with epilepsy: antiepileptic drug related mechanisms. *Seizure* **17**, 111–119 (2008).
62. Verrotti, A. *et al.* Hormonal and reproductive disturbances in epileptic male patients: emerging issues. *Reprod. Toxicol. Elmsford N* **31**, 519–527 (2011).
63. Clayton-Smith, J. & Donnai, D. Fetal valproate syndrome. *J. Med. Genet.* **32**, 724–727 (1995).
64. Genton, P., Semah, F. & Trinka, E. Valproic acid in epilepsy : pregnancy-related issues. *Drug Saf.* **29**, 1–21 (2006).
65. Ornoy, A. Valproic acid in pregnancy: how much are we endangering the embryo and fetus? *Reprod. Toxicol. Elmsford N* **28**, 1–10 (2009).

## Supplementary data

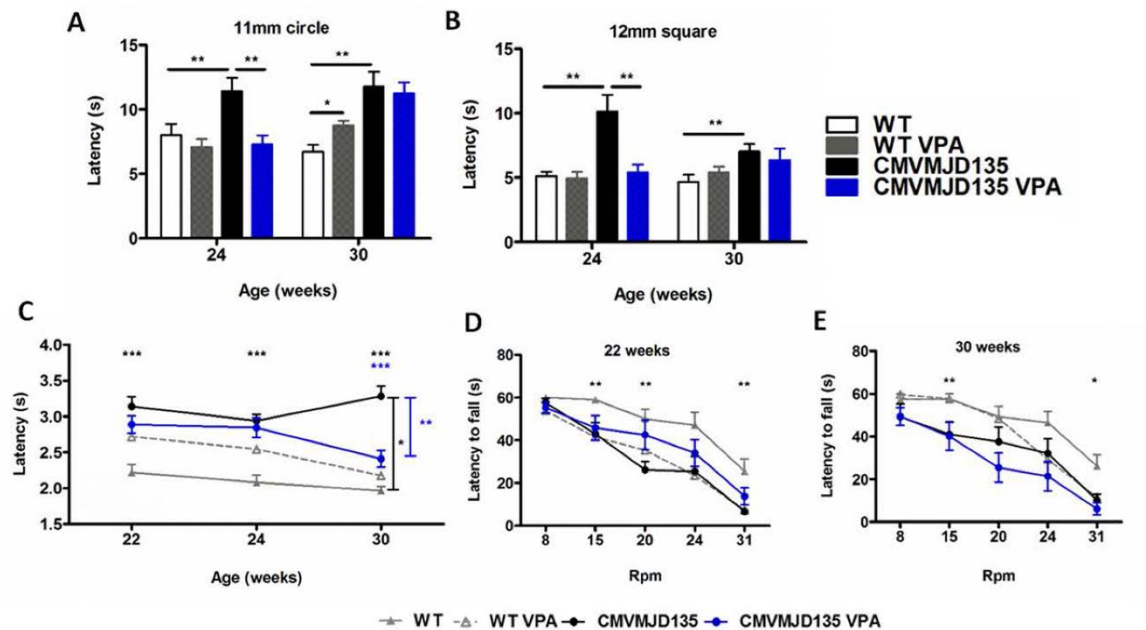


**Figure S1. Balance and motor coordination were improved at later stages upon VPA treatment given by the balance beam and motor swimming performance.** (A) Amelioration of balance and motor coordination at 24 weeks of age in 11 mm circle and (B) 12 mm square beams in beam walk test; (C) Motor swimming coordination improvement; (D,E) no improvement in increasing rotations in Rotarod were observed between VPA-treated and non-treated CMVMJD135. Bars represent the mean  $\pm$  SEM (WT veh, n=10; WT VPA, n=15, CMVMJD135 vehicle, n=10, CMVMJD135 VPA, n=13), \* represent  $p < 0.05$ , \*\* represent  $p < 0.01$  and \*\*\* represent  $p < 0.001$ , black asterisks represents the difference between WT and CMVMJD135, blue asterisks represents the difference between non-treated and VPA-treated CMVMJD135, (Repeated-measures ANOVA, Tukey correction for continuous variables, One-Way ANOVA for differences between groups in specific ages of the continuous variables and Mann-Whitney U test for continuous variables without normal distribution (Rotarod)).



## CHAPTER 3

---

Serotonergic signaling suppresses ataxin-3 aggregation, improves motor balance and coordination and exerts neuroprotection effects in a mouse model of Machado-Joseph disease

**(Part of this work was published in *Brain*, Appendix I)**

**Serotonergic signaling suppresses ataxin-3 aggregation, improves motor balance and coordination and exerts neuroprotection effects in a mouse model of Machado-Joseph disease**

Sofia Esteves<sup>1,2</sup>, Sara Duarte-Silva<sup>1,2</sup>, Anabela Silva-Fernandes<sup>1,2</sup>, Andreia Neves-Carvalho<sup>1,2</sup>, Pedro Oliveira<sup>3</sup>, Andreia Teixeira-Castro<sup>1,2</sup>, and Patrícia Maciel<sup>1,2</sup>

1) Life and Health Sciences Research Institute (ICVS), School of Health Sciences, University of Minho, 4710-057 Braga, Portugal.

2) ICVS/3Bs - PT Government Associate Laboratory, Braga/Guimarães, Portugal.

3) ICBAS-Abel Salazar Biomedical Sciences Institute, University of Porto, Porto, Portugal.



## Abstract

Polyglutamine diseases are a class of dominantly inherited neurodegenerative disorders for which there is no effective treatment. Here we provide evidence that activation of serotonergic signaling is beneficial in a mouse model of Machado-Joseph disease (MJD). Previous work in a *C. elegans* model of MJD identified citalopram, a selective serotonin re-uptake inhibitor (SSRI), in a screen of FDA-approved small molecules for suppressors of mutant ataxin-3 induced neurotoxicity. In MJD *C. elegans* model, citalopram rescued mutant ataxin-3-mediated neuronal dysfunction and reduced aggregation. In this work, we tested the therapeutic efficacy of chronic citalopram treatment in the CMVMJD135 mouse model with two different dosages. This compound reduced ataxin-3 neuronal inclusions, mitigated astrogliosis, decreased neuronal loss and strikingly ameliorated motor symptoms, together with a rescue of diminished body weight mainly at 8 mg/kg dosage. These results suggest that modulation of serotonergic signaling could be a promising therapeutic strategy for MJD, with beneficial effects in the enhancement of proteostasis.

## Introduction

Polyglutamines (PolyQ) diseases are hereditary neurodegenerative disorders caused by an expansion of a trinucleotide CAG repeat within the coding region of specific genes. This group of disorders includes Huntington's disease (HD), spinobulbar muscular atrophy (SBMA), dentatorubral-pallidoluysian atrophy (DRPLA) and six forms of spinocerebellar ataxia<sup>1</sup>. MJD (or Spinocerebellar Ataxia type 3, SCA3), the most common dominantly inherited ataxia worldwide<sup>2</sup>, is caused by an expansion of a polyQ tract in the ataxin-3 protein (ATXN3)<sup>3</sup>. This adult-onset disorder is characterized by ataxia, ophthalmoplegia and pyramidal signs, associated with dystonia, spasticity, peripheral neuropathy and amyotrophy<sup>4</sup>, however without cognitive decline. At the pathological level, there is degeneration of the deep nuclei of the cerebellum, pontine and subthalamic nuclei, substantia nigra and spinocerebellar nuclei<sup>4-6</sup> as well as the presence of ATXN3 intranuclear inclusions in these brain regions<sup>7,8</sup>.

Despite the recent efforts towards the understanding of the pathogenesis of this disorder, the molecular pathways that ultimately lead to neuronal demise remain mostly unknown and no effective treatments are yet available for MJD, as for other polyQ diseases. In the last decades several emerging therapeutic strategies have been suggested for MJD, however not yet translated to the clinic. These strategies are based on the proposed pathogenic hypothesis and comprise the pharmacologic chaperone/kinetic stabilizer approaches and the use of small molecules or gene targeting to manipulate concentration, conformation, and/or the location of ATXN3. For example, modulating the

levels of molecular chaperones HSP70, alphaB-crystallin and HSP104 can prevent or inhibit ATXN3 aggregation, and promotes its dis-aggregation<sup>9-11</sup>. Activation of autophagy, either by gene overexpression or by pharmacological activation of the pathway, can also ameliorate mutant ATXN3 pathogenesis *in vivo*<sup>12-14</sup>. Reversion of the polyQ-associated transcription down-regulation by an HDAC inhibitor (HDACi) also rescued ataxic symptoms<sup>15</sup>. Silencing of *ATXN3* offers potential, however its impact has not been promising in MJD mice<sup>16,17</sup>. For the majority of these candidate therapies, their translation to clinical trials is a very long process due to uncertainty concerning human safety. Despite the investments in drug discovery and development during the past decades, the number of new drugs introduced into the clinic has not increased significantly. The traditional approach to drug discovery, which involves *de novo* identification and validation of new molecular entities, has been costly and time-consuming. Furthermore, as the average time required for drug development has increased, there has been a new interest in drug re-purposing strategies<sup>18</sup>.

Our group has previously established a *C. elegans* model of MJD in which expression of mutant human *ATXN3* in the worm's nervous system led to its progressive aggregation in distinct neuronal subtypes and altered motor behavior<sup>19</sup>. This model was used by Teixeira-Castro *et al.*<sup>20</sup>, to screen a library of >600 FDA-approved small molecules, and to identify compounds that rescued or ameliorated mutant ATXN3-mediated neurological dysfunction (Appendix I). Citalopram, belonging to the selective serotonin re-uptake inhibitor (SSRI) class, was identified in the screening through its neurotoxicity suppression mechanism and then proven to modify also ATXN3 aggregation. The main mechanism of action of SSRI's is serotonin transporter (SERT) inhibition, increasing the serotonin (5-HT) levels, and therefore the serotonergic transmission. In spite of being a powerful platform to study neurodegenerative diseases and to perform HTS for small molecules, the direct translation from *C. elegans* outcomes to human is a huge step and may not faithfully predict the drug action in humans. Therefore, it is crucial to test the hit compounds' efficacy in a mammalian model that may more closely mirror the human disease. Here we show that citalopram was able to improve the motor balance and coordination in the CMVMJD135 mouse model of MJD, together with suppression in ATXN3 aggregation and astrogliosis, and neuroprotective effects, suggesting this FDA-approved compound as a very promising candidate to be translated to the clinic with few side effects.

## Material and Methods

**Transgenic mouse model and drug administration.** CMVMJD135 mice were generated as described previously<sup>14</sup>. DNA extraction, animal genotyping and CAG repeat size analyses were performed as previously described<sup>21</sup>. The mean repeat size ( $\pm$ SD) for all mice used was  $130 \pm 2$ . Age-matched and genetic background-matched wild-type (WT) animals were used as controls. Only male mice were used in this study. We administrated citalopram hydrobromide (CAS 59729-32-7, kindly provided by Lundbeck, Denmark) in the drinking water at two doses (8 and 13 mg/kg/day) that roughly equate the higher dosage range prescribed to human patients for depression<sup>22</sup>. Treatment was initiated at five weeks of age, one week before the expected onset of the first neurological symptoms, according to our previous knowledge of this model<sup>14</sup> and ended at 34 weeks of age. All animal procedures were conducted in accordance with European regulations (European Union Directive 2010/63/EU). Animal facilities and the people directly involved in animal experiments (SE, SDS, ASF, ATC) were certified by the Portuguese regulatory entity – Direção Geral de Alimentação e Veterinária. All the protocols were approved by the Animal Ethics Committee of the Life and Health Sciences Research Institute, University of Minho.

**Behavioral assessment.** Behavioral analysis was performed during the diurnal period in groups of 5 males per cage including CMVMJD135 hemizygous transgenic mice and WT littermates ( $n=13-16$  per genotype) treated with citalopram or with vehicle (water). All behavioral tests started in a pre-symptomatic stage (4 weeks of age) and were conducted until 30 or 34 weeks of age (Fig. 1A). Neurological tests and general health assessment were performed using a selection of tests from the SHIRPA protocol (tremors, claspings, gait quality, exploratory activity, locomotor activity, body curvature, strength to grab and hindlimb tonus) enriched with the hanging wire and vertical pole test. The dragging of the paws and the stride length were evaluated with footprinting analysis as described by Silva-Fernandes *et al.*<sup>1</sup>. Motor behavior was further assessed using the balance beam walk test (12 mm square and 17 mm round beams) and the motor swimming test. All behavioral tests were performed as previously described<sup>21</sup>. Body weight was also registered for each evaluation time point.

**Immunohistochemistry.** Thirty four week-old WT and CMVMJD135 littermate mice, citalopram-treated and non-treated ( $n=4$  for each group) were deeply anesthetized with a mixture of ketamine hydrochloride (150 mg/kg) plus medetomidine (0.3 mg/kg) and transcardially perfused with phosphate-buffered saline (PBS) followed by 4% paraformaldehyde (PFA) (Panreac, USA). Brains were

removed and post-fixed overnight in PFA and embedded in paraffin. Slides with 4- $\mu$ m-thick paraffin sections were subjected to antigen retrieval and then incubated with mouse anti-ATXN3 (1H9) (1:100, MAB5360, Milipore), rabbit anti-GFAP (1:1000, DAKO Corporation, Carpinteria) and mouse anti-Calbindin D-28K (1:1000, AB1778, Millipore, USA), which were detected by incubation with a biotinylated anti-polyvalent antibody, followed by detection through biotin-streptavidin coupled to horseradish peroxidase and reaction with the DAB (3, 3'-diaminobenzidine) substrate (Lab Vision<sup>TM</sup> Ultra-Vision<sup>TM</sup> Detection kit, Thermo Scientific). The slides were counterstained with hematoxylin 25% according to standard procedures. ATXN3 positive inclusions in the pontine nuclei (PN), reticulotegmental nucleus of the pons (RtTg), facial motor nucleus (7N) and lateral reticular nucleus (LRt), stained astrocytes (GFAP-positive) in the substantia nigra (SN) and Calbindin D-28K positive neurons in cerebellar cortex (CBX) of either vehicle or citalopram treated animals (n=4 for each conditions, 4 slides per animal) were quantified and normalized for total area using the Olympus BX51 stereological microscope (Olympus, Japan) and the Visiopharma integrator system software (Visiopharm, Denmark) as previously described<sup>21</sup>.

Thirty four week-old WT and CMVMJD135 littermate mice, vehicle- and citalopram-treated (n=4 for each group), were deeply anesthetized as mentioned above, transcardially perfused with NaCl (0,9%), and the mouse brains embedded in OCT and rapidly frozen in isopentane (CAS#78-78-4, Sigma-Aldrich, USA) chilled in liquid nitrogen. Slides with 30  $\mu$ m-thick cryostat sections were incubated with goat anti-Choline Acetyltransferase (ChAT, 1:500, AB143, Millipore, USA) and stained with VECTASTAIN<sup>®</sup> ABC system (Vector Laboratories, UK), mouse anti-NeuN (1:500, MAB377, Milipore, USA), rabbit anti-Tyrosine Hydroxylase (TH, 1:300, AB152, Milipore, USA) which were detected with Lab Vision<sup>TM</sup> Ultra-Vision<sup>TM</sup> Detection kit protocol as described above. ChAT, NeuN and TH positive neurons were quantified and normalized as described above, in the 7N, PN and Substantia nigra pars compacta (SNc), respectively.

Fifty  $\mu$ m-thick vibrotome spinal cord sections were incubated with goat anti-Choline Acetyltransferase (ChAT, 1:500, AB143, Millipore, USA) and stained with VECTASTAIN<sup>®</sup> ABC system (Vector Laboratories, UK). ChAT positive neurons in the ventral horn of the Lumbar spinal cord (LSC) were quantified and normalized for total area as described above. Fifty  $\mu$ m-thick vibrotome spinal cord sections were stained with thionin according to standard procedures for motor neuron countings. The number of large stained motor neurons in the ventral horn was quantified using ImageJ.

**Western-blot analysis.** Protein isolation from mouse brainstem tissue and Western-blot were performed as previously described<sup>21</sup>. The blots were blocked and incubated overnight at 4°C with the primary antibody rabbit anti-ataxin-3 serum (1:5000, kindly provided by Dr. Henry Paulson) and anti-GAPDH (1:1000, G8795, Sigma, USA). As a loading control, mouse ataxin-3 and GAPDH were used. Western-blot quantifications were performed using Chemidoc XRS Software with Image Lab Software (Biorad, USA), according to the manufacturer's instructions.

**Study design and statistical analysis.** Experimental design was based on power analyses for optimization of sample size. Mouse sample size calculations were performed for each behavioral test and pathological analyses assuming a power of 0.8, and a significance level of  $p < 0.05$ . Data was analyzed through the non-parametric Mann-Whitney U-test when variables were non-continuous or when a continuous variable did not present a normal distribution (Kolmogorov-Smirnov test,  $p < 0.05$ ). Continuous variables with normal distributions and with homogeneity of variance (Levene's test) were analyzed with Repeated-Measures ANOVA for longitudinal multiple comparisons and One-Way ANOVA for paired comparisons, using Tukey for post-hoc comparisons. When these two latter assumptions were not valid, an appropriate data transformation (e.g., logarithmic) was applied, and the data were reanalyzed (body weight, balance beam walk test and motor swimming test). All statistical analyses were performed using SPSS 22.0 (SPSS Inc., Chicago, IL) and G-Power 3.1.9.2 (University Kiel, Germany). A critical value for significance of  $p < 0.05$  was used throughout the study.

## Results

### **Citalopram treatment rescued weight gain and improved neurological symptoms of CMVMJD135 mice without improvement in muscle strength tests**

To validate the results previously obtained in a *C.elegans* model of MJD in a mammalian model, we assessed the therapeutic efficacy of citalopram in an MJD mouse model - CMVMJD135. As reported previously, CMVMJD135 transgenic mice displays a progressive neurological phenotype with neuropathology and intranuclear inclusions consistent with that of human patients<sup>14</sup>. Chronic treatment with citalopram 8mg/kg/day was administered in the drinking water. The treatment started at 5 weeks of age, one week before the expected onset of the first neurological symptoms, and was continued until 34 weeks. A battery of behavioral tests was performed assessing limb strength, balance, gait, coordination, and other neurological parameters like tremors or limb claspings, among others. Tests were initiated in a pre-symptomatic stage of the disease (4 weeks of age) and conducted until an age

when the phenotype is fully established (34 weeks) (study design – Fig. 1A). When no improvement trend was observed along the age, tests were stopped at 30 weeks of age.

The first sign of neurological disease in the CMVMJD135 model is the presence of grip strength abnormalities at 6 weeks of age, given by the significant decrease in the latency to fall off in the vertical pole test and in the hanging wire test. In the vertical pole test (Fig. 1B), citalopram failed to rescue the limb strength while in the hanging wire test (Fig. 1C), limited effects on the loss of limb strength were observed at some time points but no longer maintained with age. Another disease phenotype feature of the CMVMJD135 mouse model is their decreased body weight gain when compared to WT animals, which was prevented with oral administration of citalopram (Fig. 1D). While there was only marginal improvement in the dragging of the paws (Fig. 1E) and limited effects on exploratory activity, strength to grab and hindlimb tonus (Supplementary data), citalopram treatment restored stride length to WT animals at advanced stages of the trial (Fig. 1F,G). Moreover, treated animals showed reduced tremors (Fig. 1H), reduced limb clasping (Fig. 1I) and improved gait quality (Fig. 1J).

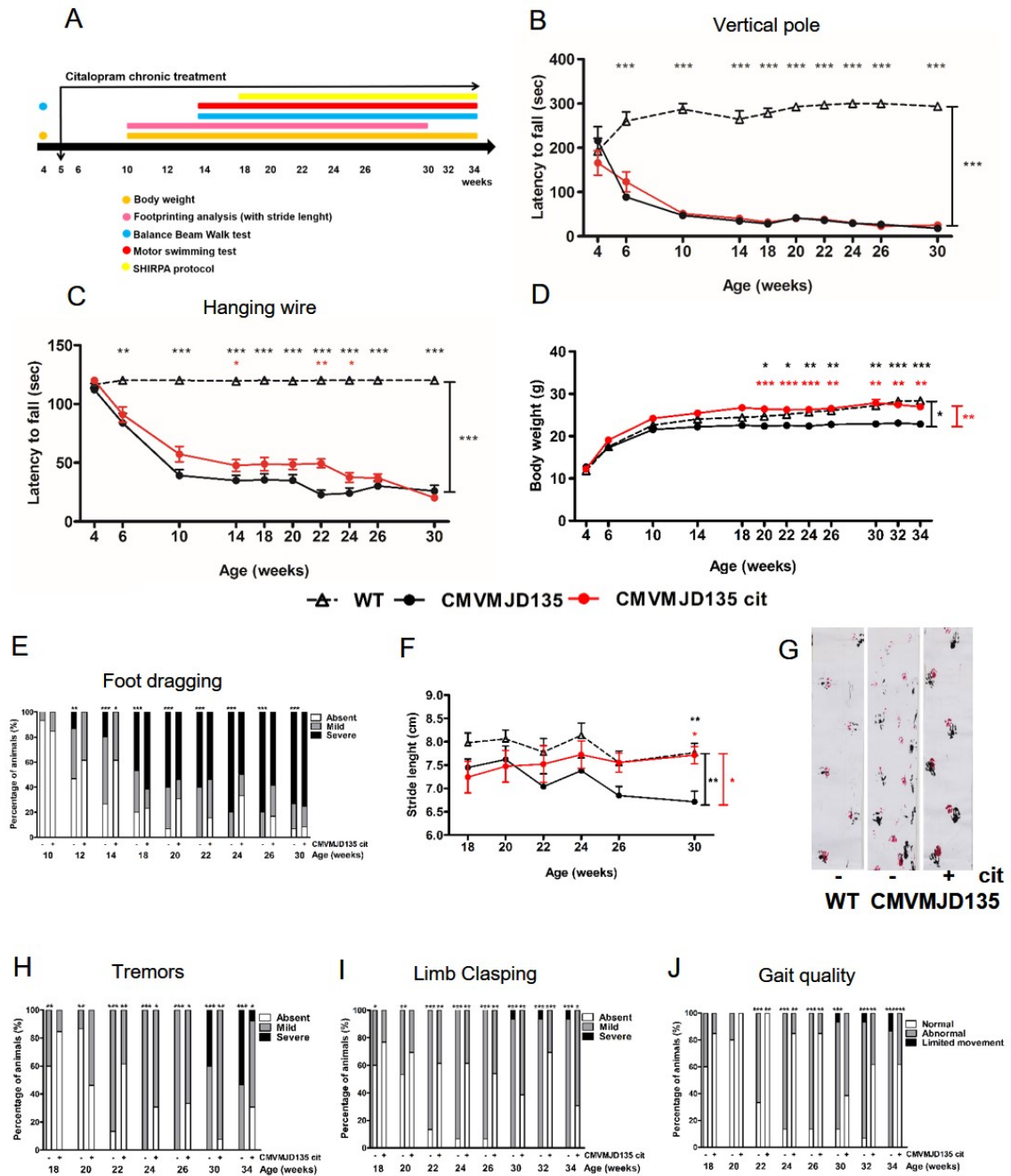


**Figure 1.** Impact of citalopram treatment at 8mg/kg/day on the neurological deficits of CMVMJD135 mice. (A) Schematic representation of the pre-clinical therapeutic trial. (B) No differences in vertical pole test and (C) limited improvement in hanging wire test upon citalopram treatment. Significant differences observed between vehicle (n=13) and cit treated CMVMJD135 mice (n=16) in (D) body weight (p=0.001, 20-34 weeks), in (E) foot dragging (p=0,035 at 14 weeks), and (F) stride length (p=0.015, 30 weeks). (G) Figure representation of stride length of WT, citalopram CMVMJD135-treated and non-treated at 30 weeks of age. (H) Tremors, (I) limb claspings and (J) gait quality were evaluated from 18 to 34 weeks of age with phenotype amelioration from 22 to 34 weeks of age. (n=13-16), \*p<0.05, \*\*p<0.01 and \*\*\*p<0.001 (Mann-Whitney U test for non-parametric variables and ANOVA, Tukey correction for continuous variables). Data presented mean  $\pm$  SEM.

**Citalopram treatment improves motor balance and coordination of CMVMJD135 mice**

Citalopram treatment resulted in a remarkable improvement in balance and motor coordination when compared to vehicle-treated CMVMJD135 mice (Fig. 2). In the balance beam walk test, we observed major improvements in time taken to cross the 12 mm square beam from 20 to 34 weeks of age (Fig. 2A) and also saw these improvements at late disease stages in a wider (17 mm) circle beam (Fig. 2B). A smaller 11 mm circle beam (Fig. 2C) was also used for assessment of motor coordination, but no major improvements in performance were detected. This beam is more challenging to the mice, particularly at late stages, when non-treated transgenic animals often fall off the beam. However, a measure of the percentage of falls in this beam, at late stages, showed that citalopram treated-CMVMJD135 mice fell significantly less than non-treated animals (Fig. 2D). The most notable benefits of citalopram were observed in the motor swimming test (Fig. 2E), since at many time points and until quite late in the trial citalopram treated animals were indistinguishable from WT, indicating that citalopram treatment significantly delayed disease progression in mice.



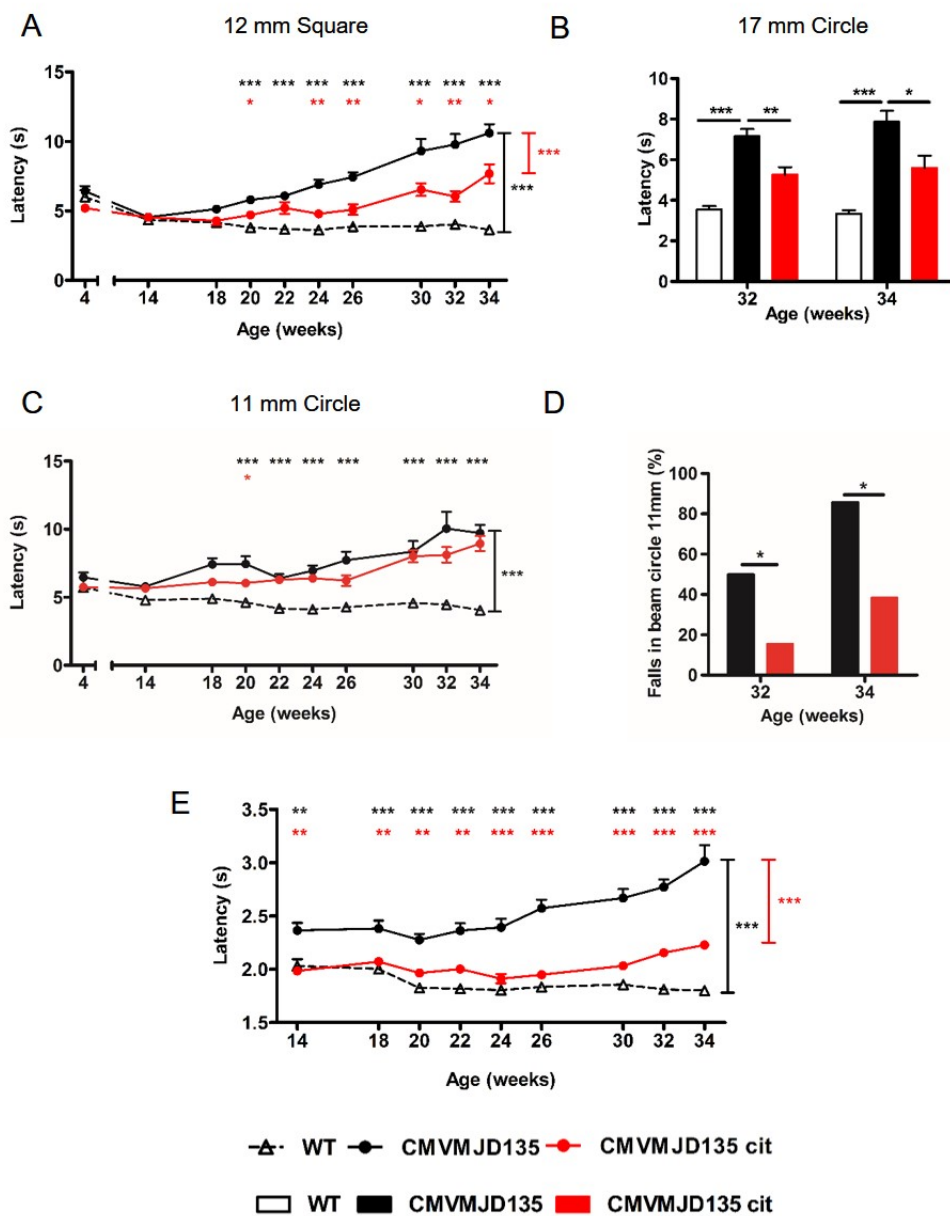


**Figure 2.** Citalopram treatment ameliorates balance and motor coordination. Significant differences observed between vehicle ( $n=13$ ) and cit treated CMVMJD135 mice ( $n=16$ ) in the (A) square beam ( $p<0.001$ , 20-34 weeks), and (B) 17 mm circle beam ( $p<0.05$ , 32-34 weeks). Significant improvement of cit treated CMVMJD135 mice at 20 weeks of age in (C) 11 mm circle ( $p<0.05$ ) with a significantly decrease in (D) percentage of falls of cit treated CMVMJD135 mice as compared with vehicle animals ( $p<0.05$ , 32-34 weeks). Significant differences since the beginning until 34 weeks of age in (E) motor swimming ( $p<0.001$ , 14-34 weeks) test. Data presented as mean  $\pm$  SEM. \* $p<0.05$ , \*\* $p<0.01$  and \*\*\* $p<0.001$  (Repeated measures ANOVA and One-way ANOVA, Tukey correction).

Importantly, citalopram treated WT mice behaved similarly to their untreated littermates, confirming the specificity of the citalopram effect in CMVMJD135 mice. Significant differences were only observed in the citalopram WT treated animals concerning body weight, which was increased (Fig. 3).

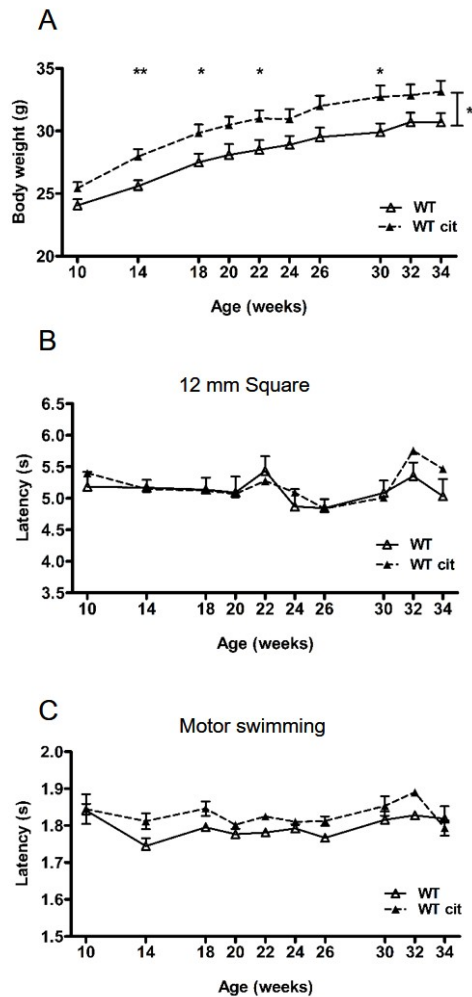


**Figure 3.** Impact of citalopram treatment at 8mg/kg/day on body weight and on motor behavior of WT mice. (A) Body weight, (B) beam walk and (C) motor swimming tests of vehicle and cit treated WT mice. Cit treatment resulted in a significant increase in body weight ( $p=0.033$ ). No differences between WT and cit treated WT mice were observed in the beam walk ( $p=0.40$ ) and motor swimming tests ( $p=0.839$ ). ( $n=10$ ), data presented as mean  $\pm$  SEM. \* $p<0.05$ , \*\* $p<0.01$  and \*\*\* $p<0.001$  (Repeated-measures ANOVA).

### Citalopram treatment reduced ATXN3 intranuclear inclusions without changing the overall levels of ATXN3 protein

The analysis of brain tissue from CMVMJD135 mice showed that citalopram treatment (8mg/kg/day) reduced ATXN3 intranuclear inclusions in the brainstem (Fig. 4A), equivalent to the decrease of neuronal aggregates observed in *C. elegans* (Appendix I). This reduction was observed in the pontine nuclei (PN), reticulotegmental nuclei of pons (RtTg) and facial motor nuclei (7N) of CMVMJD135 treated mice when compared to their vehicle-treated counterparts (Fig. 4A); the impact of citalopram was less obvious in the lateral reticular nuclei (LRt). This reduced ATXN3 aggregation did not correspond to lower ATXN3 protein levels in the brainstem (Fig. 4B), suggesting that the effect of

citalopram in mice is comparable to that in *C. elegans*, which may affect folding and solubility of ATXN3 rather than clearance of the mutant protein.

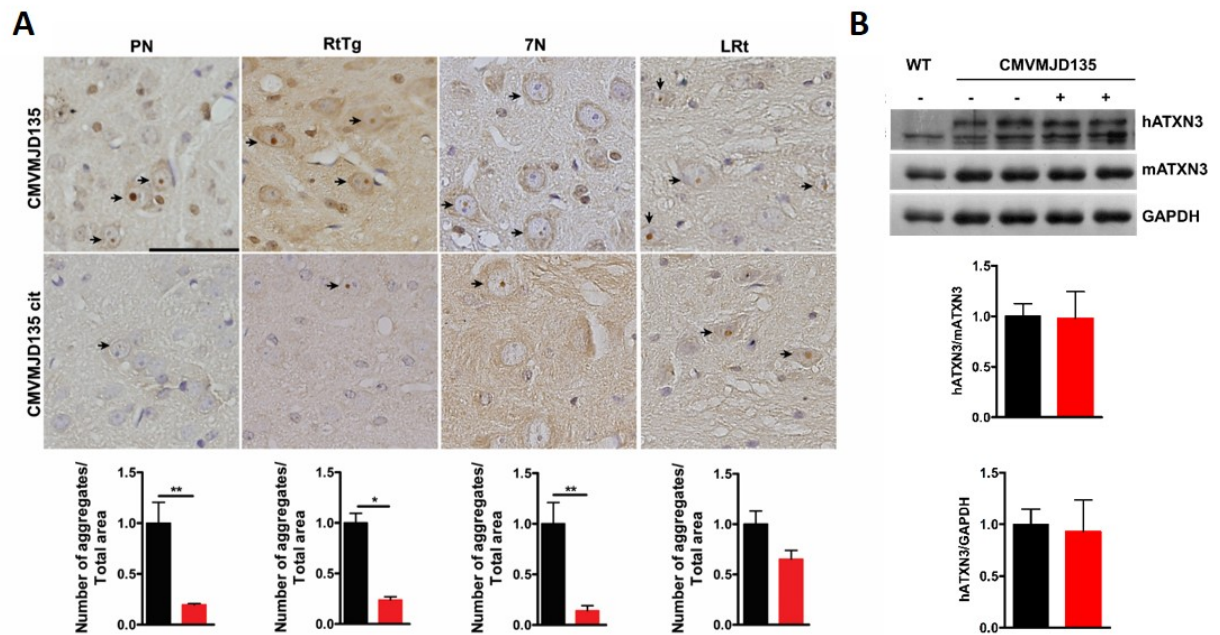


**Figure 4.** Citalopram effect in ATXN3 intranuclear inclusions and protein levels. (A) Immunohistochemistry of ATXN3 neuronal inclusions in the PN, RtTg, 7N and LRt of vehicle and cit treated CMVMJD135 mice (n=4, 34 weeks). (B) Brainstem western-blot and quantification of total human ATXN3 protein from vehicle and cit treated CMVMJD135 mice (n=5, 34 weeks). Data presented as mean  $\pm$  SEM., \*p<0.05 and \*\*p<0.01 (One-way ANOVA). Scale bars, 20  $\mu$ m. PN, pontine nuclei; RtTg, reticulotegmental nuclei of pons; 7N, facial motor nuclei; LRt, lateral reticular nuclei.

### Citalopram treatment rescued cholinergic motor neurons in 7N and increase Calbindin D-28k staining in Purkinje cells of CMVMJD135 mice

Along with mutant ATXN3 aggregation suppression in facial motor nuclei (7N) of CMVMJD135 mice, we observed that at 34 weeks of age, the loss of Choline Acetyltransferase (ChAT) positive neurons was also rescued upon citalopram treatment (Fig. 5A). Another pathological presentation of CMVMJD135 mice is the loss of Calbindin D28K staining in Purkinje cells in the cerebellar cortex (CBX) at 34 weeks of age (Fig. 5B) (without loss in Purkinje cell number – supplementary data). Although not statistically significant, possibly due to the lack of a larger animal sample, citalopram was able to relieve the loss of Calbindin D-28K positive neurons most likely contributing to the phenotype improvement observed in the behavior analysis. Even though not significant, a mild trend was also observed towards a decrease in the number of neurons (NeuN positive cells) in the pontine nuclei of CMVMJD135 mice, also with a tendency towards reversion upon citalopram treatment (Fig. 5C).

However, there was no difference in dopaminergic (TH-positive) neurons in the substantia nigra pars compacta (SNc) compared to vehicle-treated CMVMJD135 mice (Fig. 5D).

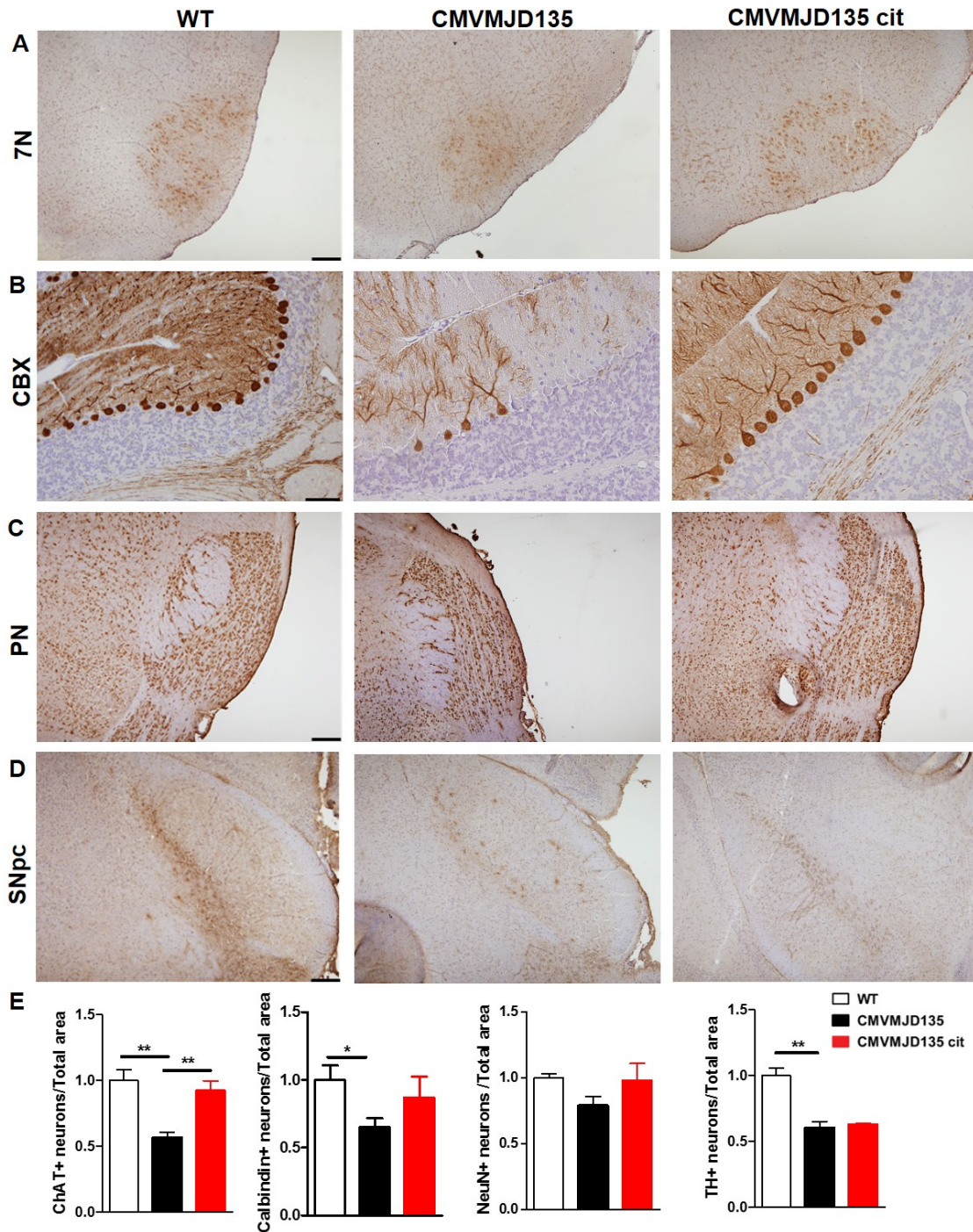


**Figure 5.** Citalopram treatment shows neuroprotective effects in CMVMJD135 mice. (A) Immunohistochemistry of ChAT-positive in the 7N, (B) Calbindin D-28K positive Purkinje cell in the CBX, (C) NeuN positive cells in PN and (D) dopaminergic (TH positive) cells in SNc from WT, vehicle and cit treated CMVMJD135 mice (n=4 per group, 34 weeks); (E) Quantification of (A), (F) Quantification of (B), (G) Quantification of (C) and (H) Quantification of (D) per total area from WT, vehicle and cit treated CMVMJD135 Data presented as mean ± SEM., \*p<0.05 and \*\*p<0.01 (One-way ANOVA). Scale bars, 200 µm (A, C and D) and 100 µm (B). CBX, Cerebellar cortex, SNc, Substantia nigra pars compacta.

### Citalopram treatment reduced reactive astrogliosis in CMVMJD135 mice

Reactive astrogliosis is observed in response to Central Nervous system (CNS) insults and strikingly evident in the substantia nigra of CMVMJD135 mice. Upon chronic citalopram treatment we saw a decrease in reactive astrogliosis observed in substantia nigra (SN), at 34 weeks of CMVMJD135 mice (Fig. 6A,B,C).

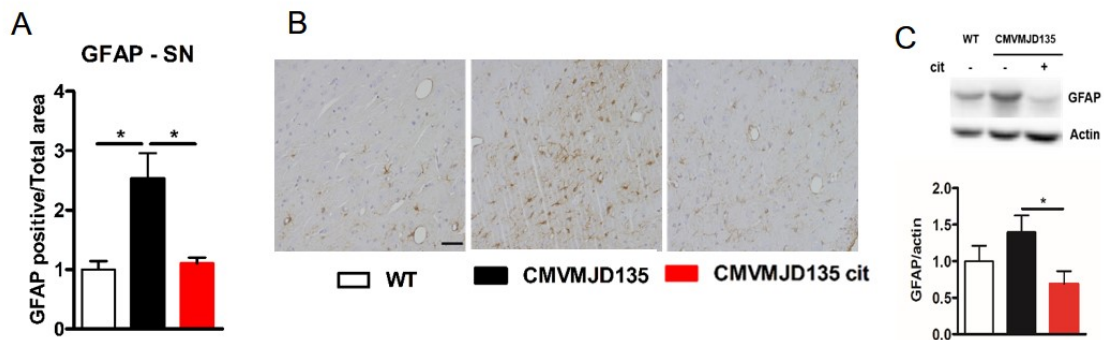


**Figure 6.** Citalopram effect in astrogliosis. (A) Quantification of GFAP-positive cells per area in SN from WT, vehicle and cit treated CMVMJD135 mice and corresponding (B) immunohistochemistry (n=5 per group, 34 weeks). (C) Brainstem western-blot and quantification of GFAP protein levels from WT, vehicle and ci treated CMVMJD135 mice (n=4 per group, 34 weeks). Data presented as mean  $\pm$  SEM., \*p<0.05 and \*\*p<0.01 (ANOVA, Tukey correction (A, B) and One-way ANOVA (C)). Scale bars, 20  $\mu$ m. GFAP, Glial fibrillary astrocytic protein.

### Motor neuron loss in the spinal cord of CMVMJD135 is mildly alleviated upon citalopram treatment

We observed a consistent motor neuron loss along the entire spinal cord of 34 week-old CMVMJD135 mice (Fig. 7A-D), being this loss of 50% in the lumbar region (LSC), which is particularly important for the flexibility and movement of the trunk. A deeper characterization of the LSC revealed a significantly decrease of the ChAT-positive neurons in this region (Fig. 7E). Although the differences were not statistically significant, citalopram showed a tendency to mitigate all these pathological features in CMVMJD135 mice.

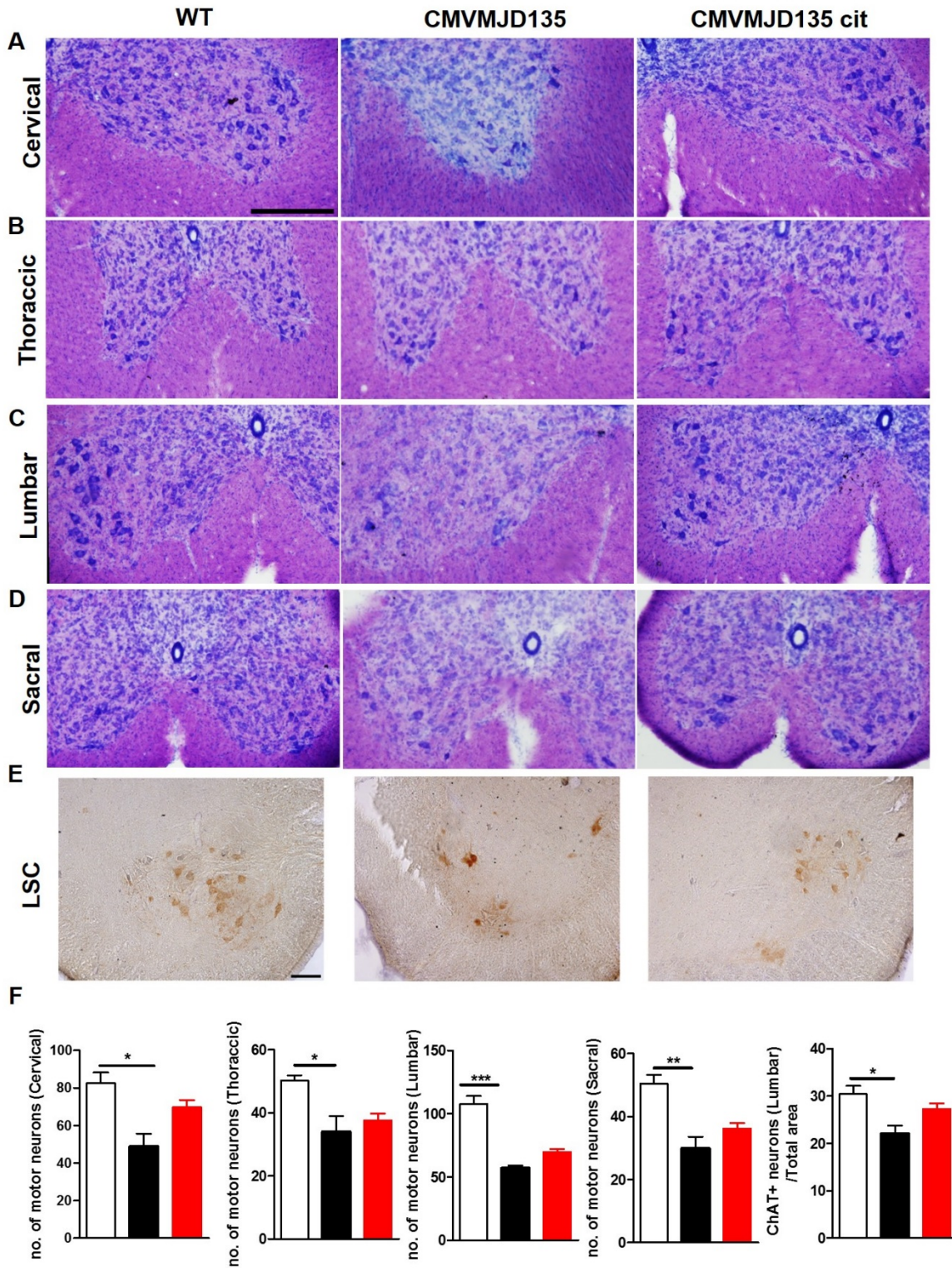


**Figure 7.** Loss of spinal motor neurons in CMVMJD135 mice. Thionin stained spinal cord and motor neuron quantification in ventral horn of (A) Cervical; (B) Thoracic; (C) Lumbar and (D) Sacral regions from WT, vehicle and cit treated CMVMJD135 mice (n=4 per group, 34 weeks); (E) Immunohistochemistry of ChAT in the LSC from WT, vehicle and cit treated CMVMJD135 mice (n=4 per group, 34 weeks). (F) Quantification of number of motor neurons and ChAT-positive cells per area in LSC. Data presented as mean ± SEM, \*p<0.05 and \*\*p<0.01 (One-way ANOVA). Scale bar, 200 µm.

### Higher dosage does not increase citalopram efficacy in CMVMJD135 mice

An increased dosage of citalopram (13mg/kg/day) was tested in CMVMJD135 mice in order to attempt to improve the response of the animals in the previously described behavioral tests. However, the results obtained with a higher dosage do not correspond to an increased effect when compared with the previous dosage tested. As occurred with 8mg/kg/day dosage, the muscle strength measured by the vertical pole and hanging wire test were not improved (Fig. 8A,B). This dosage also caused a significant increase in WT animals' body weight, but no effect in the CMVMJD135 treated animals (Fig. 8C). The dragging of the paws was not improved (Fig. 8D) nor the limb claspings (Fig. 8F). However, marginal beneficial effects were observed at late stages of the disease (30 and 34 weeks of age) for tremors and gait quality (Fig. 8E,G).

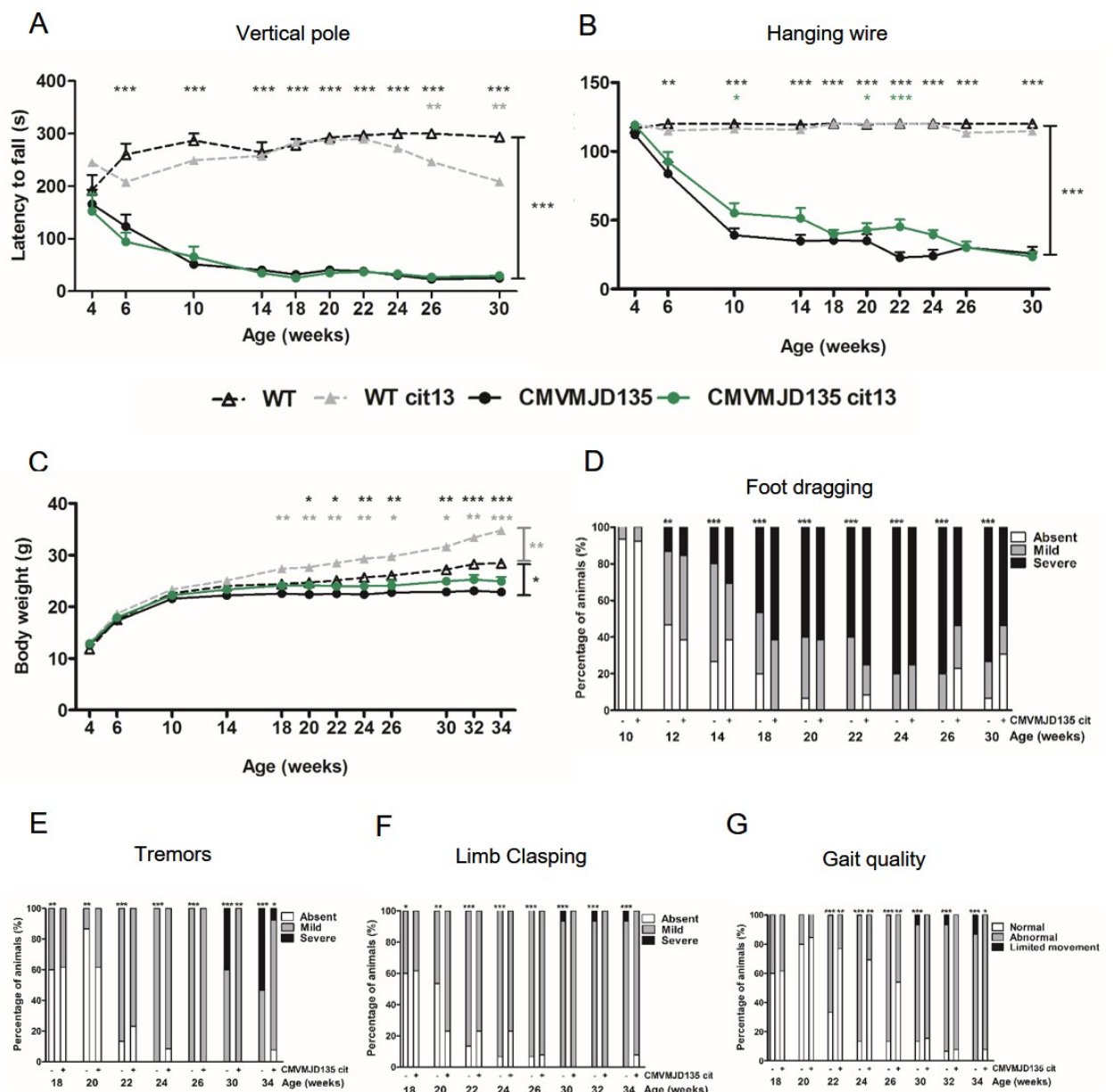


**Figure 8.** Treatment with a higher dosage of citalopram (13 mg/kg/day) led to a limited improvement of neurological symptoms of CMVMJD135 mice. (A) Vertical pole test, (B) hanging wire test, (C) body weight, (D) footprinting, (E) tremors, (F) limb claspings and (G) gait quality. (n=14) and cit treated (13 mg/kg/day) WT (WT cit13) mice (n=17) and of vehicle (n=16) and cit treated (13 mg/kg/day) CMVMJD135 mice (CMVMJD135 cit13) (n=13). No differences were observed in vertical pole, hanging wire, body weight and footprinting tests between CMVMJD135 and CMVMJD135 cit13 mice. Cit treated WT mice showed a significant increase in body weight. Marginal improvement in late stages (30 and 34 weeks) were observed for tremors and gait quality while no effect was observed in limb claspings upon treatment. Data presented as mean  $\pm$  SEM., \*p<0.05, \*\*p<0.01 and \*\*\* p<0.001. (Repeated-measures ANOVA, Tukey correction, One-way ANOVA and Mann Whitney U test for non-continuous variables).

Regarding motor balance and coordination, treatment with 13mg/kg/day citalopram was able to improve the performance in 12 mm square beam at 20 and 24 weeks, and to decrease the percentage of falls from the 11 mm circle beam at 32 and 34 weeks (Fig. 9A,D). However, no improvement was observed consistently along the trial in the majority of the beams (Fig. 9A,B,C). The major effect of this dosage was observed in the motor swimming test, however not as prominent as the 8mg/kg/day dosage (Fig. 9E). Higher dosages of citalopram, although with a trend towards improvement, did not significantly reduce the ATXN3 inclusions neither the total protein levels (Fig. 9F,G)



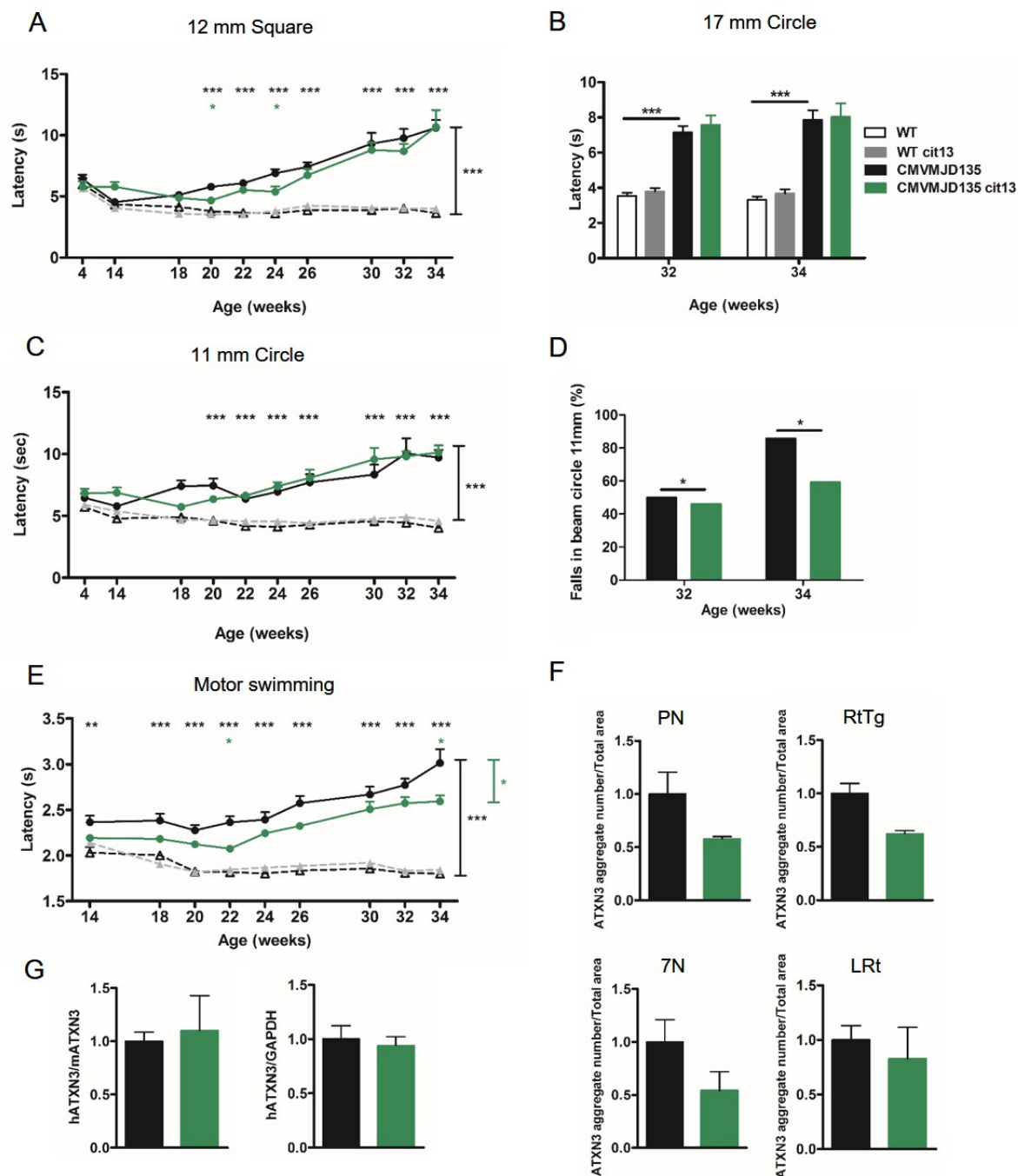


**Figure 9.** Effect of citalopram 13mg/kg/day in motor and coordination tests and in ATXN3 inclusions and protein levels. Mild amelioration at 20 and 24 weeks of age observed in (A) 12 mm square and no improvement in (B) 17 mm circle and (C) 11 mm circle beams between CMVMJD135 and CMVMJD135 cit13 mice. (D) Decrease of percentage of falls of the 11 mm circle beam and (E) improvement in motor swimming test in CMVMJD135 upon cit13 treatment. No differences observed in (F) ATXN3 inclusions in brainstem and (G) protein levels with 13mg/kg citalopram treatment. (n=13-16 for behavioral analysis and n=4-5 for pathological analysis). Data presented as mean  $\pm$  SEM., \* $p$ <0.05, \*\* $p$ <0.01 and \*\*\* $p$ <0.001. (Repeated-measures ANOVA, Tukey correction and One-way).

## Discussion

In this work, we tested citalopram, an FDA-approved compound commonly used for treating depression, with a re-purposing aim in the CMVMJD135 mouse model of MJD. The use of approved drugs has great advantages in terms of their safety and bioavailability in humans and therefore easy translation into the clinics. These compounds may also offer a quicker interpretation of pathophysiological mechanism due to their often known principal targets and mechanisms of action, and could additionally help unraveling many biological pathways and novel therapeutics targets.

Our group previously identified citalopram in a FDA/EMA-approved compounds screening in *C.elegans* model of MJD. In this screening, many serotonergic modulators were identified as suppressors of ATXN3 pathogenesis, namely decreasing the locomotion defect and ATXN3 aggregation in this model (Appendix I). The subsequent studies in a higher mammalian organism that more closely mirrors the human disease is of extreme importance prior to starting a clinical trial in humans. For that reason we studied the therapeutic efficacy of citalopram in CMVMJD135 mouse model which displays a progressive neurological phenotype and brain pathology consistent with that of human patients<sup>14</sup>. The CMVMJD135 mouse model treated with 8mg/kg/day showed striking improvements in body weight, in balance and motor coordination tests and in several other neurological parameters. This phenotype improvement was accompanied by a striking reduction of ATXN3 aggregation in specific brain regions. However, the role of protein inclusions in polyQ diseases, including MJD, is still controversial, and although the presence of nuclear aggregates has been shown to correlate with neurotoxicity, to isolate the specific toxic species within this multi-step process of aggregation, has proven to be a very hard task<sup>23-28</sup>. In this context, we have assessed the number of Choline AcetylTransferase (ChAT) positive neurons in the facial motor nuclei of the brainstem and in the lumbar ventral horn of the spinal cord and found a rescue or amelioration upon citalopram treatment in CMVMJD135 mice. The facial motor nuclei are mixed nerve brain region, with efferent (motor and vegetative) and afferent (sensitive and sensory) nerve fibers of predominantly cholinergic neurons<sup>29</sup>, which are particularly affected in MJD patients<sup>30</sup>, as well as in CMVMJD135 mice<sup>14</sup>. Citalopram was able to suppress ATXN3 aggregation but also to rescue cholinergic motor neurons in these nuclei, confirming its neuroprotective effect.

CMVMJD135 mice also present loss of Calbindin D-28K positive Purkinje cells in the cerebellar cortex at 34 weeks of age, with no decrease in total number of these cells. The essential activity mode of Purkinje cells is controlled by the sodium-potassium pump<sup>31</sup> which is one of the main responsible for the correct function of the cerebellar cortex. Loss of these neurons may lead to motor incoordination and ataxic symptoms. There was a trend towards an increase in the number of Calbindin D28K-positive

cells upon citalopram treatment that suggests a functional recovery of these neurons; the absence of statistical significance could probably be corrected by increasing the number of animals analyzed.

The pontine nuclei are involved in carrying the information from the motor cortex to the cerebellum and mostly involved in overall motor function, and they are most affected both in MJD patients<sup>32,33</sup> and in mouse models<sup>14</sup>. ATXN3 inclusions are widely present in these nuclei in both humans and CMVMJD135 mice<sup>14,34</sup>. We assessed neuronal density in the pontine nuclei of WT, citalopram-treated and non-treated CMVMJD135 mice. Despite some interesting trends, these results are not statistically different; they are however, suggestive of a neuronal dysfunction prior to a neuronal loss at 34 weeks of age in CMVMJD135 mice.

One previously established neuropathological feature of this mouse model is the loss of dopaminergic neurons (TH-positive) in the substantia nigra pars compacta, these neurons playing an important role in the control of multiple brain functions, including voluntary movement<sup>35</sup>. This pathological feature was not modified upon citalopram treatment, suggesting that this compound has no effect on dopaminergic neurons in the SNpc in this mouse model of MJD. In contrast, we observed that astrogliosis in the substantia nigra was strikingly decreased to WT levels in 34 week-old CMVMJD135 mice upon treatment.

The majority of neuropathological studies in MJD are focused on the brain (mainly brainstem, basal ganglia and cerebellum), but less is known about spinal cord pathology and its clinical relevance in the disease, with the exception of the well-known Clarke's column degeneration<sup>36</sup>. A recent paper in human MJD patients described cervical cord atrophy and antero-posterior flattening through MRI-based studies, as well as a correlation between spinal cord areas and disease severity<sup>37</sup>. MJD patients present pyramidal signs (predominantly in the legs) and urinary dysfunction<sup>38</sup>, which also suggest the involvement of spinal cord in the disease. Taking this into consideration, we assessed the motor neuron density in CMVMJD135 mice and observe a significantly loss of motor neurons (including cholinergic neurons at lumbar spinal cord) along the entire spinal cord. This loss of motor neurons was very slightly alleviated upon citalopram treatment, suggesting that its effect is more pronounced at the brain level than at the spinal cord. This is consistent with the effects seen at the motor behavior level, as motor coordination amelioration is more related to cerebellum and basal ganglia, where we observed striking improvements.

When the citalopram dosage was increased to 13mg/kg/day the symptomatic effect was mild or lost in specific tests, consistently to what happens in *C.elegans*, where a U-shaped curve was seen, meaning that this compound could have a limited range of efficacy in these two MJD models.

SERT inhibition by citalopram likely results in increased extracellular 5-HT levels, which lead to enhanced serotonergic neurotransmission. Likewise, serotonin receptor agonists could also exert serotonergic neurotransmission enhancement-like effects<sup>39</sup>. Clinical trials with 5-HT<sub>1A</sub> agonist for the treatment of cerebellar ataxia revealed promising findings<sup>40</sup>. One open label study and two case reports of MJD patients showed that treatment with buspirone and tandospirone (5-HT<sub>1A</sub> partial agonist) significantly ameliorated gait and posture, specifically in patients showing mild ataxia<sup>40,41</sup>. More recently, opposing effects of tandospirone on ataxia were found in different types of spinocerebellar degeneration, which may arise from distinct patterns of pathology<sup>42</sup>. Moreover, the degree of ataxia severity and the disease type may also determine the treatment outcome. While a previous trial with 13 MJD patients has shown no benefit of a 6-week fluoxetine treatment in motor function of MJD patients<sup>43</sup>, here we show that citalopram strongly ameliorated motor coordination and balance in MJD mice treated pre-symptomatically, starting one week before onset of disease manifestations. In HD mouse models, SSRIs treatment also resulted in striatal and memory preservation and extended survival, with no changes in huntingtin expression<sup>44</sup>. Citalopram has also been shown to be beneficial in models of Alzheimer's disease (AD) and in healthy human volunteers by reducing A $\beta$  in the CSF<sup>22</sup>. The need for chronic symptomatic treatment in MJD suggests a neuroprotective mechanism rather than immediate effects on signaling cascades<sup>22</sup> or correction of an imbalance of 5-HT levels in MJD mice, which in fact were not altered to start with (Appendix I). Additionally, the observation of citalopram impacting on the ATXN3 protein aggregation, leads us to suggest an improvement of the proteostasis state of the cell, likely not related to increased ATXN3 degradation, as the total levels of this protein remained unchanged. Indeed, it has been recently described in *C.elegans* that the release of serotonin from neurons signals to distal tissues the activation of protective mechanisms to prevent proteotoxicity<sup>45</sup>. We hypothesize that citalopram action in the neuronal environment may mediate activation of stress response(s), making the cells more resilient to the proteotoxic effect underlying MJD and other proteinopathies.

## Conclusion

The efficacy of citalopram in suppression of ATXN3 pathogenesis and its neuroprotective effects in CMVMJD135 mouse model (and in *C.elegans*, Appendix I), as well as its safety record of being widely used in depression patients, prompts us to suggest this drug for clinical trials in MJD patients.

## References

1. Ross, C. A. *et al.* Pathogenesis of neurodegenerative diseases associated with expanded glutamine repeats: new answers, new questions. *Prog. Brain Res.* **117**, 397–419 (1998).
2. Schöls, L., Bauer, P., Schmidt, T., Schulte, T. & Riess, O. Autosomal dominant cerebellar ataxias: clinical features, genetics, and pathogenesis. *Lancet Neurol.* **3**, 291–304 (2004).
3. Kawaguchi, Y. *et al.* CAG expansions in a novel gene for Machado-Joseph disease at chromosome 14q32.1. *Nat. Genet.* **8**, 221–228 (1994).
4. Coutinho, P. & Andrade, C. Autosomal dominant system degeneration in Portuguese families of the Azores Islands. A new genetic disorder involving cerebellar, pyramidal, extrapyramidal and spinal cord motor functions. *Neurology* **28**, 703–709 (1978).
5. Rosenberg, R. N. Machado-Joseph disease: an autosomal dominant motor system degeneration. *Mov. Disord. Off. J. Mov. Disord. Soc.* **7**, 193–203 (1992).
6. Sudarsky, L. & Coutinho, P. Machado-Joseph disease. *Clin. Neurosci. N. Y.* **3**, 17–22 (1995).
7. Paulson, H. L. *et al.* Machado-Joseph disease gene product is a cytoplasmic protein widely expressed in brain. *Ann. Neurol.* **41**, 453–462 (1997).
8. Perez, M. K. *et al.* Recruitment and the role of nuclear localization in polyglutamine-mediated aggregation. *J. Cell Biol.* **143**, 1457–1470 (1998).
9. Robertson, A. L. *et al.* Small heat-shock proteins interact with a flanking domain to suppress polyglutamine aggregation. *Proc. Natl. Acad. Sci. U. S. A.* **107**, 10424–10429 (2010).
10. Warrick, J. M. *et al.* Ataxin-3 suppresses polyglutamine neurodegeneration in *Drosophila* by a ubiquitin-associated mechanism. *Mol. Cell* **18**, 37–48 (2005).
11. Cushman-Nick, M., Bonini, N. M. & Shorter, J. Hsp104 suppresses polyglutamine-induced degeneration post onset in a *drosophila* MJD/SCA3 model. *PLoS Genet.* **9**, e1003781 (2013).
12. Nascimento-Ferreira, I. *et al.* Overexpression of the autophagic beclin-1 protein clears mutant ataxin-3 and alleviates Machado-Joseph disease. *Brain J. Neurol.* **134**, 1400–1415 (2011).
13. Menzies, F. M. *et al.* Autophagy induction reduces mutant ataxin-3 levels and toxicity in a mouse model of spinocerebellar ataxia type 3. *Brain J. Neurol.* **133**, 93–104 (2010).
14. Silva-Fernandes, A. *et al.* Chronic treatment with 17-DMAG improves balance and coordination in a new mouse model of Machado-Joseph disease. *Neurother. J. Am. Soc. Exp. Neurother.* **11**, 433–449 (2014).

15. Chou, A.-H., Chen, S.-Y., Yeh, T.-H., Weng, Y.-H. & Wang, H.-L. HDAC inhibitor sodium butyrate reverses transcriptional downregulation and ameliorates ataxic symptoms in a transgenic mouse model of SCA3. *Neurobiol. Dis.* **41**, 481–488 (2011).
16. Alves, S. *et al.* Silencing ataxin-3 mitigates degeneration in a rat model of Machado-Joseph disease: no role for wild-type ataxin-3? *Hum. Mol. Genet.* **19**, 2380–2394 (2010).
17. Costa, M. do C. *et al.* Toward RNAi therapy for the polyglutamine disease Machado-Joseph disease. *Mol. Ther. J. Am. Soc. Gene Ther.* **21**, 1898–1908 (2013).
18. Chong, C. R. & Sullivan, D. J. New uses for old drugs. *Nature* **448**, 645–646 (2007).
19. Teixeira-Castro, A. *et al.* Neuron-specific proteotoxicity of mutant ataxin-3 in *C. elegans*: rescue by the DAF-16 and HSF-1 pathways. *Hum. Mol. Genet.* **20**, 2996–3009 (2011).
20. Teixeira-Castro, A. *et al.* Serotonergic signalling suppresses ataxin 3 aggregation and neurotoxicity in animal models of Machado-Joseph disease. *Brain J. Neurol.* (2015). doi:10.1093/brain/awv262
21. Silva-Fernandes, A. *et al.* Motor uncoordination and neuropathology in a transgenic mouse model of Machado-Joseph disease lacking intranuclear inclusions and ataxin-3 cleavage products. *Neurobiol. Dis.* **40**, 163–176 (2010).
22. Cirrito, J. R. *et al.* Serotonin signaling is associated with lower amyloid- $\beta$  levels and plaques in transgenic mice and humans. *Proc. Natl. Acad. Sci. U. S. A.* **108**, 14968–14973 (2011).
23. Davies, S. W. *et al.* Are neuronal intranuclear inclusions the common neuropathology of triplet-repeat disorders with polyglutamine-repeat expansions? *Lancet* **351**, 131–133 (1998).
24. Arrasate, M., Mitra, S., Schweitzer, E. S., Segal, M. R. & Finkbeiner, S. Inclusion body formation reduces levels of mutant huntingtin and the risk of neuronal death. *Nature* **431**, 805–810 (2004).
25. Paulson, H. L. *et al.* Intranuclear inclusions of expanded polyglutamine protein in spinocerebellar ataxia type 3. *Neuron* **19**, 333–344 (1997).
26. Becher, M. W. & Ross, C. A. Intranuclear neuronal inclusions in DRPLA. *Mov. Disord. Off. J. Mov. Disord. Soc.* **13**, 852–853 (1998).
27. Truant, R., Atwal, R. S., Desmond, C., Munsie, L. & Tran, T. Huntington's disease: revisiting the aggregation hypothesis in polyglutamine neurodegenerative diseases. *FEBS J.* **275**, 4252–4262 (2008).
28. Ross, C. A. & Poirier, M. A. Opinion: What is the role of protein aggregation in neurodegeneration? *Nat. Rev. Mol. Cell Biol.* **6**, 891–898 (2005).
29. Toulgoat, F. *et al.* Facial nerve: From anatomy to pathology. *Diagn. Interv. Imaging* **94**, 1033–1042 (2013).

30. Rüb, U., Brunt, E. R. & Deller, T. New insights into the pathoanatomy of spinocerebellar ataxia type 3 (Machado-Joseph disease). *Curr. Opin. Neurol.* **21**, 111–116 (2008).
31. Forrest, M. D., Wall, M. J., Press, D. A. & Feng, J. The sodium-potassium pump controls the intrinsic firing of the cerebellar Purkinje neuron. *PLoS One* **7**, e51169 (2012).
32. Dürr, A. *et al.* Spinocerebellar ataxia 3 and Machado-Joseph disease: clinical, molecular, and neuropathological features. *Ann. Neurol.* **39**, 490–499 (1996).
33. Yoshizawa, T., Watanabe, M., Frusho, K. & Shoji, S. Magnetic resonance imaging demonstrates differential atrophy of pontine base and tegmentum in Machado-Joseph disease. *J. Neurol. Sci.* **215**, 45–50 (2003).
34. Yamada, M., Tsuji, S. & Takahashi, H. Pathology of CAG repeat diseases. *Neuropathol. Off. J. Jpn. Soc. Neuropathol.* **20**, 319–325 (2000).
35. Chinta, S. J. & Andersen, J. K. Dopaminergic neurons. *Int. J. Biochem. Cell Biol.* **37**, 942–946 (2005).
36. Rüb, U. *et al.* Consistent affection of the central somatosensory system in spinocerebellar ataxia type 2 and type 3 and its significance for clinical symptoms and rehabilitative therapy. *Brain Res. Rev.* **53**, 235–249 (2007).
37. Fahl, C. N. *et al.* Spinal Cord Damage in Machado-Joseph Disease. *The Cerebellum* **14**, 128–132 (2015).
38. França, M. C., D'Abreu, A., Nucci, A. & Lopes-Cendes, I. Clinical correlates of autonomic dysfunction in patients with Machado-Joseph disease. *Acta Neurol. Scand.* **121**, 422–425 (2010).
39. Morrissette, D. A. & Stahl, S. M. Modulating the serotonin system in the treatment of major depressive disorder. *CNS Spectr.* **19 Suppl 1**, 57–67; quiz 54–57, 68 (2014).
40. Takei, A., Hamada, T., Yabe, I. & Sasaki, H. Treatment of cerebellar ataxia with 5-HT1A agonist. *Cerebellum Lond. Engl.* **4**, 211–215 (2005).
41. Takei, A. *et al.* Effects of tandospirone on '5-HT1A receptor-associated symptoms' in patients with Machado-Joseph disease: an open-label study. *Clin. Neuropharmacol.* **27**, 9–13 (2004).
42. Takei, A. *et al.* Difference in the effects of tandospirone on ataxia in various types of spinocerebellar degeneration: an open-label study. *Cerebellum Lond. Engl.* **9**, 567–570 (2010).
43. Monte, T. L. *et al.* Use of fluoxetine for treatment of Machado-Joseph disease: an open-label study. *Acta Neurol. Scand.* **107**, 207–210 (2003).
44. Lauterbach, E. C. Neuroprotective effects of psychotropic drugs in Huntington's disease. *Int. J. Mol. Sci.* **14**, 22558–22603 (2013).

45. Tatum, M. C. *et al.* Neuronal serotonin release triggers the heat shock response in *C. elegans* in the absence of temperature increase. *Curr. Biol. CB* **25**, 163–174 (2015).



## Supplementary data

**Table 1.** Additional SHIRPA parameters analyzed in the citalopram pre-clinical trial with 8 and 13mg/Kg (ns=not significant).

	Phenotype (weeks)	Cit 8 (weeks)	Cit 13 (weeks)
<b>Exploratory activity</b>	18-30	24	ns
<b>Locomotor activity</b>	22-30	ns	ns
<b>Body curvature</b>	20-30	ns	ns
<b>Strenght to grab</b>	30-34	32	ns
<b>Hindlimb tonus</b>	22-34	22-24	22-24

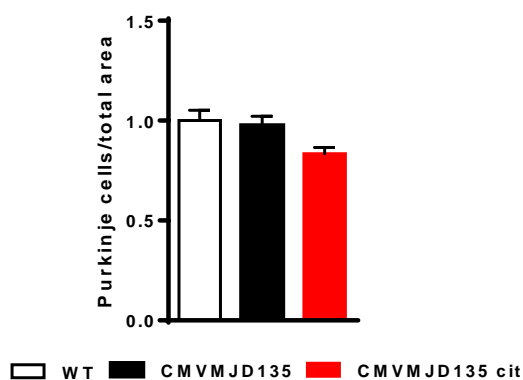


**Figure 1.** Quantification of Purkinje cell number per total area in the cerebellum cortex of WT, CMVMJD135 and CMVMJD135 cit treated animals.



# CHAPTER 4

---

Exploring the molecular mechanisms of chronic citalopram treatment in MJD mouse

Model

**Exploring the molecular mechanisms of chronic citalopram treatment in MJD mouse model**

Sofia Esteves<sup>1,2</sup>, Sara Duarte-Silva<sup>1,2</sup>, Anabela Silva-Fernandes<sup>1,2</sup>, Andreia Teixeira-Castro<sup>1,2</sup> and Patricia Maciel<sup>1,2</sup>

1) Life and Health Sciences Research Institute (ICVS), School of Health Sciences, University of Minho, 4710-057 Braga, Portugal.

2) ICVS/3Bs - PT Government Associate Laboratory, Braga/Guimarães, Portugal.

## Abstract

Machado-Joseph disease (MJD, also known as spinocerebellar ataxia type 3, SCA3), is an autosomal dominant neurological disorder, caused by an expanded polyglutamine (polyQ) repeat in the ataxin-3 (ATXN3) protein. MJD patients exhibit significant motor impairments such as gait ataxia, associated with multiple neuropathological changes including mutant ATXN3 inclusions, markedly neuronal loss and atrophy of the cerebellum. The mechanisms of neurodegeneration underlying this disease are not well understood and so far there is no effective treatment. We have previously demonstrated that chronic citalopram (a selective serotonin re-uptake inhibitor, SSRI) pre-symptomatic treatment in CMVMJD135 mice strikingly ameliorated motor coordination impairments, reduced mutant ATXN3 aggregation and astrogliosis, and exerted neuroprotective effects. Here, we explore the molecular mechanisms underlying the neuroprotective effects of citalopram in CMVMJD135 mice, by assessing candidate molecules through its RNA and protein expression levels. A trend towards an increase and/or induction of candidate molecules was observed, with no statistical differences. More specific studies, mainly RNA-seq analysis and immunohistochemistry of these candidate molecules *in situ* may shed light into the mechanism of action of citalopram in MJD, which is still unanswered.

## Introduction

Polyglutamine (polyQ) diseases are inherited, fatal neurodegenerative diseases caused by an expansion of a coding trinucleotide (CAG) repeat, which is translated to an abnormally elongated glutamine tract in the corresponding mutant proteins<sup>1</sup>. There are nine polyQ diseases, the dominantly inherited ataxia Machado Joseph Disease (MJD)/Spinocerebellar ataxia type 3 (SCA3) being the most common spinocerebellar ataxia worldwide<sup>2,3</sup>. The genes underlying these diseases have no homology with each other except for the polyQ stretch itself, suggesting a common pathogenic mechanism; however, each disease presents specific clinical and pathological symptoms. It is assumed that the common toxic gain-of-function mechanisms for the mutant polyQ protein are aggregation and deposition of misfolded proteins leading to neuronal dysfunction and eventually cell death<sup>4</sup>. Drug discovery strategies over the past few years have generated promising candidate targets and pathways which prompted to some very encouraging therapeutic advances; however, no effective treatment and/or prevention is yet available for these disorders. Some of the proposed therapeutic strategies are based on hypothetical pathogenic mechanisms and comprise: gene silencing, blocking aggregation, inducing degradation, proteolysis inhibition, mitochondrial stabilization, reduction of oxidative stress and transcription modulation among other possibilities. For many of these suggested therapies, the

translation to clinical trials may be limited by human efficacy and safety. Additionally, which of the cellular pathways is the most significant to the disease, and thus a good target, is still unclear. In this context, drug re-purposing strategies, which rely on finding new uses for existing FDA-approved compounds, has been gaining attractiveness due to the faster translation to the clinic, with predictably less safety issues<sup>5</sup>. We have previously performed an unbiased *C.elegans*-based screen of FDA/EMA-approved small molecules for modulators of mutant ataxin-3 (ATXN3) induced neurotoxicity, and identified a selective serotonin re-uptake inhibitor (SSRI), citalopram, as having a therapeutic effect *in vivo* in two different models (nematode and mouse models of MJD). Chronic citalopram pre-symptomatic treatment in CMVMJD135 mice rescued weight loss and improved gait, tremors and limb clasping. Motor coordination impairments were very strikingly ameliorated upon treatment. Mutant ATXN3 aggregation was also reduced in affected brain regions, recovery of cholinergic motor neurons loss was observed and astrogliosis mitigated. These results suggested that serotonergic signaling may be a promising therapeutic target in MJD proposing that the use of antidepressants in the clinics for neurodegenerative diseases may go beyond depression treatment. However, to be translated to clinics it is crucial to know its mechanism of action in the MJD context.

The suppression of ATXN3 aggregation suggests an improvement in the protein homeostasis (proteostasis) of neuronal cells. Several lines of evidence support neuroprotective effects of antidepressants in neurodegenerative disorders beyond treatment of depression. Neuroprotective effects including mitochondrial protection, increased BDNF expression and apoptosis have been described in Huntington's Disease (HD) models upon treatment with psychotropic drugs, including SSRI's<sup>6</sup>. Activation of the ERK signaling cascade upon stimulation of serotonin receptors was shown to reduce A $\beta$  production in Alzheimer's Disease (AD) mouse and human samples<sup>7,8</sup>. Additionally, in cellular and mouse models of Spinal and Bulbar Muscular Atrophy (SBMA), naratriptan, a serotonin receptor agonist, decreased CGRP1 expression, attenuated JNK activity and alleviated pathogenic AR-mediated neuronal damage<sup>9</sup>. More associated with the basic functioning of the proteostasis network, a recent study described that neuronal serotonin release is sufficient to activate heat shock factor 1 (HSF-1) and to upregulate molecular chaperones, suppressing protein misfolding and attenuating proteotoxic stress in *C.elegans*<sup>10</sup>. Furthermore, antidepressant treatment was also described to activate antioxidant responses by increasing HO-1 expression through NF-E2-related factor-2 (NRF2) accumulation in the nucleus and enhancing Nrf2-DNA binding activity<sup>11</sup>; and to alleviate endoplasmic reticulum stress (ER)<sup>12</sup>.

We described that MOD-5 in *C.elegans*, the ortholog of the serotonin transporter (SERT) in humans is necessary for the therapeutic efficacy of citalopram, as well as the post-synaptic receptors

SER-1 and SER-4. Moreover, HSP6, a mitochondrial chaperone, was found to be up-regulated in *C.elegans* and NRF2, an antioxidant response-related transcription factor, was found also up-regulated in MCF-7 cells upon citalopram treatment (*unpublished data*). However, the mechanism of action of citalopram, namely its effect on ATXN3 aggregation, remain unclear. Therefore, the main goal of this work was to explore and dissect the molecular changes observed in CMVMJD135 mouse nervous system upon citalopram treatment.

## Material and methods

**Gene expression quantification, qRT-PCR.** Brainstem and cerebellum total RNA was isolated from 18 and 34 week-old, vehicle- and citalopram-treated WT and CMVMJD135 littermate mice (n=4 for each group), using TRIZOL (15596-026, Invitrogen, Calrsbad, USA) according to the manufacturer's protocol. RNA samples were treated with DNase I (EN0525, Thermo Scientific®, USA) according to the manufacturer's protocol. First-strand cDNA, synthesized with iScript cDNA Synthesis kit (#170-8891, Bio-Rad, USA) was amplified by quantitative reverse-transcriptase PCR (qRT-PCR) as previously described<sup>13</sup>. Primers used for expression quantification are described in table 1. Primers were designed using PRIMER-BLAST (<http://www.ncbi.nlm.nih.gov/tools/primer-blast/>). qRT-PCR was performed in 7500 Fast Real-Time PCR System (Life Technologies) and analyzed through 7500 Software v2.3 and  $\Delta\Delta C_t$  method.

**Table 1.** List of primers used for qRT-PCR.

Primer ID	Forward	Reverse
HSC70	TGGCATTGTGTGGTCTCGT	GTGCCGAGATCAATGCCAAC
HSP105	TCTATTCTGACCCTCAAGGAGTTCC	TGTTCCAGCTTCACTGTTGTCTTGC
HSP90	CACCCTGCTCTGTACTACTACTCGG	GCCAATGCCTGTGTCCACCAAAGTC
HSP70	ATCAGTGGGCTGTACCAGGG	TTGACAGTAATCGGTGCCCAA
HSP60	CTCGGGCCTATGCCAAAGAT	TTCTTCCCTTTGGCCCCATT
HSP40	CGTACCACCCGGACAAG	GGTACCATTAGCACCACCACT
HSP27	TCACGGCTACTATGTTTCGGC	CAGAAACGCCTGGAACCTTGC
GRP75	AAGAGAGAGACAGGGGTTGATT	CCAGAAGCATCCATGGTAAGG
HO-1	CAGAAGAGGCTAAGACCGCC	GCAGTATCTTGCACCAGGCTA
NQO1	ACGGTCCTTTCCAGAATAAGAAGA	ACCTGGAAGCCACAGAACG
IV_BDNF	CAGGAGTACATATCGGCCACCA	GTAGGCCAAGTTGCCTTGTCCGT
BDNF	GACAAGGCAACTTGGCCTAC	TTCGATGACGTGCTCAAAG
LC3	TTCTTCTCCTGGTGAATGG	GTGGGTGCCTACGTTCTCAT
GFAP	GGCGAAGAAAACCGCATCAC	CCCGCATCTCCACAGTCTTT
B2m	CCTTCAGCAAGGACTGGTCT	TCTCGATCCCAGTAGACGGT

**Western-blot analysis.** Protein isolation from mouse brainstem tissue and Western-blot were performed as previously described<sup>13</sup>. The blots were blocked and incubated overnight at 4°C with the primary antibody mouse anti-GRP75 (1:1000, ab2799, Abcam), Hsp60 (1:1000, H-300, Santa Cruz Biotech), NRF2 (1:1000, C-20, Santa Cruz Biotech) and rabbit anti-GFAP (1:50000, M0761, DAKO Corporation, Carpinteria) western-blot of 18 and 34 week-old CMVMJD135 mice, either vehicle or treated with citalopram (n=4 for each condition). As a loading control, mouse anti-beta actin (1:10000, AC-15, Life technologies) was used. Western-blot detection was performed using Chemidoc XRS Software and quantifications with ImageLab Software (Biorad, USA) according to the manufacturer's instructions.

**Statistical analysis.** One-Way ANOVA was used for paired comparisons. All statistical analyses were performed using SPSS 22.0 (SPSS Inc., Chicago, IL). A critical value for significance of two-tailed  $p < 0.05$  was used throughout the study.

## Results

### Gene expression analysis in the brainstem upon citalopram treatment in 18 week-old CMVMJD135 mice

To test the hypothesis that an improvement of the proteostasis and/or homeostasis of the neuronal cells was underlying the therapeutic effect of citalopram in MJD models, we studied the expression of genes encoding components of the proteostasis network, as well as other neuroprotective molecules, first at 18 weeks of age, an age at which we already observed an improvement of the phenotype of CMVMJD135 mice upon citalopram treatment. In the brainstem (Fig. 1), citalopram treatment did not produce striking molecular changes in the expression of several heat shock proteins (Fig. 1A), neither protein levels of Hsp60 and GRP75 (Fig. 1B); antioxidant related-molecules (Fig. 1C), neither NRF2 protein levels (Fig. 1D) and neurotrophic factors (Fig. 1E). The absence of enhanced autophagy upon citalopram treatment was confirmed by the lack of significant differences in LC3 mRNA levels in the brainstem of CMVMJD135 mice (Fig. 1F). Although not statistically significant, an interesting trend towards increase upon citalopram treatment was observed for Hsp40 and GRP75 chaperones, HO-1 and BDNF.



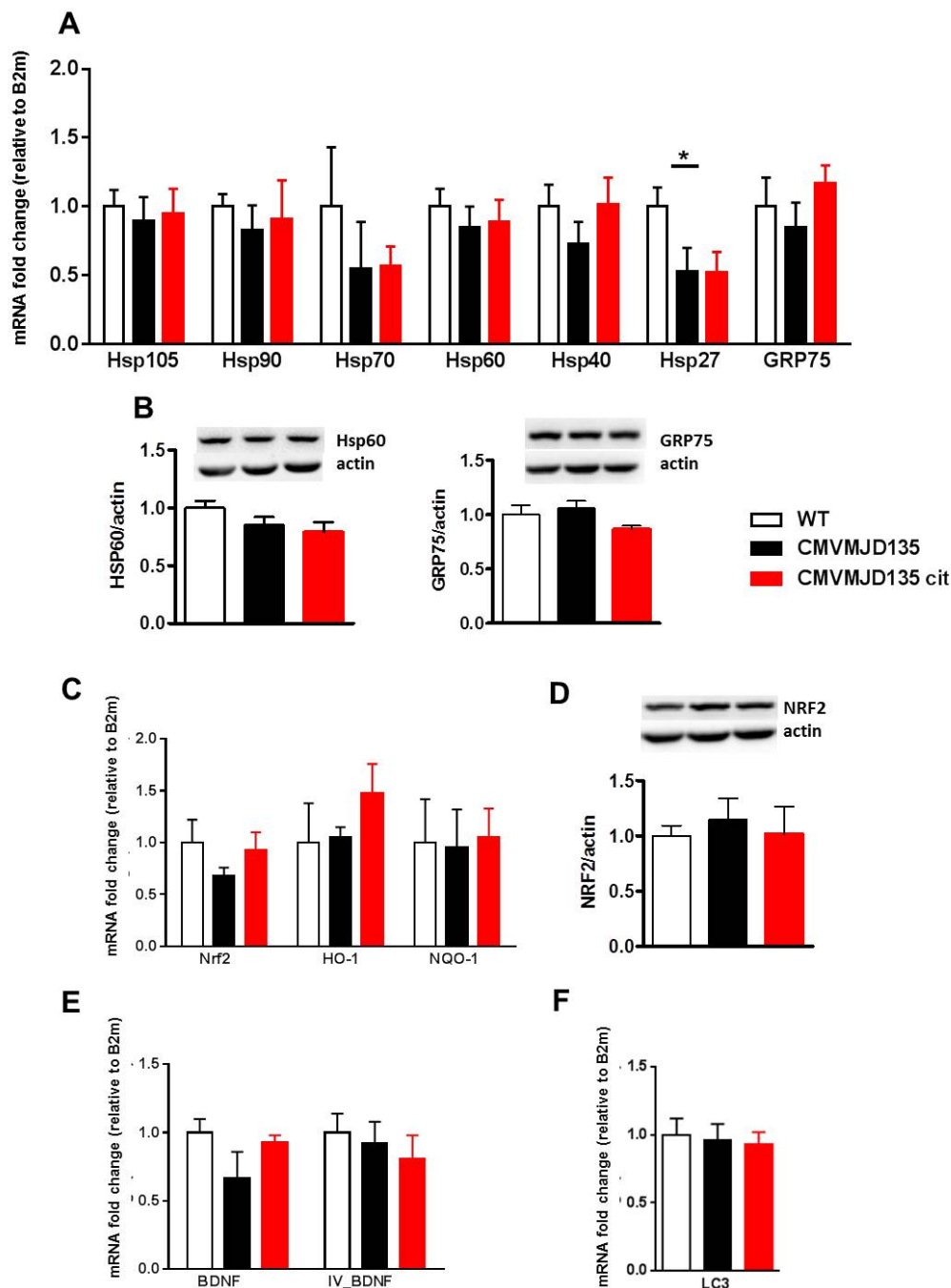


**Figure 1.** mRNA and protein level profile in brainstem upon citalopram treatment at 18 weeks of age. (A) mRNA expression levels for molecular chaperones; (B) Hsp60 and GRP75 protein levels, (C) Antioxidant-related molecules; (D) NRF2 protein levels; (E) Neurotrophic factors; (F) Autophagy-related molecules. Bar graph represents the fold changes of mRNA levels quantified by normalization to the B2m as an internal control for WT, vehicle and cit treated CMVMJD135 mice (n=4 per group, 18 weeks, n=3 technical replicates). Data presented as mean  $\pm$  SEM, \*p<0.05 (One-way ANOVA).

### **Gene expression analysis in the brainstem upon citalopram treatment in 34 week-old CMVMJD135 mice**

The same molecules were studied at the end of the pre-clinical trial, in 34 week-old CMVMJD135 mice in brainstem and cerebellum. In brainstem, after 29 weeks of citalopram chronic treatment, no striking differences were observed in the expression of several heat shock proteins (Fig. 2A), neither protein levels of Hsp60, GRP75 (Fig. 2B), antioxidant related-molecule (Fig. 2C) NRF2 (Fig. 2D) and neurotrophic factors (Fig. 2E). The absence of enhanced autophagy upon citalopram treatment was confirmed by the lack of significant differences in LC3 mRNA levels in the brainstem of CMVMJD135 mice (Fig. 2F). Other autophagy markers, namely atg1, atg5, atg7 and beclin remain to be analyzed.

Also in the cerebellum, no statistical differences were observed for molecular chaperones (Fig. 3A), antioxidant-related molecules (Fig. 3B), neurotrophic factors (Fig. 3C) and LC3 autophagy marker (Fig. 3D). High variability between animals may account for the lack of significant differences in the mRNA expression levels.

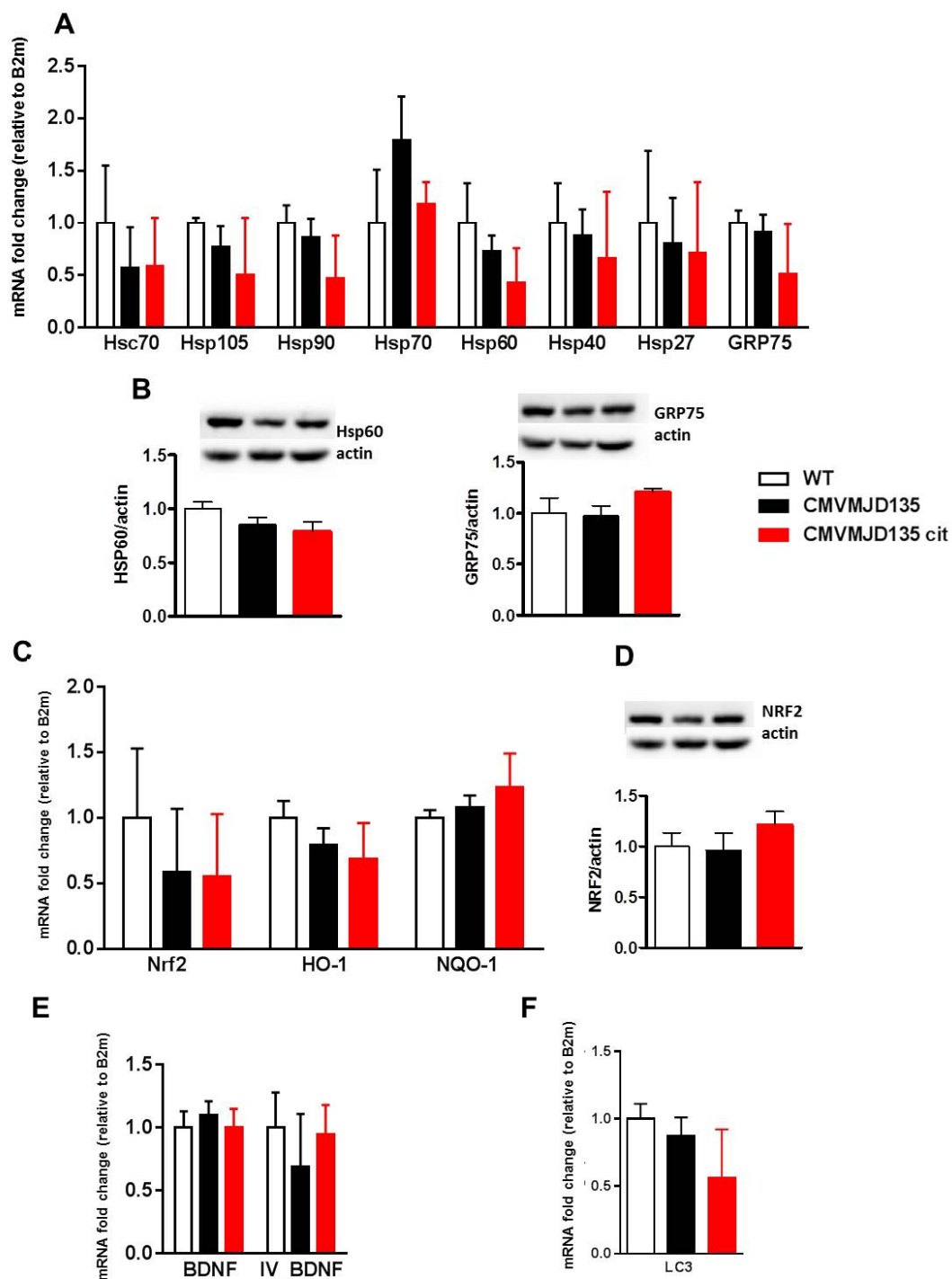


**Figure 2.** mRNA and protein level profile in the brainstem upon citalopram treatment at 34 weeks of age. (A) Molecular chaperones; (B) Hsp60 and GRP75 protein levels, (C) Antioxidant-related molecules; (D) NRF2 protein levels; (E) Neurotrophic factors; (F) Autophagy-related molecules. Bar graph represents the fold changes of mRNA levels quantified by normalization to the B2m as an internal control for WT, vehicle and cit treated CMVMJD135 mice (n=4 per group, 34 weeks, n=3 technical replicates). Data presented as mean  $\pm$  SEM, \*p<0.05 (One-way ANOVA).

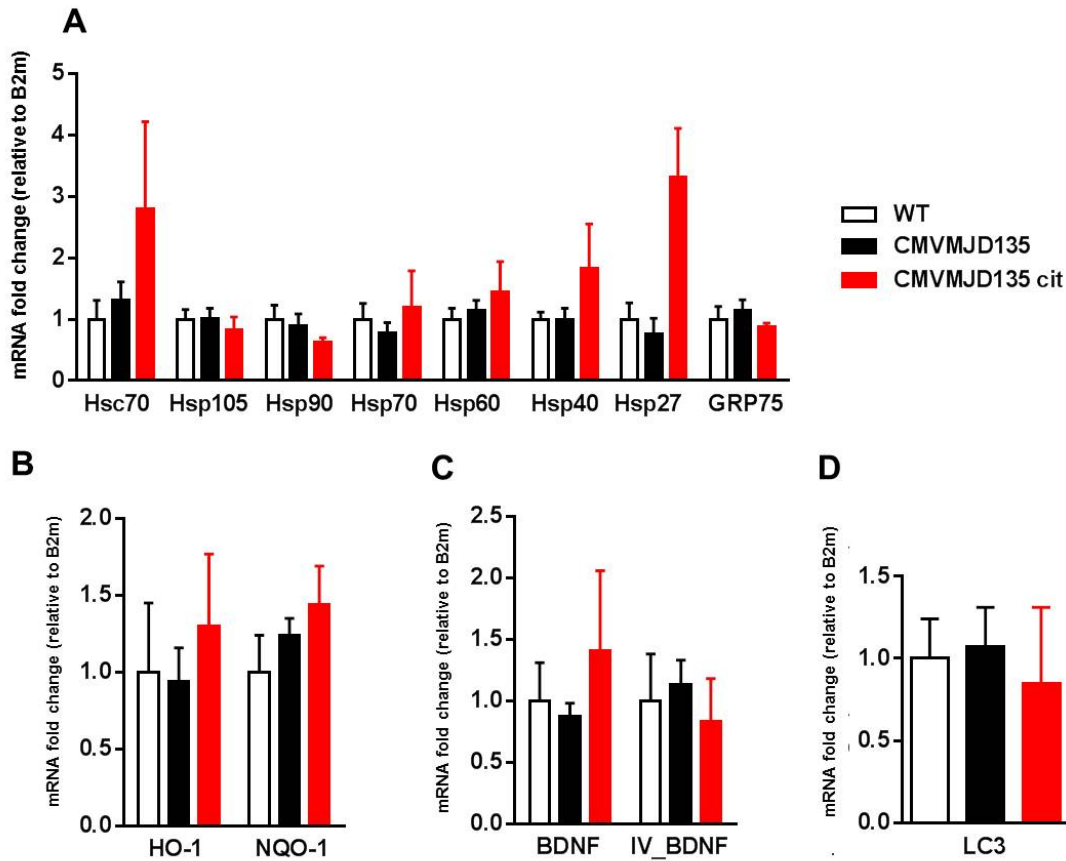


**Figure 3.** mRNA level profile in the cerebellum upon citalopram treatment at 34 weeks of age. (A) Molecular chaperones, (B) Antioxidant-related molecules, (C) Neurotrophic factors; (F) LC3 autophagy marker. Bar graph represents the fold changes of mRNA levels quantified by normalization to the B2m as an internal control for WT, vehicle and cit treated CMVMJD135 mice (n=4 per group, 34 weeks, n=3 technical replicates). Data presented as mean  $\pm$  SEM, \*p<0.05 (One-way ANOVA).

## Discussion

Even though it is remarkable to unravel and dissect the neuroprotective effect of citalopram at neuropathological level in the MJD context, its mechanism of action in terms of key cellular pathways changes upon treatment, still need to be explored.

Since citalopram strikingly reduces ATXN3 aggregation we hypothesized that this compound may be impacting on protein homeostasis. The accumulation of misfolded and aggregated proteins is a cytotoxic event implicated in the pathogenesis of several neurological diseases<sup>14</sup>. Molecular chaperones are essential components of the proteostasis network promoting efficient folding and targeting misfolding proteins for refolding and degradation. Since an increase in the molecular chaperone expression can suppress protein aggregation and toxicity in several models of neurodegenerative diseases<sup>15-19</sup>, we wonder if the citalopram is acting by this mechanism. To test this hypothesis, we

analyzed the expression levels of several molecular chaperones in citalopram-treated and non-treated CMVMJD135 mice, at two different ages, in brainstem and cerebellum. Although some interesting trends towards increased expression were found, the variability between samples did not allow us to find statistically significant differences between genotypes and treatment groups. Since we had previous evidence of upregulation of hsp6 (mouse GRP75 homolog<sup>20</sup>) in *C.elegans* upon treatment (Teixeira-Castro A., *unpublished data*) we also measured the protein levels of GRP75 and Hsp60, two mitochondrial chaperones; however, also we detected no differences.

Our group also found an upregulation of NRF2 in MSC-7 cells upon citalopram treatment (Teixeira-Castro A., *unpublished data*), leading us to focus on this transcription factor that regulates the expression of antioxidant enzymes involved in protection against oxidative damage<sup>21</sup>. Two of these antioxidant enzymes are HO-1 and NQO1, for which increased expression has been proved to exert neuroprotection in neurodegenerative diseases<sup>22-24</sup>. A trend towards an induction of HO-1 was also observed in total extracts from the cerebellum, without statistical differences.

It is widely known that SSRI's, including citalopram, increase the BDNF levels and thus contribute to neuroprotection. Here, we also assessed for BDNF levels, including mature and promotor IV-dependent BDNF, this one accounting for the majority of the neuronal activity-induced BDNF expression<sup>25,26</sup>. Isoform IV and mature BDNF expression levels were found to have a trend towards an increase in the brainstem and in the cerebellum, respectively, and therefore may be exerting neuroprotection, but these differences did not reach statistical significance.

A possible explanation for the variability between samples and therefore between groups (genotype vs treatment) may reside in the fact that MJD, like other polyQ diseases is characterized by degeneration of specific brain regions (neurospecificity) keeping others intact, in spite of the ubiquitous expression of the mutant proteins<sup>27</sup>. This pathological feature could be the explanation for the absence of striking differences when extracts from the whole brainstem and mainly the whole cerebellum are analyzed, even between WT and transgenic animals. Therefore, a transcriptomic/proteomic analysis in specific and affected (e.g. pontine nuclei, substantia nigra of the brainstem, deep cerebellar nuclei of the cerebellum or spinal cord) vs. non-affected brain regions (e.g. hippocampus), from WT and transgenic mouse brains with and without citalopram treatment could certainly identify key cellular pathways underlying the effect of this SSRI in MJD.

Another possibility to try to unravel the molecular changes in specific affected brain regions, still in the context of the proteostasis protection, is to perform immunohistochemistry of some of the molecules addressed in this study. The *in situ* characterization could provide additional information and

perhaps increased sensibility to localized effects. Although here we were mainly focused on molecules related to proteostasis and antioxidant effects, we cannot exclude that other pathways are being altered by citalopram. For instance, the effect of citalopram in excitotoxicity, in signaling post-translational modifications, in solubility of ATXN3 proteins, in mitochondria dysfunction or axonal transport could also be studied. A deep characterization of these parameters will be necessary in CMVMJD135 mouse model and their further elucidation upon citalopram chronic treatment of extremely value for the understanding of MJD pathogenesis and for the future therapy development.

## **Conclusion**

In this study we attempted to dissect the molecular mechanisms underlying the neuroprotective effects of citalopram in the context of MJD and to provide some clues for the next steps in the field. Some interesting trends was observed towards an increase in neuroprotective molecules, however; without statistical differences, therefore our question remains unanswered. The continuous efforts in understanding, at pathological and molecular levels, the mode of action of citalopram in MJD may shed light into the pathogenesis of this disease and into the identification of novel therapeutic targets.

## References

1. Orr, H. T. & Zoghbi, H. Y. Trinucleotide repeat disorders. *Annu. Rev. Neurosci.* **30**, 575–621 (2007).
2. Schöls, L., Bauer, P., Schmidt, T., Schulte, T. & Riess, O. Autosomal dominant cerebellar ataxias: clinical features, genetics, and pathogenesis. *Lancet Neurol.* **3**, 291–304 (2004).
3. Paulson, H. L. Dominantly inherited ataxias: lessons learned from Machado-Joseph disease/spinocerebellar ataxia type 3. *Semin. Neurol.* **27**, 133–142 (2007).
4. Orr, H. T. Polyglutamine neurodegeneration: expanded glutamines enhance native functions. *Curr. Opin. Genet. Dev.* **22**, 251–255 (2012).
5. Shim, J. S. & Liu, J. O. Recent advances in drug repositioning for the discovery of new anticancer drugs. *Int. J. Biol. Sci.* **10**, 654–663 (2014).
6. Lauterbach, E. C. Neuroprotective effects of psychotropic drugs in Huntington's disease. *Int. J. Mol. Sci.* **14**, 22558–22603 (2013).
7. Cirrito, J. R. *et al.* Serotonin signaling is associated with lower amyloid- $\beta$  levels and plaques in transgenic mice and humans. *Proc. Natl. Acad. Sci. U. S. A.* **108**, 14968–14973 (2011).
8. Sheline, Y. I. *et al.* An Antidepressant Decreases CSF A Production in Healthy Individuals and in Transgenic AD Mice. *Sci. Transl. Med.* **6**, 236re4–236re4 (2014).
9. Minamiyama, M. *et al.* Naratriptan mitigates CGRP1-associated motor neuron degeneration caused by an expanded polyglutamine repeat tract. *Nat. Med.* **18**, 1531–1538 (2012).
10. Tatum, M. C. *et al.* Neuronal serotonin release triggers the heat shock response in *C. elegans* in the absence of temperature increase. *Curr. Biol. CB* **25**, 163–174 (2015).
11. Lin, H.-Y. *et al.* Desipramine protects neuronal cell death and induces heme oxygenase-1 expression in Mes23.5 dopaminergic neurons. *PLoS One* **7**, e50138 (2012).
12. Omi, T. *et al.* Fluvoxamine alleviates ER stress via induction of Sigma-1 receptor. *Cell Death Dis.* **5**, e1332 (2014).
13. Silva-Fernandes, A. *et al.* Motor uncoordination and neuropathology in a transgenic mouse model of Machado-Joseph disease lacking intranuclear inclusions and ataxin-3 cleavage products. *Neurobiol. Dis.* **40**, 163–176 (2010).
14. Stefani, M. Generic cell dysfunction in neurodegenerative disorders: role of surfaces in early protein misfolding, aggregation, and aggregate cytotoxicity. *Neurosci. Rev. J. Bringing Neurobiol. Neurol. Psychiatry* **13**, 519–531 (2007).

15. Chai, Y., Koppenhafer, S. L., Bonini, N. M. & Paulson, H. L. Analysis of the role of heat shock protein (Hsp) molecular chaperones in polyglutamine disease. *J. Neurosci. Off. J. Soc. Neurosci.* **19**, 10338–10347 (1999).
16. Cummings, C. J. *et al.* Over-expression of inducible HSP70 chaperone suppresses neuropathology and improves motor function in SCA1 mice. *Hum. Mol. Genet.* **10**, 1511–1518 (2001).
17. Warrick, J. M. *et al.* Suppression of polyglutamine-mediated neurodegeneration in *Drosophila* by the molecular chaperone HSP70. *Nat. Genet.* **23**, 425–428 (1999).
18. Kobayashi, Y. *et al.* Chaperones Hsp70 and Hsp40 suppress aggregate formation and apoptosis in cultured neuronal cells expressing truncated androgen receptor protein with expanded polyglutamine tract. *J. Biol. Chem.* **275**, 8772–8778 (2000).
19. Bailey, C. K., Andriola, I. F. M., Kampinga, H. H. & Merry, D. E. Molecular chaperones enhance the degradation of expanded polyglutamine repeat androgen receptor in a cellular model of spinal and bulbar muscular atrophy. *Hum. Mol. Genet.* **11**, 515–523 (2002).
20. Yokoyama, K. *et al.* Extended longevity of *Caenorhabditis elegans* by knocking in extra copies of hsp70F, a homolog of mot-2 (mortalin)/mthsp70/Grp75. *FEBS Lett.* **516**, 53–57 (2002).
21. Dodson, M., Redmann, M., Rajasekaran, N. S., Darley-Usmar, V. & Zhang, J. KEAP1-NRF2 signalling and autophagy in protection against oxidative and reductive proteotoxicity. *Biochem. J.* **469**, 347–355 (2015).
22. Cuadrado, A. & Rojo, A. I. Heme oxygenase-1 as a therapeutic target in neurodegenerative diseases and brain infections. *Curr. Pharm. Des.* **14**, 429–442 (2008).
23. Jazwa, A. & Cuadrado, A. Targeting heme oxygenase-1 for neuroprotection and neuroinflammation in neurodegenerative diseases. *Curr. Drug Targets* **11**, 1517–1531 (2010).
24. Schipper, H. M., Song, W., Zukor, H., Hascalovici, J. R. & Zeligman, D. Heme oxygenase-1 and neurodegeneration: expanding frontiers of engagement. *J. Neurochem.* **110**, 469–485 (2009).
25. Tao, X., West, A. E., Chen, W. G., Corfas, G. & Greenberg, M. E. A calcium-responsive transcription factor, CaRF, that regulates neuronal activity-dependent expression of BDNF. *Neuron* **33**, 383–395 (2002).
26. Timmusk, T., Belluardo, N., Persson, H. & Metsis, M. Developmental regulation of brain-derived neurotrophic factor messenger RNAs transcribed from different promoters in the rat brain. *Neuroscience* **60**, 287–291 (1994).
27. Orr, H. T. Beyond the Qs in the polyglutamine diseases. *Genes Dev.* **15**, 925–932 (2001).



# CHAPTER 5

---

Assesment of chronic citalopram post-symptomatic treatment in a MJD mouse model  
of increased severity

**Assesement of chronic citalopram post-symptomatic treatment in a MJD mouse model  
with increased severity**

Sofia Esteves<sup>1,2</sup>, Sara Duarte-Silva<sup>1,2</sup>, Andreia Teixeira-Castro<sup>1,2</sup> and Patricia Maciel<sup>1,2</sup>

1) Life and Health Sciences Research Institute (ICVS), School of Health Sciences, University of Minho, 4710-057 Braga, Portugal.

2) ICVS/3Bs - PT Government Associate Laboratory, Braga/Guimarães, Portugal.

## Abstract

Machado-Joseph Disease (MJD) or spinocerebellar ataxia type 3 (SCA3) is the most common spinocerebellar ataxia worldwide, being a progressive and fatal neurodegenerative disorder caused by a polyglutamine (polyQ) expansion in the ataxin-3 gene. Its mechanisms of pathogenesis are still not well understood and there is no effective treatment so far. We have previously shown that the treatment of an MJD mouse model (CMVMJD135) with citalopram, a selective serotonin re-uptake inhibitor (SSRI), starting at pre-symptomatic stage of the disease lead to significant balance and motor coordination improvement, suppression of ataxin-3 (ATXN3) nuclear inclusions, and reduction of astrogliosis, among other neuroprotective effects. In an attempt to better mirror the clinical situation and further explore the potential of this drug, we performed a post-symptomatic citalopram treatment in a more severely affected group of CMVMJD135 mice (bearing larger CAG repeat tracts). Citalopram post-symptomatic treatment lead to mild improvement in balance and motor coordination and transient improvement in tremors, gait and limb claspings in this group of animals of this pre-clinical trial. While confirming the beneficial therapeutic effect of citalopram, our results show that the efficacy of treatment with this compound is thus reduced when the treatment is initiated later and the disease condition is too severe and well-established. This prompts us to suggest early initiation of citalopram treatment in MJD patients.

## Introduction

Machado-Joseph disease (MJD) or spinocerebellar ataxia type 3 (SCA3) is a clinically heterogeneous neurodegenerative disease characterized by variable degrees of ataxia, ophthalmoplegia, pyramidal dysfunction and peripheral neuropathy<sup>1,2</sup>. MJD is caused by an expansion of a CAG repeat that in the *ATXN3* gene, which leads to an abnormally long polyglutamine (polyQ) tract in the encoded protein, ataxin-3 (ATXN3)<sup>3</sup>. At neuropathological level, MJD is characterized by a widespread neuronal degeneration affecting multiple neuronal systems and not restricted to the cerebellum, brainstem and basal ganglia<sup>4</sup>. Currently, no effective disease modifying treatment is available for MJD.

Citalopram is a selective serotonin reuptake inhibitor (SSRI) available as an antidepressant since the 1980s in US and Europe and is overall safe and well tolerated drug<sup>5,6</sup>. Antidepressants and other psychopharmacological compounds have conventionally been prescribed to patients with neurodegenerative diseases, as a rational complementary therapy, helping them to cope with symptoms such as depression and anxiety. However, in the last years, these drugs have been explored more meticulously to assess other effects that they may have<sup>7</sup>. Several antidepressants have shown

neuroprotective effects in Alzheimer's disease (AD), Parkinson's disease (PD) Huntington's disease (HD) or Spinal and Bulbar Muscular Atrophy (SBMA)<sup>8-17</sup>. Is it clear that these drugs traditionally prescribed for depression or schizophrenia may have more pleiotropic effects than the ones currently known. In an unbiased screening of >600 FDA/EMA-approved small molecules for suppressors of *C.elegans* mutant ATXN3 induced neurotoxicity, citalopram was found to rescue neurological dysfunction and ATXN3 aggregation in this model. Chronic citalopram pre-symptomatic treatment of CMVMJD135 mice, strikingly ameliorated motor coordination impairments, reduced mutant ATXN3 aggregation and exerted neuroprotective effects (Chapter 3, Appendix I). Therefore, this compound seems to be a promising therapeutic strategy for MJD. Taking into account the promising results with citalopram pre-symptomatic treatment, we performed a follow-up citalopram pre-clinical trial with chronic treatment beginning only after the onset of the first motor coordination symptoms of the CMVMJD135 mouse model in a group with a higher CAG repeat average, and thus more severe disease. This post-symptomatic approach could more closely mirror what happens in MJD patient, and thus may serve as a validation of the potential for translation of the previous findings to the clinical context.

## **Material and Methods**

**Transgenic mouse model and drug administration.** CMVMJD135 mice were generated as described previously<sup>18</sup>. DNA extraction, animal genotyping and CAG repeat size analyses were performed as previously described<sup>19</sup>. The mean repeat size ( $\pm$ SD) for all transgenic mice used in this pre-clinical trial was  $138\pm 5$ . Age-matched and genetic background-matched WT animals were used as controls. Only male mice were used in this study. We administrated citalopram hydrobromide (CAS 59729-32-7, kindly provided by Lundbeck, Denmark) in the drinking water at a dosage of 8 mg/kg. To define the onset of symptoms we focused on the motor coordination tests that previously showed the best improvements upon treatment, i.e. the balance beam walk test and the motor swimming test. Treatment was initiated at eleven weeks of age, one week after the onset (ten weeks) of the motor coordination symptom appearance this group of animals. The trial was ended at 28 weeks of age, when the majority of the transgenic animals could not perform many of the motor tests. For analysis of genotype vs phenotype correlations, data obtained from non-treated CMVMJD135 mice of the pre-clinical trial described in Chapter 3 (mean CAG repeat size of  $130\pm 2$ ) were used together with data from non-treated CMVMJD135 mice of this pre-clinical trial. All animal procedures were conducted in accordance with European regulations (European Union Directive 2010/63/EU). Animal facilities and

the people directly involved in animal experiments (SE, SDS, ATC) were certified by the Portuguese regulatory entity — Direcção Geral de Alimentação e Veterinária. All the protocols were approved by the Animal Ethics Committee of the Life and Health Sciences Research Institute, University of Minho.

**Behavioral assessment.** Behavioral assessment was performed during the diurnal period, with 5 males per cage including CMVMJD135 hemizygous transgenic mice and WT littermates (n=15-16 per genotype) treated with citalopram or with vehicle (water). Behavioral tests started in a pre-symptomatic stage (4 weeks of age) and were conducted until 28 weeks of age (Fig. 1). Neurological tests were performed using a selection tests from the SHIRPA protocol, namely assessing tremors, gait quality and limb claspings<sup>20,21</sup>. The stride length was evaluated with footprinting analysis as previously described<sup>19</sup>. Motor behavior was assessed using the balance beam walk test (12 mm and 17 mm square and 17 mm round beams) and the motor swimming test<sup>19</sup>. All behavioral tests were performed as previously described<sup>19</sup>. Body weight was also registered for each evaluation time point. The ARRIVE guidelines were followed and taken into consideration throughout the study<sup>22</sup>.

**Immunohistochemistry and quantification of neuronal inclusions.** Twenty eight week-old WT and CMVMJD135 littermate mice, citalopram-treated and non-treated (n=4 for each group) were deeply anesthetized with a mixture of ketamine hydrochloride (150 mg/kg) plus medetomidine (0.3 mg/kg) and transcardially perfused with phosphate-buffered saline (PBS) followed by 4% paraformaldehyde (PFA) (Panreac, USA). Brains were removed and post fixed overnight in PFA and embedded in paraffin. Slides with 4- $\mu$ m-thick paraffin sections were subjected to antigen retrieval and then incubated with mouse anti-ATXN3 (1H9) (1:750, MAB5360, Milipore) which was detected by incubation with a biotinylated anti-polyvalent antibody, followed by detection through biotin-streptavidin coupled to horseradish peroxidase and reaction with the DAB (3,3'-diaminobenzidine) substrate (Lab Vision<sup>TM</sup> Ultra-Vision<sup>TM</sup> Detection kit, Thermo Scientific). The slides were counterstained with hematoxylin 25% according to standard procedures. ATXN3 positive inclusions in the pontine nuclei (PN) of either vehicle- or citalopram-treated animals (n=4 for each conditions, 4 slides per animal) were quantified and normalized for total area using the Olympus BX51 stereological microscope (Olympus, Japan) and the Visiopharma integrator system software (Visiopharm, Denmark) as previously described<sup>19</sup>.

**Genotype vs Phenotype correlation.** For analysis of genotype vs phenotype correlations, data obtained from non-treated CMVMJD135 mice of the pre-clinical trial described in Chapter 3<sup>23</sup> (mean CAG repeat size of  $130\pm 2$ ) were used together with data from non-treated CMVMJD135 mice of this pre-clinical trial. Motor performance in the balance beam walk and motor swimming tests were analyzed at 26 weeks of age for all animals ( $n=27$ ), and correlated to their CAG repeat number.

**Study design and statistical analysis.** Experimental design was based on power analyses for optimization of sample size. Mouse sample size calculations were previously performed for each behavioral test and pathological analyses assuming a power of 0.95 and 0.8, respectively, and a significance level of  $P<0.05$ <sup>23</sup>. Data was analyzed through the non-parametric Mann-Whitney U-test when variables were non-continuous or when a continuous variable did not present a normal distribution (Kolmogorov-Smirnov test,  $p<0.05$ ). Continuous variables with normal distributions and with homogeneity of variance (Levene's test) were analyzed with Repeated-Measures ANOVA for longitudinal multiple comparisons and One-Way ANOVA for paired comparisons, using Tukey test for post-hoc comparisons. Genotype-Phenotype correlations were analyzed through the Pearson correlation coefficient. All statistical analyses were performed using SPSS 22.0 (SPSS Inc., Chicago, IL) and G-Power 3.1.9.2 (University Kiel, Germany). A critical value for significance of  $p<0.05$  was used throughout the study.

## Results

### **Citalopram post-symptomatic treatment has mild limited improvement of neurological symptoms without rescuing the body weight loss**

The most striking aspect of the phenotype of CMVMJD135 mice are the presence of motor uncoordination, loss of strength and balance impairments, among other neurological symptoms<sup>18</sup>. In the experimental group of animals used in this pre-clinical trial, the severity of the phenotype was higher than in previously described groups and the symptoms appeared earlier, due to a higher CAG repeat mean. Statistically significant differences in the severity of motor symptoms (beam walk test and motor swimming test) between WT and non-treated CMVMJD135 mice were observed at ten weeks of age ( $p<0,05$ ). According to this, citalopram was administered since 11 weeks of age (Fig. 1).

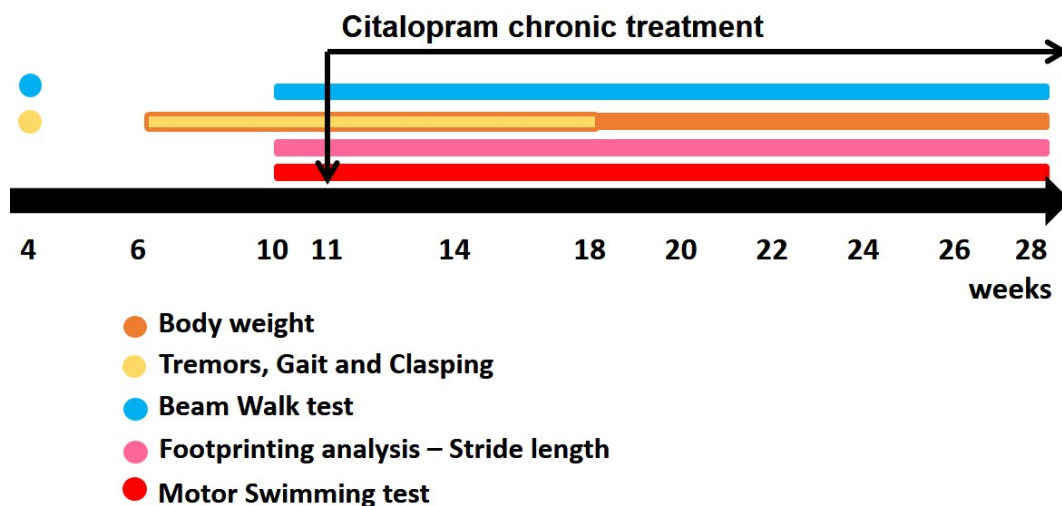


**Figure 1.** Timeline schematic representation of the pre-clinical therapeutic trial.

Citalopram post-symptomatic treatment did not rescue loss of the body weight of CMVMJD135 mice (Fig. 2A). Limited improvements were observed for tremors, which were statistically significant at 24 weeks of age, although a trend toward an improvement was observed at all ages analyzed (Fig. 2B). Also for limb clasping and gait quality, a trend towards an improvement was observed at all ages (Fig. 2C,D), the differences being statistically significant between 20 and 24 weeks of age. These ameliorations were thus transient and not maintained when the disease became more severely installed.

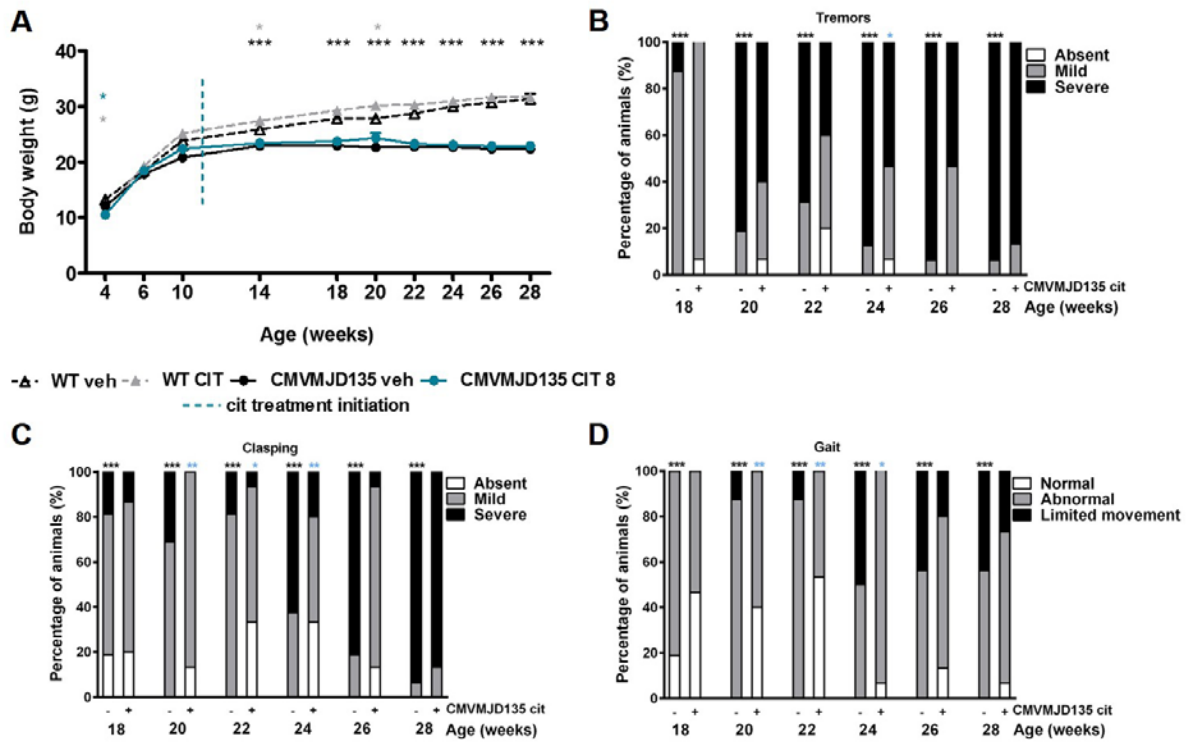


**Figure 2.** Limited effect of citalopram post-symptomatic treatment in neurological symptoms and body weight of CMVMJD135 mice. (A) Body weight, (B) Tremors, (C) Claspings, (D) Gait quality. (WT veh, n=13, WT CIT, n=17, CMVMJD135 veh, n=16, CMVMJD135 CIT, n=15) Mild improvement was observed for tremors, claspings and gait quality between 20 and 24 weeks of age, while no effect was observed in body weight upon treatment. Data presented as mean  $\pm$  SEM., \* $p$ <0.05, \*\* $p$ <0.01 and \*\*\* $p$ <0.001. (Repeated-measures ANOVA, Tukey correction, One-way ANOVA and Mann Whitney U test for non-continuous variables).

### Mild improvement in motor coordination of CMVMJD135 mice upon chronic citalopram post-symptomatic treatment

In this group of CMVMJD135 mice with a higher severity of disease, animals were not able to correctly perform the motor and coordination tests until the initially planned end of the pre-clinical trial, at 34 weeks of age, mainly for the beam walk test, in which the percentage of falls was increasing along the age in non-treated CMVMJD135 mice. Nevertheless, we observed an amelioration in motor performance with citalopram treatment in the different beams analyzed (Fig. 3A,B,C), although less striking for the 17mm circle beam. No differences were detected in the number of falls from the 17mm circle beam at 26 weeks of age (Fig. 3D). In the motor swimming test, there was a trend for citalopram-treated CMVMJD135 mice to take less time to reach the safe platform when compared to non-treated mice; however, this difference did not reach statistical differences along the pre-clinical trial (Fig. 3E). Although not so striking as in citalopram pre-symptomatic treatment (Chapter 3), an amelioration in the



stride length upon post-symptomatic treatment was observed at 28 weeks of age (Fig. 3F). Tests were not continued after this age, due to the higher severity of disease in non-treated CMVMJD135 mice, that rendered them unable to perform the beam walk and motor swimming tests, thus we were unable to confirm the continuity of amelioration of the stride length in subsequent ages.

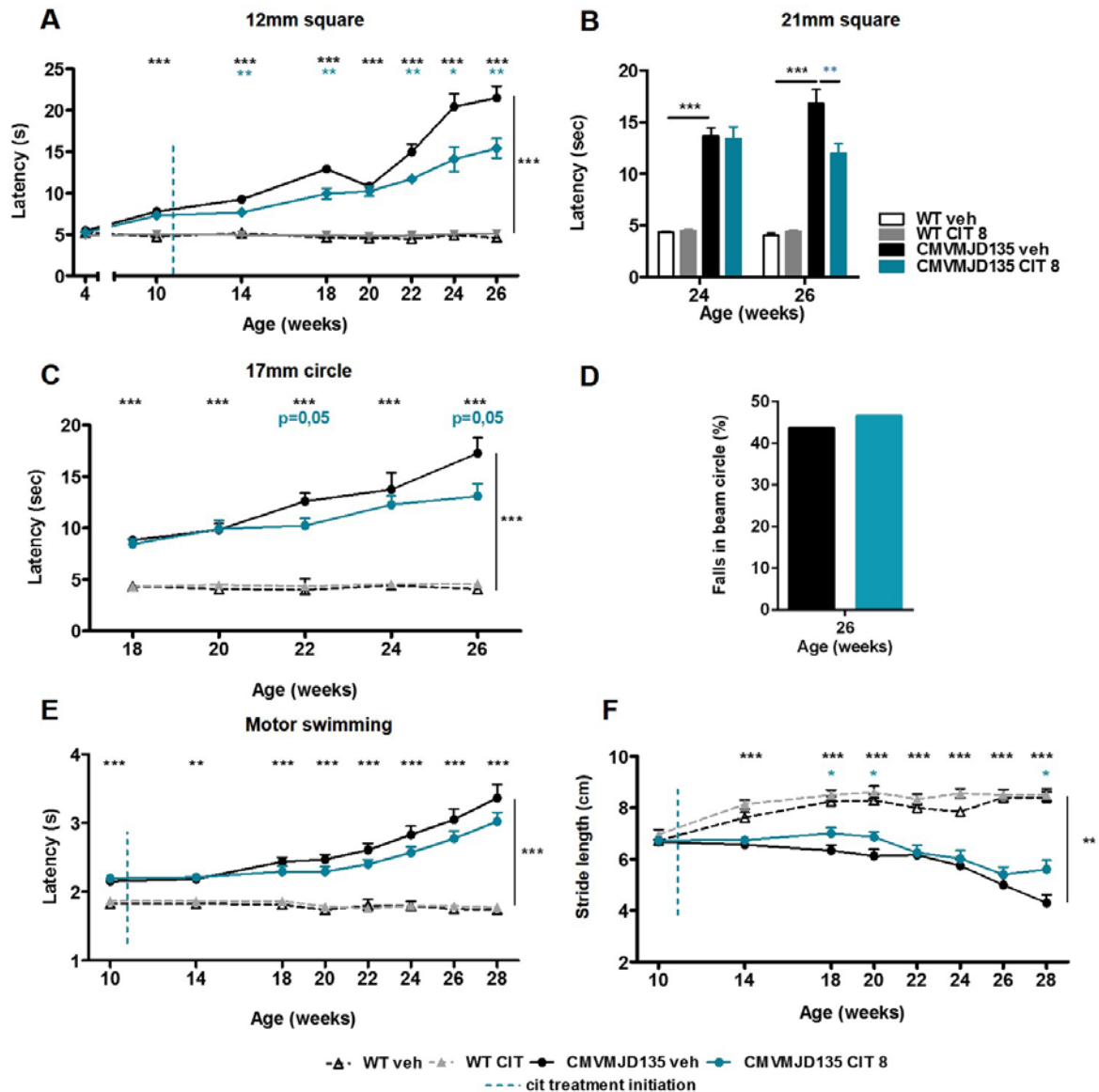


**Figure 3.** Limited effect of citalopram post-symptomatic treatment in motor coordination of CMVMJD135 mice. (A) Balance beam walk test 12mm square, (B) Balance beam walk test 21mm square, (C) Balance beam walk test 17mm circle, (D) Percentage of falls from balance beam walk test 17 mm circle, (E) Motor swimming test, (F) Stride length. (WT veh, n=13, WT CIT, n=17, CMVMJD135 veh, n=16, CMVMJD135 CIT, n=15) Mild improvements were observed in the 12 and 21 mm square balance beams and in the stride length, while no effect was observed in 17mm circle beam and in the motor swimming test upon treatment. Data presented as mean  $\pm$  SEM., \* $p$ <0.05, \*\* $p$ <0.01 and \*\*\* $p$ <0.001. (Repeated-measures ANOVA, Tukey correction and One-way ANOVA).

**CAG repeat-length correlates with phenotype severity in CMVMJD135 mouse model**

To better understand the relatively decreased effect of citalopram post-symptomatic treatment in this group of CMVMJD135 mice several comparisons were performed. The CAG number repeat of the animals from the pre-symptomatic pre-clinical trial was confirmed to be significantly less than the animals from the post-symptomatic pre-clinical trial (Fig. 4A). A genotype vs phenotype correlation was performed at 26 weeks of age, for the performance in motor swimming and beam walk tests in animals without treatment (vehicle group from the pre-<sup>23</sup> and post-symptomatic citalopram pre-clinical trial, n=23). A statistically significant correlation ( $p < 0,001$ , n=23) was obtained for both tests at this age, indicating an inverse correlation between CAG repeat length and behavior performance (Fig. 4B,C).

Consistently, the direct comparison between the groups of animals used in the pre- and post-symptomatic citalopram pre-clinical trials showed a striking difference between the groups concerning behavior performances in the beam walk and motor swimming tests, the higher CAG repeat-length group (mean  $\pm$  SD =  $138 \pm 5$ ) used for this post-symptomatic trial, showing more severe disease and faster progression than the group (mean  $\pm$  SD =  $130 \pm 2$ ) used for the previous pre-symptomatic trial (Fig. 4D,E) ( $p < 0,05$ ).

When comparing the common behavior tests from the two pre-clinical trials in terms of the symptom onset, symptom improvement (light colors corresponding to improvements and white boxes with dashed lines corresponding to the rescue of the phenotype, i.e. when the treated animals reached the WT level) and treatment onset (Fig. 4F,G) one can clearly see that in addition to our post-symptomatic treatment, the symptoms also started earlier in this pre-clinical trial due to the higher CAG repeat length of this group of animals. These two factors may underlie the differences in terms of symptom improvement from the two pre-clinical trials.

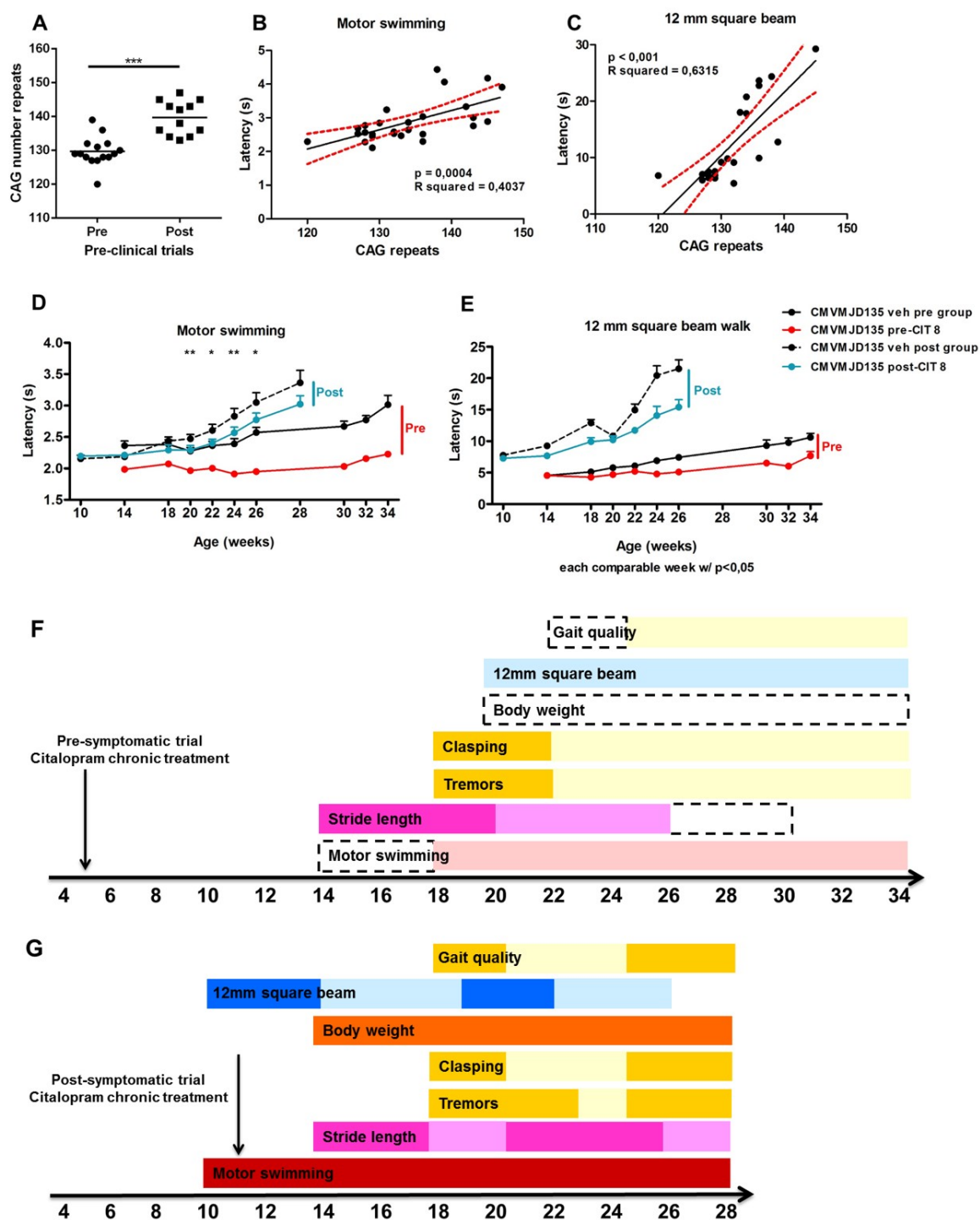


**Figure 4.** CAG-repeat length vs phenotype correlation and citalopram pre and post-symptomatic pre-clinical trial comparison. (A) CAG repeat number comparison between pre and post-symptomatic citalopram pre-clinical trials (CMVMJD135,  $n=27$ ), (B) Genotype vs phenotype correlation for the motor swimming test at 26 weeks of age (CMVMJD135,  $n=25$ ), (C) Genotype vs phenotype correlation for the beam walk test at 26 weeks of age, (CMVMJD135,  $n=23$ ). Comparison of citalopram pre- and post-symptomatic pre-clinical trials regarding performance of untreated groups in (D) the motor swimming test and (E) 12 mm square beam walk test. Data presented as mean  $\pm$  SEM., \* $p < 0.05$  and \*\* $p < 0.01$ . (Pearson correlation coefficient, Repeated-measures ANOVA, Tukey correction and One-way ANOVA). Comparison

**(Figure 4.) (cont.)** of citalopram (F) pre- and (G) post-symptomatic pre-clinical trials regarding timing and extent of improvements in the common tests. Light colors corresponding to improvements upon treatment and white boxes with dashed lines corresponding to the rescue of the phenotype, i.e. when the treated animals reached the WT level, for each behavioral test. (pre- and post-symptomatic pre-clinical trials with a range between 11 and 17 animals used per group).

### **Citalopram post-symptomatic treatment did not change the ATXN3 inclusions and neither mitigated astrogliosis**

Following the neuropathological observations upon citalopram pre-symptomatic treatment (Chapter 3), here we also evaluated the effect of citalopram post-symptomatic treatment in the abundance of ATXN3 neuronal inclusions in affected several brain regions, and of astrogliosis in the substantia nigra. The treatment with citalopram after the onset of behavior symptoms was not able to modify the course of these neuropathological alterations, not affecting the number of inclusions per total area, neither impacting in GFAP positive cells in the substantia nigra (Fig. 5).

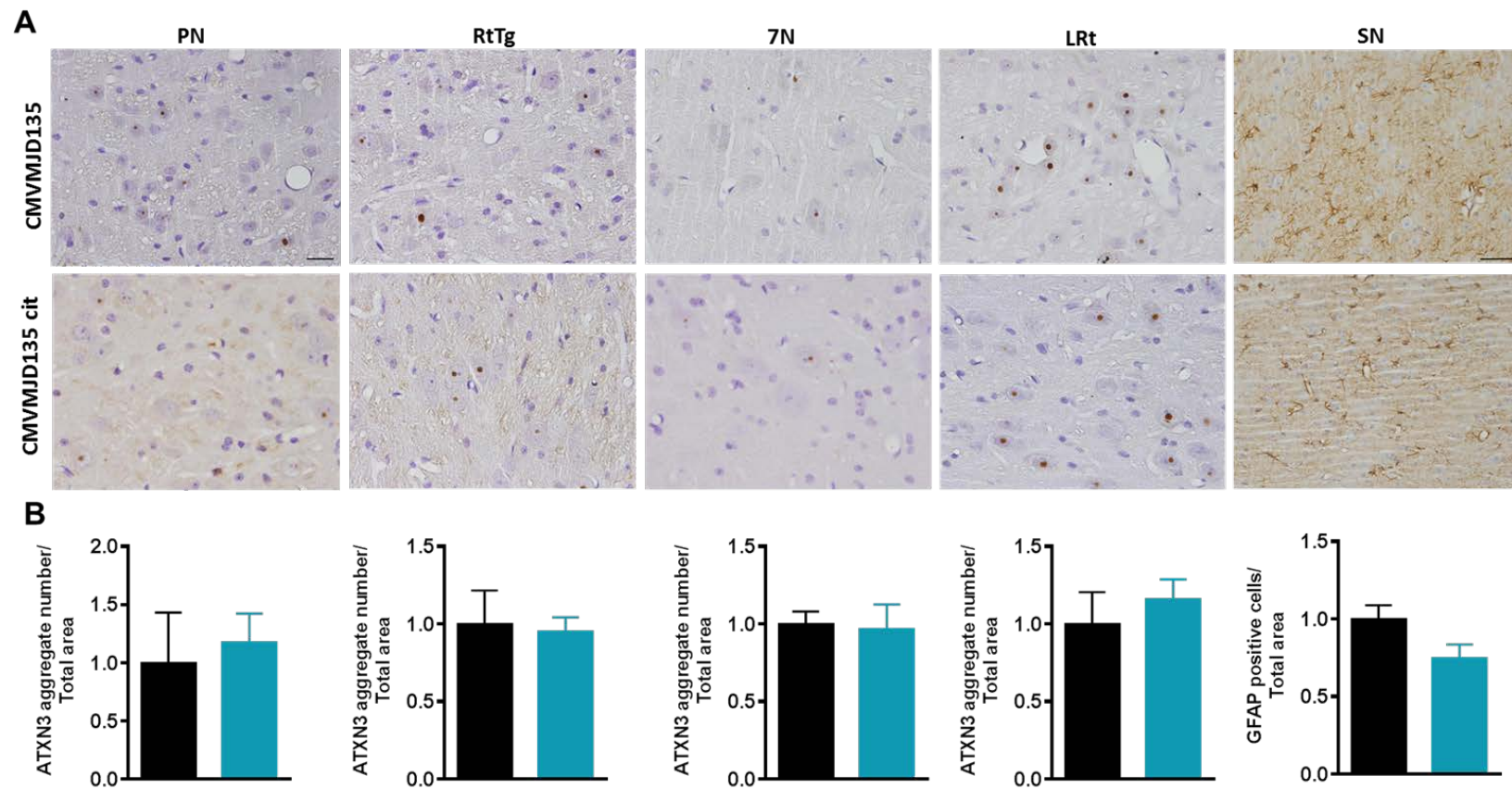


**Figure 5.** Citalopram post-symptomatic treatment effect in ATXN3 intranuclear inclusions and astrogliosis. (A) Immunohistochemistry and quantification of ATXN3 neuronal inclusions in the PN, RtTg, 7N and LRt of vehicle and cit treated CMVMJD135 mice (n=4, 28 weeks). (B) Immunohistochemistry and quantification of GFAP positive cells in substantia nigra (n=4, 28 weeks).

## Discussion

In order to explore if citalopram is able to modify the course of the symptoms after the onset of the phenotype in the CMVMJD135 mouse model of MJD, in this study we started the treatment with citalopram 8mg/kg only after the manifestation of the core motor coordination symptoms (assessed in beam walk and motor swimming tests). We chose this component of the phenotype because results from the previous pre-symptomatic pre-clinical trial (Chapter 3) showed that chronic citalopram treatment exerted its effects mostly in the more central nervous system-related symptoms rather than on the more peripheral ones (e.g. muscular strength). In this group of animals the first motor coordination symptoms occurred at 10 weeks of age. Limited effects were observed in motor coordination and balance in the beam walk test in CMVMJD135 mice upon this post-symptomatic treatment combined with a higher severity disease condition. Other neurological symptoms such as tremors, gait quality and limb claspings were also transiently attenuated upon citalopram treatment, however it did not rescue the body weight loss. Also at the neuropathological level, this post-symptomatic treatment was not able to modify the ATXN3 intranuclear inclusions neither astrogliosis.

Correlating the CAG repeat-length with the motor and balance phenotype performance in untreated CMVMJD135 mice from pre- and post-symptomatic treatment pre-clinical trial groups, we observed that animals with higher CAG repeat-length took more time to complete the tasks, thus presenting a stronger phenotype when compared to the previous pre-symptomatic treatment control groups. This correlation between CAG repeat-length and clinical features was also described in MJD patients, in which patients with higher CAG repeat length patients present earlier age at disease onset and worse clinical presentations; however, other factors than repeat size are also thought to contribute for the clinical presentation<sup>24</sup>. The CMVMJD135 mouse model has therefore, the advantage of faithfully reproducing this feature of MJD; however, one should take it into consideration, whenever possible, for the correct preparation of experimental groups for pre-clinical trials, namely for the adequate matching of control and test groups. Even with this increased severity, at an early stage of the disease progress, when the symptoms are not fully established and some of them are still absent, the neurodegenerative process could probably be overcome by treatment. As the disease progresses, however, the regeneration ability may not be sufficient to cope with the neurodegenerative process and all the symptoms appear and become strikingly established. In the CMVMJD135 mice group studied in this pre-clinical trial, the post-symptomatic treatment with citalopram had beneficial effects but it did not lead to such a marked amelioration as we have seen

in the previous pre-symptomatic trial<sup>23</sup>, which may be due to the combination of the late treatment and the increased severity of the symptoms. However, a higher efficacy of citalopram in a post-symptomatic approach cannot be excluded in a group similar to the one tested in the pre-symptomatic approach. It is therefore crucial to perform another pre-clinical trial (now currently ongoing in the lab) in order to be able to answer the question of whether citalopram is only able to delay and alleviate the symptoms when they are starting to appear, or also to modify the symptoms after their establishment in a group of comparable severity, i.e. with a similar mean number of CAG-repeats. Nonetheless, our results suggest that citalopram treatment may be less suitable for MJD patients in very late stages of the disease and/or with very severe forms of the disease.

As a dominant autosomally inherited neurodegenerative disease, MJD patients or their relatives at risk can benefit from genetic counseling, in which they can be informed of the consequences and nature of the disease as well as their probability of developing or transmitting it. A pre-symptomatic treatment of the disease would avoid or at least delay the disease onset; however, for several personal, social and/or ethical issues the majority of the clinical studies start a treatment after the onset of the symptoms (post-symptomatic treatment). Our data suggests that the pre-symptomatic gene testing for MJD and the appropriate family counselling could have a positive impact not only on subjects' quality of life, but also on the future of the disease studies. In recent years, there has been a growing number of advances and possibilities of therapeutic approaches, therefore this molecular genotyping may become of great value to families affected by this disease when an effective treatment becomes available. Although still not ongoing, a human clinical trial with citalopram treatment could be an excellent opportunity for MJD therapy, especially in a combination with pre-symptomatic genetic testing. An additional advantage is that citalopram is an SSRI with few side effects<sup>25</sup> after long term administration, which could conceivably be administered in a pre-symptomatic stage of the disease. Pre-symptomatic testing and treatment are still major ethical concerns in human patients, implying a balance of the risks of testing and treating in contrast with potential benefits; however, it is an emerging concept for several neurodegenerative diseases<sup>26,27</sup>. Another major challenge to a pre-symptomatic clinical trial is the lack of consistent and sensitive non-invasive biomarkers, not only for early stages of the disease, but also to its progression. Some recent neuroimaging and blood-based transcriptomic studies do exist<sup>28,29</sup>, however none of the resulting candidate biomarkers is ready to be introduced on clinics as a common practice. Also, for citalopram we are still lacking an efficacy biomarker limited to its mechanism of action in MJD, which could hamper the translation to clinics. Lack of financial support for a rare disease such as

MJD could also be another causes of a future delay in the development of new and potentially relevant clinical trials.

### **Conclusion**

Citalopram post-symptomatic treatment in a higher severity MJD model lead to mild motor and balance amelioration and transient improvement in tremors, gait quality and limb clasping, without rescuing the body weight loss. At the neuropathological level, post-symptomatic treatment did not change the number of ATXN3 intranuclear inclusions and did not improve astrogliosis. The possibility of better positive effects of citalopram post-symptomatic treatment is not excluded in animals with less phenotype severity. Moreover, citalopram pre-symptomatic treatment could be a rational therapeutic possibility in MJD patients having undergone genetic testing.



## References

1. Coutinho, P. & Andrade, C. Autosomal dominant system degeneration in Portuguese families of the Azores Islands. A new genetic disorder involving cerebellar, pyramidal, extrapyramidal and spinal cord motor functions. *Neurology* 28, 703–709 (1978).
2. Lima, L. & Coutinho, P. Clinical criteria for diagnosis of Machado-Joseph disease: report of a non-Azorena Portuguese family. *Neurology* 30, 319–322 (1980).
3. Kawaguchi, Y. *et al.* CAG expansions in a novel gene for Machado-Joseph disease at chromosome 14q32.1. *Nat. Genet.* 8, 221–228 (1994).
4. Rüb, U., Brunt, E. R. & Deller, T. New insights into the pathoanatomy of spinocerebellar ataxia type 3 (Machado-Joseph disease). *Curr. Opin. Neurol.* 21, 111–116 (2008).
5. Cipriani, A. *et al.* in *Cochrane Database of Systematic Reviews* (ed. The Cochrane Collaboration) (John Wiley & Sons, Ltd, 2012). at <http://doi.wiley.com/10.1002/14651858.CD006534.pub2>
6. Aboukhatwa, M., Dosanjh, L. & Luo, Y. Antidepressants are a rational complementary therapy for the treatment of Alzheimer's disease. *Mol. Neurodegener.* 5, 10 (2010).
7. Lauterbach, E. C. *et al.* Psychopharmacological neuroprotection in neurodegenerative disease: assessing the preclinical data. *J. Neuropsychiatry Clin. Neurosci.* 22, 8–18 (2010).
8. Minamiyama, M. *et al.* Naratriptan mitigates CGRP1-associated motor neuron degeneration caused by an expanded polyglutamine repeat tract. *Nat. Med.* 18, 1531–1538 (2012).
9. Cirrito, J. R. *et al.* Serotonin signaling is associated with lower amyloid- $\beta$  levels and plaques in transgenic mice and humans. *Proc. Natl. Acad. Sci. U. S. A.* 108, 14968–14973 (2011).
10. Sheline, Y. I. *et al.* An Antidepressant Decreases CSF A Production in Healthy Individuals and in Transgenic AD Mice. *Sci. Transl. Med.* 6, 236re4–236re4 (2014).
11. Omi, T. *et al.* Fluvoxamine alleviates ER stress via induction of Sigma-1 receptor. *Cell Death Dis.* 5, e1332 (2014).
12. Lin, H.-Y. *et al.* Desipramine protects neuronal cell death and induces heme oxygenase-1 expression in Mes23.5 dopaminergic neurons. *PLoS One* 7, e50138 (2012).
13. Ubhi, K. *et al.* Fluoxetine ameliorates behavioral and neuropathological deficits in a transgenic model mouse of  $\alpha$ -synucleinopathy. *Exp. Neurol.* 234, 405–416 (2012).
14. Pakaski, M. *et al.* Imipramine and citalopram facilitate amyloid precursor protein secretion in vitro. *Neurochem. Int.* 47, 190–195 (2005).

15. Chung, Y. C., Kim, S. R. & Jin, B. K. Paroxetine Prevents Loss of Nigrostriatal Dopaminergic Neurons by Inhibiting Brain Inflammation and Oxidative Stress in an Experimental Model of Parkinson's Disease. *J. Immunol.* 185, 1230–1237 (2010).
16. Duan, W. *et al.* Paroxetine retards disease onset and progression in Huntingtin mutant mice. *Ann. Neurol.* 55, 590–594 (2004).
17. Duan, W. *et al.* Sertraline slows disease progression and increases neurogenesis in N171-82Q mouse model of Huntington's disease. *Neurobiol. Dis.* 30, 312–322 (2008).
18. Silva-Fernandes, A. *et al.* Chronic treatment with 17-DMAG improves balance and coordination in a new mouse model of Machado-Joseph disease. *Neurother. J. Am. Soc. Exp. Neurother.* 11, 433–449 (2014).
19. Silva-Fernandes, A. *et al.* Motor uncoordination and neuropathology in a transgenic mouse model of Machado-Joseph disease lacking intranuclear inclusions and ataxin-3 cleavage products. *Neurobiol. Dis.* 40, 163–176 (2010).
20. Rogers, D. C. *et al.* Behavioral and functional analysis of mouse phenotype: SHIRPA, a proposed protocol for comprehensive phenotype assessment. *Mamm. Genome Off. J. Int. Mamm. Genome Soc.* 8, 711–713 (1997).
21. Rafael, J. A., Nitta, Y., Peters, J. & Davies, K. E. Testing of SHIRPA, a mouse phenotypic assessment protocol, on Dmd(mdx) and Dmd(mdx3cv) dystrophin-deficient mice. *Mamm. Genome Off. J. Int. Mamm. Genome Soc.* 11, 725–728 (2000).
22. Kilkenny, C., Browne, W. J., Cuthill, I. C., Emerson, M. & Altman, D. G. Improving bioscience research reporting: the ARRIVE guidelines for reporting animal research. *Osteoarthr. Cartil. OARS Osteoarthr. Res. Soc.* 20, 256–260 (2012).
23. Teixeira-Castro, A. *et al.* Serotonergic signalling suppresses ataxin 3 aggregation and neurotoxicity in animal models of Machado-Joseph disease. *Brain J. Neurol.* (2015). doi:10.1093/brain/aww262
24. Maciel, P. *et al.* Correlation between CAG repeat length and clinical features in Machado-Joseph disease. *Am. J. Hum. Genet.* 57, 54–61 (1995).
25. Nemeroff, C. B. Overview of the safety of citalopram. *Psychopharmacol. Bull.* 37, 96–121 (2003).
26. Katsuno, M., Tanaka, F. & Sobue, G. Perspectives on molecular targeted therapies and clinical trials for neurodegenerative diseases. *J. Neurol. Neurosurg. Psychiatry* 83, 329–335 (2012).

27. Katsuno, M., Watanabe, Hirohisa, Tanaka, Fumiaki & Sobue, Gen. Translational research on disease-modifying therapies for neurodegenerative disorders. *Neurol. Clin. Neurosci.* 1, 3–10 (2013).
28. Pacheco, L. S. *et al.* Association between Machado-Joseph disease and oxidative stress biomarkers. *Mutat. Res.* 757, 99–103 (2013).
29. Raposo, M. *et al.* Novel candidate blood-based transcriptional biomarkers of Machado-Joseph disease. *Mov. Disord. Off. J. Mov. Disord. Soc.* 30, 968–975 (2015).



# CHAPTER 6

---

General discussion and future perspectives



## 6. Introduction

In this chapter, the main findings, strengths and limitations of this PhD thesis regarding the research questions are summarized, a general discussion is made and conclusions are drawn, based on the results presented. Furthermore, suggestions for further research are put forward.

### 6.1 Pre-clinical trials design: Strengths and limitations

Drug discovery development and pre-clinical trials are challenging and expensive processes approaching hundreds of millions of dollars per drug<sup>1-3</sup>. However, most of the promising compounds identified in pre-clinical trials are not as successful in human patients, contributing to several clinical failures. These failure rates could possibly be decreased and optimized by using more stringent criteria during the pre-clinical trials. Correct design, execution and reporting of mouse model results help to make pre-clinical data more reproducible and translatable to the clinic, reducing the false positive or false negative results. Several criteria should be taken into account, as discussed below.

#### 6.1.1 Validity of mouse models of disease

Animal models are essential to bridge the translational gap between pre-clinical and clinical research. Since 1980's, several types of genetically engineered mouse models have been used in drug development and pre-clinical trials, including transgenic, knock-out, and knock-in mouse models. The best model for human diseases should assume a number of different criteria: (a) **face validity**, in which the biology and symptoms between a mouse model and human disease should be similar (being often limited by the lack of knowledge on the pathogenic mechanisms underlying the disease symptoms); (b) **construct validity**, reflecting the degree to which a model measures what it claims to be measuring and (c) **predictive validity**, in which the same drug should produce the same effects between mouse model and humans (being often limited to incomplete correlation between mouse and humans in terms of disease mechanisms or drug absorption, distribution, metabolism and excretion). Therefore, it is important to choose a model of the disease that satisfies all these criteria, exhibiting significant and well characterized phenotype and pathology relevant to the target of interest, based on the hypothesized mechanism of action of the drug being studied. However, there is no "one model" for each disease. Therefore, tests in different models are an advantage to validate the results obtained. For instance, different models of the same disease may have different genetic backgrounds, and consequently show high variability in the extent and time course of expression of disease phenotypes

and pathology patterns, may have different pharmacokinetics and pharmacodynamics to the same drug and may have different drug responses among genders (males vs females).

The CMVMJD135 mouse model used in this PhD work is the transgenic mouse model of MJD with the most extensive pathological and phenotypic characterization so far, exhibiting a high face validity. These features make this model a very useful one for pre-clinical trials and hence, the one chosen to address the questions of this PhD work. However, a combination of different models can eventually come closer to the clinical situation than a single, even highly refined model.

### **6.1.2 Sample size**

Currently, for ethical (3R policy<sup>4,5</sup>) and logistic reasons, the number of animals used in pre-clinical trials is minimized to the most. Sample size should be estimated and depends on the predictable magnitude of a specific biological effect, on the inherent variability of the target and on the parameters being measured. This number needs to be sufficient for the researcher to detect significant differences taking into account the referred variabilities, as well as the **statistical power** required to produce solid data.

In the pre-clinical trials performed in this PhD work, the sample size necessary for each behavioral test and for each molecular and pathological analysis was estimated taking into account the standard deviations obtained from previously pre-clinical trails performed in the group. We concluded that to detect a 50% of drug effect we needed a variable number of animals for different tests (Table 1 of supplementary data of the Brain paper provided in Appendix I). These precise calculations of number of animals needed to detect significant differences in these pre-clinical trials, will be of extreme value in order to better design the future pre-clinical trials, (for instance, to remove some behavioral tests that require a very large number of animals in order to detect a significant effect and could not be ethically performed).

### **6.1.3 Gender Balance, Randomization and Blindness**

These three parameters are crucial aspects of a proper pre-clinical trial design which may affect the obtained results. Mice should be separated into groups by gender (to exclude gender specific drug effects) and age and then randomly assigned to either control or treatment groups. Controls should always be included into study design, as a reference point. Due to logistic reasons, only male mice were used in the pre-clinical trials in this PhD work, but proper controls were assumed along the study. Randomization was not always possible due to treatment administration. For instance, in the



citalopram pre-clinical trial, since the drug was given in the water bottle, the animals were distributed sequentially along the boxes according to the specific treatment, making randomization also difficult. Ideally, researchers conducting the experiments and analyzing the results should be blinded to the genotype and treatments. In the case of genotype, the blinding is not possible to maintain, since as the MJD-like symptoms progresses in CMVMJD135 mice, it becomes clearly visually detectable. Blindness to the treatment was not assumed, being one of the limitations of the current pre-clinical trials, since the researcher performing, analyzing and giving the treatment was the same. Nevertheless, efforts are being made in order to re-design the following studies and comply with these parameters in the future pre-clinical trials.

#### **6.1.4 Drug treatment considerations**

Although human dosage studies are frequently performed before the clinical trials, one major concern in clinical trial failures is the inappropriate translation of a drug dosage from one animal species to another, and frequently a drug that works well in animals is apparently not effective in humans. The animal dosage should not be extrapolated to a human equivalent dosage (HED) by a simple conversion based on body weight, as was described for instance in the case of resveratrol treatment, claimed to improve the health and life span in mice<sup>6,7</sup>. In 2007, Reagan-Shaw and colleagues suggested the use of the body surface area (BSA) normalization method, based on the idea that BSA correlates well across several mammalian species with several parameters of biology, including oxygen utilization, caloric expenditure, basal metabolism, blood volume, circulating plasma proteins and renal function. According to the formula for dosage translation based on BSA [ $\text{HED (mg/kg)} = \text{Animal dosage (mg/kg)} * \text{Animal } K_m / \text{Human } K_m$ ]<sup>8</sup>, the VPA mice dosage used in the our pre-clinical trial (200mg/kg/day) would translate to 16mg/Kg/day in humans, being similar to the usual adult initial prescribed dosage by FDA in cases of epilepsy (10 to 15mg/kg/day) ([www.drugs.com](http://www.drugs.com)).

Using this approach, the citalopram dosages used in the pre-clinical trial described in Chapter 3 (8 and 13mg/kg/day) would translate to 38 and 63mg/kg/day in humans. The usual adult initial dosage of citalopram for depression is 20mg/kg/day, and the maximum dosage currently recommended in humans being 40mg/kg/day ([www.drugs.com](http://www.drugs.com)), thus the most effective dosage found in our trial is within the recommended range. Recently, this BSA method has also been questioned, and it has been proposed that other aspects should be taken into account for interspecies scaling, such as physiologic, pharmacokinetic and toxicology data, rather than the simple BSA conversion<sup>9</sup>. This is particularly important in drug discovery strategies in which often no safety and toxicity data is available

for new drugs. For the compounds studied in this PhD thesis, although still important, the safety and toxicity in humans are guaranteed since they are widely used FDA-approved compounds. Effective dosages in humans could be scaled according to the described dosages. Furthermore, one additional proof-of concept for the use of these dosages in the pre-clinical trials here performed was the fact that these dosages were already described to be non-toxic and effective in mouse models with the same genetic background<sup>10,11</sup>.

An additional question, no less important and increasingly referred in the modern translational medicine, is the gender issue. The majority of the described pre-clinical trials are performed in males and only occasionally in females. Sex is a crucial biological variable which may have deep concerns. Under-representing female animals in pre-clinical trials may result in a reduced understanding of the biological, physiological and pathological mechanisms in females compared with males. Without female experiments it is difficult to predict that the results obtained in males will also be applicable to females<sup>12</sup>. One strength of the CMVMJD135 mouse model in this aspect is that the phenotype between males and females is highly comparable. However, the compounds tested in the pre-clinical trials performed in this PhD thesis were only assessed in males, making it difficult to assume that the drug effects will be the same in females. At least for citalopram, it will be valuable to evaluate its effects also in female animals.

Treatment timing should depend on whether the goal is disease prevention, therapeutic intervention (i.e. reducing/reversing the established phenotype/pathology), or symptomatic relief. In pre-clinical trials, the treatment is often initiated before or just after the onset of the disease, i.e. in a pre-symptomatic stage of the disease. This contrasts to the clinical practice, in which treatment is usually started after the onset of the symptoms. In this work we performed two **pre-symptomatic treatment approaches** (VPA and Citalopram) aiming at prevent or delaying the onset of the symptoms, and one **post-symptomatic treatment approach** (Citalopram) aiming at reversing and relieving the established phenotype or delaying its progression. Although with promising results in citalopram pre-symptomatic treatment, we should take into account that the observed potential pharmacological effect could be overestimated in CMVMJD135 mice, as the therapeutic intervention occurred earlier in the disease process when compared to the clinical condition. However, as seen in Chapter 5, post-symptomatic treatment also had some beneficial effects, even in more severely affected animals.

Further studies on citalopram need to be performed in the CMVMJD135 mouse model; however, as a relevant proof-of concept, some of these studies are easier and fast to perform in

*C.elegans* model. In this context, we assessed the necessary treatment duration and initiation in *C.elegans* model of MJD (Appendix I). First we observed that when we take off the citalopram treatment in the course of the disease, the symptoms returns after some time (but not instantly), suggesting that we need a chronic treatment to exert the therapeutic beneficial effects. Additionally, the treatment duration suggests a chronic treatment, since less duration of treatment corresponds to less therapeutic efficacy. Finally, when we started to treat the animals one, two, three or four days after the onset of the symptoms, it was observed that as the disease becomes more established the beneficial effects are less marked. Overall, these *C.elegans* data suggest that chronic treatment with citalopram starting at pre-symptomatic stages may be the best approach.

Furthermore, the availability of genetic diagnosis for MJD together with our main findings supports that it is possible and promising to start the treatment with citalopram early in the disease or even pre-symptomatically.

### **6.1.5 Statistical methods**

The statistical methods of analysis should be chosen before the start of the study and clearly described in the methods. Assessment of population distribution (normal vs skewed) will dictate the type of the analysis (parametric vs non-parametric). Caution with outliers or high variability should also be taken, to correct analyze the data. Exclusion criteria should also be established prior to the study.

The behavioral results obtained in the pre-clinical trials performed in this work were composed of quantitative and qualitative data. Quantitative data were analyzed using parametric methods which have to assume that the residuals (i.e. deviation of each observation from its group mean) have a normal distribution, that the variances are approximately the same in each group, and that the observations are independent of each other. The first two of these assumptions was investigated through the Kolmogorov-Smirnov test to check normality of the data distribution, and Levene's test to check homogeneity of variance. When these assumptions were not valid, an appropriate data transformation (e.g., logarithmic) was applied to normalize the data. The third assumption was assumed for all methods in this study.

Continuous variables were analyzed through Repeated-Measures ANOVA for multiple comparisons to test the overall hypothesis that there are (or not) differences among groups. When no differences were found, further comparisons of means were not performed. However, when the ANOVA results were significant ( $p < 0,05$ ), Tukey post-hoc comparison *test* were performed to study the differences among individual means. Performing One-way ANOVA for each age to compare means in a

longitudinal test is not the most correct analysis to perform because it is not taking into account the pooled standard deviation. However, in this type of studies, besides the importance to know if there is a significant difference between groups, it is also relevant to know if the treatment significance is more pronounced early in the disease, if it takes several weeks to exert effects or if its therapeutic effects are only observed at later stages of the disease. For that purpose, we performed One-way ANOVA at each age to estimate the initiation of the drug therapeutic effects in the progression course of the disease.

When the assumptions needed for the ANOVA of approximately equal variation in each group and approximate normality of the residuals was not valid and no scale transformation was available to correct the heterogeneity of variance and/or non-normality, a non-parametric test was used to compare the equality of population means. For paired group comparison of Rotarod in VPA pre-clinical trial (Chapter 2) Mann-Whitney U test was used.

Categorical data, such as the footprinting analysis or SHIRPA obtained results, have a natural order such as absent, mild or severe which are also defined numerically (e.g. 0, 1 and 2, respectively). This obtained data were analyzed through the Chi-squared data and/or Mann-Whitney U test. The correlation analysis was performed with Pearson correlation to assess the strength of the linear relation between two numerical variables (e.g. correlation between CAG repeats and motor performance – Chapter 5).

Finally, each histopathological and/or molecular analysis, which are all punctual and non-continuous variables were analyzed through the One-Way ANOVA test.

### **6.1.6 Reproducibility**

The experimental results should be replicated in other laboratories to reinforce the scientific value findings and, at the end, increase the confidence to translate the results to the human clinical trials. CMVMJD135 mice phenotype and pathology was strikingly replicated among pre-clinical trials, with attention to genotype vs phenotype correlations, and in other collaborator's labs (Maria do Carmo Costa and Henry Paulson, Department of Neurology, University of Michigan, personal communication) reinforcing the reproducibility of this model. The drug treatment reproducibility is also one of the major concerns and should also be replicated as well as in other MJD mouse models. In the pre-symptomatic VPA pre-clinical trial, no striking amelioration of the phenotype and ATXN3 aggregation was observed. However, this does not exclude that the same dosage could improve other behavioral, molecular and/or pathological features in another MJD mouse model. It would be of extreme value to reinforce the confidence on therapeutic efficacy of citalopram in the context of MJD if the striking effects

observed in the CMVMJD35 mice pre-symptomatic pre-clinical trial could be replicated in more MJD mouse models. Indeed, this validation study is ongoing in the Paulson laboratory, University of Michigan (Maria do Carmo Costa et. al., *unpublished data*).

### **6.1.7 Reporting results**

Omission and/or insufficient reporting of experimental animal data may be a reason why pre-clinical several experiments are not reproduced<sup>13,14</sup>. For the studies performed in this PhD thesis, which are published and in preparation, full details of assay methods, information on the animal model used, including genetic background, CAG repeat-length, exclusion criteria and statistical analysis were provided according to the **ARRIVE guidelines**<sup>15</sup>. An additional concern in this field is that experiments with a positive and desirable outcome are more likely to be published than negative results<sup>16</sup>. It is crucial that negative results should also be reported, in peer-reviewed journals or other open-access formats, in order to increase efficiency, decrease redundant efforts and learn from others' experiences.

## **6.2 Hypothesis-based vs non-hypothesis based therapeutic approaches applied to polyQ diseases**

Despite great progress in elucidating the pathomechanisms underlying polyQ diseases, an effective treatment is still lacking, even with several efforts in the field. The current strategies towards development of therapies for these diseases can be divided in hypothesis-based and hypothesis-free approaches. The strengths of the hypothesis-based approach include the ability to apply molecular and chemical knowledge to investigate a specific molecular hypothesis. This type of approach presupposes a deep understanding of the pathogenic mechanisms of the disease in study or of related diseases. In this work, we started by using the latter strategy, simply by testing compounds shown to be promising for other polyQ diseases (or non-polyQ neurodegenerative diseases), namely in the VPA pre-clinical trial (Chapter 2).

Mechanistic targets can be identified on the basis of biological observations and the only condition that needs to be fulfilled is that affecting a single molecular mechanism will be enough to obtain a significant therapeutic effect. The therapeutic action can be achieved either if the target is involved in the pathological state or specific symptomatology or if the target can indirectly alleviate certain consequences of the disease, to produce symptomatic relief or modification of the disease process. In this context, we used VPA, which is an FDA-approved compound for treatment of epilepsy, bipolar disorder and migraine<sup>17</sup> with a relatively safe profile in clinical use. VPA has been shown to have

neuroprotective effects in animal models of HD, SBMA and ALS<sup>18-20</sup>. Also in MJD, VPA was reported to counteract neurodegeneration in a *Drosophila* model<sup>21</sup>, a human neuronal cell model<sup>22</sup> and a *C.elegans* model of the disease<sup>23</sup>. Taking into account these positive effects of VPA, we hypothesized that this compound could thereby be useful for a pre-clinical trial in an MJD mouse model, to further validate this therapeutic strategy. However, the results of our pre-clinical trial in the CMVMJD135 mouse model concerning the MJD-like neurological symptoms and ATXN3-aggregation, were not the expected neither concerning target engagement nor efficacy. Although we cannot rule out that a higher dosage could be effective in delaying disease progression. Several other molecular and pathological effects of VPA treatment in CMVMJD135 need to be further studied in the future.

A disadvantage of the hypothesis-based approach is that the proposed target may not be as relevant to the disease pathogenesis as hypothesized, or have a sufficient therapeutic impact. The lack of understanding of the entire disease mechanism may in these manner slow the progression of the candidate drugs for the disease. There has been a tendency to focus on the possible mechanisms, often identified in very simplified model systems (e.g. cell culture models) and to underestimate the complexity of physiology in the entire organism. Maybe more time and effort will be required in order to understand the complex mechanisms underlying MJD, before advancing to improved targets. At any rate, the testing of target-directed compounds is also a way to probe the relevance of candidate targets and mechanisms, thus even the “negative” results found in our work can contribute to advance knowledge.

In the last years, hypothesis-free approaches for polyQ therapies are also gaining relevance due do their numerous advantages and the novel technical possibilities for screening. High-throughput screening allows the testing of the effects of thousands of drug-like compounds across a panel of targets. This approach does not involve a prior deep understanding of the molecular mechanisms and frequently reveals interesting disease-modifying agents by the identification of molecules that modify the disease phenotype by acting on a previously undescribed target or by acting simultaneously on more than one target. This type of strategy is thus contributing not only to provide new avenues for defining the pathomechanisms of the disease, but also for direct pathways to therapy.

Our group established a *C. elegans* model of MJD<sup>23</sup> and screened a library of FDA/EMA-approved compounds for their ability to prevent or delay the neurological dysfunction and the ATXN3 aggregation in this model. This screening relied primarily on the phenotypic measures of response (percentage of locomotion defective animals) requiring, *a priori*, few mechanist assumptions. Several promising molecules were identified, citalopram being one of the most striking compounds able to reduce the

locomotion defective and subsequent ATXN3 aggregation in this MJD model. Although not questionable in terms of their value for drug discovery and molecular mechanism studies of the disease, there is a need to fill the gap between *C.elegans* and humans. Therefore, a citalopram pre- and post-symptomatic pre-clinical trials using CMVMJD135 mice was performed in this PhD thesis to assess the impact of this compound in the multiple symptoms and pathology shown by this model. We show that activation of serotonergic signaling with citalopram lead to very striking improvement of the symptoms and pathology of CMVMJD135 mice. Taking into consideration the pathogenic mechanisms already suggested for MJD, and also our own neurochemical analysis of the CMVMJD135 mice, finding serotonergic signaling as a relevant target was surprising.

### 6.3 Selective Serotonin Reuptake Inhibitors (SSRI's) for neurodegenerative disorders

Selective Serotonin Reuptake Inhibitors (SSRI's) are a class of compounds used to treat depression by improving symptoms such as mood, sleep, appetite and concentration by increasing the serotonergic signaling. However, current research suggests that SSRIs not only can help treat depression, but also may have therapeutic potential as neuroprotective agents. For instance, **paroxetine** administration to HD mutant mice increased serotonin levels, delayed the onset of neurodegeneration and motor dysfunction, improved energy metabolism and mouse lifespan<sup>24</sup>. **Fluoxetine**, another SSRI, improved neurogenesis in HD mutant mice by increasing brain neurotrophic factors<sup>25</sup>. **Sertraline**, also increased neurogenesis and slowed disease progression in another model of HD<sup>26</sup>. Even **citalopram** was described to decrease de A $\beta$  production in human subjects<sup>11,27</sup>. It is clear that drugs traditionally prescribed for disorders such as depression or anxiety may have more pleiotropic effects than previously anticipated.

#### 6.3.1 Citalopram for MJD: future perspectives

In accordance to the recent findings of SSRI's in neurodegenerative diseases, we identified citalopram as exerting striking improvements in symptoms and pathology of CMVMJD135 mice. An attempts towards understanding of additional neuroprotective effects of citalopram in MJD *C.elegans* and mouse model is ongoing through analysis of several candidate hypotheses (Fig. 1).

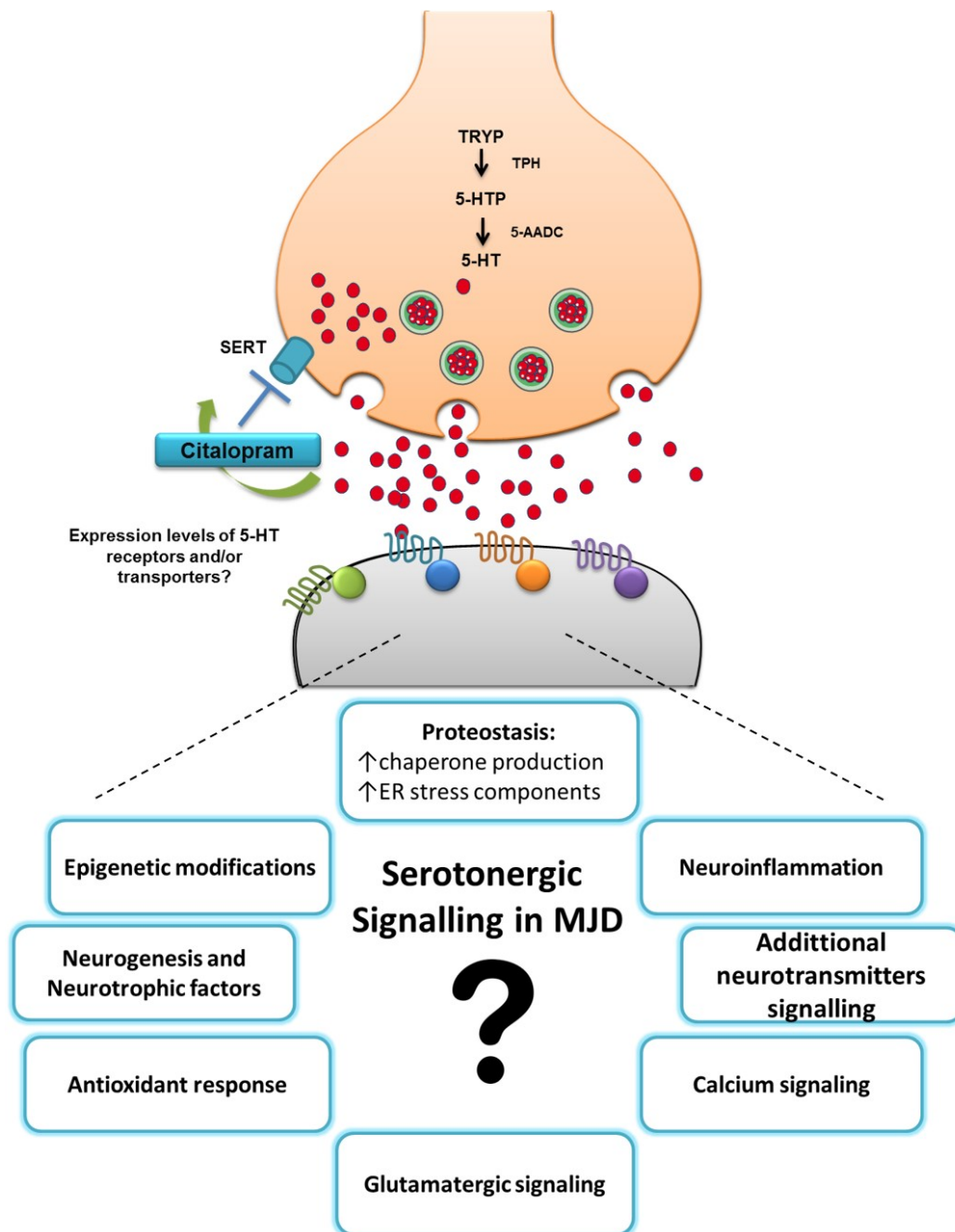


**Figure 1.** Hypothesis model for serotonergic signaling effects through citalopram treatment in MJD models.

The brain serotonin system modulates a diverse array of behavioral and physiological processes, including the regulation of motor output that is mediated by central pattern generators<sup>28-30</sup>, such as locomotion. Experimental data have shown that impairment of the serotonergic cerebellar system can induce cerebellar ataxia<sup>31</sup>. However, this system has not been specifically described as affected in MJD patients and indeed the structural integrity of the serotonergic raphe nuclei seems preserved, and supports the view that depressive symptoms observed in MJD patients are not primarily related to the underlying pathological process, but rather are a reactive nature<sup>32,33</sup>. Likewise, our data also don't confirm an *a priori* depletion of serotonin in CMVMJD135 mice nor a serotonin turnover problem in



the brain (Appendix I), which suggests that the increase in the serotonergic signaling by citalopram is not correcting a neurotransmitter deficiency but exerting other pleiotropic effects. The expression levels of the serotonin receptors and/or transporters still need to be addressed in order to understand the physiological status of serotonergic signaling in CMVMJD135 mouse model. The fact is that, even in the absence of a serotonergic signaling deficiency, the increase in the serotonin levels by citalopram was highly effective in rescuing motor symptoms and, more unexpectedly, ATXN3 aggregation. Since the total ATXN3 protein levels were measured and no differences were found, we hypothesize that citalopram is not acting by promoting degradation of the mutant protein (through autophagy, for instance) but exerting a direct link to proteostasis that should be further explored. Although no major differences were found in several candidate chaperones (Chapter 3), we do not exclude that differences could be detected in specific brain regions, which we were not able to detect in a whole brainstem or cerebellum RNA extraction. We hope that the already ongoing transcriptomic analysis of specific affected and spared regions in citalopram-treated and non-treated CMVMJD135 mice may provide new avenues for treatment and perhaps disclose novel pathogenic mechanisms involved in MJD. A related question that remains to be addressed in the CMVMJD135 mice is the effect of citalopram in ATXN3 solubility, as we observed in *C.elegans* model of MJD (Appendix I) in which the citalopram was able to increase the ATXN3 protein solubility. Several other components of ER stress and/or mitochondria UPR may together contribute to a decrease of ATXN3 aggregation, however, not forgetting that aggregation is still a matter of discussion in terms of its pathogenicity or its protection shield function from the other toxic forms (i.e. intermediate species of aggregation).

Nevertheless, the citalopram effects were not solely based on aggregation, since a decrease in the astrogliosis (neuroinflammation) and a restoration of the cholinergic and Calbindin D-28K positive neurons was observed upon treatment. CMVMJD135 mice display astrogliosis measured by the GFAP positive astrocytes in the substantia nigra; however, the complete characterization of the inflammatory status, for instance in terms of microglia involvement and up or down-regulation of pro- and anti-inflammatory cytokines is an ongoing study in the lab. A quantitative assessment of the effect of citalopram in these molecules may reveal additional contributions to this drug's neuroprotective effects. Also, the midbrain cholinergic system is affected in MJD patients<sup>32</sup>, and in the CMVMJD135 mouse model in which we detected a loss of cholinergic neurons in facial nuclei and in the spinal cord. Citalopram is one of the more specific SSRI's, with little effect in histaminergic, cholinergic, dopaminergic, or  $\alpha$ -adrenergic receptors and also one of the most tolerable SSRI's due to its lack of drug interactions and low incidence of side effects compared with other molecules. However, in the

case of the CMVMJD135 mouse model treated with citalopram, the data suggests that cholinergic and serotonergic signaling may be linked, even indirectly, producing positive effects, which still need to be explored in the future.

The loss of Calbindin D-28K positive cells in the cerebellum of CMVMJD135 mouse model observed in this PhD work allowed us a double achievement, first the indirect confirmation that perturbation of calcium-signaling in Purkinje cells may play a role in the pathogenesis of MJD and second, that citalopram is also playing a neuroprotective role by (directly and indirectly) restoring this signaling. Calbindin-D28K is a major calcium-binding protein found in mammalian brain<sup>34,35</sup> exerting essential roles as neuronal buffer<sup>36</sup>, and in aging and neurodegenerative diseases<sup>37-40</sup>. In fact, deranged calcium signaling was already implicated in neurodegeneration when studied in the YAC84Q mouse model of MJD<sup>41</sup>. It is possible that disruption of Purkinje cell calcium signaling may lead to initial cerebellar dysfunction and ataxic symptoms and eventually proceed the Purkinje cell death, although as this animals' age (34 weeks) we still did not observe Purkinje cell loss (Chapter3). These findings suggest that the differential expression of calcium-binding proteins in Purkinje cells of CMVMJD135 mouse model may contribute to their ability to survive excitotoxic insults and that citalopram may be helping neurons to cope with deranged neuronal calcium signaling, a hypothesis that needs to be further clarified. Also related to calcium signaling is the glutamatergic signaling, dysfunction of which may lead to excitotoxicity events, this being one of the pathogenic mechanism widely associated with polyQ diseases, including MJD. It was described that L-glutamate-induced excitation of MJD patient-specific induced pluripotent stem cell (iPSC)-derived neurons initiates calcium-dependent proteolysis of ATXN3 followed by the formation of SDS-insoluble aggregates<sup>42</sup>, and, more recently, that nuclear accumulation of mutant ataxin-3 was able to disrupt dendritic differentiation and mGluR-signaling in MJD mouse Purkinje cells<sup>43</sup>. Although not explored in this PhD work, since citalopram was able to reduce the ATXN3 aggregation, it seems that calcium and glutamatergic signaling may be explored and hypothesized as possible citalopram targets in the CMVMJD135 mouse model, underlying the cleavage of ATXN3 protein and promoting its aggregation in specific brain regions.

Also not deeply studied in this PhD work, but a promising hypothesis lies in the antioxidant response effects. Citalopram was described to reduce the oxidative stress in patients with major depression<sup>44</sup> and other SSRIs were already described to increase the levels of several antioxidant enzymes<sup>45</sup>, suggesting that augmentation of antioxidant defenses may be one of the mechanisms underlying the neuroprotective effects of antidepressants and possible with implications also for MJD.

In another perspective, SSRI's are widely prescribed for the chronic treatment of major depressive disorder (MDD). Likewise, in this PhD work we observed also citalopram chronic treatment was also necessary to exert the neuroprotective effects in MJD models. The molecular changes already described to underlie SSRI treatment effects in models of depression include increased production and/or increase of neurotrophic factors (i.e. BDNF), increased levels of cell proliferation and neuronal migration markers, reduced expression of serotonin autoreceptors and induction of molecules that modulate neuronal remodeling. Therefore, it will be valuable to address these alterations in the CMVMJD135 mouse model and possible could make a link between the SSRI effects for these two different groups of CNS disorders.

Antidepressant-like effects may also involve epigenetic modifications like DNA acetylation and/or most likely DNA methylation. For instance, it was already described that several antidepressants caused epigenetic modifications associated with changes in HDAC expression in C56BL/6 mice<sup>46</sup>, that antidepressant response may vary according to epigenetic regulation of BDNF expression<sup>47</sup>, and that some genes may be controlled by epigenetic mechanisms that can be affected by antidepressant treatments<sup>48</sup>. Therefore, epigenetic mechanisms in the CMVMJD135 mouse model and upon citalopram treatment may be also one of the further hypothesis to be explored in terms of its possible mechanisms in MJD.

Obviously, more research work should be performed to unravel the neuroprotective actions of citalopram in MJD and to replicate these positive findings also in female animals and in other MJD mouse models, before undertaking citalopram clinical trials in patients. However, in the absence of disease modifying drugs for MJD so far, the recent findings on citalopram, provide and additional hope for the future therapeutic developments in MJD, mainly due to the fact that this compound is frequently provided for long-term treatment in clinical practice without major side-effects.

#### **6.4 Main findings and conclusions of this work**

1. Chronic Valproic acid pre-symptomatic treatment at 200mg/kg/day led to limited and mild symptomatic effects at later stages in the CMVMJD135 mouse model;
2. Chronic Valproic acid treatment did not alter ATXN3 aggregation at 30 weeks of age;
3. Chronic Citalopram pre-symptomatic treatment with 8mg/kg/day led to striking amelioration of motor coordination in the CMVMJD135 mice model;
4. Chronic Citalopram pre-symptomatic treatment with 8mg/kg/day reduced ATXN3 aggregation and astrogliosis at 34 weeks of age;
5. Chronic citalopram pre-symptomatic treatment with a higher dosage of 13mg/kg/day led to limited and mild improvements in the CMVMJD135 mouse model;
6. Chronic post-symptomatic citalopram treatment led to mild improvements in a group of CMVMJD135 mice with higher CAG repeat length and more severe disease.

## References

1. DiMasi, J. A., Hansen, R. W. & Grabowski, H. G. The price of innovation: new estimates of drug development costs. *J. Health Econ.* **22**, 151–185 (2003).
2. Frederix, G. W. J., Hövels, A. M., Severens, J. L., Raaijmakers, J. a. M. & Schellens, J. H. M. [Threshold value for reimbursement of costs of new drugs: cost-effectiveness research and modelling are essential links]. *Ned. Tijdschr. Geneesk.* **159**, A7728 (2015).
3. Freedman, L. P., Cockburn, I. M. & Simcoe, T. S. The Economics of Reproducibility in Preclinical Research. *PLoS Biol.* **13**, e1002165 (2015).
4. Bulger, R. E. Use of animals in experimental research: a scientist's perspective. *Anat. Rec.* **219**, 215–220 (1987).
5. Russell, W. M. S. The development of the three Rs concept. *Altern. Lab. Anim. ATLA* **23**, 298–304 (1995).
6. Baur, J. A. *et al.* Resveratrol improves health and survival of mice on a high-calorie diet. *Nature* **444**, 337–342 (2006).
7. A compound in red wine makes mice live longer, healthier. *Mayo Clin. Health Lett. Engl. Ed* **25**, 4 (2007).
8. Reagan-Shaw, S., Nihal, M. & Ahmad, N. Dose translation from animal to human studies revisited. *FASEB J.* **22**, 659–661 (2007).
9. Blanchard, O. L. & Smoliga, J. M. Translating dosages from animal models to human clinical trials—revisiting body surface area scaling. *FASEB J. Off. Publ. Fed. Am. Soc. Exp. Biol.* **29**, 1629–1634 (2015).
10. Rouaux, C. *et al.* Sodium valproate exerts neuroprotective effects in vivo through CREB-binding protein-dependent mechanisms but does not improve survival in an amyotrophic lateral sclerosis mouse model. *J. Neurosci. Off. J. Soc. Neurosci.* **27**, 5535–5545 (2007).
11. Cirrito, J. R. *et al.* Serotonin signaling is associated with lower amyloid- $\beta$  levels and plaques in transgenic mice and humans. *Proc. Natl. Acad. Sci. U. S. A.* **108**, 14968–14973 (2011).
12. Sandberg, K., Umans, J. G. & Georgetown Consensus Conference Work Group. Recommendations concerning the new U.S. National Institutes of Health initiative to balance the sex of cells and animals in preclinical research. *FASEB J. Off. Publ. Fed. Am. Soc. Exp. Biol.* **29**, 1646–1652 (2015).

13. Kilkenny, C., Browne, W. J., Cuthill, I. C., Emerson, M. & Altman, D. G. Improving bioscience research reporting: the ARRIVE guidelines for reporting animal research. *Osteoarthr. Cartil. OARS Osteoarthr. Res. Soc.* **20**, 256–260 (2012).
14. Hooijmans, C. R., de Vries, R., Leenaars, M., Curfs, J. & Ritskes-Hoitinga, M. Improving planning, design, reporting and scientific quality of animal experiments by using the Gold Standard Publication Checklist, in addition to the ARRIVE guidelines. *Br. J. Pharmacol.* **162**, 1259–1260 (2011).
15. Kilkenny, C. *et al.* Animal research: reporting in vivo experiments—the ARRIVE guidelines. *J. Cereb. Blood Flow Metab. Off. J. Int. Soc. Cereb. Blood Flow Metab.* **31**, 991–993 (2011).
16. Sena, E. S., van der Worp, H. B., Bath, P. M. W., Howells, D. W. & Macleod, M. R. Publication bias in reports of animal stroke studies leads to major overstatement of efficacy. *PLoS Biol.* **8**, e1000344 (2010).
17. Rosenberg, G. The mechanisms of action of valproate in neuropsychiatric disorders: can we see the forest for the trees? *Cell. Mol. Life Sci. CMLS* **64**, 2090–2103 (2007).
18. Tsai, L.-K., Tsai, M.-S., Ting, C.-H. & Li, H. Multiple therapeutic effects of valproic acid in spinal muscular atrophy model mice. *J. Mol. Med. Berl. Ger.* **86**, 1243–1254 (2008).
19. Feng, H.-L. *et al.* Combined lithium and valproate treatment delays disease onset, reduces neurological deficits and prolongs survival in an amyotrophic lateral sclerosis mouse model. *Neuroscience* **155**, 567–572 (2008).
20. Zádori, D., Geisz, A., Vámos, E., Vécsei, L. & Klivényi, P. Valproate ameliorates the survival and the motor performance in a transgenic mouse model of Huntington's disease. *Pharmacol. Biochem. Behav.* **94**, 148–153 (2009).
21. Yi, J. *et al.* Sodium valproate alleviates neurodegeneration in SCA3/MJD via suppressing apoptosis and rescuing the hypoacetylation levels of histone H3 and H4. *PLoS One* **8**, e54792 (2013).
22. Lin, X. P. *et al.* Valproic acid attenuates the suppression of acetyl histone H3 and CREB activity in an inducible cell model of Machado-Joseph disease. *Int. J. Dev. Neurosci. Off. J. Int. Soc. Dev. Neurosci.* **38**, 17–22 (2014).
23. Teixeira-Castro, A. *et al.* Neuron-specific proteotoxicity of mutant ataxin-3 in *C. elegans*: rescue by the DAF-16 and HSF-1 pathways. *Hum. Mol. Genet.* **20**, 2996–3009 (2011).
24. Duan, W. *et al.* Paroxetine retards disease onset and progression in Huntingtin mutant mice. *Ann. Neurol.* **55**, 590–594 (2004).
25. Grote, H. E. *et al.* Cognitive disorders and neurogenesis deficits in Huntington's disease mice are rescued by fluoxetine. *Eur. J. Neurosci.* **22**, 2081–2088 (2005).

26. Duan, W. *et al.* Sertraline slows disease progression and increases neurogenesis in N171-82Q mouse model of Huntington's disease. *Neurobiol. Dis.* **30**, 312–322 (2008).
27. Sheline, Y. I. *et al.* An Antidepressant Decreases CSF A Production in Healthy Individuals and in Transgenic AD Mice. *Sci. Transl. Med.* **6**, 236re4–236re4 (2014).
28. Harris-Warrick, R. M. Neuromodulation and flexibility in Central Pattern Generator networks. *Curr. Opin. Neurobiol.* **21**, 685–692 (2011).
29. MacKay-Lyons, M. Central pattern generation of locomotion: a review of the evidence. *Phys. Ther.* **82**, 69–83 (2002).
30. Guertin, P. A. Central Pattern Generator for Locomotion: Anatomical, Physiological, and Pathophysiological Considerations. *Front. Neurol.* **3**, (2013).
31. Chan-Palay, V. Indoleamine neurons and their processes in the normal rat brain and in chronic diet-induced thiamine deficiency demonstrated by uptake of 3H-serotonin. *J. Comp. Neurol.* **176**, 467–493 (1977).
32. Rüb, U., Brunt, E. R. & Deller, T. New insights into the pathoanatomy of spinocerebellar ataxia type 3 (Machado-Joseph disease). *Curr. Opin. Neurol.* **21**, 111–116 (2008).
33. Cecchin, C. R. *et al.* Depressive symptoms in Machado-Joseph disease (SCA3) patients and their relatives. *Community Genet.* **10**, 19–26 (2007).
34. Celio, M. R. *et al.* Monoclonal antibodies directed against the calcium binding protein Calbindin D-28k. *Cell Calcium* **11**, 599–602 (1990).
35. Zhang, J. H., Morita, Y., Hironaka, T., Emson, P. C. & Tohyama, M. Ontological study of calbindin-D28k-like and parvalbumin-like immunoreactivities in rat spinal cord and dorsal root ganglia. *J. Comp. Neurol.* **302**, 715–728 (1990).
36. Schwaller, B., Meyer, M. & Schiffmann, S. 'New' functions for 'old' proteins: the role of the calcium-binding proteins calbindin D-28k, calretinin and parvalbumin, in cerebellar physiology. Studies with knockout mice. *Cerebellum Lond. Engl.* **1**, 241–258 (2002).
37. Yuan, H.-H., Chen, R.-J., Zhu, Y.-H., Peng, C.-L. & Zhu, X.-R. The neuroprotective effect of overexpression of calbindin-D(28k) in an animal model of Parkinson's disease. *Mol. Neurobiol.* **47**, 117–122 (2013).
38. Riascos, D. *et al.* Age-related loss of calcium buffering and selective neuronal vulnerability in Alzheimer's disease. *Acta Neuropathol. (Berl.)* **122**, 565–576 (2011).
39. Sasaki, S. *et al.* Parvalbumin and calbindin D-28k immunoreactivity in transgenic mice with a G93A mutant SOD1 gene. *Brain Res.* **1083**, 196–203 (2006).

40. Geula, C. *et al.* Loss of calbindin-D28k from aging human cholinergic basal forebrain: relation to neuronal loss. *J. Comp. Neurol.* **455**, 249–259 (2003).
41. Chen, X. *et al.* Deranged calcium signaling and neurodegeneration in spinocerebellar ataxia type 3. *J. Neurosci. Off. J. Soc. Neurosci.* **28**, 12713–12724 (2008).
42. Koch, P. *et al.* Excitation-induced ataxin-3 aggregation in neurons from patients with Machado-Joseph disease. *Nature* **480**, 543–546 (2011).
43. Konno, A. *et al.* Mutant ataxin-3 with an abnormally expanded polyglutamine chain disrupts dendritic development and metabotropic glutamate receptor signaling in mouse cerebellar Purkinje cells. *Cerebellum Lond. Engl.* **13**, 29–41 (2014).
44. Khanzode, S. D., Dakhale, G. N., Khanzode, S. S., Saoji, A. & Palasodkar, R. Oxidative damage and major depression: the potential antioxidant action of selective serotonin re-uptake inhibitors. *Redox Rep. Commun. Free Radic. Res.* **8**, 365–370 (2003).
45. Behr, G. A., Moreira, J. C. F. & Frey, B. N. Preclinical and Clinical Evidence of Antioxidant Effects of Antidepressant Agents: Implications for the Pathophysiology of Major Depressive Disorder. *Oxid. Med. Cell. Longev.* **2012**, 1–13 (2012).
46. Ookubo, M., Kanai, H., Aoki, H. & Yamada, N. Antidepressants and mood stabilizers effects on histone deacetylase expression in C57BL/6 mice: Brain region specific changes. *J. Psychiatr. Res.* **47**, 1204–1214 (2013).
47. Lopez, J. P. *et al.* Epigenetic regulation of BDNF expression according to antidepressant response. *Mol. Psychiatry* **18**, 398–399 (2013).
48. Melas, P. A. *et al.* Antidepressant treatment is associated with epigenetic alterations in the promoter of P11 in a genetic model of depression. *Int. J. Neuropsychopharmacol. Off. Sci. J. Coll. Int. Neuropsychopharmacol. CINP* **15**, 669–679 (2012).



## **Appendix I**

---



## Serotonergic signalling suppresses ataxin 3 aggregation and neurotoxicity in animal models of Machado-Joseph disease

Andreia Teixeira-Castro,<sup>1,2,3,4,\*</sup> Ana Jalles,<sup>1,2,\*</sup> Sofia Esteves,<sup>1,2,\*</sup> Soosung Kang,<sup>3,5,6</sup> Liliana da Silva Santos,<sup>1,2</sup> Anabela Silva-Fernandes,<sup>1,2</sup> Mário F. Neto,<sup>3,4</sup> Renée M. Brielmann,<sup>3,4</sup> Carlos Bessa,<sup>1,2</sup> Sara Duarte-Silva,<sup>1,2</sup> Adriana Miranda,<sup>1,2</sup> Stéphanie Oliveira,<sup>1,2</sup> Andreia Neves-Carvalho,<sup>1,2</sup> João Bessa,<sup>1,2</sup> Teresa Summavielle,<sup>7</sup> Richard B. Silverman,<sup>3,5,6</sup> Pedro Oliveira,<sup>8</sup> Richard I. Morimoto<sup>3,4</sup> and Patrícia Maciel<sup>1,2</sup>

\*These authors contributed equally to this work.

Polyglutamine diseases are a class of dominantly inherited neurodegenerative disorders for which there is no effective treatment. Here we provide evidence that activation of serotonergic signalling is beneficial in animal models of Machado-Joseph disease. We identified citalopram, a selective serotonin reuptake inhibitor, in a small molecule screen of FDA-approved drugs that rescued neuronal dysfunction and reduced aggregation using a *Caenorhabditis elegans* model of mutant ataxin 3-induced neurotoxicity. MOD-5, the *C. elegans* orthologue of the serotonin transporter and cellular target of citalopram, and the serotonin receptors SER-1 and SER-4 were strong genetic modifiers of ataxin 3 neurotoxicity and necessary for therapeutic efficacy. Moreover, chronic treatment of CMVMJD135 mice with citalopram significantly reduced ataxin 3 neuronal inclusions and astrogliosis, rescued diminished body weight and strikingly ameliorated motor symptoms. These results suggest that small molecule modulation of serotonergic signalling represents a promising therapeutic target for Machado-Joseph disease.

1 Life and Health Sciences Research Institute (ICVS), School of Health Sciences, University of Minho, 4710-057 Braga, Portugal

2 ICVS/3Bs - PT Government Associate Laboratory, Braga/Guimarães, Portugal

3 Department of Molecular Biosciences, Northwestern University, Evanston, Illinois 60208, USA

4 Rice Institute for Biomedical Research, Northwestern University, Evanston, Illinois 60208, USA

5 Department of Chemistry, Northwestern University, Evanston, Illinois 60208, USA

6 Chemistry of Life Processes Institute and Center for Molecular Innovation and Drug Discovery, Northwestern University, Evanston, Illinois 60208, USA

7 IBMC - Instituto de Biologia Molecular e Celular, Universidade do Porto, Rua do Campo Alegre, 823, 4150-180 Porto, Portugal

8 ICBAS-Abel Salazar Biomedical Sciences Institute, University of Porto, Porto, Portugal

Correspondence to: Patrícia Maciel, PhD

Life and Health Sciences Research Institute (ICVS);

School of Health Sciences; University of Minho;

Gualtar Campus, 4710-057 Braga,

Portugal

E-mail: pmaciel@ecsau.de.uminho.pt

**Keywords:** spinocerebellar ataxia type 3; ataxin 3 aggregation; therapy; selective serotonin reuptake inhibitor, citalopram

**Abbreviations:** 5-HT = serotonin; SCA3 = spinocerebellar ataxia type 3; SSRI = selective serotonin reuptake inhibitor

## Introduction

The expansion of trinucleotide CAG repeats causes hereditary adult-onset neurodegenerative disorders such as Huntington's disease, spinobulbar muscular atrophy, dentatorubral-pallidolusian atrophy and six forms of spinocerebellar ataxia (Ross *et al.*, 1998). Machado-Joseph disease (or spinocerebellar ataxia type 3, SCA3), the most common dominantly inherited SCA worldwide (Schols *et al.*, 2004), is characterized by ataxia, ophthalmoplegia and pyramidal signs, associated with dystonia, spasticity, peripheral neuropathy and amyotrophy (Coutinho and Andrade, 1978), without cognitive decline. Pathologically, there is degeneration of the deep nuclei of the cerebellum, pontine and subthalamic nuclei, substantia nigra and spinocerebellar nuclei. The genetic basis of Machado-Joseph disease is the expansion of a polyglutamine tract within the protein ataxin 3 (ATXN3) (Kawaguchi *et al.*, 1994). When the polyglutamine tract exceeds 60 consecutive glutamines, ATXN3 becomes highly aggregation prone, leading to an imbalance in cellular proteostasis, as aggregation-associated proteotoxicity dominates over folding and clearance (Balch *et al.*, 2008; Morimoto, 2008).

Currently there is no treatment for Machado-Joseph disease that effectively slows disease progression. Efforts to improve patient quality of life and to sustain independence address the restless legs and extrapyramidal syndromes, treatment of cramps and of the effects of fatigue (D'Abreu *et al.*, 2010). Not yet translated to clinical practice are therapeutic strategies that include the use of small molecules or gene targeting to manipulate the concentration, conformation, and/or location of ATXN3. For example, it is known that modulating the levels of molecular chaperones Hsp70, alphaB-crystallin and Hsp104 could prevent or inhibit ATXN3 aggregation, and promote its disaggregation (Warrick *et al.*, 2005; Robertson *et al.*, 2010; Cushman-Nick *et al.*, 2013). Treatment with Hsp90 inhibitors that increase chaperone expression had beneficial effects, although it failed to achieve the predicted molecular effect of chaperone induction in animal models of Machado-Joseph disease (Silva-Fernandes *et al.*, 2014). Likewise, activation of autophagy, either genetic or pharmacological, lessened ATXN3 pathogenesis *in vivo* (Menzies *et al.*, 2010; Nascimento-Ferreira *et al.*, 2013). In rodents, reversion of the expanded polyglutamine-associated transcription down-regulation by a histone deacetylase (HDAC) inhibitor rescued ataxic symptoms (Chou *et al.*, 2011). Dantrolene administration (targeting intracellular calcium homeostasis) improved motor performance and prevented neuronal loss (Chen *et al.*, 2008). While silencing of ATXN3 offers potential, the impact of this type of treatment to date has not been promising in Machado-Joseph disease mice (Costa Mdo *et al.*, 2013; Nobrega *et al.*, 2013). For many proposed therapies, translation into clinical practice will be further limited by human safety. The traditional approach to drug discovery, which involves *de novo* identification and validation of new molecular targets, is costly and

time-consuming, thus limiting the number of new drugs introduced into the clinic (Shim and Liu, 2014). Moreover, as the average time required for drug development continues to increase, there has been renewed interest in drug repurposing strategies (Chong and Sullivan, 2007; Shim and Liu, 2014). On the other hand, in past years, the primary cause of new drug candidate failures has been low therapeutic efficacy in clinical trials. Among the most frequently proposed reasons for this shortcoming is the lack of translation of *in vitro* and recombinant drug activity to therapeutic *in vivo* whole organism systems. As an approach to identify novel therapeutic strategies, we used *Caenorhabditis elegans* (*C. elegans*), a powerful platform to model neurodegenerative disease and for characterization of small bioactive molecules (Kaletta and Hengartner, 2006). Previously, we established a *C. elegans* model for Machado-Joseph disease pathogenesis in which expression of mutant ATXN3 in the nervous system led to its progressive aggregation in distinct neuronal subtypes and altered motor behaviour (Teixeira-Castro *et al.*, 2011a). Here, we used this model to screen a library of FDA-approved small molecules, and identified compounds that rescued or ameliorated mutant ATXN3-mediated neurological dysfunction. By combining compound treatment with genetic tools, we demonstrate that modulation of serotonergic signalling by selective serotonin reuptake inhibitors (SSRIs) suppressed mutant ATXN3 aggregation and neurotoxicity in both *C. elegans* and mice. This reveals the utility of the approach by which safe and highly effective bioactive small molecules can be repurposed to benefit rare diseases lacking effective therapies. The finding that serotonin recapture inhibition modulates proteotoxicity may be relevant for other protein conformation disorders.

## Materials and methods

### Study design

The overall objective of the study was to find novel therapeutic targets for Machado-Joseph disease. The first part of this study was designed to identify novel suppressor compounds of mutant ATXN3 pathogenesis *in vivo*, using a hypothesis-free approach. The second aim of the study was to validate one of the identified drugs in a vertebrate model of the disease. To achieve the two goals, a small molecule screening of a FDA-approved library was conducted using a transgenic *C. elegans* model of the disease (Teixeira-Castro *et al.*, 2011a). The most promising hit of the screening regarding human safety, target specificity and conservation across evolution was tested in CMVMJD135 mice (Silva-Fernandes *et al.*, 2014). For all animal experiments, we ensured blinded outcome assessment. Experimental design was based on power analyses for optimization of sample size. *C. elegans* (Supplementary Table 1) and mice (Supplementary Table 2) sample size calculations were performed for each behavioural test and pathological analyses assuming a power of 0.95 and 0.8, respectively, and a significance level of  $P < 0.05$ . The effect size was calculated aiming for a 50% improvement. In general, we used  $n = 3-4$

per genotype/treatment of *C. elegans* for motility assays,  $n = 8$ – $14$  for aggregation (with three replicates) and  $n = 4$  for immunoblotting. For mice, we used  $n = 13$ – $16$  per genotype/treatment for behavioural tests, and a group size of four animals per group for quantification of ATXN3 intranuclear inclusions, assessment of astrogliosis and western blot analysis. All experiments were designed with commitment to the principles of refinement, reduction, and replacement and performed according to the FELASA guidelines to minimize discomfort, stress, and pain to the animals, with defined humane endpoints (1994).

## Nematode strains and general methods

For a list of strains used in this work and abbreviations, see [Supplementary Table 3](#). All the strains were backcrossed to Bristol strain N2 five to eight times. Standard methods were used for culturing and observing *C. elegans*, unless otherwise noted (Brenner, 1974). Nematodes were grown on nematode growth medium plates seeded with *Escherichia coli* OP50 strain at 20°C.

## Compounds

All the compounds were obtained from the commercial vendors indicated below and were used without further purification. The Prestwick Chemical Library<sup>TM</sup> (Prestwick Chemical) used for the *C. elegans* screening comprised 1120 chemical and pharmacologically diverse small molecules. Other compounds used, including the 11 hits selected for validation, were reordered from a different manufacturer before repetition of experiments: 17-(allylamino)-17-demethoxygeldanamycin (17-AAG) CAS 75747-14-7 (Biomol); nisoxetine hydrochloride CAS 57754-86-6 (Sigma); scoulerine CAS 6451-73-6 (Toronto Research); eburnamonine CAS 4880-88-0 (Santa Cruz); piperlongumine CAS 20069-09-4 (Biotrend); chlortetracycline hydrochloride CAS 64-72-2 (Sigma); tiapride hydrochloride CAS 51012-33-0 (Sigma); clemizole hydrochloride CAS 1163-36-6 (Sigma); metixene hydrochloride CAS 7081-40-5 (Sigma); budesonide CAS 51333-22-3 (Sigma); noscapine CAS 128-62-1 (Sigma); estrone CAS 53-16-7 (Sigma); fluoxetine CAS 56296-78-7 (Kemprotec Ltd.); zimelidine CAS 61129-30-4 (Sigma); lysergol CAS 602-85-7 (Sigma); pindolol CAS 13523-86-9 (Sigma); trazodone hydrochloride CAS 25332-39-2 (Sigma); citalopram hydrobromide CAS 59729-32-7 (Kemprotec Ltd.); escitalopram (S-citalopram) hydrobromide CAS 219861-08-2 (Kemprotec Ltd). Citalopram used for studies in mice and vabicaserin were kindly provided by Lündbeck.

## Drug toxicity assay

Bristol strain N2 was used to screen the Prestwick Chemical Library<sup>TM</sup> for compound toxicity. The assay was performed in 96-well plate format, in liquid culture (Voisine *et al.*, 2007). Each well contained a final volume of 60  $\mu$ l, comprising 20–25 animals in egg stage, drug at the appropriate concentration and OP50 bacteria to a final OD<sub>595</sub> of 0.6–0.8 measured in the microplate reader (Bio-Rad microplate reader 680). To obtain the age synchronized population of eggs, gravid adults were treated with alkaline hypochlorite solution (0.5 M NaOH, ~2.6% NaClO)

for 7 min. The animals were then washed in M9 buffer, resuspended in S-medium to the appropriate egg number and transferred into the 96-well plate. The OP50 bacteria were grown overnight at 37°C and 150 rpm in Luria Broth (LB) media, pelleted by centrifugation, inactivated by four to six cycles of freeze/thawing, frozen at –80°C and then resuspended in S-medium supplemented with cholesterol, streptomycin, penicillin and nystatin (Sigma). Worms were grown with continuous shaking at 180 rpm at 20°C (Shel Lab) for 7 days. The compound library was prepared in 100% dimethyl sulphoxide (DMSO, Sigma) and tested at dilutions corresponding to a maximum concentration of 1% DMSO to avoid solvent-specific developmental defects and toxicity. For each compound, two final concentrations were tested (50  $\mu$ M and 25  $\mu$ M). The effect of compounds on *C. elegans* physiology was monitored by the rate at which the *E. coli* food suspension was consumed, as a read out for *C. elegans* growth, survival or fecundity. The absorbance (OD<sub>595</sub>) was measured daily. OP50-only (S-medium, no vehicle), DMSO 1% (vehicle) and DMSO 5% (toxic condition) controls were used.

## *C. elegans* assays for motility defects and aggregation

Wild-type (WT, N2), wild-type ATXN3 (AT3WT) and mutant ATXN3 (AT3q130) animals were grown in liquid culture in a 96-well plate format, with the chemical compounds, as described above. Four-day-old animals were transferred from the 96-well plates onto an unseeded nematode growth medium plate (equilibrated at 20°C). Plates were allowed to dry for 1 h before starting the assays. Motility assays were performed at 20°C as previously described (Gidalevitz *et al.*, 2006; Teixeira-Castro *et al.*, 2011a). Motor behaviour assays were run in triplicates or quadruplicates ( $n = 3$  or 4), with a total of at least 150 animals tested per genotype and/or compound. For confocal dynamic imaging and quantification of ATXN3 aggregation, live animals were immobilized with 3 mM levamisole (Sigma) and mounted on a 3% agarose pad. All images were captured on an Olympus FV1000 (Japan) or Zeiss LSM 510 (Germany) confocal microscopes, under a  $\times 60$  oil (NA = 1.35) or  $\times 63$  water (NA = 1.0) objectives. Z-series imaging was acquired for all vehicle- and compound-treated animals, using a 515/514 nm laser excitation line for yellow fluorescent protein fusion proteins. The pinhole was adjusted to 1.0 Airy unit of optical slice, and a scan was acquired every ~0.5  $\mu$ m along the z-axis. The quantification of the aggregates was performed as previously described (Teixeira-Castro *et al.*, 2011a, b). Three parameters were measured: area of aggregates/total area; number of aggregates/total area; and number of aggregates. Values shown are the mean (normalized to vehicle treated control) of eight or more animals per group, unless noted otherwise.

## Chemical and pharmacological classification of the hits

Hits were manually inspected to categorize them into chemical and pharmacological classes based on MeSH tree (Medical Subject Headings; PubMed), ChEBI Ontology (Chemical Entities of Biological Interest), and ATC (Anatomical Therapeutic Chemical) fourth level classifications. The majority of the hits were sorted into heterocyclic, alkaloid, steroid,

polycyclic, and  $\beta$ -amino alcohol chemical classes, and further classified into neurotransmitter, anti-infective, cardiovascular, anti-inflammatory, analgesic, and hormone pharmacological classes. For a drug that has multiple therapeutic applications, all classes were equally considered. However, if a new multi-therapeutic drug shares the same structural and pharmacological class with a high scored single therapeutic compound, we considered only a single therapeutic application and clustered the new molecule into the same class. This classification allowed us simple observation of the chemical and pharmacological classes of the hits.

### C. *elegans* citalopram time course assays

For time course experiments, animals were grown on nematode growth medium plates with OP50 supplemented with citalopram. OP50 cultures were prepared as described above and concentrated 10 $\times$  with S-media supplemented with streptomycin, penicillin and nystatin (Sigma). Stock solutions of citalopram (2.5 mM and 0.5 mM) (Kemprotec) or vehicle (DMSO) were prepared and added to OP50 cultures to a final concentration of 25  $\mu$ M or 5  $\mu$ M. Plates were seeded with 200  $\mu$ l of OP50-citalopram/vehicle and left at room temperature to dry for at least 3 days. Fresh plates were prepared two to three times a week to prevent drug degradation. OFF-drug effect was evaluated by treating the animals for 4 days and after that time animals were transferred to DMSO plates (vehicle), shown in Fig. 2D as AT3q130::cit OFF. During the reproductive period, animals were transferred into new fresh plates every day.

### Immunoblotting analysis

For determination of the steady-state protein levels of ATXN3, the animals were incubated in liquid culture with the chemical compounds in a 96-well plate format as described above. Four-day-old animals were transferred from the liquid culture onto an unseeded nematode growth medium plate (equilibrated at 20°C). After 1 h of acclimation 25 individual young adult animals were picked, boiled for 15 min in sodium dodecyl sulphate (SDS) sample buffer (to destroy all the aggregates) and the resulting extracts resolved on a 10% SDS gel, as previously described (Gidalevitz *et al.*, 2009; Teixeira-Castro *et al.*, 2011). Immunoblots were probed with anti-ATXN3 mouse (1H9, MAB5360, Milipore; 1:1000 or 1:150) and anti-tubulin mouse antibodies (T5168, Sigma; 1:5000); and detected with horseradish peroxidase-coupled secondary antibodies (Bio-Rad) and chemiluminescence (ECL western-blotting detecting reagents, Amersham Pharmacia). Protein isolation from mouse brainstem tissue and western blot were performed as previously described (Silva-Fernandes *et al.*, 2010). The blots were blocked and incubated overnight at 4°C with the primary antibody rabbit anti-ataxin 3 serum (kindly provided by Dr Henry Paulson) (1:5000) and mouse anti-GAPDH (G8795, Sigma, 1:1000). As a loading control, mouse ataxin 3 and GAPDH were used. Western blot quantifications were performed using Chemidoc XRS Software with ImageLab Software (Bio-Rad) or ImageJ software (NIH), according to the manufacturer's instructions. ATXN3 fractionation assays were performed as previously described (Koch *et al.*, 2011), with the following modifications: AT3q130 animals were grown for 4 days in

nematode growth medium-citalopram/vehicle plates. Nematodes were collected and washed in M9 buffer, and re-suspended in RIPA buffer [50 mM Tris, 150 mM NaCl, 0.2% Triton<sup>TM</sup> X-100, 25 mM EDTA, supplemented with complete protease inhibitor (Roche)] before shock freezing in liquid nitrogen. After three freeze-thawing cycles, the worm pellet was ground with a motorized pestle, and lysed on ice, in the presence of 0.025 U/ml benzonase (Sigma). The lysate was centrifuged at 1000 rpm for 1 min in a table-top centrifuge to pellet the carcasses (Nussbaum-Krammer *et al.*, 2013). Protein concentration was determined using Bradford assay (Bio-Rad) and was set to a final concentration of 3–4  $\mu$ g/ $\mu$ l in all experimental conditions and followed by a 22 000 g centrifugation for 30 min at 4°C. The pellet fractions were separated from supernatants (Triton<sup>TM</sup> X-100-soluble fraction) and homogenized in 150  $\mu$ l RIPA buffer containing 2% SDS followed by a second centrifugation step at room temperature. The supernatants (SDS-soluble fraction) were removed, and the remaining pellets were incubated for 16 h in 100% formic acid at 37°C. After formic acid evaporation at 37°C, the pellet was dissolved in 25  $\mu$ l Laemmli buffer (SDS-insoluble fraction) followed by pH adjustment with 2 M Tris-base for SDS-polyacrylamide gel electrophoresis analysis. Gels were loaded with 50  $\mu$ g of the Triton<sup>TM</sup> X-100 fraction, 40  $\mu$ l of the SDS-soluble fraction and the complete SDS-insoluble fraction. Western blot analyses were performed as described above.

### Lifespan

Assays were performed at 20°C as previously described (Morley and Morimoto, 2004). Approximately 100 hermaphrodites were cultured on each Petri dish and were transferred to fresh plates every day until the cessation of progeny production, and about every 1–3 days thereafter. Animals were scored as dead if they showed no spontaneous movement or response when prodded. Dead animals that displayed internally hatched progeny, extruded gonad or desiccation were excluded.

### Transgenic mouse model and drug administration

CMVMJD135 mice were generated as described previously (Silva-Fernandes *et al.*, 2014). DNA extraction, animal genotyping and CAG repeat size analyses were performed as previously described (Silva-Fernandes *et al.*, 2010). The mean repeat size [ $\pm$  standard deviation (SD)] for all mice used was 130  $\pm$  2. Age-matched and genetic background-matched wild-type animals were used as controls. Only male mice were used in this study. We administered citalopram hydrobromide CAS 59729-32-7 (Lundbeck, Denmark) in the drinking water at two doses (8 and 13 mg/kg/day) that roughly equate to the high dosage range prescribed to human patients for depression (Cirrito *et al.*, 2011). Treatment was initiated at 5 weeks of age, one week before the expected onset of the first neurological symptoms. The trial was ended at 34 weeks of age, according to the humane endpoints established for the non-treated CMVMJD135 mice. All animal procedures were conducted in accordance with European regulations (European Union Directive 86/609/EEC). Animal facilities and the people directly involved in animal experiments (A.T.C., S.E., A.S.F., S.D.S.) were certified by the Portuguese regulatory

entity - Direcção Geral de Alimentação e Veterinária. All of the protocols performed were approved by the Animal Ethics Committee of the Life and Health Sciences Research Institute, University of Minho.

## Neurochemical quantification

CMVMJD135 and wild-type male littermate mice ( $n = 5-8$ ) were sacrificed at 24 weeks of age by decapitation, their brains were rapidly removed, snap frozen in liquid nitrogen and dissected. Serotonin (5-HT) and 5-hydroxyindoleacetic acid (5-HIAA) levels were measured in the substantia nigra, medulla oblongata and cerebellum by high performance liquid chromatography, combined with electrochemical detection (HPLC/EC), as described previously (Santos *et al.*, 2010). Concentrations of neurotransmitters were calculated using standard curves and results were expressed in terms of 5-HT and metabolism content per amount of protein.

## Behavioural assessment

Behavioural analysis was performed during the diurnal period in groups of five males per cage including CMVMJD135 hemizygous transgenic mice and wild-type littermates ( $n = 13-16$  per genotype) treated with citalopram or with vehicle (water). All behavioural tests started in a presymptomatic stage (4 weeks) and were conducted until 30 or 34 weeks of age. Neurological tests and general health assessment were performed using the SHIRPA protocol, enriched with the hanging wire test. The dragging of the paws and the stride length were evaluated with footprint analysis. Motor behaviour was further assessed using the balance beam walk test (12-mm square and 17-mm round beams) and the motor swimming test. All behavioural tests were performed as previously described (Silva-Fernandes *et al.*, 2014). Body weight was also registered for each evaluation time point.

## Immunohistochemistry and quantification of neuronal inclusions

Thirty-four-week-old wild-type and CMVMJD135 littermate mice, vehicle- and citalopram-treated ( $n = 4$  for each group) were deeply anaesthetized [a mixture of ketamine hydrochloride (150 mg/kg) plus medetomidine (0.3 mg/kg)] and transcardially perfused with phosphate-buffered saline (PBS) followed by 4% paraformaldehyde (Panreac). Brains were removed and post-fixed overnight in paraformaldehyde and embedded in paraffin. Slides with 4- $\mu$ m thick paraffin sections were subjected to antigen retrieval and then incubated with mouse anti-ATXN3 (1H9, MAB5360, Millipore; 1:100), rabbit anti-GFAP (Dako Corporation; 1:1000) or rabbit anti-Calbindin D-28 K (AB1778, Millipore, 1:1000) antibodies, which were detected by incubation with a biotinylated anti-polyvalent antibody, followed by detection through biotin-streptavidin coupled to horseradish peroxidase and reaction with the DAB (3, 3'-diaminobenzidine) substrate (Lab Vision™ Ultra-Vision™ Detection kit, Thermo Scientific). The slides were counterstained with haematoxylin 25% according to standard procedures. Fifty-micrometre thick vibratome spinal cord sections were incubated with goat Anti-Choline Acetyltransferase (ChAT, Millipore, 1:500) and stained according to

VECTASTAIN® ABC system (Vector Laboratories). Thirty-four-week-old wild-type and CMVMJD135 littermate mice, vehicle- and citalopram-treated ( $n = 4$  for each group), were deeply anaesthetized as mentioned above, transcardially perfused with NaCl (0.9%) and the mouse brains embedded in O.C.T. and rapidly frozen in isopentane (Sigma, CAS#78-78-4) chilled in liquid nitrogen. Slides with 30- $\mu$ m thick cryostat sections were incubated with anti-ChAT according to the Lab Vision™ Ultra-Vision™ Detection kit instructions. ATXN3 positive inclusions in the pontine nuclei, reticulotegmental nucleus of the pons, facial motor nucleus and lateral reticular nucleus; stained astrocytes (GFAP-positive) in the substantia nigra; Calbindin D-28 K positive neurons in the cerebellar cortex; ChAT-positive neurons in the facial motor nucleus and in the ventral horn of the lumbar spinal cord of either vehicle- or citalopram-treated animals ( $n = 3-4$  for each condition, four slides per animal) were quantified and normalized for total area using the Olympus BX51 stereological microscope (Olympus) and the Visiopharma integrator system software (Visiopharm) as previously described (Silva-Fernandes *et al.*, 2014).

## Statistical analysis

Data were analysed through the non-parametric Mann-Whitney U-test when variables were non-continuous or when a continuous variable did not present a normal distribution (Kolmogorov-Smirnov test,  $P < 0.05$ ). Continuous variables with normal distributions and with homogeneity of variance (Levene's test) were analysed with repeated measures ANOVA for longitudinal multiple comparisons and one-way ANOVA or Student's *t*-test for paired comparisons, using Tukey or Bonferroni tests for *post hoc* comparisons. When these two latter assumptions were not valid, an appropriate data transformation (e.g. logarithmic) was applied, and the data were re-analysed (body weight, balance beam walk test and motor swimming test). When logarithmic data transformation did not reduce the heterogeneity of variances (hanging wire test), several mathematical models were applied. In this test, the best fit model was the logarithmic and the treatment differences were analysed according to the *R* squares of the CMVMJD135 groups, with a normal residual distribution. Statistical analysis of *C. elegans* survival assays was performed using the log rank (Mantel-Cox) test. All statistical analyses were performed using SPSS 20.0/22.0 (SPSS Inc.) and G-Power 3.1.9.2 (University Kiel, Germany). A critical value for significance of  $P < 0.05$  was used throughout the study.

## Results

### A whole animal screen identifies small molecules that ameliorate mutant ataxin 3-mediated neuronal dysfunction

To identify small bioactive molecules with therapeutic value for Machado-Joseph disease, we screened a commercially available compound library, composed mainly of FDA/EMA-approved drugs, using a *C. elegans* model of

Machado-Joseph disease pathogenesis (AT3q130) in which mutant ATXN3 expressed in neurons caused aggregation and motility defects (Teixeira-Castro *et al.*, 2011). The strategy, validation approach and compound safety assays are depicted in Supplementary Figs 1 and 2. In the primary screen we identified 48 compounds (Fig. 1A) that ameliorated mutant ATXN3-mediated locomotion defects, showing a percentage of effect to non-treated animals higher than 50% within a confidence interval of 95% (Supplementary Fig. 3A). The hit compounds were categorized into chemical and pharmacological classes based on MeSH tree, ChEBI Ontology, and ATC fourth level classifications. While the chemical structure classification of the hit compounds revealed marked heterogeneity, they were enriched for specific pharmacological activities, namely modulators of neurotransmission (adrenergic, serotonergic, cholinergic, dopaminergic and histaminergic), anti-infectious, cardiovascular, anti-inflammatory, analgesic and hormone-related actions (Supplementary Fig. 3B).

A representative compound for each pharmacological cluster (Table 1) was further assessed for safety (Supplementary Fig. 2B) and ability to ameliorate motility impairment of mutant ATXN3 animals (Fig. 1B). The motility of wild-type animals was not increased by any of these hit compounds, suggesting that their action is specifically targeting mutant ATXN3-mediated pathogenesis (data not shown). Next, we examined whether these compounds affected protein aggregation in neurons of AT3q130 animals *in vivo*, and showed that the majority also decreased mutant ATXN3 aggregation (Fig. 1C). The reduction in ATXN3 aggregation was not due to decreased steady state levels of ATXN3 protein, suggesting a mechanism more likely related to folding stability than enhanced clearance (Fig. 1D). In summary, this *C. elegans* AT3q130 repurposing screen identified compounds with novel activity as suppressors of ATXN3 pathogenesis.

## Pharmacological and genetic inhibition of *C. elegans* SERT suppresses ATXN3 pathogenesis

Among the largest class of compounds that suppressed mutant ATXN3-mediated pathogenesis were those that affected serotonergic neurotransmission and modulated 5-HT-mediated signalling (Fig. 1E). Of these, citalopram is a SSRI with a proven safety record that is widely used for treatment of depression (Mandrioli *et al.*, 2012). The primary molecular target of citalopram is the 5-HT transporter (SERT, encoded by *SLC6A4*), which is responsible for 5-HT reuptake by serotonergic neurons (Blakely *et al.*, 1994). This target specificity and conservation prompted us to further examine the effects of citalopram on Machado-Joseph disease pathogenesis. Treatment with citalopram caused complete rescue of mutant ATXN3-mediated neuronal dysfunction (Fig. 1E), with a dose-response profile and a derived half-maximal effective concentration (EC<sub>50</sub>) value of 1  $\mu$ M (Supplementary

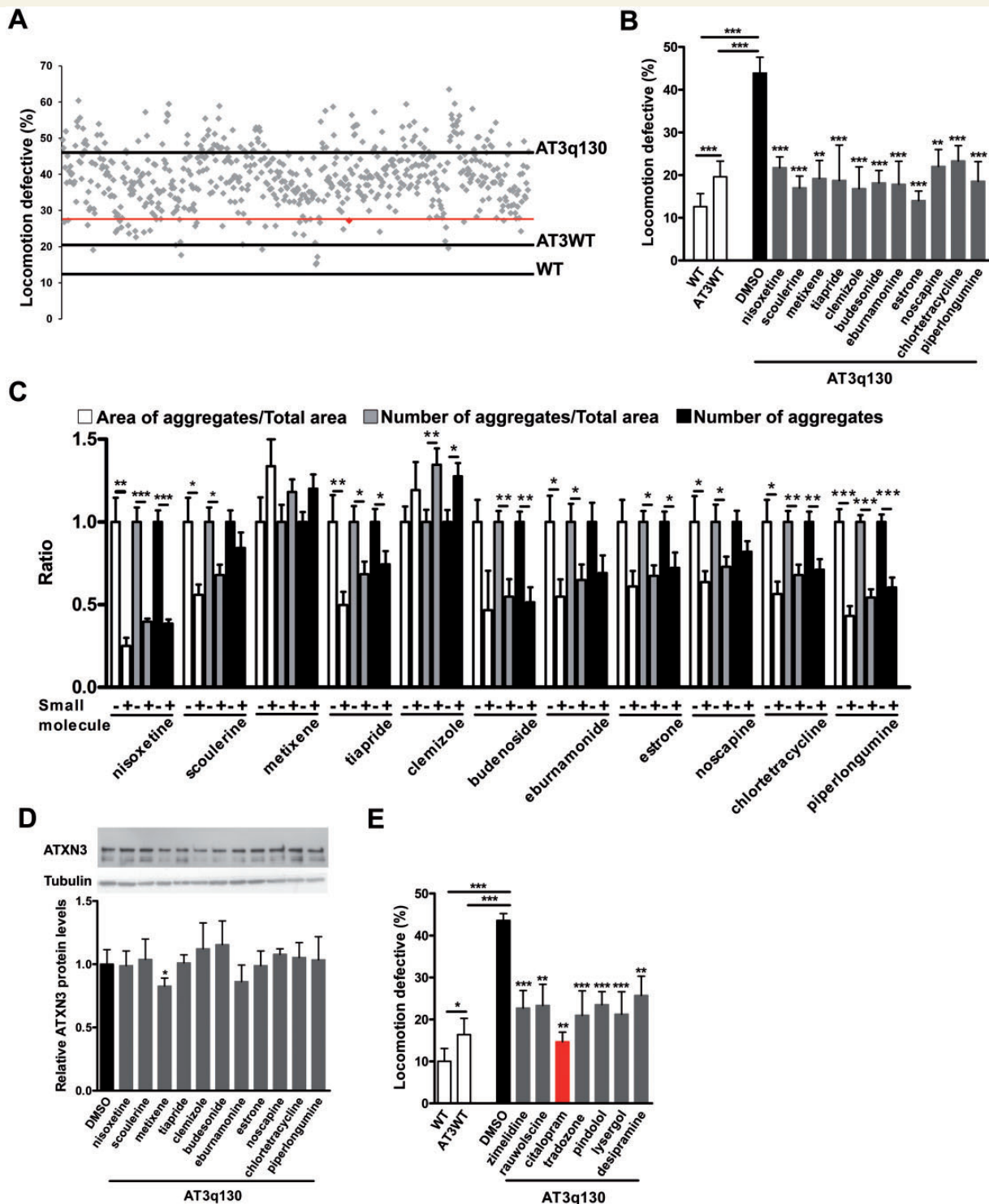
Fig. 4A). Citalopram exists as a racemic mixture but its effects are largely due to the S-enantiomer, escitalopram; this and other SSRIs also had beneficial effects on AT3q130 animals (Supplementary Fig. 4B). Normal behaviour and motility, development and fecundity in wild-type animals were not affected by SSRI treatment (Supplementary Fig. 4C). Importantly, citalopram treatment significantly reduced mutant ATXN3 aggregation in *C. elegans* neurons (Fig. 2A), and increased ATXN3 solubility (Fig. 2B), as assessed by biochemical fractionation (Koch *et al.*, 2011), without affecting the overall level of protein (Fig. 2C).

On continuous exposure to citalopram, the survival of AT3q130 animals was rescued (Supplementary Fig. 4D and E) and their neuronal dysfunction was restored through to Day 14 of age (Fig. 2D). This beneficial effect declined when citalopram was withdrawn, and neurotoxicity returned after 3-4 days OFF treatment (AT3q130::cit OFF, Fig. 2D). Maximum protection required early treatment (from the egg stage through to Day 4 of adulthood) (Fig. 2E); moreover, the extent of drug exposure period was critical, as 2 days of treatment were insufficient to exert beneficial effects (Fig. 2F).

In *C. elegans*, there is one 5-HT transporter orthologue of the vertebrate SERT, MOD-5 (Ranganathan *et al.*, 2001). To confirm the beneficial effect of pharmacological inhibition of serotonin recapture, we showed that genetic ablation of MOD-5 rescued mutant ATXN3-mediated motor dysfunction and aggregation in *C. elegans* (Fig. 2G). Pharmacogenetic analysis also supported MOD-5 as a cellular target of citalopram in the nematode, as drug treatment did not further ameliorate mutant ATXN3-mediated pathogenesis in the absence of MOD-5. In contrast, estrone (a steroid hormone) was able to further reduce the motility impairment of *mod-5*; AT3q130 animals (Fig. 2G), which is consistent with independent modes of action for these two compounds.

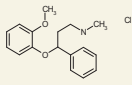
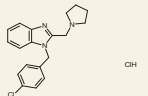
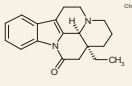
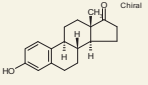
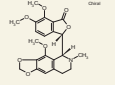
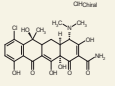
The role of 5-HT receptors was examined using pharmacological and pharmacogenetic approaches (Fig. 3A). Activation of postsynaptic 5-HT receptors by the 5-HT<sub>2C</sub> receptor (*HTR2C*) agonist vabicaserin (Dunlop *et al.*, 2011) and stimulation of the presynaptic 5-HT autoreceptors by buspirone (Takei *et al.*, 2005), dihydroergotamine (Villalon *et al.*, 2003) (Fig. 3B), lysergol (Pertz *et al.*, 1999) or pindolol (Corradetti *et al.*, 1998) (Fig. 1D) ameliorated mutant ATXN3-mediated motor dysfunction. Consistent with this, genetic ablation of the 5-HT postsynaptic G-protein coupled receptor SER-1 (Hamdan *et al.*, 1999) enhanced AT3q130 aggregation and locomotion defects (Fig. 3C). Likewise, the effect of citalopram was also dependent on these receptors. Additionally, ablation of the SER-4 (Olde and McCombie, 1997) autoreceptor, which by eliminating the negative feedback likely increases 5-HT availability, restored locomotion and reduced ATXN3 aggregation *in vivo* (Fig. 3D). Taken together, these results support the idea that pharmacological and genetic inhibition of MOD-5 restores motility and suppresses aggregation of AT3q130 through modulation of 5HTR activity.





**Figure 1 Identification of small-molecule suppressors of ATXN3 pathogenesis.** (A) Graphical representation of the results of the *C. elegans*-based screening in which we assessed a subset of 599 compounds of the Prestwick Chemical library. Black lines represent the mean percentage of animals with locomotion impairment for untreated AT3q130, AT3WT and wild-type animals. Grey dots show the mean of percentage of locomotion impaired AT3q130 animals upon treatment for each compound. The red line represents the assay cut-off to a minimum of 50% of effect in animals' motor behaviour. The red dot represents the percentage of locomotion impaired AT3q130 animals upon citralopram treatment, as obtained in the primary screen. (B) Motility analysis of AT3q130 animals treated with the top 11 hit compounds found in the screen ( $n = 4$ ,  $\pm$  SD),  $^{***}P < 0.001$ ,  $^{**}P < 0.01$  (Student's *t*-test). (C) Quantification of AT3q130 aggregation by confocal imaging and fluorescence intensity ( $n \geq 10$ ,  $\pm$  SD)  $^{*}P < 0.05$ ,  $^{**}P < 0.01$ ,  $^{***}P < 0.001$  (ANOVA, Bonferroni's test). (D) Human ATXN3 expression in AT3q130 animals treated with the top hit compounds ( $n = 4-6 \pm$  SEM).  $^{*}P < 0.05$  (Student's *t*-test). (E) Motility analysis of AT3q130 animals treated with compounds targeting serotonergic neurotransmission found in the screen ( $n = 4$ ,  $\pm$  SD),  $^{*}P < 0.05$ ,  $^{**}P < 0.01$ ,  $^{***}P < 0.001$  (Student's *t*-test). WT = wild-type; AT3WT = wild-type ATXN3 expressing animals; AT3q130 = mutant ATXN3 expressing animals.

**Table 1** Small molecule suppressors of ATXN3 pathogenesis grouped by their pharmacological action

Cluster	Pharmacological action	Drug	Structure	Number of hit compounds
1	Neurotransmitter Adrenergic	Nisoxetine HCl		8
2	Neurotransmitter Serotonergic	Scoulerine	<b>Propylamine</b> 	8
3	Neurotransmitter Cholinergic	Metixene HCl	<b>Alkaloid</b> 	2
4	Neurotransmitter Dopaminergic	Tiapride HCl	<b>Heterocyclic</b> 	2
5	Neurotransmitter Histaminergic	Clemizole HCl	<b>Benzamide</b> 	3
6	Anti-inflammatory	Budesonide	<b>Heterocyclic</b> 	5
7	Cardiovascular	Eburnamonine	<b>Steroid</b> 	5
8	Hormones/Hormone substituents	Estrone	<b>Alkaloid</b> 	4
9	Analgesic	Noscapine	<b>Steroid</b> 	2
10	Anti-infective	Chlortetracycline HCl	<b>Alkaloid</b> 	8
11	Etc.	Piperlongumine	<b>Polycyclic</b>  <b>Heterocyclic</b>	9

\*HCl = hydrochloride.

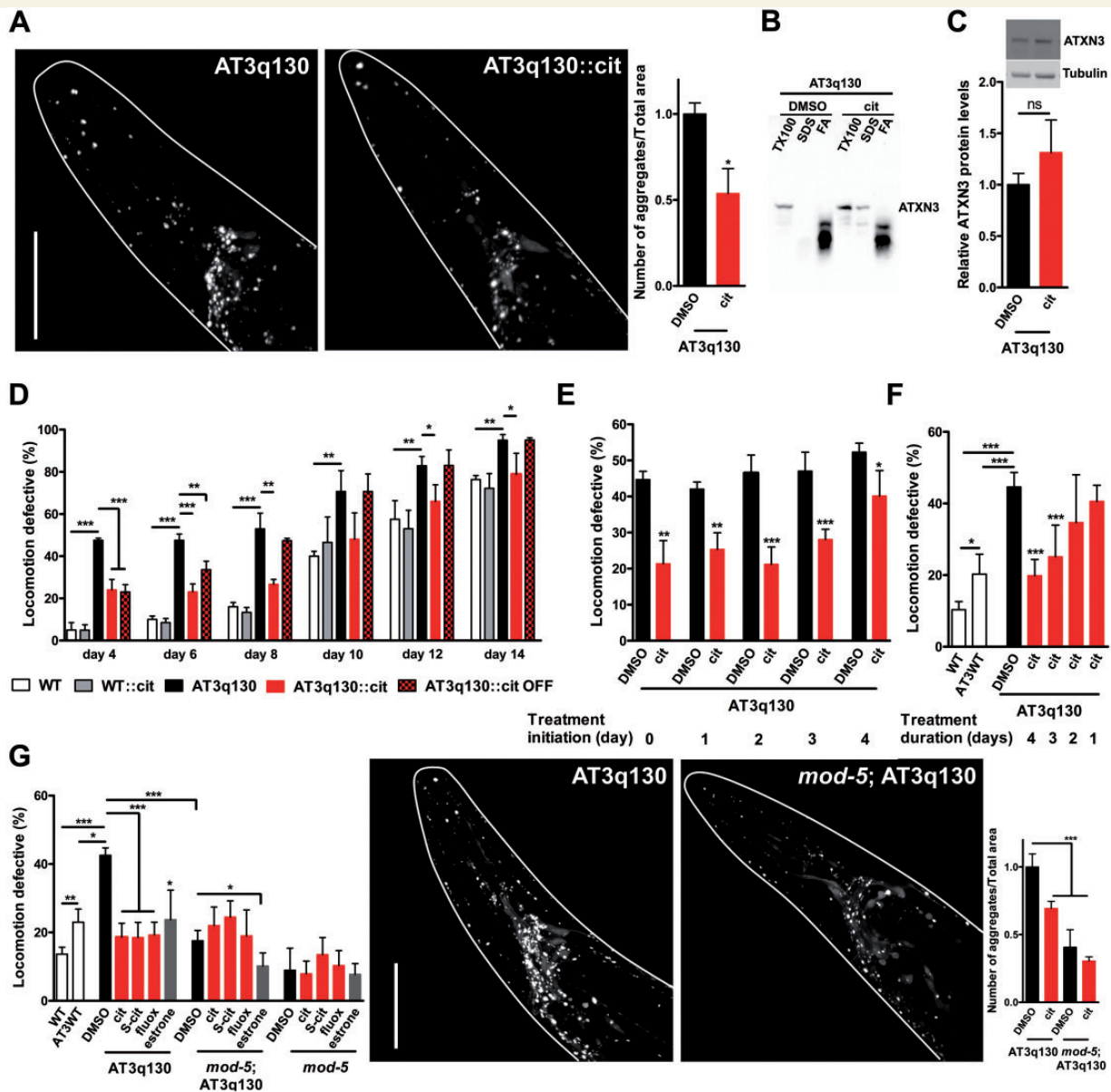


**Figure 2 Early life chronic citalopram treatment suppressed mutant ATXN3 aggregation and neuronal dysfunction in *C. elegans*.** (A) Aggregate quantification in AT3q130 animals upon citalopram (cit) treatment. (B) Representative western blot analysis of ATXN3 protein upon biochemical fractionation of AT3q130 protein extracts (out of  $n = 3$ ). (C) Human ATXN3 protein levels in AT3q130 cit animals. (D) Motility of citalopram-treated wild-type (WT::cit) and AT3q130 (AT3q130::cit) animals and OFF-drug effect (AT3q130::cit OFF) as disease progressed. (E) Motor behaviour of AT3q130 cit animals treated for 4 days, with treatment initiation at the indicated days and (F) treatment duration for the indicated days. (G) Locomotion impairment and aggregation load of AT3q130 animals in the *mod-5* background and upon treatment with citalopram, S-citalopram and fluoxetine. For motor behaviour assays: ( $n = 3-4 \pm SD$ ), \* $P < 0.05$ , \*\* $P < 0.01$ , \*\*\* $P < 0.001$  (Student's *t*-test). For aggregate quantification: ( $n \geq 8 \pm SD$ ), \* $P < 0.05$ , \*\* $P < 0.01$ , \*\*\* $P < 0.001$  (ANOVA, Bonferroni's test). For western blot: ( $n = 4 \pm SD$ ),  $P > 0.05$  (Student's *t*-test). TX100 = Triton™ X-100; FA = formic acid; cit = citalopram; S-cit = S-citalopram; fluox = fluoxetine; WT = wild-type.

## Citalopram treatment improves motor balance and coordination of CMVMJD135 mice

To further investigate the therapeutic potential of citalopram, we used a transgenic mouse model of Machado-Joseph disease, CMVMJD135, that displays progressive Machado-Joseph disease-like motor decline and

neuropathology, including ATXN3-positive intranuclear inclusions in the CNS (Silva-Fernandes *et al.*, 2014). Although CMVMJD135 mice showed no changes in baseline 5-HT levels measured by HPLC (Fig. 4), oral administration of citalopram (8 mg/kg) to these animals (study design; Fig. 5A) prevented their decreased body weight gain (Fig. 5B) and had significant beneficial effects on the motor phenotype. While there was only marginal

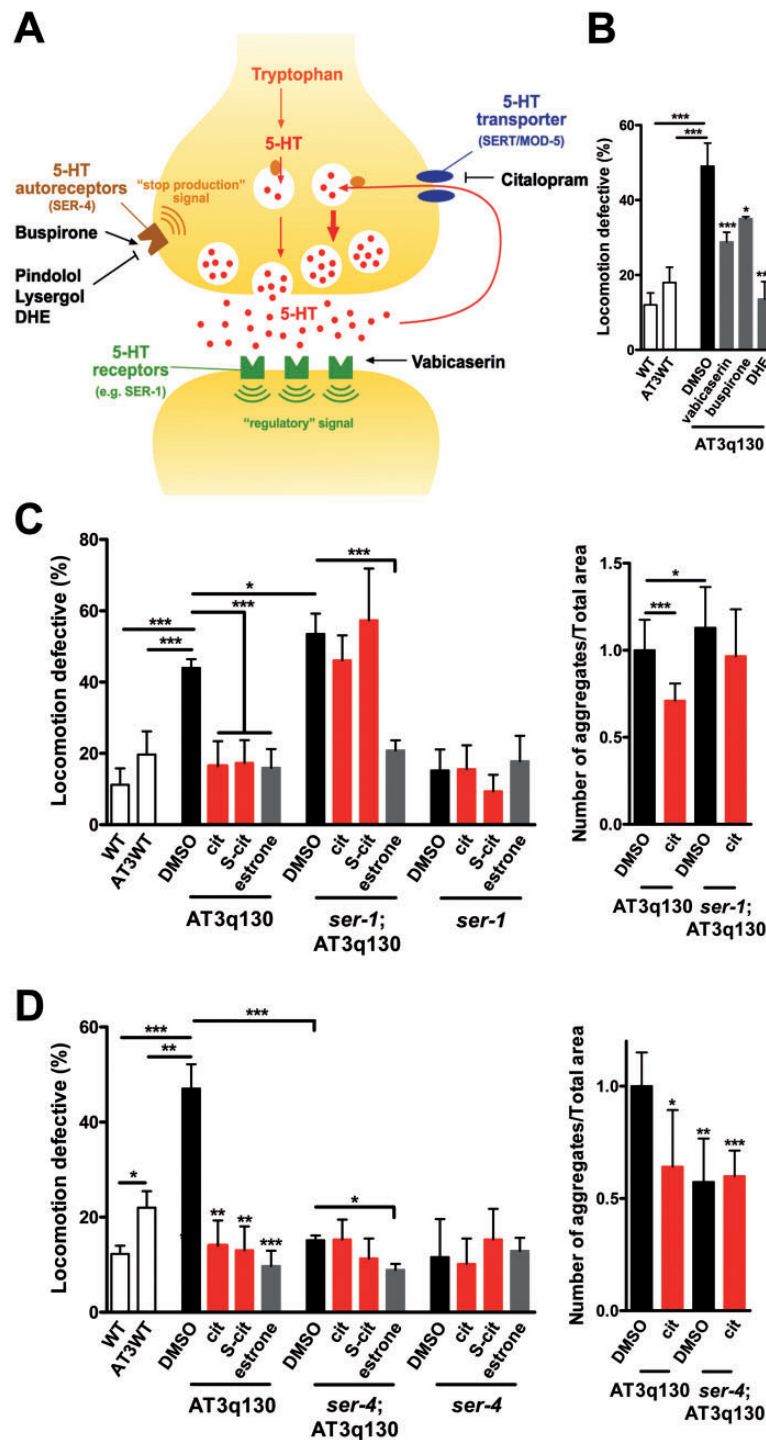


**Figure 3 Serotonergic signalling improves ATXN3 pathogenesis in a G-protein coupled receptor-dependent manner. (A)** Schematic of a serotonergic synapse showing that 5-HT is synthesized and released into the synaptic cleft, where it activates postsynaptic 5-HT receptors. Vabicaserin may activate the regulatory signalling coupled with SER-1. Pindolol, lysergol and DHE probably antagonize the 5-HT autoreceptor SER-4, whereas the 5-HT1A receptor agonist buspirone may desensitize the receptor, shutting down the stop production signal mediated by 5-HT autoreceptors in presynaptic neurons. **(B)** Motor behaviour of AT3q130 animals treated with vabicaserin, buspirone and dihydroergotamine. **(C)** Motility defects and aggregation load of AT3q130 animals in a *ser-1* genetic background, with and without cit, S-citalopram and estrone treatments. **(D)** Motility performance and mutant ATXN3 aggregation phenotypes of AT3q130 animals in the absence of SER-4. For motor behaviour assays: ( $n = 3-4$ ,  $\pm$  SD), \* $P < 0.05$ , \*\* $P < 0.01$ , \*\*\* $P < 0.001$  (Student's *t*-test). For aggregate quantification: ( $n \geq 12$ ,  $\pm$  SD) \* $P < 0.05$ , \*\* $P < 0.01$ , \*\*\* $P < 0.001$  (ANOVA, Bonferroni's test). DHE = dihydroergotamine; DMSO = dimethyl sulphoxide; cit = citalopram; S-cit = S-citalopram; fluox = fluoxetine.

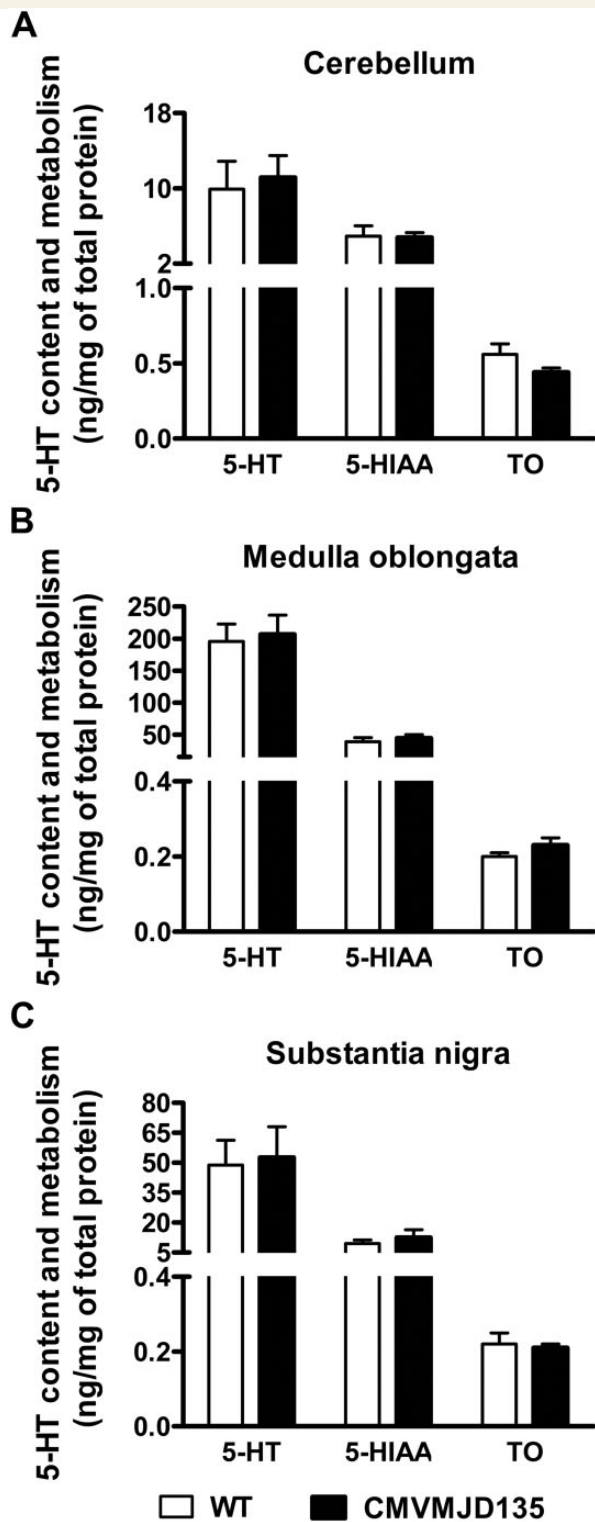


**Figure 4** CMVMJD135 mice show normal levels of 5-HT and 5-HT metabolic turn over at fully symptomatic stages of disease. Levels of 5-HT, 5-HIAA and 5-HT turnover (5-HIAA/5-HT) were measured by HPLC (A) in the cerebellum ( $n = 5$  wild-type;  $n = 7$  CMVMJD135), (B) medulla oblongata ( $n = 6$  wild-type;  $n = 8$  CMVMJD135) and (C) substantia nigra ( $n = 5$  wild-type;  $n = 5$  CMVMJD135) at 24 weeks of age. Data presented as the mean  $\pm$  SEM.  $P > 0.05$  (Student's  $t$ -test). TO = turnover; WT = wild-type.

improvement in the dragging of the paws (Supplementary Fig. 5A) and limited effects on exploratory activity (Supplementary Fig. 5B), grip strength (Supplementary Fig. 5C) and hindlimb tonus (Supplementary Fig. 5D), citalopram treatment restored stride length to wild-type levels at advanced stages of the trial (Fig. 5C). Moreover, treated animals showed reduced tremors (Fig. 5D), reduced limb claspings (Fig. 5E), and improved gait quality (Fig. 5F). Citalopram treatment also resulted in a striking improvement in balance and motor coordination as compared to vehicle-treated CMVMJD135 mice. In the balance beam walk test, we observed major improvements in the 12 mm square beam from 20 to 34 weeks of age (Fig. 6A and Supplementary Video 1) and also in a wider (17 mm) round beam (Supplementary Fig. 5E). The most remarkable benefits of citalopram were observed in the motor swimming test (Fig. 6B), since at many time points and until quite late in the trial citalopram treated animals were indistinguishable from wild-type (Supplementary Video 2). Overall, these results demonstrate that citalopram can reduce the impairment in motor coordination of the Machado-Joseph disease mouse, with less benefit on strength, suggesting effects at the level of the brainstem, midbrain or cerebellum, rather than on spinocerebellar tracts and muscle innervation. Treatment also significantly delayed disease progression in mice.

Citalopram treated wild-type mice behaved similarly to their untreated littermates, confirming the specificity of the effect (Supplementary Fig. 6). Moreover, CMVMJD135 mice treated with a dosage of 13 mg/kg showed more limited improvements when compared to vehicle-treated controls in all paradigms mentioned above (Supplementary Fig. 7).

The analysis of brain tissue from CMVMJD135 mice showed that citalopram treatment (8 mg/kg) mitigated reactive astrogliosis (Fig. 6C) and decreased ATXN3 intranuclear inclusions in the brainstem (Fig. 6D), analogous to the reduction of neuronal aggregates in *C. elegans*. This reduction was observed in the pontine nuclei, reticulotegmental nuclei of pons and facial motor nuclei of CMVMJD135-treated mice when compared to their vehicle-treated counterparts (Fig. 6D); the impact of citalopram was less marked in the lateral reticular nuclei. This reduced ATXN3 aggregation did not correspond to lower levels of ATXN3 protein levels in the brainstem (Fig. 6E), suggesting that the effect of citalopram in mice is similar to that in *C. elegans*, affecting folding and stability of ATXN3 rather than clearance of the mutant protein. Citalopram treatment also had neuroprotective effects, rescuing loss of ChAT-positive motor neurons in the facial motor nuclei (Fig. 7A). The same trend was observed for motor neurons of the ventral horn of the lumbar spinal cord (Fig. 7B), albeit without statistical significance, in agreement with the observed phenotypic effects upon treatment. The mild reduction in Calbindin D28-K-positive cells seen in the cerebellar cortex of CMVMJD135 mice was also circumvented by citalopram treatment (Fig. 7C).

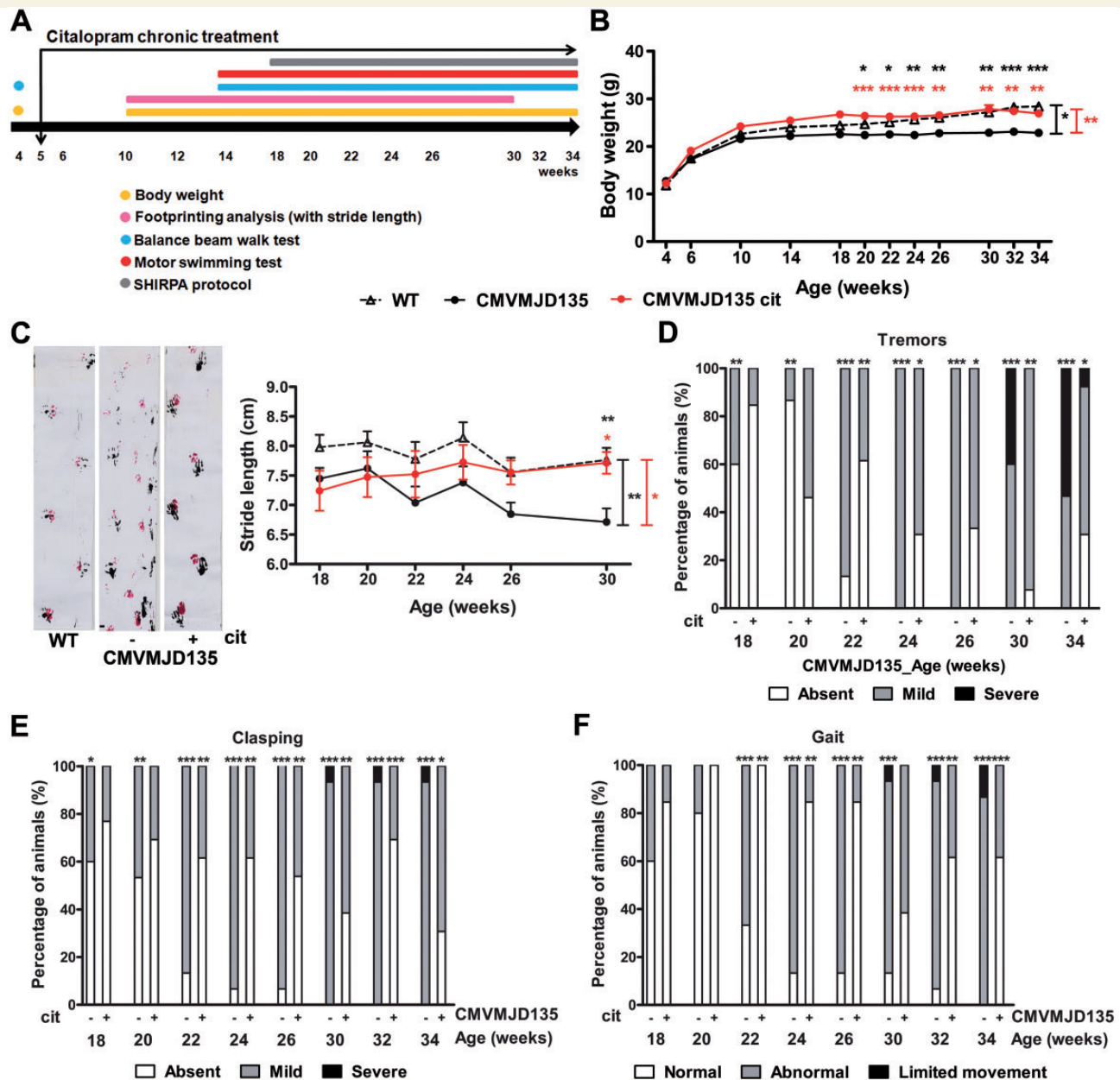


**Figure 5** Impact of citalopram treatment at 8 mg/kg on the neurological deficits of CMVMJD135 mice. (A) Schematic representation of the preclinical therapeutic trial. Significant differences observed between vehicle ( $n = 13$ ) and citalopram-treated CMVMJD135 mice ( $n = 16$ ) in (B) body weight ( $P = 0.001$ , 20–34 weeks) and (C) stride length ( $P = 0.015$ , 30 weeks). (D) Tremors, (E) limb clasping and (F) gait were evaluated from 18 to 34 weeks of age with phenotype amelioration from 22 to 34 weeks of age. ( $n = 13$ –16,  $\pm$  SD), \* $P < 0.05$ , \*\* $P < 0.01$  and \*\*\* $P < 0.001$  (Mann-Whitney U-test for non-parametric variables and ANOVA, Tukey correction for continuous variables). cit = citalopram.

## Discussion

In this study we describe a small molecule screen using a collection of FDA/EMA-approved drugs to identify modulators of neuronal dysfunction in transgenic *C. elegans* expressing mutant ATXN3. By using two model systems, we combined the ease and speed of screening in *C. elegans*, the ability to use genetics and selected small molecule agonists and antagonists of receptors and transporters to validate pathways, and the relevance of subsequent confirmation

in a vertebrate model of Machado-Joseph disease. This led to the identification of neuroactive compounds, among which modulators of the serotonergic pathway that strongly suppressed Machado-Joseph disease pathogenesis *in vivo*. In support of this screening strategy, many of the suppressors of ATXN3 pathogenesis identified in our study have been shown to be effective in other neurodegenerative disorders, including Parkinson's and Alzheimer's disease, and also in Machado-Joseph disease (Clarke *et al.*, 1966; Perenyi *et al.*, 1985; Kanai *et al.*,

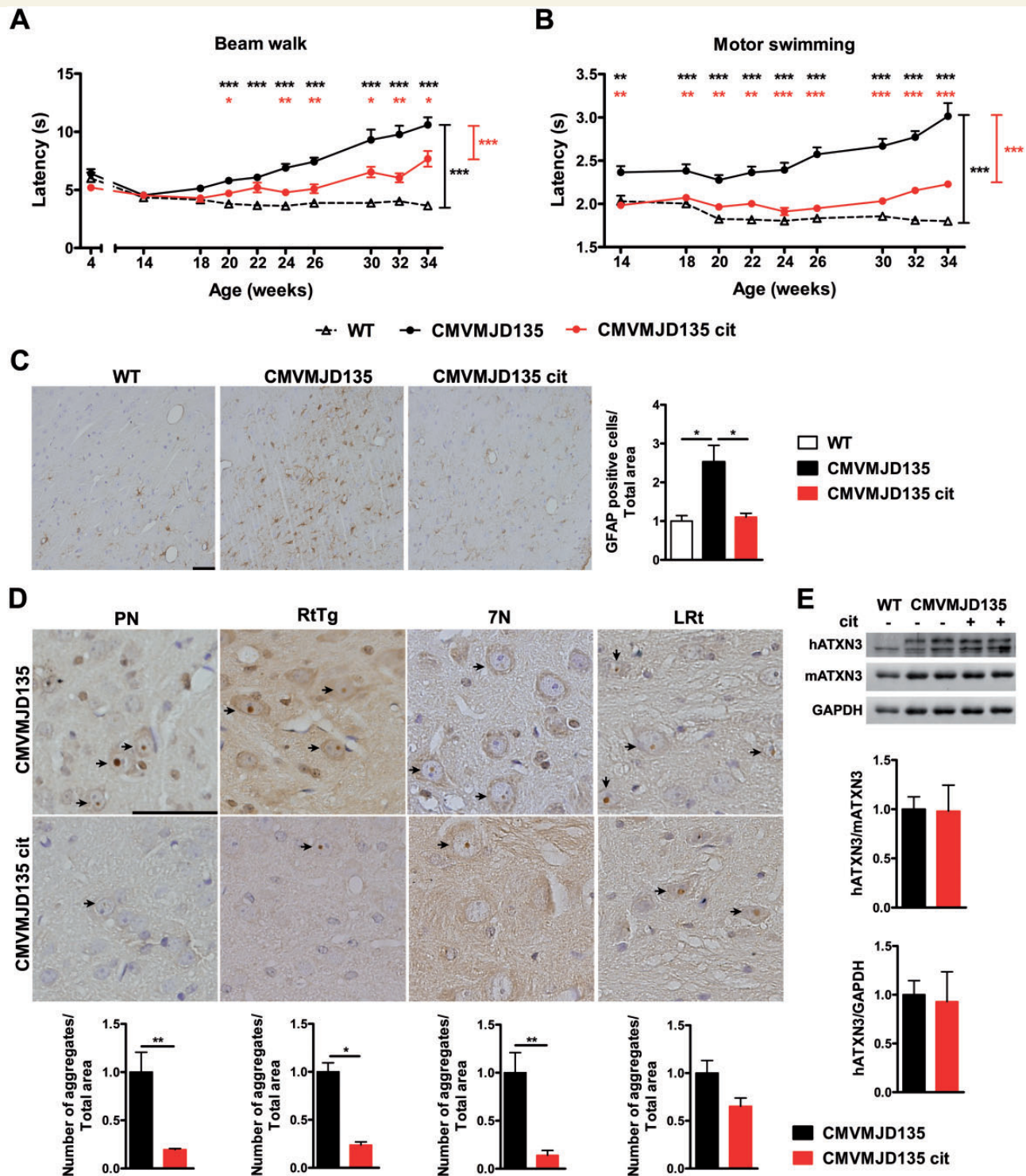
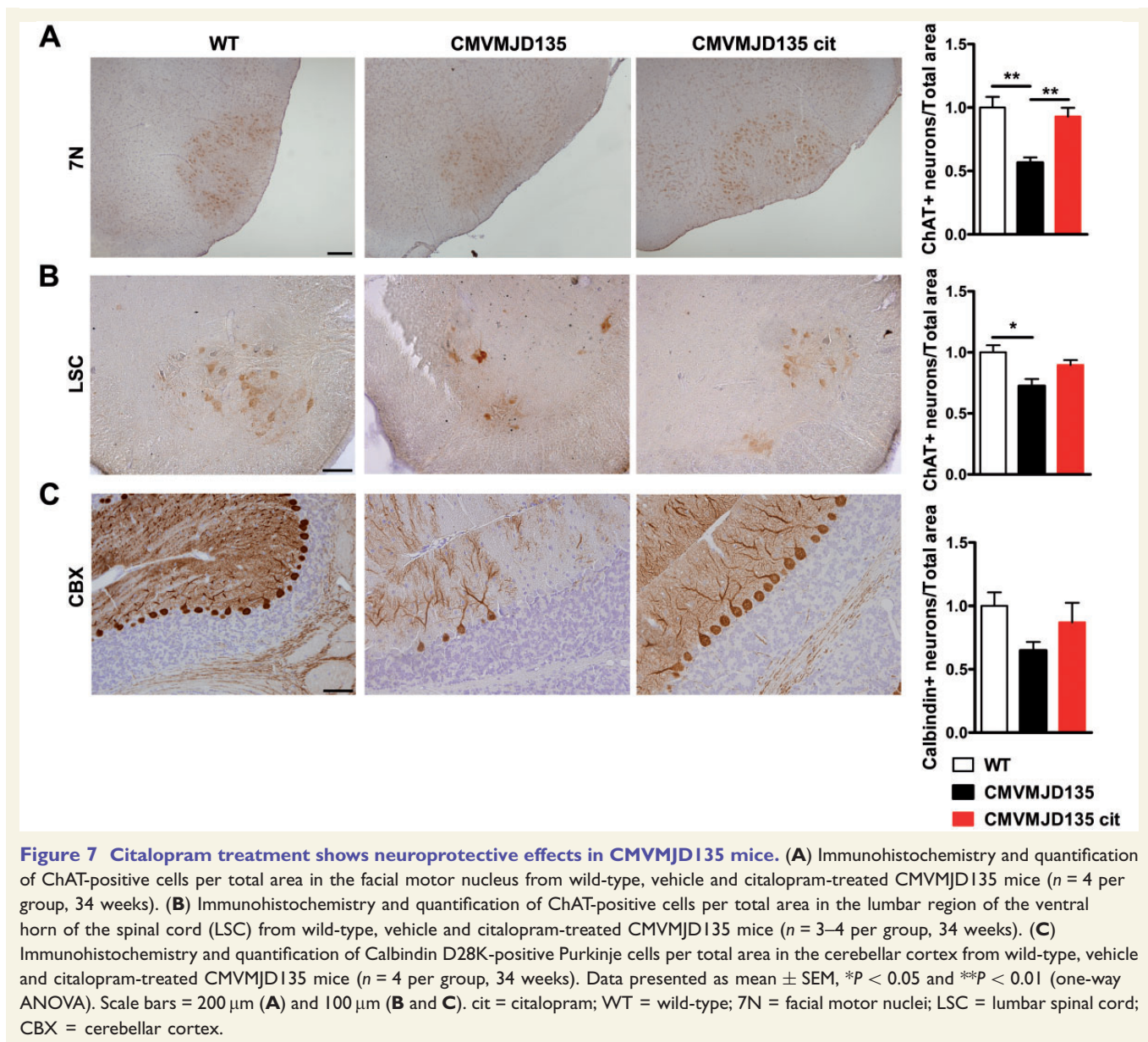


**Figure 6 Citalopram treatment ameliorates balance and motor coordination and suppresses mutant ATXN3 aggregation in Machado-Joseph disease mice.** Significant differences observed between vehicle ( $n = 13$ ) and citalopram-treated CMVMJD135 mice ( $n = 16$ ) in the (A) square beam ( $P < 0.001$ , 20–34 weeks) and (B) motor swimming ( $P < 0.001$ , 14–34 weeks) tests. (C) Immunohistochemistry and quantification of GFAP-positive cells per area in substantia nigra from wild-type, vehicle- and citalopram-treated CMVMJD135 mice ( $n = 5$  per group, 34 weeks). (D) Neuronal inclusions in the pontine nuclei, reticulotegmental nucleus of the pons, facial motor nucleus and lateral reticular nucleus of vehicle and citalopram-treated CMVMJD135 mice ( $n = 4$ , 34 weeks). (E) Brainstem immunoblots and quantification of total human ATXN3 protein from vehicle and citalopram-treated CMVMJD135 mice ( $n = 5$ , 34 weeks). Data presented as mean  $\pm$  SEM, \* $P < 0.05$  and \*\* $P < 0.01$  [ANOVA, Tukey correction (A and B) and one-way ANOVA (C–E)]. Scale bars = 20  $\mu$ m. cit = citalopram; WT = wild-type; SN = substantia nigra; PN = pontine nuclei; RtTg = reticulotegmental nuclei of pons; 7N = facial motor nuclei; LRt = lateral reticular nuclei.



2003; Cho *et al.*, 2009; Cirrito *et al.*, 2011). A more in-depth understanding of the mechanism of action of these suppressors of expanded ATXN3 toxicity and their ability to modulate aggregation offers new opportunities for small-molecule therapeutics for Machado-Joseph disease and other protein conformational diseases.

Citalopram and other SSRIs suppressed Machado-Joseph disease pathogenesis in the *C. elegans* and mouse models, showing beneficial effects on motility/coordination, aggregation of mutant ATXN3, and disease progression. MOD-5 (and SERT) inhibition by citalopram likely results in increased extracellular 5-HT levels and enhanced serotonergic neurotransmission that can elicit 5-HT dependent effects on neuronal activities, adaptation (Blier and de Montigny, 1999; El Mansari *et al.*, 2005; Schilstrom *et al.*, 2011), and remodelling (Musazzi *et al.*, 2010;

Bessa *et al.*, 2013). Indeed, ablation of the postsynaptic receptor SER-1 (Hamdan *et al.*, 1999), which is pharmacologically similar to the mammalian 5-HT<sub>2</sub> receptor, aggravated ATXN3 pathogenesis. The beneficial action of citalopram required SER-1, suggesting that the downstream effects of this drug are mediated by signalling cascades involving this receptor. Furthermore, ablation of SER-4, which shares similarity to vertebrates' 5-HT<sub>1</sub> autoreceptors, rescued motor neuron dysfunction and reduced ATXN3 aggregation *in vivo*.

The therapeutic effects of SSRIs for amelioration of mutant ATXN3-mediated neurotoxicity in both *C. elegans* and mice required chronic treatment; likewise, citalopram prolonged treatment is necessary in depression (Blier and de Montigny, 1999). Such SSRI treatment modalities result in 5-HT<sub>1A</sub> autoreceptor desensitization (Blier and De



Montigny, 1983; Lanfumey *et al.*, 2008), which inactivates the negative feedback mechanism taking place in presynaptic neurons, thereby increasing 5-HT availability and activating postsynaptic receptors (Lanfumey and Hamon, 2004). Pindolol, a  $\beta$ -adrenergic receptor partial agonist with 5-HT<sub>1A</sub> receptor antagonist properties, when combined with SSRIs, results in a significant decrease in time to first response compared with SSRIs alone. Moreover, a faster desensitization of 5-HT<sub>1A</sub> autoreceptors by a direct agonist (e.g. buspirone) may also accelerate the therapeutic efficacy of SSRIs (Blier and Ward, 2003). Consistently, targeting 5-HT autoreceptors by chronic treatment ameliorated mutant ATXN3-mediated pathogenesis in *C. elegans*. Serotonin receptors in nematodes and mammals, while homologous, may not be functionally identical (Komuniecki *et al.*, 2004); therefore, it would be important to identify the specific 5-HT receptors required for citalopram's effect on toxicity and aggregation of mutant ATXN3 in mice.

In Huntington's disease mouse models, SSRI treatment resulted in striatal and memory preservation and extended survival (Lauterbach, 2013). Citalopram has also been shown to be beneficial in models of Alzheimer's disease and in healthy human volunteers by reducing amyloid- $\beta$  in the CSF (Cirrito *et al.*, 2011; Sheline *et al.*, 2014). The need for chronic and early symptomatic treatment in Machado-Joseph disease suggests a neuroprotective mechanism rather than immediate effects on signalling cascades (Sheline *et al.*, 2014) or correction of an imbalance of 5-HT in Machado-Joseph disease mice. Moreover, the effect of citalopram and MOD-5 inactivation on aggregation ATXN3 is consistent with an impact of serotonergic neurotransmission on the rebalance of proteostasis state of the organism. Indeed, it has been recently described that the release of serotonin from neurons signals to distal tissues the activation of protective mechanisms to prevent proteotoxicity (Tatum *et al.*, 2015).

Comparing the effects obtained with citalopram with those described in the literature for other molecules with positive effect in Machado-Joseph disease models, this SSRI appears to have a higher therapeutic efficacy. From our own work, when we compare the current results with the previous findings for the Hsp90 inhibitor 17-DMAG (Silva-Fernandes *et al.*, 2014), we observe a more pronounced therapeutic effect of citalopram. Namely, the manifestation of motor swimming defects was delayed 8 weeks by 17-DMAG treatment versus at least 20 weeks by citalopram treatment; also, at 30 weeks, the percentage of effect of 17-DMAG in this test was 33%, and that of citalopram was 79%. The difference in performance between the treated groups (normalized to the respective non-treated groups) in the two experiments was statistically significant at this age ( $P = 0.018$ ).

In conclusion, the efficacy of citalopram in suppression of ATXN3 pathogenesis in two disease models, as well as its safety record of being widely used in depression patients,

prompts us to suggest this drug for clinical trials in patients with Machado-Joseph disease.

## Acknowledgements

We are grateful to members of the Maciel and Morimoto laboratories for sharing reagents, for critical analysis of the data and discussions on the manuscript. We also thank Lündbeck for providing citalopram for the preclinical trial in mice and Drs Karina Fog and Søren Møller for discussions on experimental planning and data. We are grateful to Dr Veena Prahlad and Dr Michael Ailion for comments on *C. elegans* pharmacogenetic experiments. Thanks to the *Caenorhabditis Genetics Center* (CGC), which is funded by the National Institutes of Health – National Center for Research Resources, for some of the nematode strains.

## Funding

This work was supported by Fundação para a Ciência e Tecnologia (FCT) and COMPETE through the projects [PTDC/SAU-GMG/112617/2009] (to P.M.) and [EXPL/BIM-MEC/0239/2012] (to A.T.C.), by National Ataxia foundation (to P.M.), by Ataxia UK (to P.M.), by National Institutes of Health (NIH) [GM038109, GM081192, AG026647, and NS047331] (to R.I.M.), by The Chicago Biomedical Consortium (to R.I.M.) and by the Ellison Medical Foundation (to R.I.M.). A.T.C., A.J., S.E., L.S.S., C.B., S.D.S., A.S.F. and A.N.C. were supported by the FCT individual fellowships SFRH/BPD/79469/2011, SFRH/BD/76613/2011, SFRH/BD/78554/2011, SFRH/BD/84650/2012, SFRH/BPD/74452/2010, SFRH/BD/78388/2011, SFRH/BPD/91562/2012 and SFRH/BD/51059/2010, respectively. FCT fellowships are co-financed by POPH, QREN, Governo da República Portuguesa and EU/FSE.

## Supplementary material

Supplementary material is available at *Brain* online.

## References

- Balch WE, Morimoto RI, Dillin A, Kelly JW. Adapting proteostasis for disease intervention. *Science* 2008; 319: 916–9.
- Bessa JM, Morais M, Marques F, Pinto L, Palha JA, Almeida OF, et al. Stress-induced anhedonia is associated with hypertrophy of medium spiny neurons of the nucleus accumbens. *Transl Psychiatry* 2013; 3: e266.
- Blakely RD, De Felice LJ, Hartzell HC. Molecular physiology of norepinephrine and serotonin transporters. *J Exp Biol* 1994; 196: 263–81.
- Blier P, De Montigny C. Electrophysiological investigations on the effect of repeated zimelidine administration on serotonergic neurotransmission in the rat. *J Neurosci* 1983; 3: 1270–8.

- Blier P, de Montigny C. Serotonin and drug-induced therapeutic responses in major depression, obsessive-compulsive and panic disorders. *Neuropsychopharmacology* 1999; 21 (2 Suppl): 91S–8S.
- Blier P, Ward NM. Is there a role for 5-HT1A agonists in the treatment of depression? *Biol Psychiatry* 2003; 53: 193–203.
- Brenner S. The genetics of *Caenorhabditis elegans*. *Genetics* 1974; 77: 71–94.
- Chen X, Tang TS, Tu H, Nelson O, Pook M, Hammer R, et al. Deranged calcium signaling and neurodegeneration in spinocerebellar ataxia type 3. *J Neurosci* 2008; 28: 12713–24.
- Cho Y, Son HJ, Kim EM, Choi JH, Kim ST, Ji IJ, et al. Doxycycline is neuroprotective against nigral dopaminergic degeneration by a dual mechanism involving MMP-3. *Neurotox Res* 2009; 16: 361–71.
- Chong CR, Sullivan DJ, Jr. New uses for old drugs. *Nature* 2007; 448: 645–6.
- Chou AH, Chen SY, Yeh TH, Weng YH, Wang HL. HDAC inhibitor sodium butyrate reverses transcriptional downregulation and ameliorates ataxic symptoms in a transgenic mouse model of SCA3. *Neurobiol Dis* 2011; 41: 481–8.
- Cirrito JR, Disabato BM, Restivo JL, Verges DK, Goebel WD, Sathyan A, et al. Serotonin signaling is associated with lower amyloid-beta levels and plaques in transgenic mice and humans. *Proc Natl Acad Sci USA* 2011; 108: 14968–73.
- Clarke S, Hay GA, Vas CJ. Therapeutic action of methixene hydrochloride on Parkinsonian tremor and a description of a new tremor-recording transducer. *Br J Pharmacol Chemother* 1966; 26: 345–50.
- Corradetti R, Laaris N, Hanoun N, Laporte AM, Le Poul E, Hamon M, et al. Antagonist properties of (-)-pindolol and WAY 100635 at somatodendritic and postsynaptic 5-HT1A receptors in the rat brain. *Br J Pharmacol* 1998; 123: 449–62.
- Costa Mdo C, Luna-Cancelon K, Fischer S, Ashraf NS, Ouyang M, Dharia RM, et al. Toward RNAi therapy for the polyglutamine disease Machado-Joseph disease. *Mol Ther* 2013; 21: 1898–908.
- Coutinho P, Andrade C. Autosomal dominant system degeneration in Portuguese families of the Azores Islands. A new genetic disorder involving cerebellar, pyramidal, extrapyramidal and spinal cord motor functions. *Neurology* 1978; 28: 703–9.
- Cushman-Nick M, Bonini NM, Shorter J. Hsp104 suppresses polyglutamine-induced degeneration post onset in a drosophila MJD/SCA3 model. *PLoS Genet* 2013; 9: e1003781.
- D'Abreu A, Franca MC, Jr, Paulson HL, Lopes-Cendes I. Caring for Machado-Joseph disease: current understanding and how to help patients. *Parkinsonism Relat Disord* 2010; 16: 2–7.
- Dunlop J, Watts SW, Barrett JE, Coupet J, Harrison B, Mazandarani H, et al. Characterization of vabicaserin (SCA-136), a selective 5-hydroxytryptamine 2C receptor agonist. *J Pharmacol Exp Ther* 2011; 337: 673–80.
- El Mansari M, Sanchez C, Chouvet G, Renaud B, Haddjeri N. Effects of acute and long-term administration of escitalopram and citalopram on serotonin neurotransmission: an *in vivo* electrophysiological study in rat brain. *Neuropsychopharmacology* 2005; 30: 1269–77.
- Gidalevitz T, Ben-Zvi A, Ho KH, Brignull HR, Morimoto RI. Progressive disruption of cellular protein folding in models of polyglutamine diseases. *Science* 2006; 311: 1471–4.
- Gidalevitz T, Krupinski T, Garcia S, Morimoto RI. Destabilizing protein polymorphisms in the genetic background direct phenotypic expression of mutant SOD1 toxicity. *PLoS Genet* 2009; 5: e1000399.
- Hamdan FF, Ungrin MD, Abramovitz M, Ribeiro P. Characterization of a novel serotonin receptor from *Caenorhabditis elegans*: cloning and expression of two splice variants. *J Neurochem* 1999; 72: 1372–83.
- Kaletta T, Hengartner MO. Finding function in novel targets: *C. elegans* as a model organism. *Nat Rev Drug Discov* 2006; 5: 387–98.
- Kanai K, Kuwabara S, Arai K, Sung JY, Ogawara K, Hattori T. Muscle cramp in Machado-Joseph disease: altered motor axonal excitability properties and mexiletine treatment. *Brain* 2003; 126 (Pt 4): 965–73.
- Kawaguchi Y, Okamoto T, Taniwaki M, Aizawa M, Inoue M, Katayama S, et al. CAG expansions in a novel gene for Machado-Joseph disease at chromosome 14q32.1. *Nat Genet* 1994; 8: 221–8.
- Koch P, Breuer P, Peitz M, Jungverdorben J, Kesavan J, Poppe D, et al. Excitation-induced ataxin-3 aggregation in neurons from patients with Machado-Joseph disease. *Nature* 2011; 480: 543–6.
- Komuniecki RW, Hobson RJ, Rex EB, Hapiak VM, Komuniecki PR. Biogenic amine receptors in parasitic nematodes: what can be learned from *Caenorhabditis elegans*? *Mol Biochem Parasitol* 2004; 137: 1–11.
- Lanfumeij L, Hamon M. 5-HT1 receptors. *Curr Drug Targets CNS Neurol Disord* 2004; 3: 1–10.
- Lanfumeij L, Mongeau R, Cohen-Salmon C, Hamon M. Corticosteroid-serotonin interactions in the neurobiological mechanisms of stress-related disorders. *Neurosci Biobehav Rev* 2008; 32: 1174–84.
- Lauterbach EC. Neuroprotective effects of psychotropic drugs in Huntington's disease. *Int J Mol Sci* 2013; 14: 22558–603.
- Mandrioli R, Mercolini L, Saracino MA, Raggi MA. Selective serotonin reuptake inhibitors (SSRIs): therapeutic drug monitoring and pharmacological interactions. *Curr Med Chem* 2012; 19: 1846–63.
- Menzies FM, Huebener J, Renna M, Bonin M, Riess O, Rubinsztein DC. Autophagy induction reduces mutant ataxin-3 levels and toxicity in a mouse model of spinocerebellar ataxia type 3. *Brain* 2010; 133(Pt 1): 93–104.
- Morimoto RI. Proteotoxic stress and inducible chaperone networks in neurodegenerative disease and aging. *Genes Dev* 2008; 22: 1427–38.
- Morley JF, Morimoto RI. Regulation of longevity in *Caenorhabditis elegans* by heat shock factor and molecular chaperones. *Mol Biol Cell* 2004; 15: 657–64.
- Musazzi L, Mallei A, Tardito D, Gruber SH, El Khoury A, Racagni G, et al. Early-life stress and antidepressant treatment involve synaptic signaling and Erk kinases in a gene-environment model of depression. *J Psychiatr Res* 2010; 44: 511–20.
- Nascimento-Ferreira I, Nobrega C, Vasconcelos-Ferreira A, Onofre I, Albuquerque D, Aveleira C, et al. Beclin 1 mitigates motor and neuropathological deficits in genetic mouse models of Machado-Joseph disease. *Brain* 2013; 136 (Pt 7): 2173–88.
- Nobrega C, Nascimento-Ferreira I, Onofre I, Albuquerque D, Hirai H, Deglon N, et al. Silencing mutant ataxin-3 rescues motor deficits and neuropathology in Machado-Joseph disease transgenic mice. *PLoS One* 2013; 8: e52396.
- Nussbaum-Krammer CI, Park KW, Li L, Melki R, Morimoto RI. Spreading of a prion domain from cell-to-cell by vesicular transport in *Caenorhabditis elegans*. *PLoS Genet* 2013; 9: e1003351.
- Olde B, McCombie WR. Molecular cloning and functional expression of a serotonin receptor from *Caenorhabditis elegans*. *J Mol Neurosci* 1997; 8: 53–62.
- Pain and distress in laboratory rodents and lagomorphs. Report of the Federation of European Laboratory Animal Science Associations (FELASA) Working Group on Pain and Distress accepted by the FELASA Board of Management November 1992. *Lab Anim* 1994; 28: 97–112.
- Perenyi A, Arato M, Bagdy G, Frecska E, Szucs R. Tiapride in the treatment of tardive dyskinesia: a clinical and biochemical study. *J Clin Psychiatry* 1985; 46: 229–31.
- Pertz HH, Brown AM, Gager TL, Kaumann AJ. Simple O-acylated derivatives of lysergol and dihydrolysergol-I: synthesis and interaction with 5-HT2A, 5-HT2C and 5-HT1B receptors, and alpha1 adrenergic receptors. *J Pharm Pharmacol* 1999; 51: 319–30.
- Ranganathan R, Sawin ER, Trent C, Horvitz HR. Mutations in the *Caenorhabditis elegans* serotonin reuptake transporter MOD-5 reveal serotonin-dependent and -independent activities of fluoxetine. *J Neurosci* 2001; 21: 5871–84.
- Robertson AL, Headey SJ, Saunders HM, Ecroyd H, Scanlon MJ, Carver JA, et al. Small heat-shock proteins interact with a flanking

- domain to suppress polyglutamine aggregation. *Proc Natl Acad Sci USA* 2010; 107: 10424–9.
- Ross CA, Margolis RL, Becher MW, Wood JD, Engelender S, Cooper JK, et al. Pathogenesis of neurodegenerative diseases associated with expanded glutamine repeats: new answers, new questions. *Prog Brain Res* 1998; 117: 397–419.
- Santos M, Summavielle T, Teixeira-Castro A, Silva-Fernandes A, Duarte-Silva S, Marques F, et al. Monoamine deficits in the brain of methyl-CpG binding protein 2 null mice suggest the involvement of the cerebral cortex in early stages of Rett syndrome. *Neuroscience* 2010; 170: 453–67.
- Schilstrom B, Konradsson-Geuken A, Ivanov V, Gertow J, Feltmann K, Marcus MM, et al. Effects of S-citalopram, citalopram, and R-citalopram on the firing patterns of dopamine neurons in the ventral tegmental area, N-methyl-D-aspartate receptor-mediated transmission in the medial prefrontal cortex and cognitive function in the rat. *Synapse* 2011; 65: 357–67.
- Schols L, Bauer P, Schmidt T, Schulte T, Riess O. Autosomal dominant cerebellar ataxias: clinical features, genetics, and pathogenesis. *Lancet Neurol* 2004; 3: 291–304.
- Sheline YI, West T, Yarasheski K, Swarm R, Jasielec MS, Fisher JR, et al. An antidepressant decreases CSF Abeta production in healthy individuals and in transgenic AD mice. *Sci Transl Med* 2014; 6: 236re4.
- Shim JS, Liu JO. Recent Advances in Drug Repositioning for the Discovery of New Anticancer Drugs. *Int J Biol Sci* 2014; 10: 654–63.
- Silva-Fernandes A, Costa Mdo C, Duarte-Silva S, Oliveira P, Botelho CM, Martins L, et al. Motor uncoordination and neuropathology in a transgenic mouse model of Machado-Joseph disease lacking intranuclear inclusions and ataxin-3 cleavage products. *Neurobiol Dis* 2010; 40: 163–76.
- Silva-Fernandes A, Duarte-Silva S, Neves-Carvalho A, Amorim M, Soares-Cunha C, Oliveira P, et al. Chronic treatment with 17-DMAG improves balance and coordination in a new mouse model of Machado-Joseph disease. *Neurotherapeutics* 2014; 11: 433–49.
- Takei A, Hamada T, Yabe I, Sasaki H. Treatment of cerebellar ataxia with 5-HT1A agonist. *Cerebellum* 2005; 4: 211–5.
- Tatum MC, Ooi FK, Chikka MR, Chauve L, Martinez-Velazquez LA, Steinbush HWM, et al. Neuronal serotonin release triggers the heat shock response in *C. elegans* in the absence of temperature increase. *Curr Biol* 2015; 52: 163–74.
- Teixeira-Castro A, Ailion M, Jalles A, Brignull HR, Vilaca JL, Dias N, et al. Neuron-specific proteotoxicity of mutant ataxin-3 in *C. elegans*: rescue by the DAF-16 and HSF-1 pathways. *Hum Mol Genet* 2011a; 20: 2996–3009.
- Teixeira-Castro A, Dias N, Rodrigues P, Oliveira JF, Rodrigues NF, Maciel P, et al. An image processing application for quantification of protein aggregates in *Caenorhabditis elegans*. In: Rocha MP, Corchado JM, Fdez Riverola F, Valencia A, editors. *Advances 55 in Intelligent and Soft Computing Series*. Vol. 93. Springer-Verlag; 2011b. (ISBN 978-3-642-19913-4).
- Villalon CM, Centurion D, Valdivia LF, de Vries P, Saxena PR. Migraine: pathophysiology, pharmacology, treatment and future trends. *Curr Vasc Pharmacol* 2003; 1: 71–84.
- Voisine C, Varma H, Walker N, Bates EA, Stockwell BR, Hart AC. Identification of potential therapeutic drugs for huntington's disease using *Caenorhabditis elegans*. *PLoS One* 2007; 2: e504.
- Warrick JM, Morabito LM, Bilen J, Gordesky-Gold B, Faust LZ, Paulson HL, et al. Ataxin-3 suppresses polyglutamine neurodegeneration in *Drosophila* by a ubiquitin-associated mechanism. *Mol Cell* 2005; 18: 37–48.

## Supplementary material

### **Serotonergic signaling suppresses ataxin-3 aggregation and neurotoxicity in animal models of Machado-Joseph disease**

Andreia Teixeira-Castro,<sup>1,2,3,4,9</sup> Ana Jalles,<sup>1,2,9</sup> Sofia Esteves,<sup>1,2,9</sup> Soosung Kang,<sup>3,5,6</sup> Liliana da Silva Santos,<sup>1,2</sup> Anabela Silva-Fernandes,<sup>1,2</sup> Mário F. Neto,<sup>3,4</sup> Renée M. Briemann,<sup>3,4</sup> Carlos Bessa,<sup>1,2</sup> Sara Duarte-Silva,<sup>1,2</sup> Adriana Miranda,<sup>1,2</sup> Stéphanie Oliveira,<sup>1,2</sup> Andreia Neves-Carvalho,<sup>1,2</sup> João Bessa,<sup>1,2</sup> Teresa Summavielle,<sup>7</sup> Richard B. Silverman,<sup>3,5,6</sup> Pedro Oliveira,<sup>8</sup> Richard I. Morimoto<sup>3,4</sup> and Patrícia Maciel<sup>1,2,\*</sup>

<sup>1</sup> Life and Health Sciences Research Institute (ICVS), School of Health Sciences, University of Minho, 4710-057 Braga, Portugal.

<sup>2</sup> ICVS/3Bs - PT Government Associate Laboratory, Braga/Guimarães, Portugal.

<sup>3</sup> Department of Molecular Biosciences, Northwestern University Evanston, Illinois 60208, USA.

<sup>4</sup> Rice Institute for Biomedical Research, Northwestern University Evanston, Illinois 60208, USA.

<sup>5</sup> Department of Chemistry, Northwestern University, Evanston, Illinois 60208, USA.

<sup>6</sup> Chemistry of Life Processes Institute and Center for Molecular Innovation and Drug Discovery, Northwestern University, Evanston, Illinois 60208, USA.

<sup>7</sup> BMC - Instituto de Biologia Molecular e Celular, Universidade do Porto, Rua do Campo Alegre, 823, 4150-180 Porto, Portugal.

<sup>8</sup> ICBAS-Abel Salazar Biomedical Sciences Institute, University of Porto, Porto, Portugal.

<sup>9</sup> These authors contributed equally to this work.

\*Correspondence to Patrícia Maciel, PhD, Associate Professor

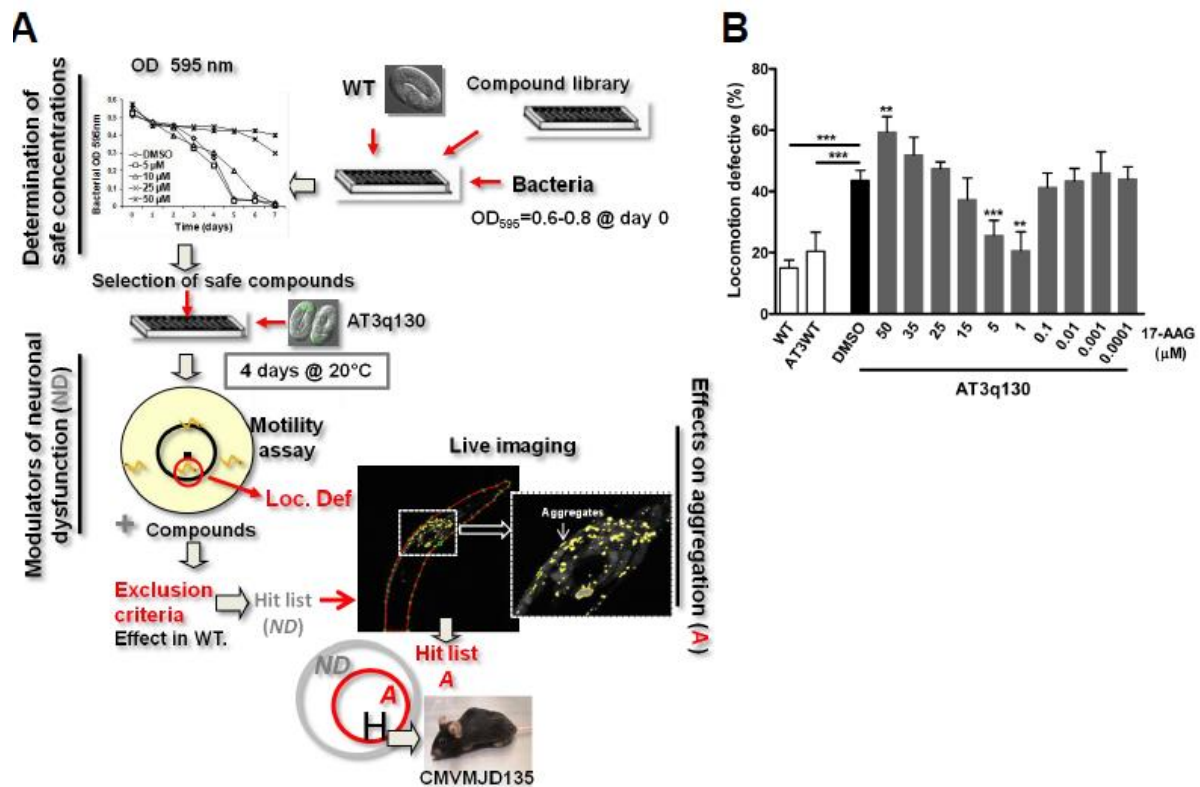
Life and Health Sciences Research Institute (ICVS); School of Health Sciences; University of Minho;

Gualtar Campus

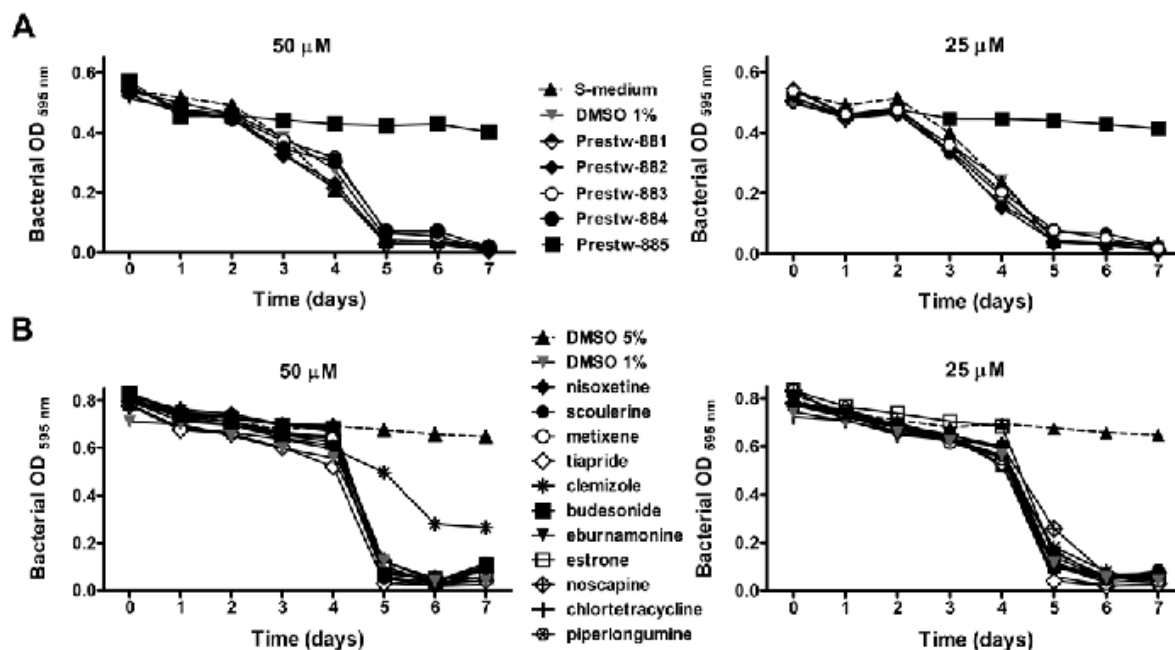
4710-057 Braga, Portugal

[Tel:+351253604824](tel:+351253604824); Fax:+351253604820; E-mail: [pmaciel@ecea.uminho.pt](mailto:pmaciel@ecea.uminho.pt)

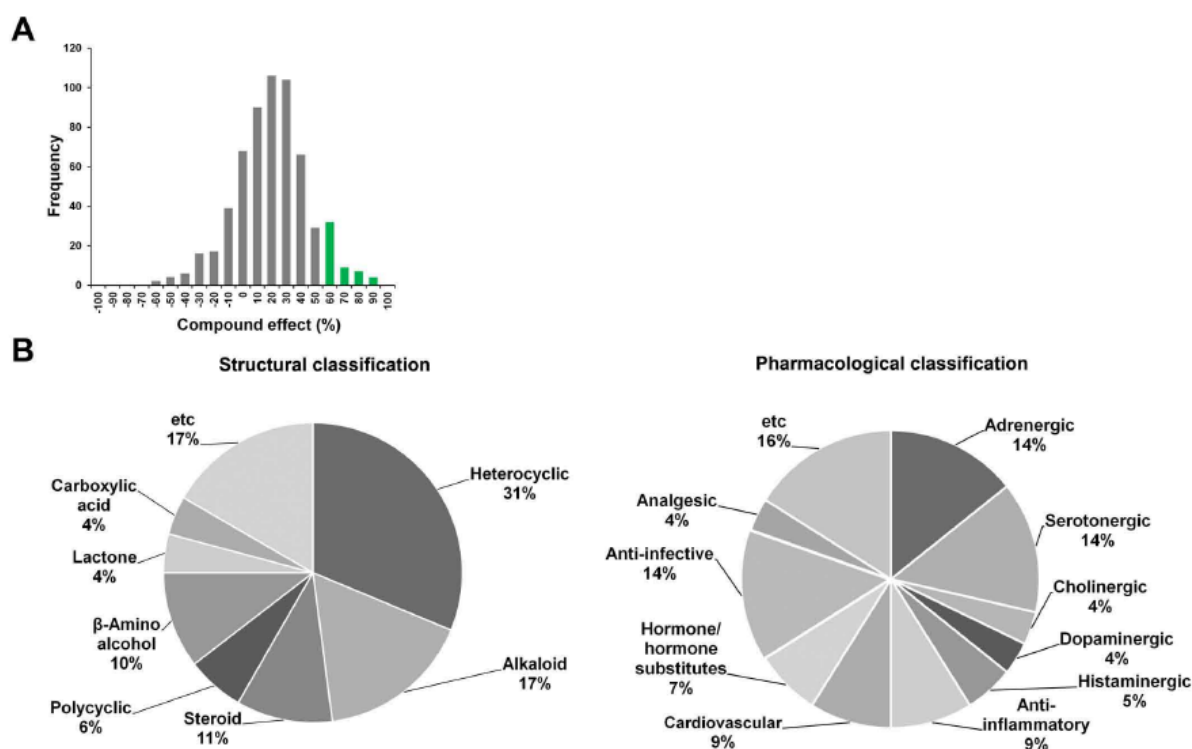
Running title: Serotonergic signaling suppresses MJD



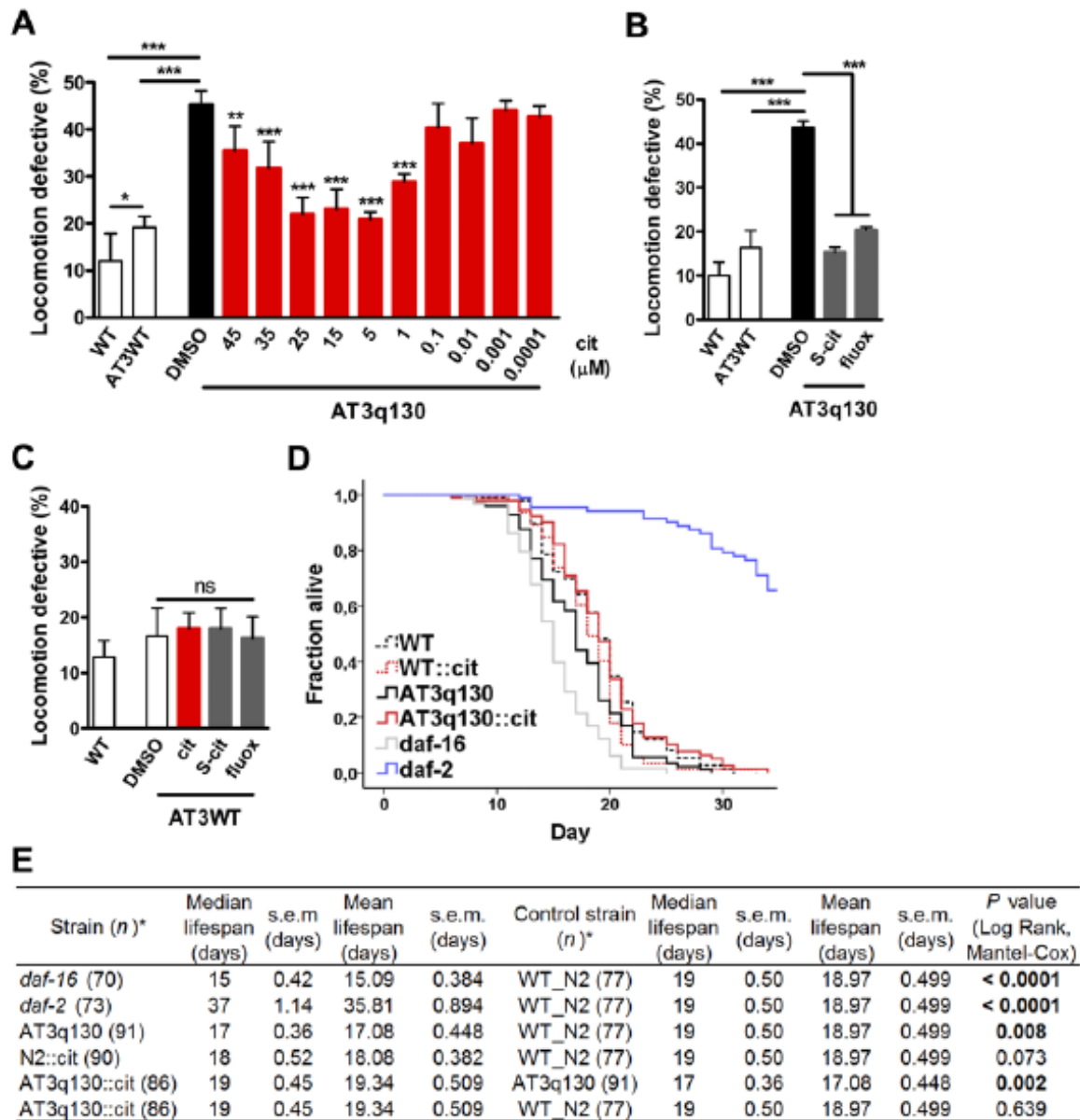
**Supplementary Figure 1.** Strategy used in the *C. elegans* small molecules screening and validation using 17-AAG. (A) Strategy used in the *C. elegans* screening: (i) determination of safe concentrations for each compound; (ii) identification of compounds that rescued or ameliorated AT3q130-mediated locomotion impairment; (iii) and determination of the impact on mutant ATXN3 aggregation of the top hit compounds. (iv) One selected suppressor of ATXN3 pathogenesis in *C. elegans* was tested in the CMVMJD135 mouse model. (B) AT3q130 animals were treated with 17-AAG (previously shown to decrease motility impairment in this model (Teixeira-Castro *et al.*, 2011)) at the indicated concentrations, and percentage of locomotion defective animals was determined ( $n = 3$ ,  $\pm$  s.d.), \* $P < 0.05$ , \*\* $P < 0.01$  and \*\*\* $P < 0.001$  (Student's *t*-test). OD, optical density; WT, wild-type animals; AT3q130, mutant ATXN3 expressing animals; Loc. Def, locomotion defective; ND, modulators of neuronal dysfunction; A, Aggregation.



**Supplementary Figure 2.** Prestwick library compound toxicity evaluation using the food clearance assay. (A) Example of five of the 1,120 compounds tested is given here. The OD of the *E. coli* OP50 suspension was measured daily of WT animals treated with each drug at 50 and 25  $\mu$ M. The mean OD was calculated for each day from triplicate samples and plotted over time. In this example, Prestw-885 administration to WT animals prevented food consumption, as OD levels remained high during the seven days, and was therefore classified as not safe at the concentrations tested. The other compounds shown were classified as safe, as the OD decrease paralleled the one of control samples. Control DMSO (DMSO 1%) corresponds to drug vehicle and Control S-medium to OP50-only S-medium (no vehicle). (B) Food clearance assay for a new batch of the hit compounds selected from the primary screen. Control DMSO (DMSO 1%) corresponds to drug vehicle and DMSO at 5% (DMSO 5%) was used as positive (toxic compound) control. Food consumption was slower when WT animals were treated with clemizole at 50  $\mu$ M, and similar to control (DMSO 1%) when treated with a lower dosage of 25  $\mu$ M. Therefore, subsequent clemizole treatments were set to 25  $\mu$ M, as this concentration was deemed safe to the nematodes. WT, wild-type.

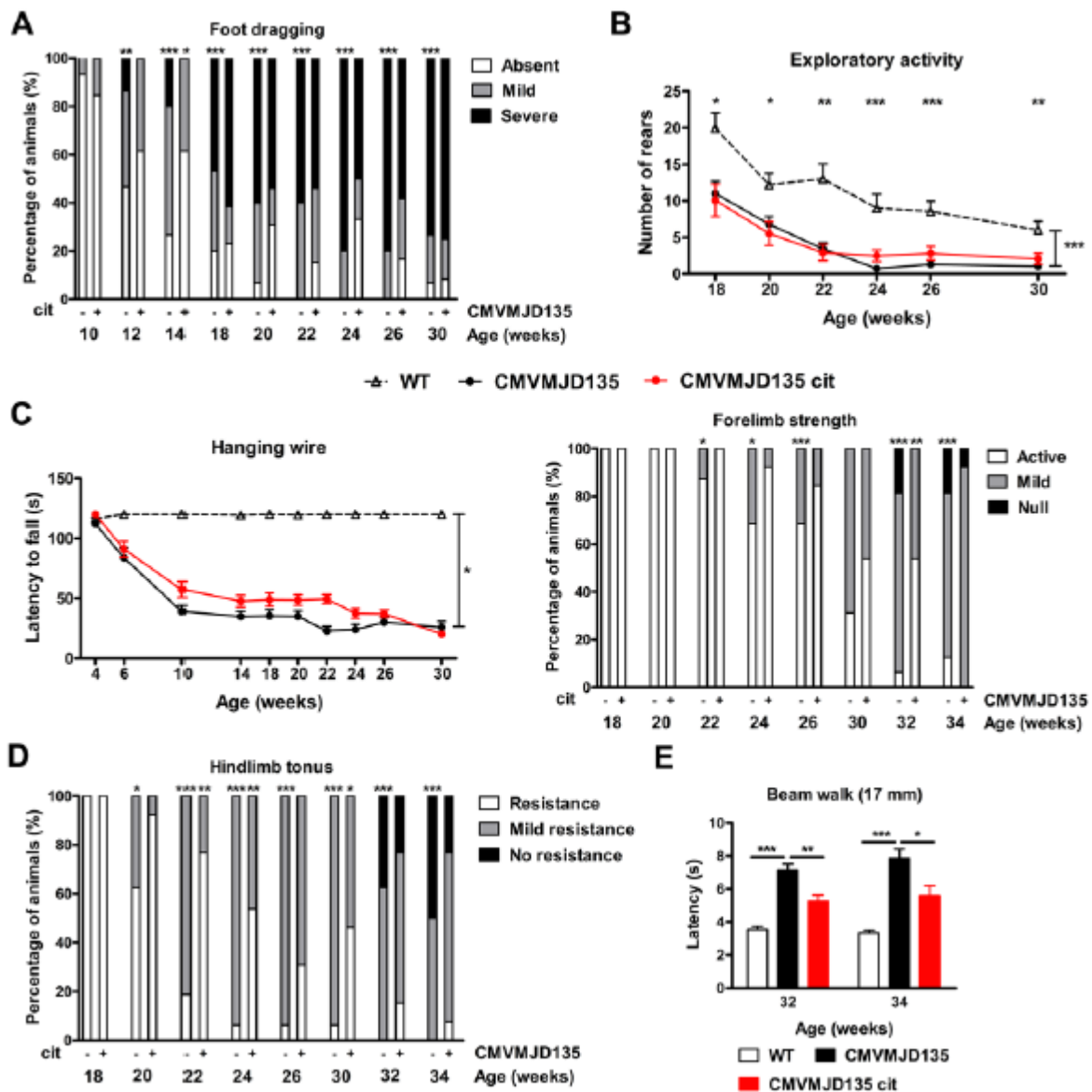


**Supplementary Figure 3.** *C. elegans*-based small molecule screening for suppressors of mutant ATXN3- mediated neurotoxicity. (A) Histogram shows percentage of effect frequency for the 599 Prestwick library compounds tested. Green bars show hit compounds of the screening, i.e. those which show a percentage of effect greater than 50%, within a 95% confidence interval. (B) Pharmacological and structural classification of the small molecules that actively ameliorated mutant-ATXN3 mediated neurological dysfunction in *C. elegans*. Pharmacological classification identified eleven major clusters, whereas at the chemical structure level the hit compounds found were clustered into nine groups. A subset of the compounds was included in more than one pharmacologic category, as they may have multiple targets. Scoulerine, for example, has been described to target 5-HT-,  $\alpha$ -adreno- and GABA-receptors (Ko *et al.*, 1993, Eisenreich *et al.*, 2003).

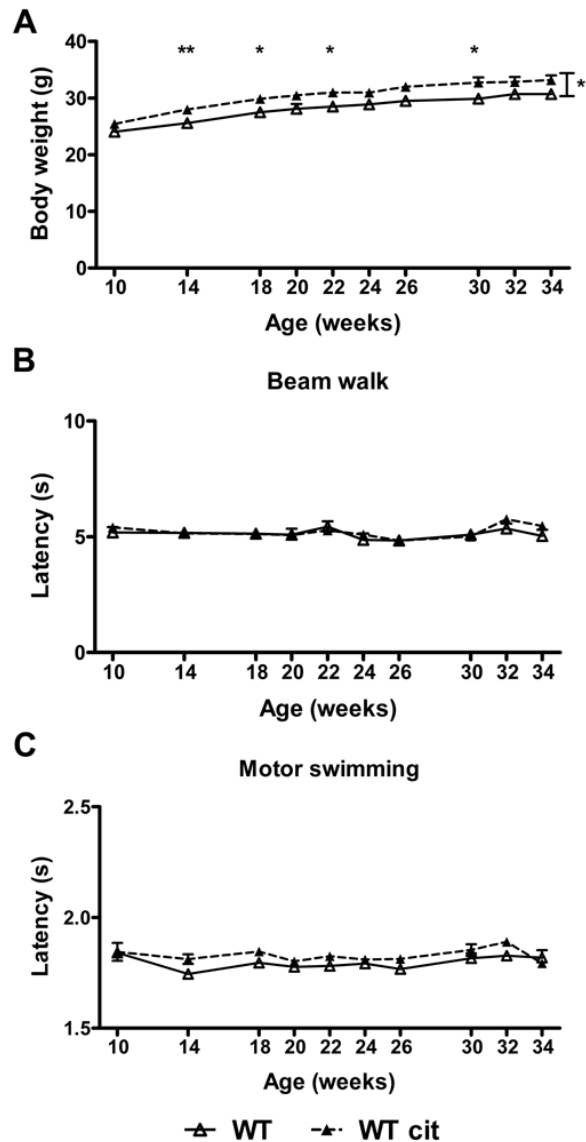


**Supplementary Figure 4.** SSRI treatment restores motility and survival of AT3q130 animals. (A) Dose-response profile of locomotion defects of AT3q130 animals upon cit treatment. (B), Other SSRIs - S-cit and fluox - showed similar effect on motor behavior of the AT3q130 animals. (C) Motility performance of AT3WT upon cit, S-cit and fluox treatments ( $n = 3-4 \pm$  s.d.), \* $P < 0.05$ , \*\* $P < 0.01$ , \*\*\* $P < 0.001$  (Student's  $t$ -test). (D) Survival of AT3q130 animals upon cit treatment and (E) statistics. cit, citalopram; S-cit, S-citalopram; fluox, fluoxetine; AT3WT, wild-type ATXN3 animals.

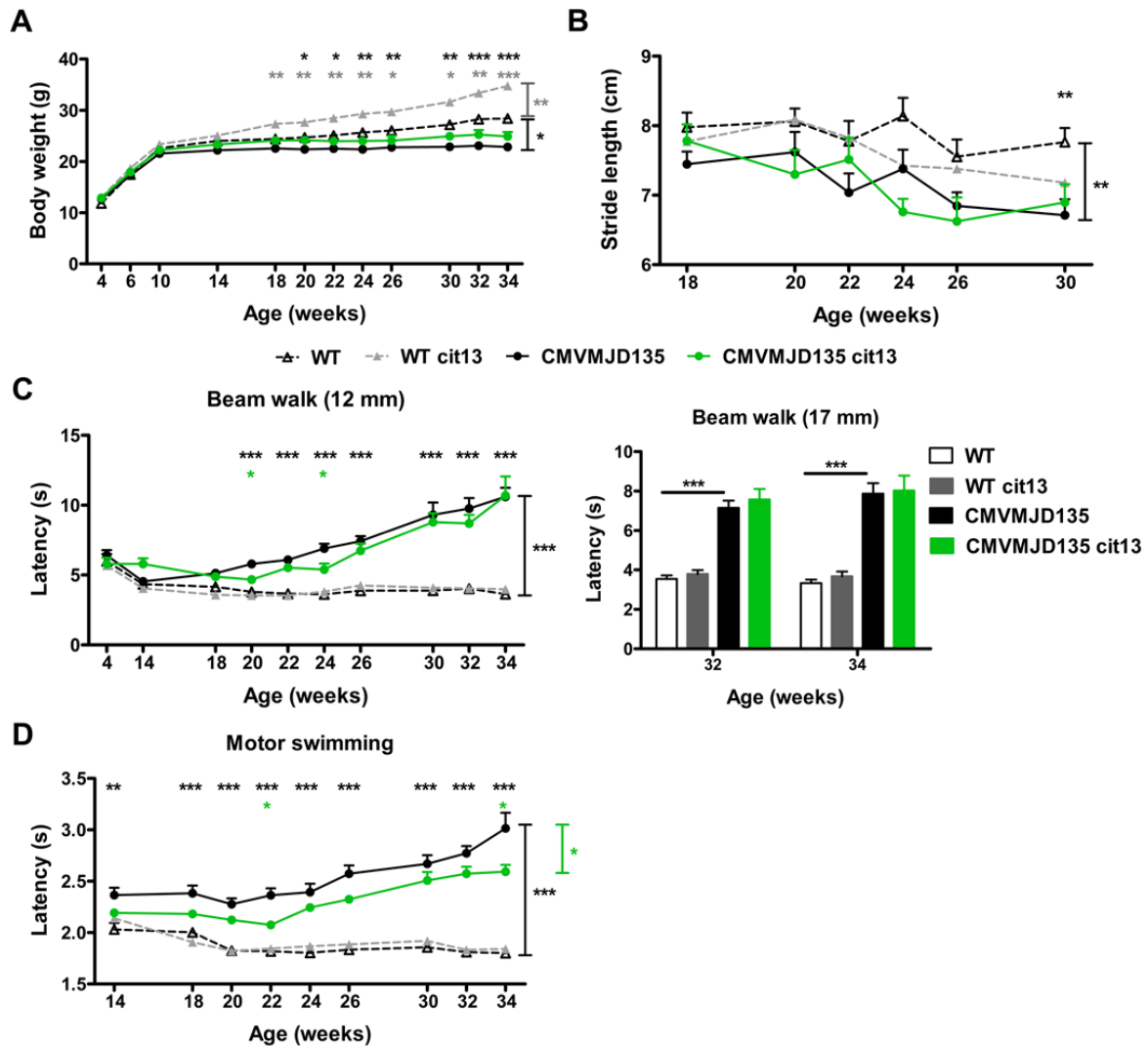




**Supplementary Figure 5.** Impact of citalopram treatment at 8 mg/kg on the neurological deficits and muscle strength of CMVMJD135 mice. (A) Mild improvement in the dragging of the paws at 14 weeks of age. (B) No improvement in exploratory activity. (C) No effect on muscle strength tests: hanging wire and forelimb strength, and on (D) hindlimb tonus. (E) Effects of cit treatment on balance of CMVMJD135 mice when crossing a round 17 mm beam at 32-34 weeks, ( $n = 13-16$ ,  $\pm$  s.d.),  $*P < 0.05$ ,  $**P < 0.01$  and  $***P < 0.001$  (Mann-Whitney U test for non-parametric variables and ANOVA, Tukey correction for continuous variables. For hanging wire test:  $R$  squares comparison of the logarithmic model for CMVMJD135 groups). cit, citalopram.



**Supplementary Figure 6.** Impact of citalopram treatment at 8 mg/kg on body weight and on motor behavior of WT mice. (A) Body weight, (B) beam walk and (C) motor swimming tests of vehicle and cit treated WT mice. Cit treatment resulted in a significant increase in body weight (Treatment:  $F_{1,18} = 5.337$ ,  $P = 0.033$ ). No differences between WT and cit treated WT mice were observed in the beam walk (Treatment:  $F_{1,16} = 0.748$ ,  $P = 0.40$ ) and motor swimming tests (Treatment:  $F_{1,14} = 0.043$ ,  $P = 0.839$ ). ( $n = 10 \pm$  s.e.m.), \* $P < 0.05$ , \*\* $P < 0.01$  and \*\*\* $P < 0.001$  (Repeated-measures ANOVA). cit, citalopram; WT, wild-type.



**Supplementary Figure 7.** Treatment with a higher dosage of citalopram (13 mg/kg) led to a limited improvement of neurological symptoms of CMVMJD135 mice. (A) Body weight, (B) stride length, (C) beam walk and (D) motor swimming tests of vehicle ( $n = 14$ ) and cit treated (13 mg/kg) WT (WT cit13) mice ( $n = 17$ ) and of vehicle ( $n = 16$ ) and cit treated (13 mg/kg) CMVMJD135 mice (CMVMJD135 cit13) ( $n = 13$ ). No differences were observed in body weight between CMVMJD135 and CMVMJD135 cit13 mice (Genotype:  $F_{1,67} = 31.335$ ,  $P < 0.001$ ; Treatment:  $F_{2,67} = 14.181$ ,  $P = 0.000007$ ; Genotype\*Treatment  $F_{1,67} = 1.425$ ,  $P = 0.237$ ; Post-hoc Tukey test (vehicle versus cit treated CMVMJD135 mice,  $P = 0.431$ ). Cit treated WT mice showed a significant increase in body weight (Tukey test,  $P = 0.007$ ). No differences were observed in stride length upon treatment. Regarding the balance beam walk test, a marginal amelioration was detected at 20 and 24 weeks of age (One-way ANOVA, Tukey test,  $P = 0.03$  and  $P = 0.031$ , respectively; Genotype:  $F_{1,49} = 124.181$ ,  $P < 0.001$ ; Treatment:  $F_{1,49} = 2.478$ , Genotype\*Treatment:  $F_{1,49} = 2.478$ ,  $P = 0.122$ ). In the motor swimming test, significant differences upon treatment were observed only at 22 and 34 weeks of age (One-way ANOVA, Tukey test,  $p = 0.016$  and  $p = 0.041$ , respectively, Genotype:  $F_{1,64} = 118.157$ ,  $P < 0.001$ , Treatment:  $F_{2,64} = 19.959$ ,  $P < 0.001$ ; Genotype\*Treatment:  $F_{1,64} = 6.3$ ,  $P = 0.015$ ). Data presented as mean  $\pm$  s.e.m., \* $P < 0.05$ , \*\* $P < 0.01$  and \*\*\* $P < 0.001$  (Repeated-measures ANOVA, Tukey correction). cit13, citalopram at 13 mg/kg; WT, wild-type.

**Supplementary Table 1.** Power analyses of the *C. elegans* behavior and pathological phenotypes.  $n$  needed is the number of subjects or observations needed for the specified power. The power of each statistical test was set to 95%, which is the probability that it correctly rejects the null hypothesis when it is false. The  $P$ -values were calculated by Students  $t$ -test or One-Way ANOVA followed by Bonferroni *post hoc* analysis. If  $P < 0.05$ , they are labeled as red bold letters. When actual  $n \geq n$  needed, they are labeled as blue bold letters.

Test	Improvement effect	Day	Effect size	$n$ needed	Strain comparison	$P$ -value	Actual $n$
Motility assay (treatment in plates)	25%	4	3.77	3	Q130 vs N2	<0.001	3
					Q130 vs Q130_cit	<0.001	
		6	3	4	Q130 vs N2	<0.001	4
					Q130 vs Q130_cit	<0.001	
		8	1.75	8	Q130 vs N2	<0.001	4
					Q130 vs Q130_cit	<0.01	
	10	0.66	18	Q130 vs N2	<0.01	4	
				Q130 vs Q130_cit	>0.05		
	12	1.05	21	Q130 vs N2	<0.01	4	
				Q130 vs Q130_cit	<0.05		
	14	0.61	59	Q130 vs N2	<0.001	4	
				Q130 vs Q130_cit	<0.05		
	50%	4	7.2	2	Q130 vs N2	<0.001	4
					Q130 vs Q130_cit	<0.001	
		6	6.33	2	Q130 vs N2	<0.001	4
					Q130 vs Q130_cit	<0.001	
		8	3.5	3	Q130 vs N2	<0.001	4
					Q130 vs Q130_cit	<0.01	
	10	1.41	12	Q130 vs N2	<0.01	4	
				Q130 vs Q130_cit	>0.05		
	12	2.5	6	Q130 vs N2	<0.01	4	
				Q130 vs Q130_cit	<0.05		
	14	1.38	13	Q130 vs N2	<0.001	4	
				Q130 vs Q130_cit	<0.05		
	75%	4	10.98	2	Q130 vs N2	<0.001	4
					Q130 vs Q130_cit	<0.001	
		6	9.33	2	Q130 vs N2	<0.001	4
					Q130 vs Q130_cit	<0.001	
		8	5.24	3	Q130 vs N2	<0.001	4
					Q130 vs Q130_cit	<0.01	
	10	2.17	6	Q130 vs N2	<0.01	4	
				Q130 vs Q130_cit	>0.05		
	12	3.33	3	Q130 vs N2	<0.01	4	
				Q130 vs Q130_cit	<0.05		
	14	1.99	7	Q130 vs N2	<0.001	4	
				Q130 vs Q130_cit	<0.05		
	95%	4	3.72	2	Q130 vs N2	<0.001	4
					Q130 vs Q130_cit	<0.001	
		6	12	2	Q130 vs N2	<0.001	4
					Q130 vs Q130_cit	<0.001	
		8	6.8	2	Q130 vs N2	<0.001	4
					Q130 vs Q130_cit	<0.01	
10	2.73	4	Q130 vs N2	<0.01	4		
			Q130 vs Q130_cit	>0.05			
12	4.03	3	Q130 vs N2	<0.01	4		
			Q130 vs Q130_cit	<0.05			
14	2.6	5	Q130 vs N2	<0.001	4		
			Q130 vs Q130_cit	<0.05			
Motility assay (96-well plates)	25%	4	1.83	8	Q130 vs N2 Q130 vs Q130_cit	<0.01	3
	50%		3.94	3			3
	75%		5.78	2			3
	95%		7.35	2			3
	25%	4	1.84	8	Q130 vs Q14 Q130 vs Q130_cit	<0.01	3
	50%		3.41	3			3
	75%		4.99	3			3
	95%		6.57	3			3

Supplementary Table 1. (cont.) Power analyses of the *C. elegans* behavior and pathological phenotypes.

Test	Improvement effect	Day	Effect size	<i>n</i> needed	Strain comparison	P-value	Actual <i>n</i>
ATXN3 Western-blot	25%	4	1.34	13	Q130 vs Q130_cit	>0.05	4
	50%		2.66	4			4
	75%		4	3			4
	95%		5.06	3			4
ATXN3 aggregation	25%	4	0.78	36	Q130 vs Q130_cit	<0.05	8-14
	50%		1.31	14			
	75%		2.71	6			
	95%		2.73	4			

Supplementary Table 2. Power analyses of the behavior and pathological phenotypes in CMVMJD135 mice.

Test	Week	Effect size	<i>n</i> needed	Group comparison	P-value	Actual <i>n</i>		
Body weight	14	0,55	57	CMVMJD135 vs WT	>0.05	13-16		
				CMVMJD135 vs CMVMJD135_cit	<0.01			
	18	0,54	57	CMVMJD135 vs WT	>0.05			
				CMVMJD135 vs CMVMJD135_cit	<0.001			
	20	0,80	26	CMVMJD135 vs WT	>0.05			
				CMVMJD135 vs CMVMJD135_cit	<0.001			
	22	0,81	25	CMVMJD135 vs WT	<0.05			
				CMVMJD135 vs CMVMJD135_cit	<0.01			
	24	0,98	17	CMVMJD135 vs WT	<0.01			
				CMVMJD135 vs CMVMJD135_cit	<0.01			
26	0,84	25	CMVMJD135 vs WT	<0.05				
			CMVMJD135 vs CMVMJD135_cit	<0.01				
30	0,96	18	CMVMJD135 vs WT	<0.01				
			CMVMJD135 vs CMVMJD135_cit	<0.01				
32	1,31	10	CMVMJD135 vs WT	<0.01				
			CMVMJD135 vs CMVMJD135_cit	0.011				
34	1,50	8	CMVMJD135 vs WT	<0.001				
			CMVMJD135 vs CMVMJD135_cit	<0.05				
Motor swimming test	14	1,87	5	CMVMJD135 vs WT	<0.01	13-16		
				CMVMJD135 vs CMVMJD135_cit	<0.001			
	18	4,39	2	CMVMJD135 vs WT	<0.001			
				CMVMJD135 vs CMVMJD135_cit	<0.01			
	20	2,65	5	CMVMJD135 vs WT	<0.001			
				CMVMJD135 vs CMVMJD135_cit	<0.01			
	22	5,16	3	CMVMJD135 vs WT CMVMJD135 vs CMVMJD135_cit	<0.001 <0.001			
							24	6,77
26	9,81	2						
			30			14,84	2	
32	8,10	2						
			34			12,92	2	
Stride length	18	0,31						175
			CMVMJD135 vs CMVMJD135_cit			>0.05		
	20	0,32	142	CMVMJD135 vs WT	>0.05			
				CMVMJD135 vs CMVMJD135_cit	>0.05			
	22	0,37	142	CMVMJD135 vs WT	>0.05			
				CMVMJD135 vs CMVMJD135_cit	>0.05			
	24	0,43	77	CMVMJD135 vs WT	>0.05			
				CMVMJD135 vs CMVMJD135_cit	>0.05			
26	0,49	49	CMVMJD135 vs WT	>0.05				
			CMVMJD135 vs CMVMJD135_cit	>0.05				
30	0,72	29	CMVMJD135 vs WT	<0.01				
			CMVMJD135 vs CMVMJD135_cit	<0.05				

Supplementary Table 2. (cont.) Power analyses of the behavior and pathological phenotypes in CMVMJD135 mice.

Test	Week	Effect size	n needed	Group comparison	P-value	Actual n
Balance beam walk test (12 mm square)	18	0,44	72	CMVMJD135 vs WT	>0.05	13-16
				CMVMJD135 vs CMVMJD135_cit	>0.05	
	20	1,0	17	CMVMJD135 vs WT	<0.001	
				CMVMJD135 vs CMVMJD135_cit	<0.05	
	22	0,89	19	CMVMJD135 vs WT	<0.001	
				CMVMJD135 vs CMVMJD135_cit	>0.05	
	24	1,4	9	CMVMJD135 vs WT	<0.001	
				CMVMJD135 vs CMVMJD135_cit	<0.01	
	26	1,27	10	CMVMJD135 vs WT	<0.001	
				CMVMJD135 vs CMVMJD135_cit	<0.01	
30	1,09	15	CMVMJD135 vs WT	<0.001		
			CMVMJD135 vs CMVMJD135_cit	<0.05		
32	1,0	15	CMVMJD135 vs WT	<0.001		
			CMVMJD135 vs CMVMJD135_cit	<0.001		
34	1,39	9	CMVMJD135 vs WT	<0.001		
			CMVMJD135 vs CMVMJD135_cit	<0.05		
Balance beam walk test (17 mm circle)	32	1,27	11	CMVMJD135 vs WT	<0.001	13-16
	34	1,05	15	CMVMJD135 vs WT	<0.05	
				CMVMJD135 vs CMVMJD135_cit	<0.05	
Locomotory activity (number of squares)	22	0,46	77	CMVMJD135 vs WT	<0.01	13-16
	24	0,94	19	CMVMJD135 vs WT	<0.001	
				CMVMJD135 vs CMVMJD135_cit	>0.05	
	26	1,00	17	CMVMJD135 vs WT	<0.001	
				CMVMJD135 vs CMVMJD135_cit	>0.05	
30	0,84	23	CMVMJD135 vs WT	<0.001		
CMVMJD135 vs CMVMJD135_cit	>0.05					
Rears (exploratory activity)	18	0,62	41	CMVMJD135 vs WT	<0.05	13-16
				CMVMJD135 vs CMVMJD135_cit	>0.05	
	20	0,54	55	CMVMJD135 vs WT	<0.05	
				CMVMJD135 vs CMVMJD135_cit	0.982	
	22	1,3	10	CMVMJD135 vs WT	<0.05	
	24	2,28	4	CMVMJD135 vs WT	<0.001	
				CMVMJD135 vs CMVMJD135_cit	>0.05	
	26	1,57	7	CMVMJD135 vs WT	<0.001	
CMVMJD135 vs CMVMJD135_cit				>0.05		
30	1,09	14	CMVMJD135 vs WT	0.006		
CMVMJD135 vs CMVMJD135_cit	>0.05					
ATXN3 Western-blot	34	2.02	4	CMVMJD135 vs WT	<0.001	4
CMVMJD135 vs CMVMJD135_cit	>0.05					
ATXN3 inclusions (7N)	34	6.1	2	CMVMJD135 vs WT	<0.001	4
CMVMJD135 vs CMVMJD135_cit	<0.05					
ATXN3 inclusions (PN)	34	1.97	5	CMVMJD135 vs WT	<0.001	4
CMVMJD135 vs CMVMJD135_cit	>0.05					
ATXN3 inclusions (Rttg)	34	1.45	7	CMVMJD135 vs WT	<0.001	4
CMVMJD135 vs CMVMJD135_cit	>0.05					
ATXN3 inclusions (LRT)	34	2.07	4	CMVMJD135 vs WT	<0.001	4
CMVMJD135 vs CMVMJD135_cit	>0.05					
GFAP immunohistochemistry	34	1.15	5-10	CMVMJD135 vs WT	<0.001	4
CMVMJD135 vs CMVMJD135_cit	<0.05					

Supplementary Table 3. List of strains, abbreviations and crosses used in this work.

Strain (ref.)	Abbreviation	Protein	Genotype
AM510 (Teixeira-Castro <i>et al.</i> , 2011)	AT3q14	AT3q14::YFP	<i>rmls228[P<sub>F25B3.3</sub>::AT3v1-1q14::yfp]</i>
AM685 (Teixeira-Castro <i>et al.</i> , 2011)	AT3q130	AT3q130::YFP	<i>rmls263[P<sub>F25B3.3</sub>::AT3v1-1q130::yfp]</i>
AM599 (Teixeira-Castro <i>et al.</i> , 2011)	AT3q130	AT3q130::YFP	<i>rmls261[P<sub>F25B3.3</sub>::AT3v1-1q130::yfp]</i>
AQ866 (Olde and McCombie, 1997)	<i>ser-4</i>		<i>ser-4(ok512) III</i>
MAC72 <sup>‡</sup>	<i>ser-4</i> ; AT3q130	AT3q130::YFP	<i>ser-4(ok512) III;rmls263[P<sub>F25B3.3</sub>::AT3v1-1q130::yfp]</i>
MT8944 (Ranganathan <i>et al.</i> , 2001)	<i>mod-5</i>		<i>mod-5(n822) I</i>
MAC73 <sup>‡</sup>	<i>mod-5</i> ; AT3q130	AT3q130::YFP	<i>mod-5(n822) I;rmls263[P<sub>F25B3.3</sub>::AT3v1-1q130::yfp]</i>
MT9772 (Ranganathan <i>et al.</i> , 2001)	<i>mod-5</i>		<i>mod-5(n3314) I</i>
MAC74 <sup>‡</sup>	<i>mod-5</i> ; AT3q130	AT3q130::YFP	<i>mod-5(n3314) I;rmls263[P<sub>F25B3.3</sub>::AT3v1-1q130::yfp]</i>
DA1814 (Hamdan <i>et al.</i> , 1999)	<i>ser-1</i>		<i>ser-1(ok345) X</i>
MAC75 <sup>‡</sup>	<i>ser-1</i> ; AT3q130	AT3q130::YFP	<i>ser-1(ok345) X;rmls263[P<sub>F25B3.3</sub>::AT3v1-1q130::yfp]</i>
CB1370 (Kimura <i>et al.</i> , 1997)	<i>daf-2</i>		<i>daf-2(e1370) III</i>
CF1038 (Lin <i>et al.</i> , 1997)	<i>daf-16</i>		<i>daf-16(mu86) I</i>

<sup>‡</sup>this study

## Legends of Supplementary Videos

**Supplementary Video 1.** Citalopram treatment improved the balance, coordination and time spent to reach the platform of CMVMJD135 mice in the beam walk test. Balance beam walk test of 30 week-old WT, vehicle and citalopram treated CMVMJD135 mice.

**Supplementary Video 2.** Citalopram treatment ameliorated the coordination and time spent to reach the platform in the motor swimming test of CMVMJD135 mice. Motor swimming test of 30 week-old WT, vehicle and citalopram treated CMVMJD135 mice.

## References cited in this section

- Eisenreich WJ, Hofner G, Bracher F. Alkaloids from *Croton flavens* L. and their affinities to GABA-receptors. *Nat Prod Res.* 2003;17(6):437-40.
- Hamdan FF, Ungrin MD, Abramovitz M, Ribeiro P. Characterization of a novel serotonin receptor from *Caenorhabditis elegans*: cloning and expression of two splice variants. *J Neurochem.* 1999;72(4):1372-83.
- Kimura KD, Tissenbaum HA, Liu Y, Ruvkun G. *daf-2*, an insulin receptor-like gene that regulates longevity and diapause in *Caenorhabditis elegans*. *Science.* 1997;277(5328):942-6.
- Ko FN, Yu SM, Su MJ, Wu YC, Teng CM. Pharmacological activity of (-)-discretamine, a novel vascular alpha-adrenoceptor and 5-hydroxytryptamine receptor antagonist, isolated from *Fissistigma glaucescens*. *Br J Pharmacol.* 1993;110(2):882-8.
- Lin K, Dorman JB, Rodan A, Kenyon C. *daf-16*: An HNF-3/forkhead family member that can function to double the life-span of *Caenorhabditis elegans*. *Science.* 1997;278(5341):1319-22.
- Olde B, McCombie WR. Molecular cloning and functional expression of a serotonin receptor from *Caenorhabditis elegans*. *J Mol Neurosci.* 1997;8(1):53-62.
- Ranganathan R, Sawin ER, Trent C, Horvitz HR. Mutations in the *Caenorhabditis elegans* serotonin reuptake transporter MOD-5 reveal serotonin-dependent and -independent activities of fluoxetine. *J Neurosci.* 2001;21(16):5871-84.
- Teixeira-Castro A, Ailion M, Jalles A, Brignull HR, Vilaca JL, Dias N, et al. Neuron-specific proteotoxicity of mutant ataxin-3 in *C. elegans*: rescue by the DAF-16 and HSF-1 pathways. *Hum Mol Genet.* 2011;20(15):2996-3009.